FN-EDA domain knock-in and knock-out mice, as a model for the study of the hepatic fibronectin (FN) functions

Thesis

FN-EDA DOMAIN KNOCK-IN AND KNOCK-OUT MICE, AS A MODEL FOR THE STUDY OF THE HEPATIC FIBRONECTIN (FN) FUNCTIONS

Federico Andrea Moretti

A Thesis Submitted in Fulfillment of the Requirements of the Open University (UK) for the Degree of Doctor of Philosophy

Life Sciences

International Centre for Genetic Engineering and Biotechnology (ICGEB)

Trieste, Italy

Director of Studies: Andrés F. Muro, Ph.D.

External Supervisor: Javier Caceres, Ph.D.

September 2007

TEXT BOUND CLOSE TO THE SPINE IN THE ORIGINAL THESIS

Alle mie nipotine Carlotta e Matilde

To my little nieces Carlotta and Matilde

ACKNOWLEDGMENTS

The present thesis was carried out in the *Mouse Molecular Genetics Group* at the *International Centre for Genetic Engineering and Biotechnology* (ICGEB), Trieste, Italy. I am profoundly grateful to *Prof. Francisco E. Baralle* for his constant encouragement and support throughout the development of this thesis work and also for supporting my enrollment to the Open University (UK).

A special heartfelt thank and all my gratitude go to *Dr. Andrés F. Muro* for his constant guidance and patience, for his precious advises and for sustaining me in any difficulties.

I would also like to thank sincerely my external supervisor *Dr. Javier Cáceres* (MRC Human Genetics Unit, Western general Hospital, Edinburgh, UK) for his precious support, *Dr. Marcello Raspa* (European Mutant Mouse Archive, Monterotondo-Scalo, Rome, Italy) for providing me the murine strain TG-Alf-p-CRE, and *Dr. Eric White* (University of Michigan Health System, Chicago, USA) for providing me some of the histological protocols describes in the thesis and his important data obtained working on lungs. I have also to thank *Fabiola Porro* and *Alessandra Iaconcig* for their excellent technical support, all the component of the ICGEB Animal House, in particular *Giancarlo Lunazzi*, *Mauro Sturnega* and *Stefano Artico* for the animal care and handling, *Dr. Maurizio Romano* and *Gabriele Talotti* for their precious help in the use of the computer software, and *Dr. Rodolfo Garcia* and *Ann Crum* for critical reading of the manuscript and for comments regarding the use of English.

Finally I would like to express my gratitude to all members of the *Molecular Pathology Group*, the *Human Molecular Genetics Group* and to my precious lab-mates *Luisa Costessi* e *Giulia Bortolussi* for their cooperation and friendship during these years.

TABLE OF CONTENTS

LIST OF FIGURES

LIST OF ABBREVIATIONS

FN = Fibronectin.

pFN = plasma Fibronectin.

cFN = cellular Fibronectin.

ECM = Extracellular Matrix.

EDA = Extra-Domain A.

EDB = Extra-Domain B.

IIICS = Type III Homology Connecting Segment.

V = Variable Segment or IIICS.

$EDA^{wt/wt}$ = Wild-type mouse.

$EDA^{+/+}$ = EDA knock-in mouse.

$EDA^{-/-}$ = EDA knock-out mouse.

$EDA^{+/+CRE}$ = Liver-specific EDA-null mouse.

ESE = Exonic Splicing Enhancer.

ESS = Exonic Splicing Silencer.

neo = Aminoglycoside phosphotransferase gene.

tk = Thymidine kinase.

LoxP = Locus of Crossover in bacteriophage P1.

CRE = Cyclization Recombination Protein.

Floxed = Flanked by LoxP sites.

HSC = Hepatic Stellate Cell.

SEC = Sinusoidal Endothelial Cell.

αSMA = Smooth Muscle α-Actin.

β-Tub = β-Tubulin.

TGFβ = Transforming Growth Factor-β.

CCl_4 = Carbon Tetracloride.

BDL = Bile Duct Ligation.

ABSTRACT

Fibronectin (FN) is a multidomain glycoprotein found in plasma and tissue extracellular matrices (ECM). Plasma FN (pFN) is produced and secreted into the bloodstream by the liver. Liver ECM-FN and pFN are characterized by the absence of the EDA domain, one of the three FN exons undergoing alternative splicing. However, in pathological situations such as wound healing, the liver produces and accumulates huge amounts of $EDA^{+}FN$ in sinusoidal ECM. In order to study the functions of the FN isoforms produced by the liver, we used two mouse strains devoid of EDA-exon alternative splicing, which constitutively include ($EDA^{+/+}$ strain) or exclude ($EDA^{-/-}$ strain) the EDA domain.

The $EDA^{+/+}$ strain is characterized by an important decrease of FN levels both in plasma and tissues. Here, we show that the atypical presence of the EDA domain in hepatocytes affects pFN secretion into the bloodstream and we demonstrate that a high proportion of tissue ECM-FN is supplied by plasma. In fact, removal of the EDA exon only from the liver, by hepatocyte-specific deletion of the EDA exon, restores normal levels of FN in both plasma and tissues of the $EDA^{+/+}$ animals. This finding not only suggests that plasma behaves as a sort of FN reservoir for tissue maintenance but also shows for the first time that the pFN contribution to the ECM of tissues is roughly equal to that produced locally.

The $EDA^{-/-}$ strain was used to study the role of the EDA domain in the onset of liver fibrosis. In two different liver fibrosis models, we observed that $EDA^{-/-}$ animals develop attenuated fibrosis in comparison to control mice. The important role of the EDA domain in the activation and proliferation of the hepatic stellate cells (HSCs), these are the key cells responsible for the ECM protein overproduction in the fibrotic processes, is demonstrated for the first time *in vivo*. $EDA^{-/-}$ livers treated to induce fibrosis, present a striking reduction in the number of myofibroblasts or activated HSCs, suggesting that the EDA domain could be a potential target for the treatment of liver fibrosis.

1. INTRODUCTION

1.1 FIBRONECTINS.

Fibronectins (FNs) are a large family of multifunctional and multidomain glycoproteins mainly found in the extracellular matrix (ECM) of tissues and in plasma. FN is organized in functional domains as "beads on a string" that are arranged in a "modular fashion" and used by the protein to fulfill diverse interactions (Hynes and Yamada, 1982; Yamada, 1983). FNs have been implicated in a wide variety of cellular processes, particularly those involving the interactions of cells with other ECM proteins. These processes include cell-adhesion, -migration and -differentiation, ECM and cytoskeletal organization, wound healing, embryogenesis, oncogenic transformation, and hemostasis (Hynes, 1990). The basic role of FN in these processes is that of a ligand between various intracellular and extracellular molecules for the regulation and maintenance of the normal cell and tissue functions. The interaction of FN with specific transmembrane receptors called integrins is considered fundamental for cell regulation and signal transduction (Plow et al., 2000).

1.1.1 Fibronectin functional domains.

The FN functional molecule consists of two similar or identical subunits of 220-250 kDa that are held together by two disulfide-bonds near their carboxyl-termini and forming a dimer. Each monomer is made of several compact globular domains separated by short, flexible and extendable connecting regions (Figure 1). Three different types of homologous and repeating domains, termed Type I, II, and III, exist (Hynes, 1990). Each of the twelve Type I modules is made of ~ 40 amino acids (aa) forming five anti-parallel β-strands, originating two anti-parallel β-sheets stabilized by two disulfide bonds (Baron et al., 1990). There are only two Type II modules that are made of ~ 60 aa forming four anti-

parallel β-strands and stabilized by two disulfide bonds (Constantine et al., 1991; Petersen et al., 1983).

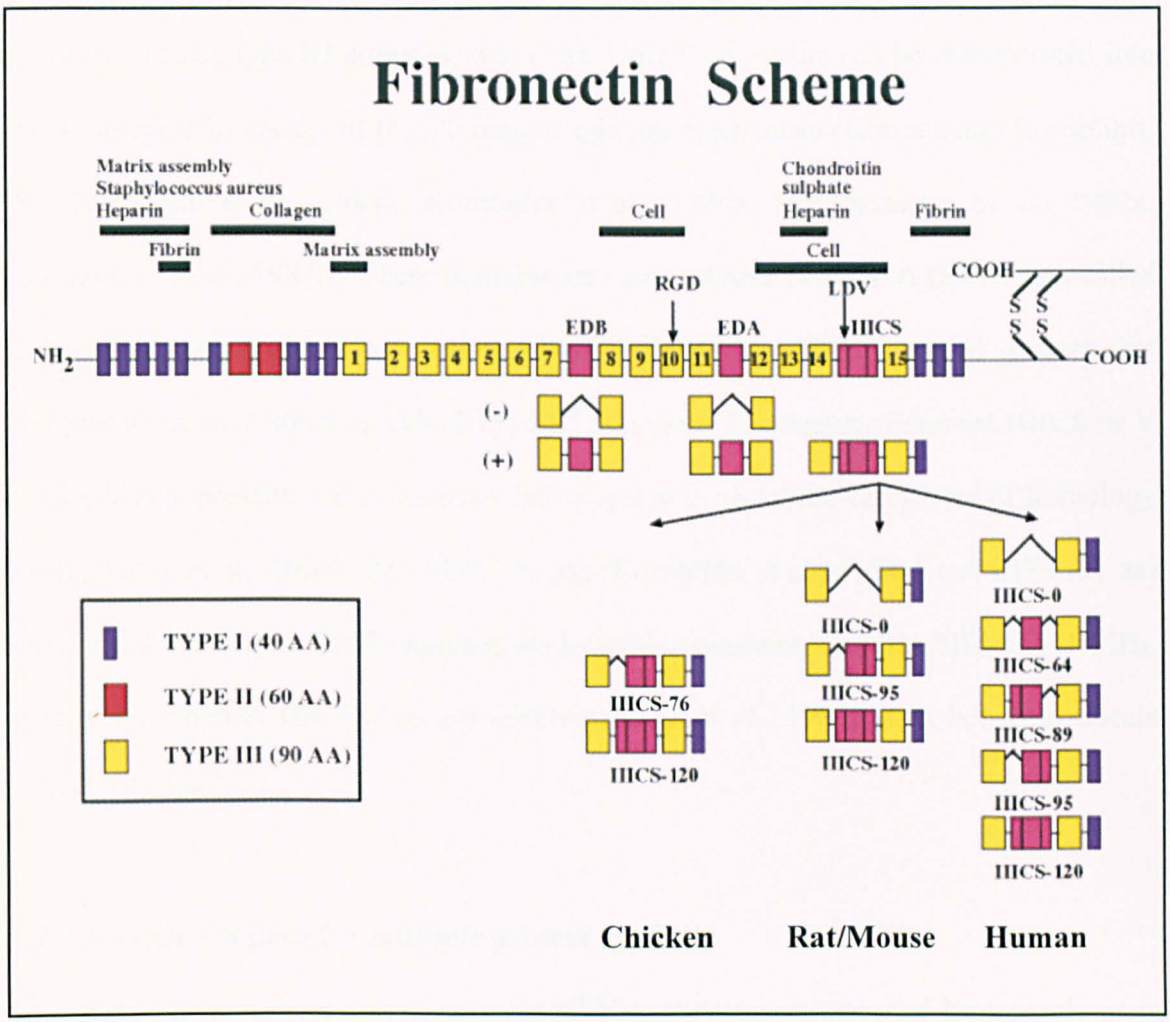

Figure 1. Schematic representation of the fibronectin protein and its interactions.
Upper part. Type I (violet), Type II (red boxes) and Type III (yellow boxes) are the repeating homologous domains present in the FN polypeptide. EDB, EDA, and IIICS are the alternatively spliced domains. EDA and EDB are Type III domains, whereas IIICS does not fall into any of the homology category. Type I, Type II, EDB, EDA and IIICS domains are each encoded by a single exon. Most of the type III domains are instead encoded by two exons. Interaction of FN functional domains with other extracellular matrix proteins, cells and itself is shown in the top.
Lower part. Representation of the FN splicing pattern. While EDA and EDB exons can be simply spliced in or out from the FN mRNA, IIICS undergoes a much more complex splicing pattern, leading to the generation of two, three and five splicing variants in chickens, rodents and human, respectively.

The fifteen Type III modules constitute the largest part of the FN polypeptide (Figure 1). The 90 aa are organized in seven β-strands forming a sandwich of two anti-parallel β-sheets (Baron et al., 1992). There are no disulfide bonds present. One of the most intriguing features of the Type III modules in fibronectin is that their number is modulated through the alternative splicing of the single FN pre-mRNA (Figure 1). Besides the constitutive fifteen type III domains, two extra Type III domains can be incorporated into the FN molecule by means of the alternative splicing mechanism (Gutman and Kornblihtt, 1987; Kornblihtt et al., 1984a; Kornblihtt et al., 1984b; Schwarzbauer et al., 1987a; Schwarzbauer et al., 1987b). These domains are termed Extra-Domain A (EDA, also called EIIIA or EDI) and B (EDB, also called EIIIB or EDII). In addition, a third element that undergoes alternative splicing, called Type III homology Connecting Segment (IIICS or V for Variable) is present, but it does not fall into any of the three categories of homology (Schwarzbauer et al., 1983). The EDA (90 aa) (Kornblihtt et al., 1984a) and EDB (91 aa) (Gutman and Kornblihtt, 1987) domains are located between repeats III_{11}/III_{12} and III_7/III_8, respectively, whereas IIICS (120 aa) (Schwarzbauer et al., 1983) is in between repeats III_{14}/III_{15} (Figure 1).

1.1.2 A single FN gene for multiple protein variants.

It has already been established that all FNs variants are encoded by a single gene (George et al., 1993; Kornblihtt et al., 1983; Schwarzbauer et al., 1983). The FN gene has been mapped to chromosome 1 and 2, in mouse (Skow et al., 1987) and human (Prowse et al., 1986), respectively. However, multiple FN mRNAs, and consequently multiple protein isoforms, can arise due to the alternative splicing mechanism of the FN pre-mRNA (ffrench-Constant, 1995; Kornblihtt et al., 1996). Whereas EDA and EDB exons can be simply included or excluded from FN mRNA by the splicing machinery, the IIICS element undergoes a more complicated splicing pattern (Pankov and Yamada, 2002). In fact, it can be completely included (V120) or excluded (V0), or partially included, according to the

species (Figure 1). Two variants are present in chicken (Norton and Hynes, 1987), three in both rat and mouse (Schwarzbauer et al., 1983), and five in human (Hershberger and Culp, 1990). As the single splicing events in the three regions of variability are independent from each other (Caputi et al., 1995a; Chauhan et al., 2004), at least 8 different polypeptides could be generated from the FN gene in chicken, 12 in rat and mouse and up to 20 in human (Pankov and Yamada, 2002). Even though the mechanism by which the FN gene produces protein variants has been known for a long time, the different properties of the single isoforms in different processes such as ligand-binding, cell-adhesion, -activation or -differentiation, solubility, composition of the ECM are poorly understood especially *in vivo*.

1.1.3 Plasma and cellular fibronectins.

In vivo analyses have shown that FNs are found in most body fluids such as plasma, bile and amniotic fluids, in the ECM of all connective tissues, and on the cell surfaces and most basement membranes (Hynes, 1990). *In vitro* experiments have revealed that FNs are synthesized by a wide variety of cell types such as fibroblasts, endothelial cells and hepatocytes that are the most important producers, and by macrophages, platelets, myoblasts, epithelial-, amniotic- and glial-cells that synthesize FNs at lower levels (Hynes and Yamada, 1982). Overall, FNs can be subdivided in two major forms: the plasma (pFN) and the cellular (cFN) fibronectin. pFN is soluble and secreted by the hepatocytes (Owens and Cimino, 1982; Tamkun and Hynes, 1983a) into the bloodstream at a concentration of 300 μg/ml and 580 μg/ml in human (Yamada, 1983) and mice (George et al., 1993), respectively. On the contrary, cFN is insoluble; it is assumed that it is locally produced by fibroblasts and other cell types, and assembled into the ECM of the tissues (Hayashi and Yamada, 1981; Yamada and Kennedy, 1979) even though hepatocytes are also able to produce and incorporate cFN (lacking both the EDA and EDB domains) into the ECM of liver (Marceau et al., 1980; Voss et al., 1979). Plasma and cellular FNs are structurally and

functionally very similar but they are not identical. Whereas pFN remains as a soluble, compact heterodimer lacking both the EDA and EDB domains, although V0 and V+ splicing variants are present, cFN is deposited as insoluble polymers, forming a three-dimensional fibrillar matrix embedding all the cells forming a tissue. Furthermore, cFN contains EDA and EDB domains at variable proportions depending on the specific tissue (ffrench-Constant, 1995; Hynes, 1990; Kornblihtt et al., 1996). FNs are also characterized by different levels of glycosylation (Tajiri et al., 2005; Zhu and Laine, 1985), phosphorylation (Ali and Hunter, 1981; Teng and Rifkin, 1979) and sulfation (Dunham and Hynes, 1978). The structural differences in the FN polypeptide chains due to alternative splicing and post-translation modifications may explain the diverse biochemical behavior of the two types of FN, such as solubility and electrophoretic mobility (Hayashi and Yamada, 1981; Olden et al., 1979; Tamkun and Hynes, 1983a; Yamada and Kennedy, 1979). The exclusive presence of EDA and/or EDB in cFN may be responsible for its lower solubility and its higher tendency to aggregate and form fibrils.

1.1.4 Interaction of fibronectin with other molecules.

The most important characteristic of fibronectins [*fibre* = fiber + *nectere* = to bind, to connect] is their capablility of interacting specifically with cells and with a wide variety of other macromolecules present in the ECM (Hynes, 1990; Yamada, 1983). Due to the organization of its functional domains in a modular fashion, FN appears to mediate or modify cell adhesion and several other complex biological events by mechanisms that are being intensively investigated. Expression of recombinant FN fragments or limited digestion of FN with a variety of proteases generate a collection of fragments that are sometimes referred to as functional domains due to their ability to interact with other macromolecules. The best-established interactions, for which evidence exists both for their occurrence *in vivo* and for their specificity *in vitro*, are those with collagens and gelatin (denatured collagen), fibrin, fibrinogen, glycosaminoglycans and proteoglycans, integrins

and FN itself (Hynes, 1990; Pankov and Yamada, 2002; Yamada, 1983) (Figure 1). A region of 30-40 kDa in size, including repeats I_{6-9} and $II_{1,2}$, near the amino-terminus of FN is retained to interact with collagens. It has been suggested that the physiological function of the collagen/gelatin-binding domain is related to both the binding and clearance of denatured collagenous materials from blood and tissues, and mediation of cell-attachment to collagen (Leikina et al., 2002; Pankov and Yamada, 2002). Two major heparin-binding domains, located at the C-terminal and N-terminal ends of the protein, interact with widely distributed glycosaminoglycans such as heparin, heparan and chondroitin sulfate, hyaluronic acid, and also bacteria. It seems that interactions between FN and glycosaminoglycans may provide structural organization to the extracellular matrix where FN functions as a cross-linking molecule stabilizing the matrix around cells (Mostafavi-Pour et al., 2001; Pankov and Yamada, 2002).

FN binds to fibrin and fibrinogen through two major fibrin-binding sites localized at the N- and C-terminals. The interaction of FN with fibrin is important for cell adhesion or cell migration into fibrin clots during hemostasis. FN-fibrin interaction is also important during wound healing, providing a substrate for fibroblasts migrating into the wounds to initiate the repair process (Yamada, 1983).

A striking feature of cFN is its ability to arrange into fibrils as a result of FN-FN associations. Although pFN circulating in blood is in a closed, reportedly non-active form, most of the FN activities in the body have been ascribed to the insoluble form of FN that exists as an important part of the tissue ECM. The creation and deposit of insoluble FN fibrils into the ECM is a tightly regulated, cell-mediated process termed FN matrix assembly or fibrillogenesis (Geiger et al., 2001; Pankov and Yamada, 2002). A critical step in this process is the self-association of FN into aggregates and fibrils that is directed by multiple binding sites that have been identified along the molecule. An example is the first Type III domain (III_1, Figure 1). Some of these self-interaction sites are exposed and available for binding, while others are cryptic and become accessible only after

conformational changes, for example, by cell-driven mechanical stretching of the FN molecule. In comparison to cFN, pFN has a minor tendency to undergo self-aggregation (Yamada, 1983).

The binding of FN to the cell surface requires a specific region of the molecule termed cell-binding domain (Figure 1). The cell-binding site lies in the central part of the molecule and binds transmembrane receptors termed integrins (Yamada, 1983). Integrins are structurally and functionally related transmembrane heterodimeric ($\alpha\beta$) receptors that link the ECM with the intracellular cytoskeleton (Pankov and Yamada, 2002; Plow et al., 2000) (Figure 2). In particular, integrins serve as FN receptors at the cell surface, and this interaction is crucial for the ability of FNs to affect cellular activity (Giancotti and Ruoslahti, 1999; Hynes, 1992; Yamada, 2000). The well-known tripeptides Arg-Gly-Asp (RGD), located close to the C-terminus of repeat III_{10} and its synergic site PHSRN in the repeat III_9 are retained to promote specific binding of $\alpha5\beta1$ integrin to FN (Hynes, 1992; Pierschbacher and Ruoslahti, 1984) (Figure 1). The stability of individual modules is often affected by interactions with neighboring modules and such interactions have important implications for the overall shape of the protein. However, binding of $\alpha_5\beta_1$ integrin to FN is not restricted only to repeats III_9 and III_{10}. It can also interact with an N-terminal fragment containing repeats $I_{1\text{-}9}$ and $II_{1\text{-}2}$, which also promotes $\alpha_5\beta_1$ integrin-mediated cell-adhesion (Pankov and Yamada, 2002). It is possible that interaction with this N-terminal region triggers integrin-mediated intracellular signals that are distinct from those generated in response to ligation with the RGD sequence. On the other hand, the tripeptide RGD also interacts with other integrins such as $\alpha_{IIb}\beta_3$ and $\alpha_v\beta_3$, that seem to play a central role in the platelet adhesive reactions (Plow et al., 2000). Recently, binding of $\alpha_4\beta_1$ as well as $\alpha_9\beta_1$ integrins to the EDGIHEL sequence located within the alternatively spliced EDA segment has been reported (Liao et al., 2002), suggesting a possible role of EDA domain in cell-adhesion and gene expression. Two other cell-recognition sequences, LDV and REDV, were also identified in the alternatively spliced segments CS-1 and CS-4 of the IIICS

region. Both of them are recognized by $\alpha_4\beta_1$ as well as $\alpha_4\beta_7$ integrins (Komoriya et al., 1991; Pankov and Yamada, 2002). By means of the cell-binding region, FN can mediate the attachment and spreading of many cell types such as fibroblasts, phagocytes, neurons, glial cells and bacteria and affect their cellular activities. Moreover, the observation that some integrins bind specific sequences within alternatively spliced segments indicates the existence of a novel mechanism by which cell adhesion to fibronectin is regulated by the alternative splicing process.

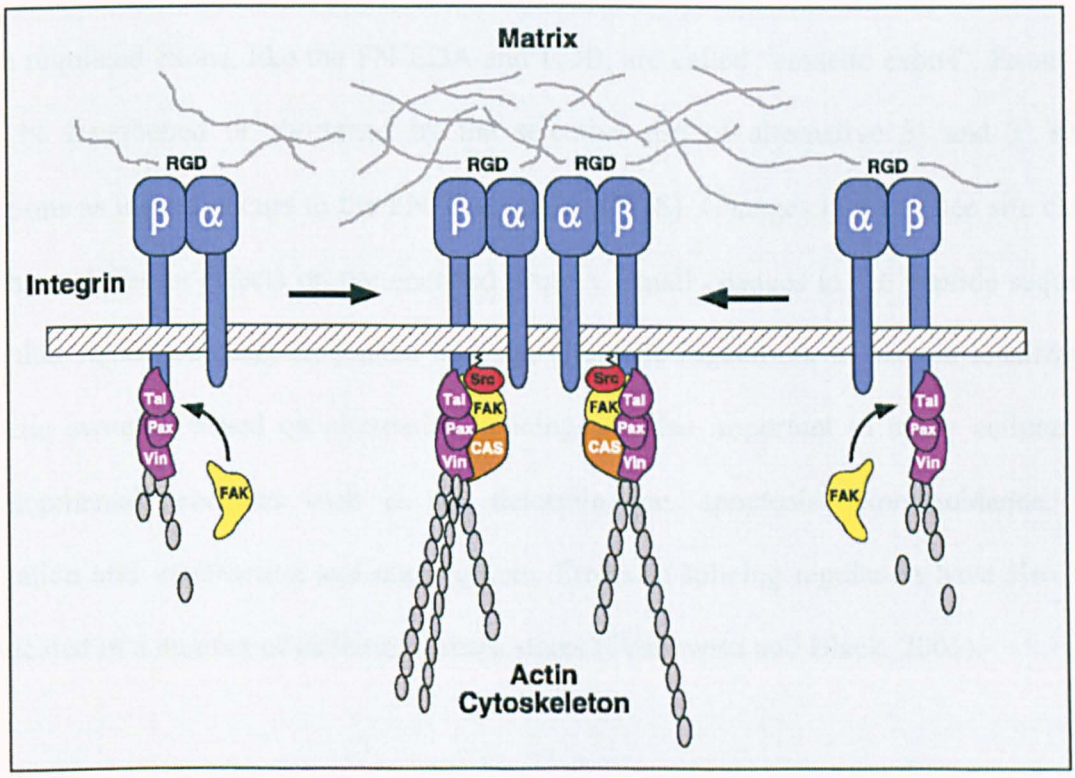

Figure 2. Schematic representation of the extracellular matrix.
Fibronectins along with other extracellular macromolecules form a sort of fibrillar network or matrix surrounding the cell surfaces, involved in the cell and tissue morphology organization and maintenance. Cell-activation, -migration and -adhesion are processes that normally need specific interaction of FN with cell-surface receptors called integrins. Integrins are transmembrane receptors, made of two subunits termed α and β, which integrate the extra-cellular matrix with the intra-cellular cytoskeleton.

1.2 THE ALTERNATIVE SPLICING OF EDA EXON.

The splicing reaction that assembles eukaryotic mRNAs from their much longer precursors provides a uniquely versatile means of genetic regulation. Alterations in the splice site choice can have many different effects on the mRNA and protein products of a gene. Commonly, alternative splicing patterns determine the inclusion or exclusion of an exon in the mRNA eventually giving rise to protein isoforms that differ in their peptide sequence and hence chemical and biological activity (Black, 2003). Alternative splicing is a major contributor to protein diversity in eukaryotic organisms. Most of the gene exons are constitutive, always being included in the final mRNA. Instead, several exons undergo alternative splicing as they are sometimes included and excluded from the final mRNA. Such regulated exons, like the FN EDA and EDB, are called "cassette exons". Exons can also be lengthened or shortened by the selective use of alternative 5' and 3' splice junctions as indeed occurs to the FN V segment (IIICS). Changes in the splice site choice can have different effects on the encoded protein. Small changes in the peptide sequence can alter ligand binding, enzymatic activity, allosteric regulation, or protein localization. Genetic switches based on alternative splicing are also important in many cellular and developmental processes such as sex determination, apoptosis, axon guidance, cell-excitation and -contraction and many others. Errors in splicing regulation have also been implicated in a number of different disease states (Grabowski and Black, 2001).

1.2.1 The splicing reaction.

The splicing reaction consists of excision of the introns from a pre-mRNA and joining of the exons. It is directed by special sequences at the intron/exon boundaries called "splice sites" (Gesteland, 1999) (Figure 3). The 5' splice site marks the exon/intron junction at the 5'-end of the intron. This includes a GU dinucleotide at the intron end encompassed within a larger, less conserved consensus sequence. At the other end of the intron, the 3' splice site region has three conserved sequence elements: the branch point,

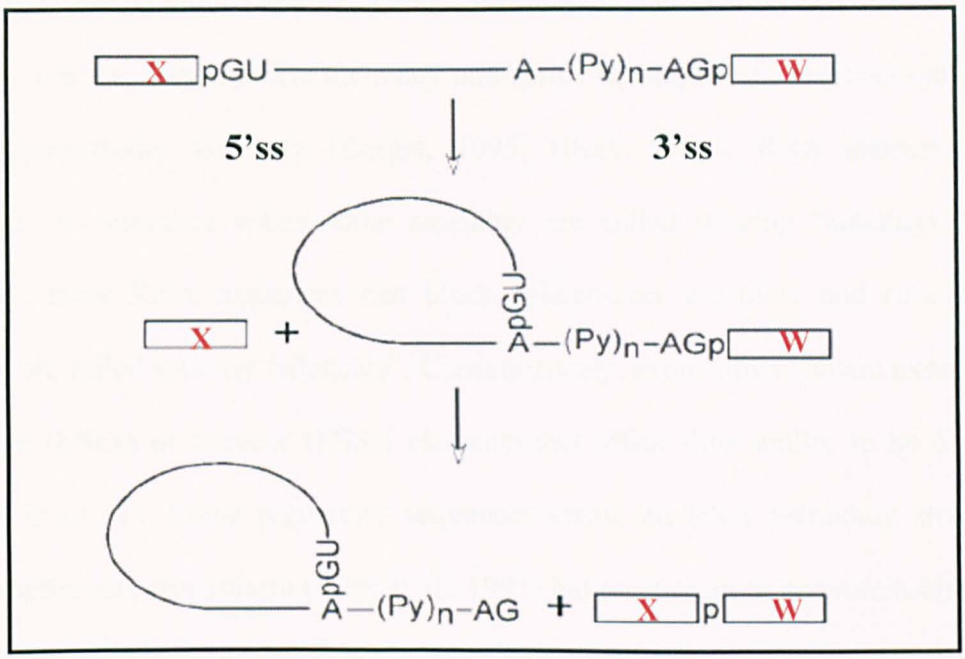

Figure 3. Schematic representation of the splicing reaction.
Splicing takes place in two transesterification steps. The first step results in two reaction intermediates: the detached 5'-exon and an intron/3'-exon fragment in a lariat structure. The second step ligates the two exons and releases the intron lariat. See text for details. X and W are joined exons; 5'ss, 5'splice site; 3'ss, 3'splice site; A, branch point; (Py)n, poly-pyrimidine tract (Black, 2003).

followed by a polypyrimidine tract, and subsequently a terminal AG at the extreme 3'-end of the intron. In the first step of the splicing reaction, the 2-hydroxyl group of a specific A residue at the branch point attacks the phosphate at the 5' splice site. This step produces two reaction intermediates: a detached 5' exon and, an intron/3'-exon fragment in a lariat configuration containing a branched A nucleotide at the branch point. In the second step, the phosphate at the 3'-end of the intron is attacked by the 3-hydroxyl of the detached 5' exon. This reaction ligates the two exons and releases the intron, that is still in the form of a lariat (Black, 2003). A large macromolecular complex called "spliceosome", made-up of a set of five small nuclear ribonucleoproteins (snRNPs) and numerous accessory proteins (splicing factors), is assembled on each intron/exon boundary and catalyzes the two steps of the splicing reaction (Brow, 2002; Gesteland, 1999). The information contained in the

splice site sequences is generally not sufficient to determine whether a site will assemble a functional spliceosome complex. Other information and interactions are necessary to activate their use. Indeed, there are many non-splice site regulatory sequences that strongly affect spliceosome assembly (Berget, 1995; Black, 2003). RNA elements that act positively to stimulate spliceosome assembly are called splicing "enhancers". On the contrary, those RNA sequences that block spliceosome assembly and certain splicing choices are called splicing "silencers". Consequencely, exons often contain exonic splicing enhancer (ESEs) or silencer (ESSs) elements that affect their ability to be defined and spliced in or out. Some regulatory sequences create an RNA secondary structure that affects splice site recognition (Libri et al., 1991) but most seem to be protein-binding sites. The ESE elements are normally recognized by specific splicing regulatory proteins called Serine/Arginine proteins (SR proteins) facilitating the binding of snRNPs and other splicing factors at the 3' and 5' splice sites of a regulated exon (Graveley, 2000). The ESS elements are instead retained to interact with the heterogeneous nuclear ribonucleoproteins (hnRNPs), a large group of molecules identified in splicing as factors that counteract SR protein activity (Krecic and Swanson, 1999).

1.2.2 Regulation of EDA exon alternative splicing.

Interesting studies of the regulatory sequences involved in the recognition of the EDA exon by the splicing machinery have been performed during the last two decades. It is now clear that an 81-nucleotide regulatory-region, bearing two brief sequences with the function of splicing enhancer (ESE) and silencer (ESS) and located in the centre of EDA exon (Figure 4A), is involved in the regulation of EDA exon alternative splicing (Caputi et al., 1994; Mardon et al., 1987). Indeed, it seems that the ESE and ESS sequences regulate the inclusion/exclusion process of the EDA exon from the FN mRNA, determining the relative proportion of the EDA^+ and EDA^- mRNAs that are present in the diverse cell types or tissues. The accurate exon definition in the pre-mRNA by the splicing machinery

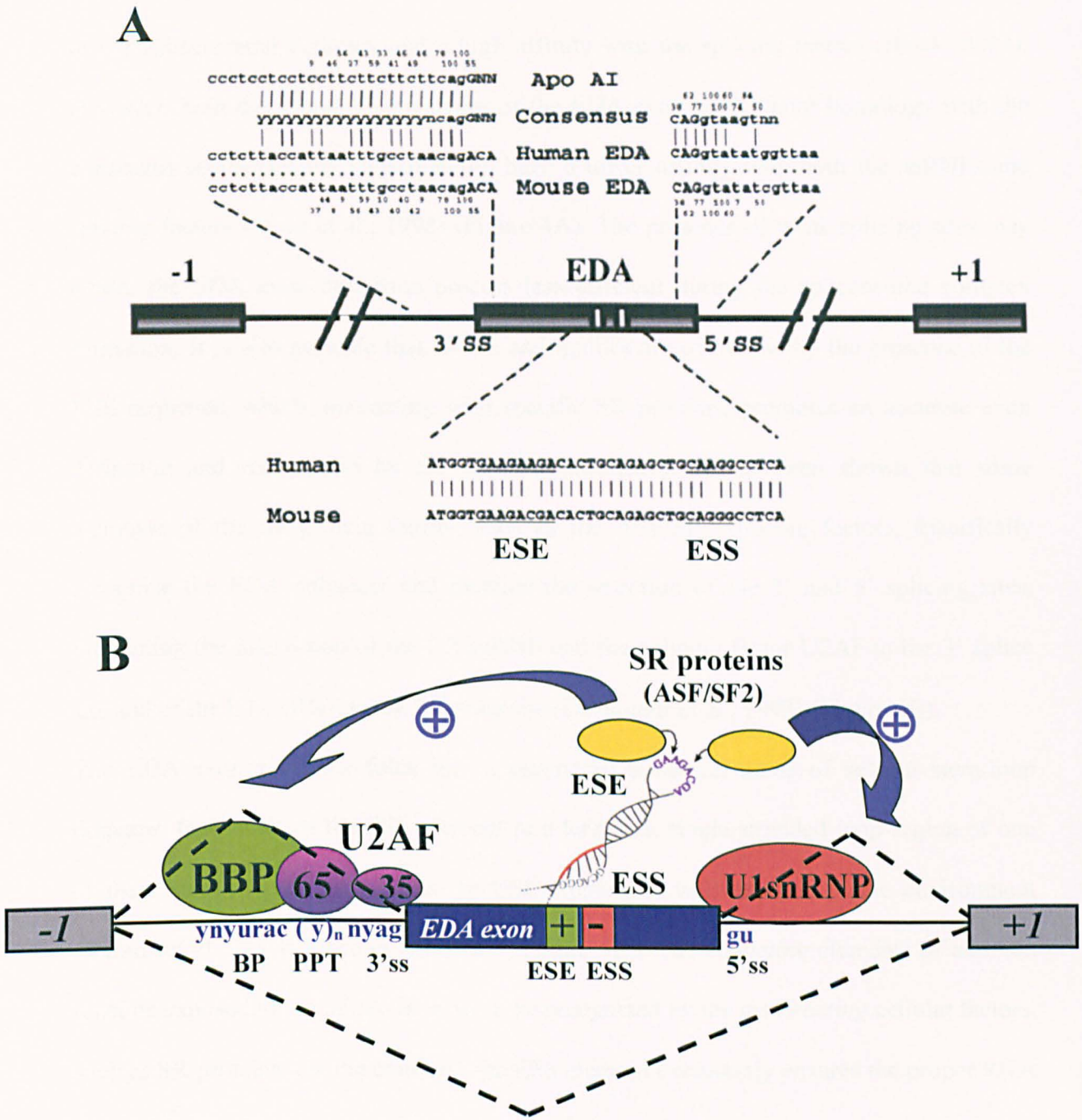

Figure 4. Mouse splicing *cis-acting* elements (Panel A) and *trans-acting* factors (Panel B) that controls alternative splicing of the EDA exon.

A. A schematic representation of the EDA region of FN gene and its regulatory cassette. The sequences of the mouse and human 3' and 5' splicing sites (ss) are compared with the consensus sequence, and the exonic region sequences involved in EDA splicing regulation are indicated. Enhancer (ESE) and silencer (ESS) sequences are underlined. Individual base frequencies are also indicated (Muro et al., 1998). **B.** Interaction of the ESE element with SR proteins facilitates the binding of snRNP and other splicing factors (BBP, U2AF) on the 5' and 3' splicing sites, respectively, enhancing the EDA exon inclusion in the FN mRNA. Exons and introns are shown as boxes and lines, respectively; Y, pyrimidine; n, generic base; BP, branch point; PPT, poly-pyrimidine tract.

requires a good base-pairing interaction between the 3' and 5' splice sites and the snRNPs of the spliceosomal complex and a high affinity with the splicing factors (Black, 2003). However, both the 5' and 3' splice sites of the EDA exon have a poor homology with the consensus sequences and consequently, have a lower affinity with both the snRNPs and splicing factors (Muro et al., 1998) (Figure 4A). The presence of weak splicing sites may render the EDA exon definition process less efficient during the spliceosome complex formation. It is also possible that all the ambiguities are overcome by the presence of the ESE sequence, which, interacting with specific SR proteins, promotes an accurate exon definition and recognition by the splicing machinery. It has been shown that some members of the SR-protein family, such as the ASF/SF2 splicing factors, specifically recognize the EDA enhancer and mediate the selection of the 3' and 5' splicing sites, facilitating the interaction of the U2-snRNP and the splicing factor U2AF to the 3' splice site and of the U1-snRNP to the 5' splice site (Lavigueur et al., 1993) (Figure 4B).

The EDA exon sequence folds into a secondary structure, made of several stem-loop domains, that localizes the ESE element in a terminal, single-stranded loop-region of one of these stem-loop domains, thus the ESE element is well exposed to the environment (Buratti et al., 2004; Muro et al., 1999) (Figure 4B). The *cis-acting* elements of an exon must be exposed to the milieu in order to be recognized by the *trans-acting* cellular factors, such as SR proteins. On the contrary, the ESS element exclusively ensures the proper RNA conformation, since it lies in a double-stranded stem-region of the same stem-loop domain (Muro et al., 1999). Although it has been demonstrated that the ESE within the EDA exon specifically interacts with the ASF/SF2 splicing factor (Buratti et al., 2004), it is not yet known if any of the *trans-acting* factors interacts with the ESS. However, we can hypothesize that a possible competition between the EDA-ESE linking SR proteins and antagonistic splicing factors such as the hnRNPs, can positively or negatively affect the formation of the RNA secondary structure and determine the EDA^+/EDA^- mRNA ratio. The EDA exon inclusion/exclusion ratio is strictly regulated in a developmentally-, age-

and tissue-specific manner (Caputi et al., 1995a; Chauhan et al., 2004; Magnuson et al., 1991; Pagani et al., 1991) (Figure 5). RT-PCR analysis of total RNA, prepared from various embryo organs, showed a high inclusion percentage of the EDA exon in the FN mRNA. The EDA exon is completely excluded from the FN mRNA in adult liver and skin, but in other tissues its inclusion gradually decreases with the age (Chauhan et al., 2004) (Figure 5). We can envision several, parallel splicing regulatory circuits interacting with various regulatory *trans-acting* factors, to explain the peculiar spectrum of EDA exon inclusion observed in different tissues, at different developmental stages and under different experimental conditions.

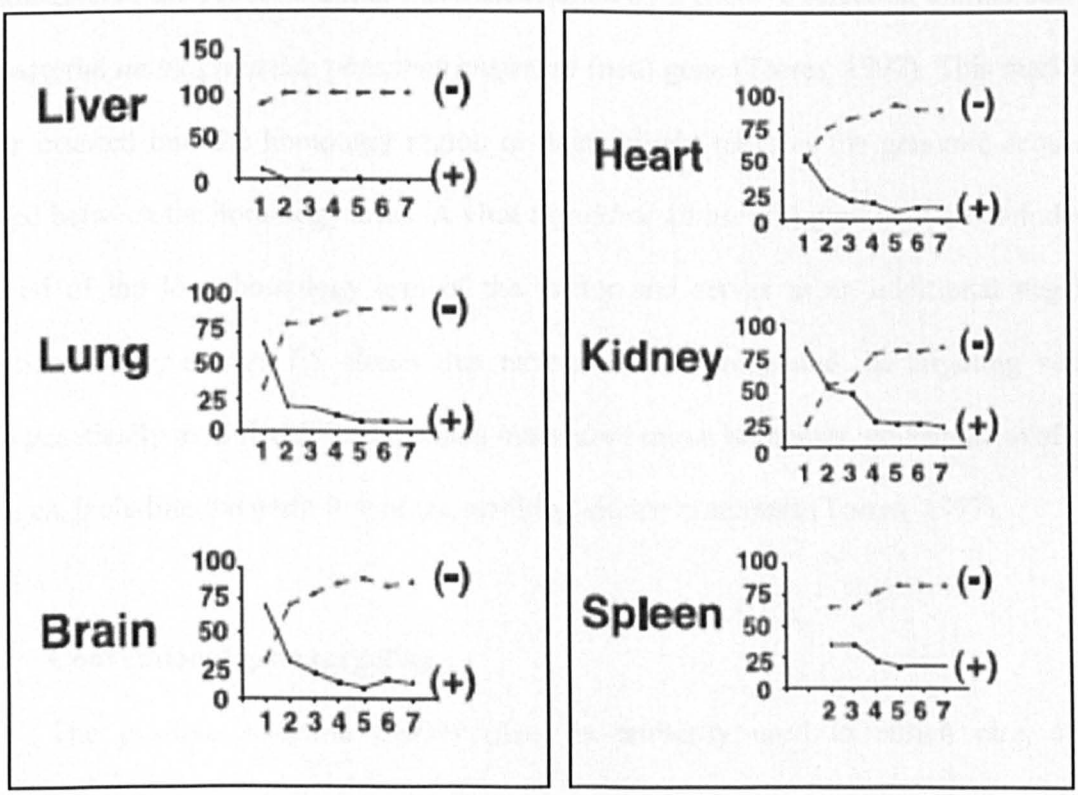

Figure 5. Splicing pattern variation of the EDA exon in the FN pre-mRNA at different ages and at the various tissues.
The graphs shows the percentage of each alternatively spliced form as a function of the age. The different ages are indicated as numbers from 1 to 7 (E13.5, 1-day-old, 14-day-old, 2-month-old, 6-month-old, 15-month-old and 24-month-old, respectively). Spleen analysis in the E13.5 stage was not performed due to low amount of material recovered from the embryo. (+), EDA^+ isoform; (–), EDA^- isoform (Chauhan et al. 2004).

1.3 GENE TARGETING STRATEGY.

Gene targeting, defined as the introduction of site-specific modifications into the mouse genome by homologous recombination, is generally used for the production of mutant animals to study gene function *in vivo* (Torres, 1997). The only efficient gene targeting method presently established utilizes pluripotent murine embryonic stem (ES) cell lines. Using these cells, the identification of the rare, homologous recombinant ES cell clones can be easily accomplished *in vitro* by both the positive and negative selection. As a substrate for homologous recombination, vectors of the replacement type are most frequently used for gene targeting in ES cells and usually to simply inactivate gene function (Figure 6A and B). A typical replacement vector consists of two regions of DNA homologous to the genomic target locus interrupted by a positive selection marker such as the bacterial *aminoglycoside phosphotransferase* (neo) gene (Torres, 1997). This marker is either inserted into the homology region or alternatively replaces the genomic sequence located between the homology arms. A viral *thymidine kinase* (tk) gene is often included at the end of the long homology arm of the vector and serves as an additional negative selection marker against ES clones that have randomly integrated the targeting vector. Such genetically modified ES cells, when introduced into a blastocyst, contribute to all cell lineages, including the germ line of the resulting chimeric animals (Torres, 1997).

1.3.1 Conventional gene targeting.

The positive selection marker (neo) is primarily used to enrich rare, stably transfected ES cell clones. It frequently serves in the generation of site-specific mutagenesis by insertion of the marker gene into a coding exon or the replacement of coding exons of the target gene by the marker (Figure 6A). In any case, the end product of a targeting experiment using a replacement type vector, that includes a positive selection marker, is the presence of the selection marker gene in the targeted locus which cannot be further modified.

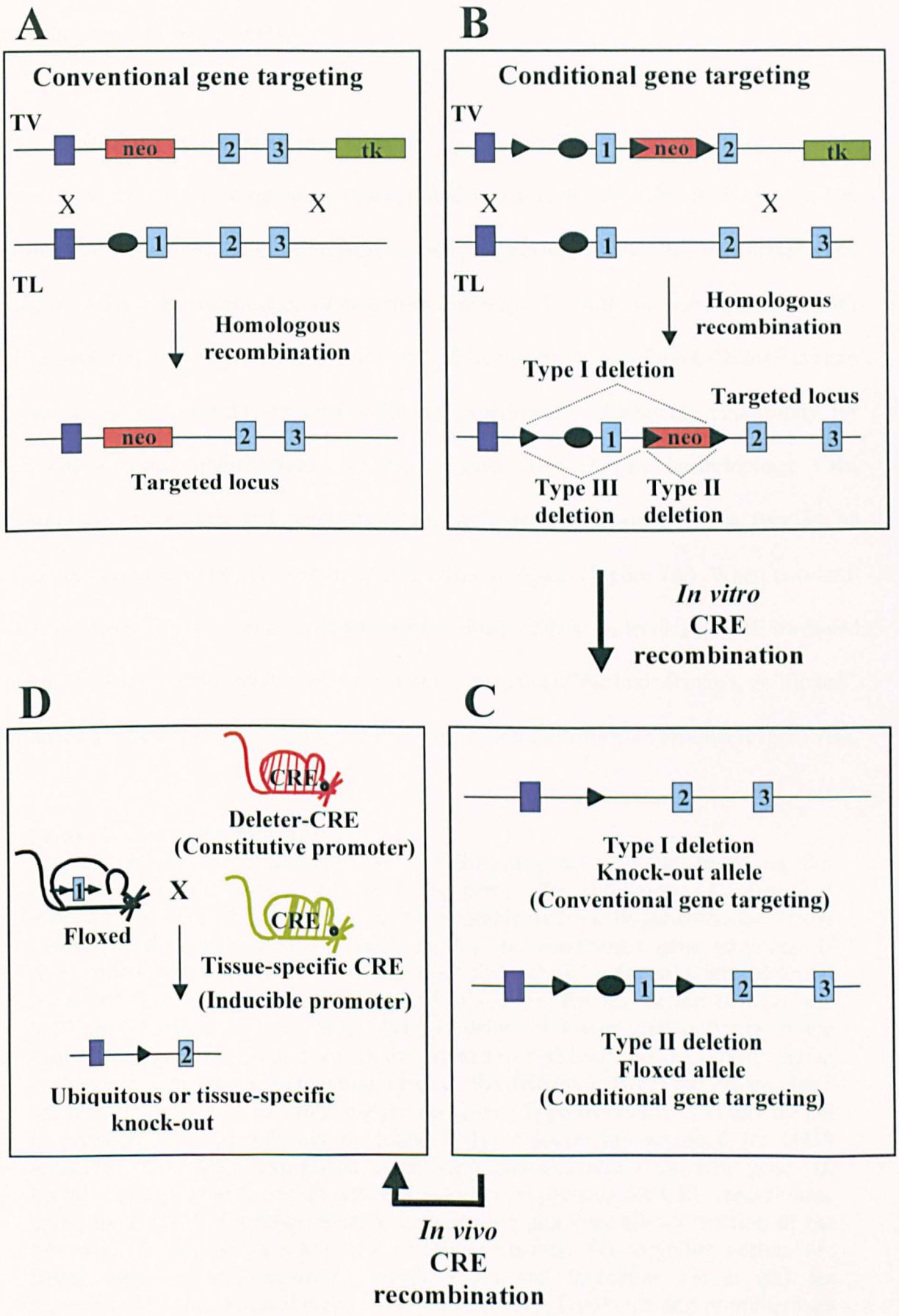
A
Conventional gene targeting
TV
neo
2
3
tk
X
X
1
2
3
TL
Homologous recombination
neo
2
3
Targeted locus
B
Conditional gene targeting
TV
1
neo
2
tk
X
X
1
2
3
TL
Homologous recombination
Type I deletion
Targeted locus
1
neo
2
3
Type III deletion
Type II deletion
In vitro CRE recombination
D
CRE
Deleter-CRE
(Constitutive promoter)
1
Floxed
X
CRE
Tissue-specific CRE
(Inducible promoter)
2
Ubiquitous or tissue-specific knock-out
C
2
3
Type I deletion
Knock-out allele
(Conventional gene targeting)
1
2
3
Type II deletion
Floxed allele
(Conditional gene targeting)
In vivo CRE recombination

Thus, this gene targeting strategy is only suitable for the generation of a nonfunctional (knock-out) allele of a target gene. This type of gene inactivation is called "conventional gene targeting" (Torres, 1997).

1.3.2 CRE/loxP recombination system.

The use of a recombination system, and in particular the CRE/loxP system, has considerably improved the gene targeting technique (Torres, 1997). CRE/loxP-based gene targeting allows the introduction of mutations into target loci with the subsequent removal of the selection marker gene (Figure 6B and C). Moreover, the use of the CRE/loxP system allows a greater versatility in gene targeting experiments offering the opportunity for "conditional gene modifications" *in vivo* (Figure 6D). The P1 bacteriophage CRE recombinase recognizes and mediates site-specific recombination between two 34 bp sequences referred to as loxP (Sauer and Henderson, 1988) (Figure 7A). When two loxP sites are placed in the same orientation on a linear DNA molecule, a CRE-mediated intramolecular recombination event results in the excision of the loxP-flanked, or "floxed", sequence as circular molecule with one loxP site left on each reaction product (Figure 7B).

Figure 6. Gene targeting strategy.
A. Conventional gene targeting. **B.** Conditional gene targeting based on the introduction of three loxP sites in the genome (flox-and-delete). **C.** Transient expression of the CRE recombinase in the recombinant ES cells generates the floxed version of the targeted allele, necessary for the conditional gene targeting. If recombination occurs between the outer loxP sites (Type I deletion) a large deletion is created that should inactivate or modify the gene. Recombination between the loxP sites flanking the neo gene (Type II deletion) leaves one loxP site in the genome that generates, together with the isolated (outer) loxP site, the floxed version of the gene. The third recombination product, the deletion between the isolated loxP site and the inner loxP site flanking the neo gene (Type III deletion), is usually not of practical use and will not be found if ES colonies are screened for G418 sensitivity after CRE expression since such colonies retain the neo gene. **D.** Crossbreeding of the floxed mouse with a mouse expressing the CRE recombinase under the control of a tissue-specific or inducible promoter allows deletion of the floxed DNA segment in a temporal or spatial manner. TG, targeting vector; TL, target locus; exons, neomycin cassette (neo) and thymidine kinase (tk) are represented as blue, red and green boxes, respectively. LoxP sites and promoters are represented as black triangle and dots, respectively.

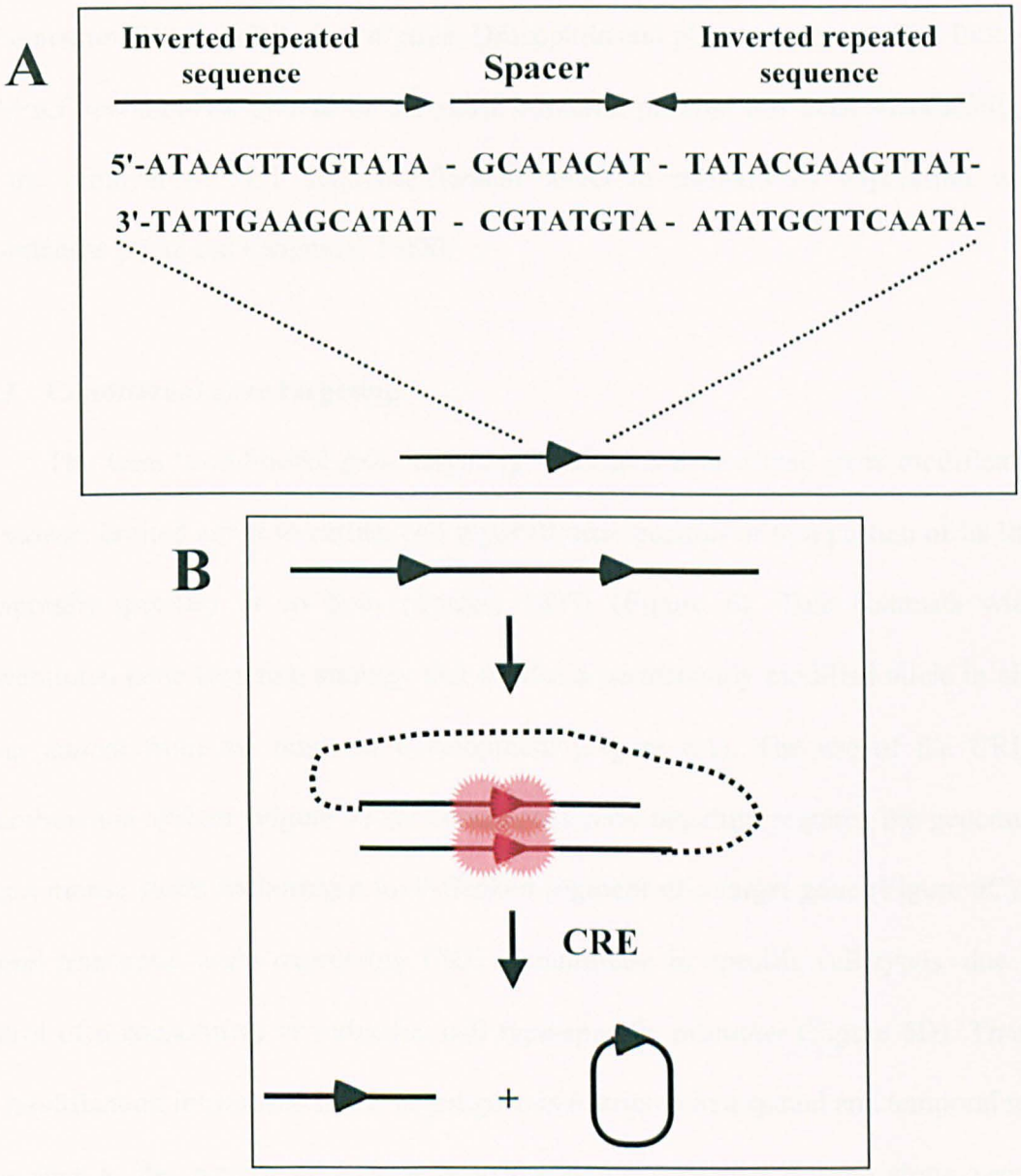

Figure 7. CRE/loxP site-specific recombination system.
A. LoxP sites (locus of crossover (x) in P1; black triangles) are composed of two 13-bp inverted repeated sequences separated by an 8-bp non-palindromic sequence which dictates the orientation of the overall sequence (spacer). **B.** By inserting two directed loxP sites it is possible to delete the floxed DNA stretch following transient *in vitro* or *in vivo* expression of the CRE recombinase. CRE recombinase (causes recombination; red stars) specifically recognizes and recombines two consecutive loxP sequences, generating both a linear and a circle subproduct, each with a single loxP site (flox-and-delete-strategy). Each of the two repeats within a loxP site is bound by one molecule of CRE and a staggered 6-bp cut is generated. In the life-cycle of the P1 phage, CRE recombinase serves to ensure the segregation of the cyclic unit-copy P1 plasmid prophage and the cyclization of the linear viral genome after infection of bacteria.

If the two loxP sites are placed in opposing orientations the floxed sequence will be inverted. An alternative recombination system can be used for gene manipulation not only of the mammalian cells but also of yeast, Drosophila and plants (Torres, 1997). Indeed, the FLP/FRT recombinase system of the yeast 2-micron plasmid has been successfully used for the removal of FRT sequence-flanked selection markers by expression of FLP recombinase (Veit and Fangman, 1988).

1.3.3 Conditional gene targeting.

The term "conditional gene targeting" indicates a restricted gene modification in the mouse, limited either to certain cell types (tissue-specific) or to a portion of its lifetime (temporally-specific) or to both (Torres, 1997) (Figure 6). This contrasts with the conventional gene targeting strategy that creates a permanently modified allele in all cells of an animal from the onset of development (Figure 6A). The use of the CRE/loxP recombination system (Figure 7) for conditional gene targeting requires the generation of both a mouse strain harboring a loxP-flanked segment of a target gene (Figure 6C) and a second transgene strain expressing CRE recombinase in specific cell types, due to the control of a constitutive or inducible cell type-specific promoter (Figure 6D). Therefore, the modification introduced in the target gene is restricted in a spatial and temporal manner according to the pattern of CRE expression in the particular murine strain used. The regional specificity of conditional gene targeting allows both to test the function of widely expressed molecules in a particular cell lineage and to investigate gene function post-natally. The latter point is particularly usefull in the case the conventional (complete) gene inactivation leads to a severe or lethal phenotype during embryonic development, preventing a more detailed *in vivo* analysis (Torres, 1997). The use of an inducible or tissue-specific promoter for CRE expression has the important additional advantage that the wild-type gene product is present throughout ontogeny until the time of induction.

1.3.4 Flox-and-delete strategy.

The "flox-and-delete" strategy can be used for conditional gene inactivation and is especially useful if lethality is anticipated in conventional mutants (Torres, 1997). A minimal flox-and-delete gene-targeting vector contains three loxP sites in the same orientation, two sites flanking a selection marker gene and an isolated site within one arm of homology (Figure 6B). After identification of homologous recombinant ES clones, that have cointegrated the isolated loxP site, transient *in vitro* CRE expression leads to three different recombination products (Figure 6C). The ES cell clones with deletion of the marker gene are used to produce a strain with the floxed allele for conditional gene inactivation, while clones with deletion of the fragment flanked by the external loxP sites can be used to generate mice harboring the inactivated version (knock-out) of the gene of interest (Figure 6D).

1.3.5 Site-specific recombination in hepatocytes.

In order to obtain an hepatocyte-specific recombination of a DNA segment flanked by loxP sites, a transgenic mouse has been generated that expresses the CRE recombinase open reading frame under the control of both the mouse albumin regulatory elements and the α-fetoprotein enhancer (Alf-p-CRE Trangene, Figure 8) (Kellendonk et al., 2000). This configuration has been chosen to mimic the genomic organization of the mouse albumin gene, which is specifically activated in hepatocytes. In mammals, the albumin gene is located upstream of the α-fetoprotein (AFP) gene and its expression is thought to be influenced by the AFP enhancers located between both genes. In mice, the albumin gene starts its expression during embryogenesis shortly after the appearance of the liver bud (day 9.5 pc) and mRNA levels increase following liver development. CRE is active before day 10.5 pc but not before day 9.5 pc. Thus, the Alf-p-CRE expression vector seems to allow the expression of CRE recombinase in mice at the time, during embryogenesis, coincident with activation of the endogenous albumin gene.

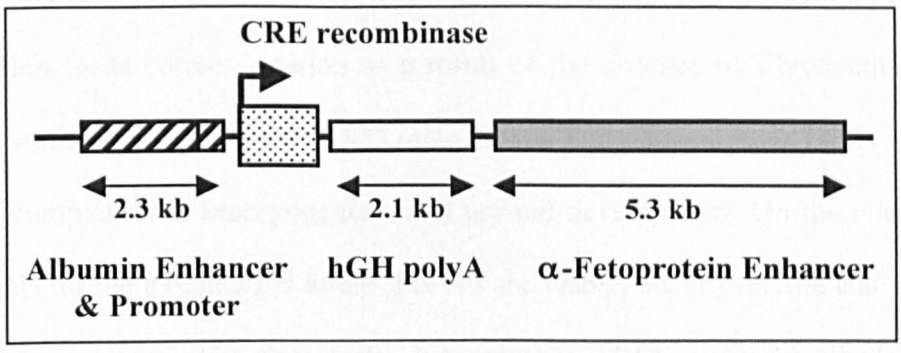

Figure 8. Schematic representation of CRE recombinase transgene (TG Alf-p-CRE).
When the CRE recombinase gene is expressed under the control of specific promoter/enhancer sequences is possible to condition the removal of a floxed DNA stretch from the genome either temporally or spatially. A CRE recombinase transgene, that under the control of the mouse albumin enhancer and promoter and alpha-fetoprotein enhancer is specifically expressed in the hepatocytes, is represented. hGH polyA is a human polyadenylation site (Kellendonk et al., 2000).

1.4 GENETICALLY MODIFIED-FN GENE-MURINE MODELS.

In order to study *in vivo* the biological role of FN and its alternative spliced segments, different genetic manipulations have been introduced in the gene. Conventional and conditional knock-out mice, and specific alternative splicing modifications of the FN gene have been generated and are briefly described below:

1.4.1 Conventional fibronectin knock-out mouse.

The importance of FN in embryonic development was shown for the first time by George *et al.* (George et al., 1993) through the generation of a conventional FN knock-out (KO) mouse strain, constitutively devoid of the protein. The promoter region and the first exon of the mouse FN gene were replaced with a selection marker (neo), thus preventing FN gene transcription. Mice homozygous for the targeted FN allele ($FN^{-/-}$) die during early gastrulation (E8.0) due to severe defects in mesodermally-derived tissues such as notochord and somites that are absent. Mutant embryos also display a shortened anterior-posterior axis, deformed neural tube, heart and embryonic vasculature, and defective yolk sac, extra-embryonic vasculature and amnion. All of these abnormalities can be interpreted

as a consequence of severe deficits in mesodermal adhesion, differentiation, proliferation, and migration to its correct location as a result of the absence of fibronectin. Thus, the early embryonic lethality of the FN KO mice proves that deposition of FN is required for successful completion of embryogenesis and normal development. On the contrary, mice heterozygous for the targeted FN allele ($FN^{wt/-}$) are viable, healthy, fertile and of the same size of wild-type mice, even though the concentration of FN in the blood plasma is one half (~ 233 μg/ml) of that found in wild-type mice (~ 580 μg/ml). This finding indicates that the wild-type allele does not up-regulate to compensate for the null-allele.

1.4.2 Conditional pFN-null mouse.

Due to the early embryonic lethality, the conventional KO mouse of the FN gene could not be used to address the role of FNs in adult physiology and pathology. To examine the functions of FN in adult tissues, and in particular the role of pFN in hemostasis and tissue repair, Sakai *et al.* (Sakai et al., 2001) generated a conditional liver-specific FN-null mouse using the CRE/loxP system. CRE-mediated recombination at the two inserted loxP sites removed the start codon (ATG), the signal sequence and the exon/intron border of exon 1, thus generating the null allele. To induce the conditional deletion of the floxed DNA segment in the adult liver, mice bearing the floxed FN alleles were crossed with two transgenic strains expressing CRE recombinase under the control of the interferon-/polyinosinic-polycytidic acid (pI-pC)-inducible Mx promoter and the tissue-specific albumin promoter, respectively. An important role of pFN in hemostasis is demonstrated by several evidences such as i) the high concentration of pFN in blood, ii) the abundant amount of platelet-derived FN that becomes secreted upon platelet activation, iii) the ability of pFN to crosslink with fibrin or fibrinogen and to bind to the FN receptors (integrins) on the platelet surface during the formation of the blood clots. However, the initial data obtained performing experiments using pFN-deficient mice (both in plasma and in platelets) did not confirm this hypothesis. Indeed, *in vitro* and *in vivo* measurements of

the clotting and bleeding time, respectively, or *in vitro* platelet-aggregation tests carried on the Sakai's conditional pFN-null mice (Sakai et al., 2001), on the George's FN heterozygous ($FN^{wt/-}$) mice (Matuskova et al., 2006) and on the Muro's $EDA^{+/+}$ mice (unpublished data, see next paragraph) showed that the differences with the respective control mice were not significant. An explanation for this unexpected finding could be the presence of cFN in platelets derived from pFN-deficient mice or, alternatively, several other blood coagulation factors compensating for the absence of pFN. Conditional pFN-null mice were also used to study tissue-repair processes such as skin wound healing and brain injury after focal cerebral ischemia. No differences in skin reepithelization process were observed in pFN-null mice in comparison with control mice. The abundant deposition of cFn on the surface of the wounds made by platelets, keratinocytes, macrophages and fibroblasts, that transmigrate to close the wound (Clark, 1990; Ffrench-Constant et al., 1989) is a likely explanation for the normal cutaneous wound healing in pFN-null mice (Sakai et al., 2001). Thus, this model initially did not show a direct involvement of pFN either in blood clotting or in skin wound healing. However pFN was found to fulfill an important role in the brain wound healing after induction of an injury by focal ischemia. Ischemia leads to a blood-brain barrier damage resulting in the extravasation of plasma but not of blood cells in brain (Garcia et al., 1994). As expected, pFn was found throughout the infarcts in normal mice but no pFN was found in the infarcts of pFn-null mice that were also larger than those of the control animals. Several factors could contribute to the increase in infarct size of pFn-null mice. pFn could provide a matrix for adherence, migration and proliferation of those blood cells necessary to repair the tissue damage. This is not possible in the pFn-null mice.

1.4.3 EDA exon knock-in and knock-out mice.

The study of the function of the different FN protein isoforms is difficult *in vivo* due to the simultaneous presence of more than one variant at a given specific

developmental time and tissue. To address this issue a novel genetic approach was previously designed in our lab (Muro et al., 2003) without modifying the coding sequence of the FN gene. Taking advantage of the detailed knowledge of the elements involved in EDA splicing regulation (Caputi et al., 1994; Mardon et al., 1987; Muro et al., 1999; Muro et al., 1998) (Figure 4) and the gene targeting technique (Figure 6 and 7), knock-in ($EDA^{+/+}$) and knock-out ($EDA^{-/-}$) murine strains for the FN EDA exon (Figure 9) were generated. In brief, the 5' splice site was mutated to that of the consensus sequences and the 3' splice site was replaced by that of the constitutively spliced-in second exon of the apolipoprotein AI gene that exactly matches the 3' splice site consensus (Figure 4A). The targeting construct consisted of 11.5 kb of mouse genomic DNA (Figure 9A and B). Three loxP sites were included in the targeting vector flanking the neo-tk marker cassette and the EDA exon, and an additional marker gene, the *diphtheria toxin* (DTA) gene, was linked at the end of the long arm of homology. The homologous recombinant clones obtained underwent a second step of recombination by transient expression of the CRE recombinase *in vitro* (Figure 9C and D). The recombinant clones, containing the deleted neo-tk cassette and the loxP flanked EDA in one of the FN alleles, were used to obtain chimeras. Heterozygous offsprings ($EDA^{wt/+}$) were then mated to each other to produce the $EDA^{+/+}$ mice that include the modified EDA exon in both the FN alleles. $EDA^{wt/+}$ mice were also mated with CRE-recombinase transgenic mice (Deleter-CRE, Figure 6D) to obtain $EDA^{wt/-}$ progeny that were subsequently mated to each other to obtain $EDA^{-/-}$ animals (Figure 9E). The EDA exon, that is normally spatially and temporally regulated during development and ageing (Figure 5), is now constitutively either present or absent from the FN mRNA of the $EDA^{+/+}$ and $EDA^{-/-}$ strains, respectively (Figure 10). Radioactive RT-PCR analysis of total RNA extracts of various organs from $EDA^{wt/wt}$, $EDA^{+/+}$ and $EDA^{-/-}$ adult mice

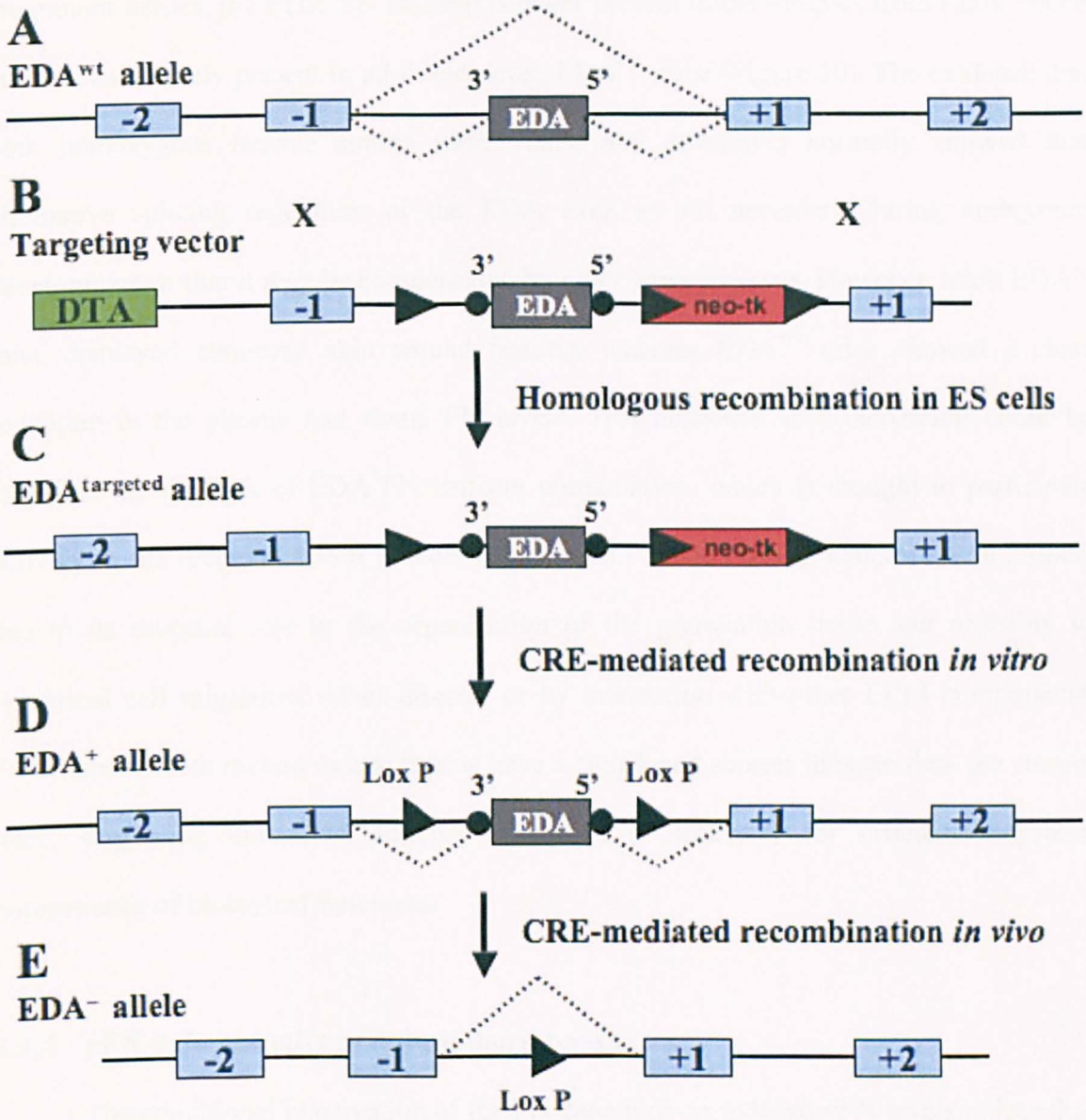

Figure 9. Strategy for the generation of mouse strains lacking regulated splicing at the EDA exon of the FN gene.

A. Partial map of the wild-type FN allele. **B.** The targeting vector. **C.** The targeted allele. **D.** The EDA-floxed allele. **E.** The EDA-null alleles. Exons, neo-tk, and diphtheria toxin (DTA) are shown as light-blue, red and green boxes, respectively. The EDA exon and its internal splicing regulatory elements, ESE and ESS, are indicated as grey, blue and red boxes, respectively. Lox P sites and optimized 3' and 5' splice sites are indicated as black triangles and dots, respectively. The recombinant ES cells were transiently transfected with a CRE-recombinase expressing plasmid, to remove the neo-tk cassette (Panel C and D). $EDA^{+/wt}$ heterozygote cells were used for blastocyst microinjection. $EDA^{+/wt}$ mice were mated with a CRE-expressing transgenic mouse strain to obtain the $EDA^{-/wt}$ mice.

confirmed the lack of regulated splicing of the EDA exon in both mutant mouse strains. In the mutant tissues, the $EDA^{+}FN$ isoform is never present in the samples from $EDA^{-/-}$ mice but is constitutively present in all tissues from $EDA^{+/+}$ mice (Figure 10). The evidence that both homozygous murine strains were viable and developed normally showed that alternative splicing regulation of the EDA exon is not necessary during embryonic development or that it may be compensated by other gene products. However, adult $EDA^{-/-}$ mice displayed abnormal skin wound healing, whereas $EDA^{+/+}$ mice showed a clear reduction in the plasma and tissue FN levels. This abnormal reepithelization could be explained by the lack of $EDA^{+}FN$ isoform upregulation, which is thought to participate actively in the reepithelization process (Clark et al., 1983; Ffrench-Constant et al., 1989) due to its essential role in the organization of the granulation tissue and probably in epidermal cell migration, either directly or by interaction with other ECM components. Furthermore, both mutant mouse strains have a significant shorter lifespan than the control mice, suggesting that EDA splicing regulation is necessary for efficient long-term maintenance of biological functions.

1.4.4 pFN-deficient mice and thromboembolism.

The conditional inactivation of the FN gene in liver reduced pFN levels to less than 2% and the platelet FN levels to about 20% of the levels of the control mice (Ni et al., 2003; Sakai et al., 2001). Heterozygous mice for FN ($FN^{wt/-}$) were found to have 55% of reduction in pFN levels and 21% of reduction in platelet FN content, when compared to the levels of control animals (George et al., 1993; Matuskova et al., 2006). $EDA^{+/+}$ are instead characterized by a reduction of about 70-80% in the pFN content (Muro et al., 2003) and a reduction of about 50-60% in the platelet FN content (unpublished data). All these pFN-deficient mice were tested in a model of thromboembolism to evaluate their capacity to form thrombi, following induction of arterial injuries by topical application of ferric chloride. Interestingly, both the partial and the total pFN deficiency of the $FN^{wt/-}$

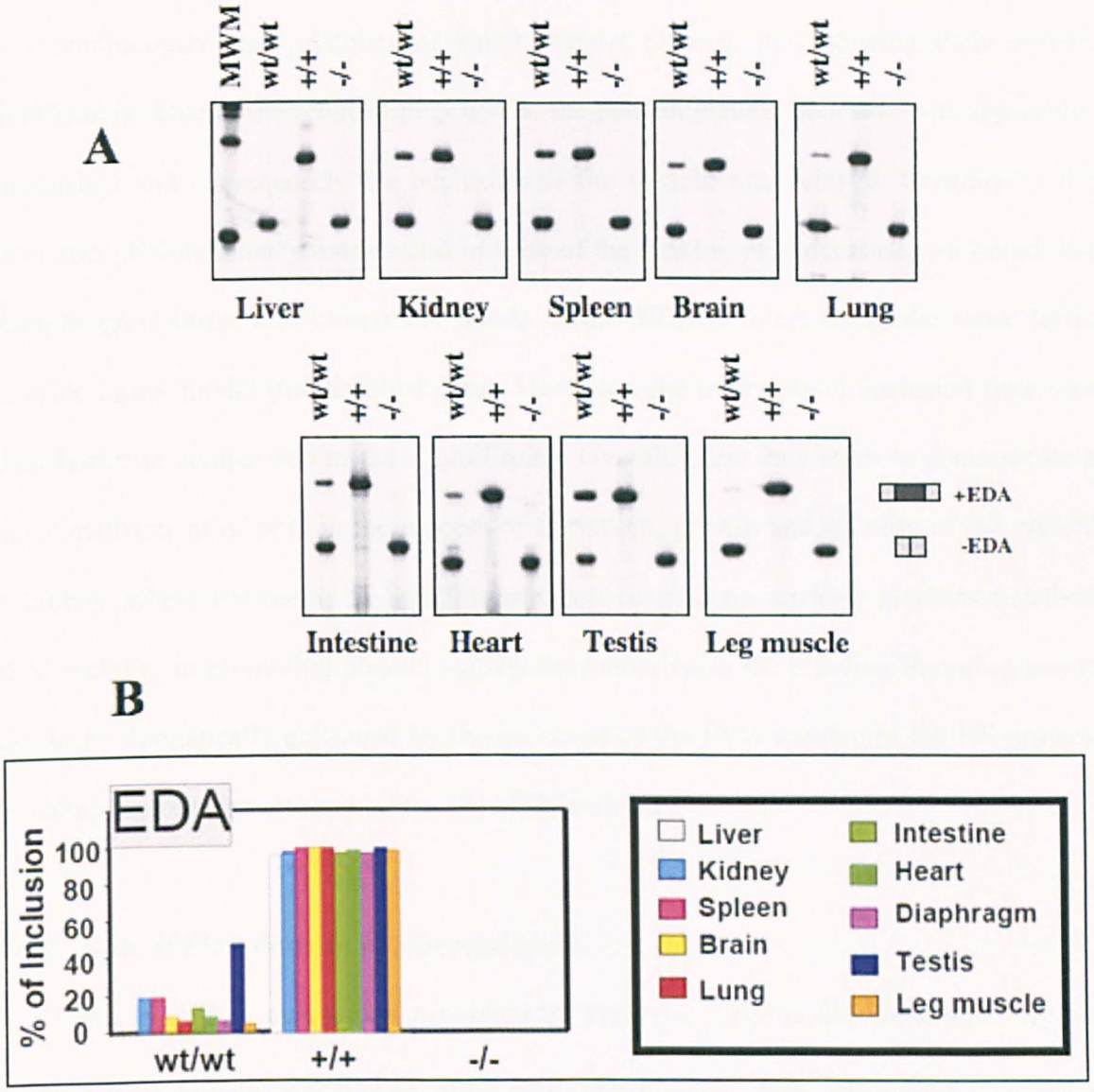

Figura 10. RT-PCR analysis of the splicing patterns of adult mutant and control mice.

A. Radioactive RT-PCR analysis of total RNA prepared from different organs from 4-month-old adult $EDA^{wt/wt}$, $EDA^{+/+}$ and $EDA^{-/-}$ mice for the EDA alternatively spliced region. The inclusion of the EDA exon within the wt FN mRNA is subjected to a tight tissue-specific regulation. The most dramatic example is seen in liver, where EDA exon is completely excluded from the mRNA. On the other hand, the highest inclusion of EDA exon is seen in testis, where the EDA^{+}FN form outnumbers the EDA^{-}FN form. In all other tissues the inclusion is lower but always present. In the mutant mice is always present only one of the two variants, EDA^{+} or EDA^{-} mRNA. **B.** Quantification of the radioactive PCR products. The percentage of EDA inclusion for each genotype is indicated by the coloured graph-bars (Chauhan et al. 2004).

(Matuskova et al., 2006) and conditional pFN-null mice (Ni et al., 2003), respectively, resulted in an evident delay in the formation of thrombi after vessel wall injury. Moreover, even though the thrombi formed in both models were stably anchored to the vessel wall, they continuously shed platelets or small platelet clumps, thus slowing their growth significantly. Due to the reduced pFN levels, the platelet/platelet cohesion was apparently diminished and consequently the occlusion of the vessels was delayed. Contrary to the other two pFN-deficiency models and in spite of the striking pFN decrease, we found that thrombi grew faster and were more stable in our $EDA^{+/+}$ mice, using the same ferric chloride injury model (unpublished data). Moreover, the mean vessel occlusion time was also shorter in comparison to the control mice. Overall, these data seem to demonstrate a clear involvement of pFN in the process of formation, growth and stability of the arterial thrombus, where FN seems to function as a sort of glue for sticking platelets together. pFN' s ability in promoting platelet aggregation/cohesion in the growing thrombus seems also to be dramatically enhanced by the inclusion of the EDA domain in the FN protein, revealing a prothrombotic role of the $EDA^{+}FN$ isoform.

1.4.5 Role of EDA domain in atherosclerosis.

An $EDA^{-/-}$ ko mouse was generated by Tan *et al.* (Tan et al., 2004) similarly but independently to that generated by Muro *et al.* (see above). $EDA^{-/-}$ mice were then mated to apolipoprotein E (ApoE)-null mice ($ApoE^{-/-}$) to generate $EDA^{-/-}ApoE^{-/-}$ double KO mice. $ApoE^{-/-}$ mice are animals that develop hypercholesterolemia and atherosclerotic lesions in arterial wall, following a high-fat, high-cholesterol diet (Plump et al., 1992). Immunohistochemistry with monoclonal antibodies revealed that $EDA^{+}FN$ variant is prominent in atherosclerotic lesions of the $ApoE^{-/-}$ mice. Morphometric measurement of the extent of the atherosclerotic plaques both in $EDA^{-/-}ApoE^{-/-}$ and control $ApoE^{-/-}$ mice revealed that the $EDA^{-/-}ApoE^{-/-}$ mice have reduced, thinner lesions, containing less quantity of lipids. Additionally, cholesterol concentrations in $EDA^{-/-}ApoE^{-/-}$ plasma were

slighty lower than the $ApoE^{-/-}$ controls. These studies provide an *in vivo* evidence for a role of the alternatively spliced EDA segment of FN in atherogenesis, suggesting a pro-atherogenic function in the pathophysiology of the disease. However, our $EDA^{+/+}$ and $EDA^{-/-}$ mouse strains (Muro et al., 2003) revealed a 40% reduction in atherosclerotic lesions after a fat-diet treatment, in comparison to control mice ($EDA^{wt/wt}$) (Babaev et al., 2007. In press in Atherosclerosis). These results seem to rule out a pro-atherogenic role of the EDA domain and suggest that the observed reduction of atherosclerosis in both the $EDA^{+/+}$ and $EDA^{-/-}$ strains might be associated with the impossibility to modify the steady state levels of the EDA domain due to the absence of regulated splicing in both mutant strains.

1.4.6 EDB exon knock-out mice.

A first attempt to study the *in vivo* role of the FN-EDB domain by gene targeting was made by Georges-Labouesse *et al.* (Georges-Labouesse et al., 1996). The EDB exon and part of the flanking intronic sequences were deleted and replaced by a marker cassette (neo) in order to generate a constitutive EDB-null strain. On the other hand, the EDB exon and the two flanking exons (III7b and III8a) were replaced by the corresponding III7b-EDB-III8a cDNA segment in an attempt to generate a constitutive EDB^{+} strain. The neo cassette was inserted into the intron downstream of the exon III8a. Although the heterozygous animals from both strains ($EDB^{wt/+}$ and $EDB^{wt/-}$) appeared normal in size and fecundity and presented no obvious defects after more than 2 years of age, it was found that the pFN levels were about half of the levels of control littermates. Furthermore, none of the homozygous mutant embryos ($EDB^{-/-}$) survived over the tenth day of gestation (E10). Both mutations resulted to be recessive embryonic lethal as already observed in the conventional FN KO animals (George et al., 1993). The reason for the non-functionality of the FN alleles containing the deletion of the EDB exon or its replacement with a corresponding cDNA segment is not clear. However, the presence of the marker cassette

inside the FN gene or the presence of a long artificial exon (III7b-EDB-III8a) may have altered its expression, generating a defective phenotype similar to that obtained by George *et al.* (George et al., 1993). It is noteworthy that also Fukuda *et al.* (Fukuda et al., 2002) examined the function of the FN-EDB exon by generating mice lacking the EDB exon ($EDB^{-/-}$) in which the neo marker was deleted *in vivo*. The EDB domain is prominently expressed during embryonic development, wound healing and malignant transformation although it is mostly eliminated from FN in normal adult tissues (Ffrench-Constant and Hynes, 1989; Oyama et al., 1993; Oyama et al., 1989a; Oyama et al., 1989b), similarly to what occurs in the EDA domain. Analysis of the EDB-null mice revealed the absence of any significant abnormal phenotypes *in vivo*, upon anatomical inspection of major organs. Mice developed normally and were fertile, even though embryonic fibroblasts grew slower *in vitro* and deposited less FN in the pericellular matrix than fibroblasts from wild-type mice. These results indicate that expression of EDB^{+} isoforms is dispensable during embryonic development, even though it may play a regulatory role in the FN matrix assembly and growth of the connective tissue cells. Given that matrix-assembled FNs is supposed to transduce signals that stimulate cell cycle progression via interaction with integrins (Assoian and Schwartz, 2001), decreased FN matrix assembly may well explain the reduced proliferative potential of EDB-null fibroblasts *in vitro*.

1.5 PLASMA AS A RESERVOIR OF PROTEINS FOR THE TISSUES.

Previous experiments have shown that the bloodstream could behave as an important reservoir of FN and other plasma proteins to supply to the tissues for the formation and/or maintenance of the extracellular matrixes and the regulation of many other cell activities. Initial evidences supporting this hypothesis came from *in vivo* studies where purified human pFN was intravenously injected into mice. By immunostaining, human FN was detected in the tissues of mice and its distribution was found indistinguishable from the mouse endogenous cFN (Oh et al., 1981). *In vitro* experiments

performed with human fibroblast cultures showed that exogenous pFN added to the cultures was incorporated into the culture ECM to form fibrils on the fibroblast cell surface along with the endogenous cFN (Bae et al., 2004; McKeown-Longo and Mosher, 1983; Peters et al., 1990). These data indicate that soluble FN may be insolubilized and assembled into the multimeric, insoluble matrices characteristic of connective tissues, most likely via specific cell-surface receptors, but quantification of the FN incorporated has never been assessed.

1.6 ROLE OF EDA$^+$FN VARIANT IN WOUND HEALING.

The ability of repairing damaged tissues represents an important response to injury that is common to all complex organisms. Just as in embryonic development, the repair process involves proliferation, migration, and differentiation of a number of different cell types. Therefore, it is likely that wound healing might share many of the molecular mechanisms used during development. For example, the EDA$^+$FN variant is highly expressed in early embryonic tissues where proliferation, migration, and an undifferentiated state of cells are prevalent. Similarly, the EDA$^+$FN isoform is highly expressed in many pathological situations characterized by dedifferentiation, cell proliferation, and migration such as wound healing (Ffrench-Constant and Hynes, 1988; Ffrench-Constant et al., 1989) (Ffrench-Constant and Hynes, 1989; Norton and Hynes, 1987; Oyama et al., 1989a; Oyama et al., 1989b; Pagani et al., 1991; Peters and Hynes, 1996). The experimentally induced injury in both liver and skin represents an excellent procedure to study the role of the EDA$^+$FN variant in the wound healing process. This is due to the fact that those tissues do not synthesize EDA$^+$FN mRNA in normal conditions. It has been shown that EDA$^-$FN mRNA comprises ~ 70% and 100% of the total FN mRNA in fetal and adult liver, respectively, both in human (Oyama et al., 1989b) and in mice (Chauhan et al., 2004). However, in situations such as fibro-pathologies, tumorigenesis or other pathological circumstances, the EDA segment is again included at

high levels (Brown et al., 1993; Ffrench-Constant et al., 1989; Glukhova et al., 1990; Glukhova et al., 1989; Jarnagin et al., 1994; Knowlton et al., 1992; Oyama et al., 1993). This deregulation of the EDA exon alternative splicing mechanism that resembles an embryonic condition is one of the main features of the liver during the processes of regeneration, fibrosis and malignancy, and of the skin during wound healing.

1.6.1 Liver regeneration.

An example of up-regulation of the EDA exon in pathological situations comes from the analysis of the splicing pattern of regenerating liver after partial hepatectomy. After partial resection of the liver, normally quiescent hepatic cells are stimulated to reenter the cell cycle and proliferate in order to restore the original liver mass in 7-10 days. This means that during the regeneration process, a significant reprogramming of the cellular activities (Arai et al., 2003; Su et al., 2002), including the alternative splicing process (Caputi et al., 1995b; Du et al., 1997), occurs. It has been reported that in rat regenerating liver, 24 hrs after 70% organ resection, there is an abnormal over-production of FN mRNAs (up to three fold) including an up-regulation of the EDA^+FN isoforms. The EDA^+FN mRNA arises from almost 0% up to 20% of the total amount of FN mRNA (Caputi et al., 1995b). This finding is consistent with the observation that hepatocytes start producing EDA^+FN after being 3 days in culture, suggesting that the EDA domain has a role in cell-proliferation and tissue modeling (Odenthal et al., 1992). Interestingly, an increased inclusion of the EDB exon but not of the EDA exon is observed in the FN transcript within the first few hours posthepatectomy (Du et al., 1997). We can speculate that the changes in both the EDA and EDB splicing patterns, generating increased EDA^+FN EDB^+FN/total FN mRNA ratios, serve to provide a more adequate extracellular matrix facilitating tissue repair by promoting cell-activation, -proliferation and -migration. However, the fact that EDA exon does not appear in the early phases of normal liver

regeneration lends support to the idea that the EDA and EDB alternative splicing are regulated by different mechanism and may have different functions.

1.6.2 Liver fibrosis.

The fibroproliferative disorders are not well understood, even though major efforts are being made to elucidate the pathogenic mechanisms. These disorders are characterized by three important events: i) a tissue injury, ii) an abnormal activation and differentiation of fibroblasts or other cell types such as the hepatic stellate cells (HSCs) into myofibroblasts; they are indeed the key cells of the fibrotic process in most organs, and iii) a dramatic increase in the production and deposition of ECM proteins in injured tissues (Bataller and Brenner, 2005; Bissell, 2001). It has been reported that collagen is the predominant ECM protein identified in fibrotic lesions and is the hallmark of fibroproliferative diseases. EDA^+FN variant is also present in abnormally large quantities and localized in areas of active fibrogenesis where it seems to participate in the activation of fibroblasts (Jarnagin et al., 1994). In a rat model in which liver fibrosis was experimentally induced by ligation of the bile duct, the most conspicuous event in FN expression is the sharp increase of the synthesis of both total FN mRNAs (up to 7-fold) and EDA^+FN mRNAs. The EDA^+FN variant is almost undetectable in the whole normal liver extract. The *in vitro* analysis of FN synthesis of each cell type constituting the liver, before and after the injury, revealed that two types of non-parenchymal cells are principally involved in the overproduction of EDA^+FN mRNA: firstly, the sinusoidal endothelial cells (SECs) that line blood capillaries and secondly the HSCs that are fat-storing cells (also called Ito cells or lipocytes) present in the liver space of Disse (Figure 11). Both of the SECs and HSCs normally express very little FN mRNA, but after the injury the EDA^+FN/total FN mRNA ratio is dramatically increased (Jarnagin et al., 1994). Indeed, the EDA^+ mRNAs in the SECs increase rapidly and constitute most (> 80%) of the total FN mRNA within 24 hrs, while in the HSCs increase from ~7% to 42% within 7 days

after the liver injury. On the contrary, in the hepatocytes, the level of total FN mRNA remains constant and the EDA exon is almost undetectable up to 14 days after the bile duct ligation. The appearance of the EDA domain during development (Ffrench-Constant and Hynes, 1989; Oyama et al., 1989b; Pagani et al., 1991), its nearly total disappearance in the adult liver and reappearance in a context of wound healing clearly suggest a specific biological role for the $EDA^{+}FN$ variant. The fibrotic process that follows a liver injury is characterized by the appearance and proliferation of myofibroblast-like cells (Bissell, 1990; Friedman, 2000; Serini and Gabbiani, 1999). These cells seem to arise in part from the HSCs through a conversion process called "activation" (Jarnagin et al., 1994; Lotersztajn et al., 2005; Magness et al., 2004). In normal liver, HSCs are synthetically quiescent, notable mainly for their abundant stores of retinoid esters. Once they are active, the HSCs start proliferation, synthesis of cytokine receptors and secretion of ECM proteins. It is thought that HSCs activation is regulated by soluble products of inflammation such as cytokines and growth factors, and by the ECM itself (Friedman et al., 1989; George et al., 2000). Studies performed *in vitro* by plating HSCs on substrata with various FN matrixes, containing or not containing the EDA domain, revealed that the presence of the EDA domain in the matrix is an important factor for the activation of the HSCs (Jarnagin et al., 1994). The activation of HSCs was monitored by quantitation of one of the protein markers for the activated HSCs such as the smooth muscle α-actin (αSMA). The fresh isolates contained no detectable αSMA, but in culture on a collagen substrate, they underwent spontaneous activation that was detectable after 2-3 days and increased progressively. HSCs plated for the same period of time on a matrix containing $EDA^{+}FN$ (cFN) or $EDA^{-}FN$ (pFN) expressed substantially higher levels of αSMA, but strikingly the αSMA level in the HSCs incubated on $EDA^{+}FN$ matrix was twice the level of αSMA of the HSCs incubated on $EDA^{-}FN$ matrix. Moreover, the activation effect of the $EDA^{+}FN$ matrix was completely blocked by the use of anti-EDA antibodies, confirming that the activation of the HSCs was related to the presence of the EDA segment (Jarnagin et al.,

1994). During wound healing, it has been shown that non-parenchymal cells have a predominant role in respect to parenchymal cells, due to their increased production of both the EDA$^+$FN and collagen mRNAs (Jarnagin et al., 1994; Maher and McGuire, 1990). However the role played by the non-parenchymal cells in the pathophysiology of the liver fibrosis has never been firmly established *in vivo*.

1.6.3 Liver tumorigenesis.

Many studies have been performed in order to investigate the splicing pattern of FN in human liver diseases such as chronic hepatitis, cirrhosis and hepatocellular carcinoma. The scenario looks to be very similar to that of animal models for wound healing. It has been shown that EDA$^+$FN mRNA expression is upregulated in human liver malignant and fibrotic tissues, as occurs during development. The physiological significance of the increased expression of the EDA$^+$FN variant in tumorigenesis has not yet been well understood. It is possible that the EDA$^+$FN variant is involved in the manifestation of the invasive properties such as migration and proliferation of the malignant tumor cells (Matsui et al., 1997; Oyama et al., 1993; Oyama et al., 1989a; Tavian et al., 1994).

1.6.4 Skin wound healing.

Similarly to liver, skin of adult animals does not contain the EDA domain in the FN protein. However, the EDA$^+$FN variant is thought to participate actively in the reepithelization process (Clark et al., 1983; Ffrench-Constant et al., 1989). It has been observed that after skin wounding, FN gene is highly expressed in the cells at the base and edge of the wound and in the subjacent uninjured muscle and dermis. Interestingly, the splicing pattern of FN mRNA is different in these areas. In adjacent dermis and muscle, the splicing pattern remains identical to that of normal adult skin with exclusion of EDA exon from the FN mRNA. On the contrary, EDA exon is included in the FN mRNA present in the cells at the base and edge of the wound (Ffrench-Constant et al., 1989). These data are

in agreement with the abnormal skin wound healing of adult $EDA^{-/-}$ mice, following full thickness excision of skin (Muro et al., 2003). A factor that promotes the EDA domain inclusion into FN is the transforming growth factor-β (TGF-β). TGF-β is a multifunctional cytokine that is implicated in a broad range of processes such as tissue development and repair, including the pathogenesis of fibroproliferative disorders (Ellingsworth et al., 1986). It has been shown that the treatment of cultured human skin fibroblasts with picomolar quantities of TGF-β results in two- to three-fold increase in the relative amount of $EDA^{+}FN$ (Balza et al., 1988; Borsi et al., 1990). Additionally, $EDA^{+}FN$ variant over-production exerts a sort of synergic effect on the initial TGF-β-mediated stimulation of fibroblasts (Serini et al., 1998). Following the early $EDA^{+}FN$ deposit and the EDA-dependent auto-stimulation, fibroblasts start the intracitoplasmatic accumulation of αSMA and the secretion of collagen. TGF-β stimulation of fibroblasts plated on gelatin substrata containing a specific anti-EDA antibody showed a dramatic inhibition of αSMA and collagen induction. Conversion of fibroblasts to a myofibroblast-like phenotype mediated by both the EDA domain and cytokines such as TGF-β, is an important event to generate contraction and closure of the skin wounds (Montesano and Orci, 1988; Serini and Gabbiani, 1999). The expression of smooth muscle α-actin (αSMA) in stress fibers increases the contractile activity of cultured fibroblasts and this perfectly correlates with wound contraction efficiency *in vivo* (Hinz and Gabbiani, 2003).

1.7 EXPERIMENTAL MODELS FOR LIVER FIBROSIS

Liver fibrosis results from chronic damage to the liver in conjunction with the accumulation of ECM proteins, which is a characteristic of most types of chronic liver diseases. The main causes of liver fibrosis in industrialized countries include chronic hepatitis C virus (HCV) infection, alcohol abuse and nonalcoholic steatohepatitis (diabetes mellitus, obesity and hypertriglyceridemia) (Bataller and Brenner, 2005; Friedman, 2003). Animal models of chronic hepatic fibrosis are excellent tools to study cells and molecular

mediators involved in the onset of fibrosis, in a serial manner during both progression and/or recovery. Several approaches towards induction of fibrosis have been described. Of these, carbon tetrachloride (CCl_4) intoxication and bile duct ligation (BDL) in rodents are the most widely studied and applied. However, the importance of studying human diseases using animal models should not be overemphasized as, at best, only a snapshot of a disease process which may develop over months or few years can be provided. Nevertheless, mechanistic studies combining knock-out or transgenic animals with CCl_4 or BDL experimental models have provided unparalleled insight into mechanism underlying hepatic fibrosis (Constandinou et al., 2005). The hepatotoxicity of CCl_4 involves two main phases. Firstly, CCl_4 is metabolized to trichloromethyl radical by the cytochrome P450 that is highly expressed in centrilobular hepatocytes. Trichloromethyl radicals are responsible for lipid peroxidation and membrane damage. The second phase is an inflammatory response that is launched by resident hepatic macrophages or Kupffer cells. After activation, these cells secrete cytokines such as TGF-β, chemokines, and other proinflammatory factors (Novobrantseva et al., 2005). In addition to their direct cytotoxic effects, these factors attract and activate other monocytes as well as neutrophils and lymphocytes, all of which contribute to tissue damage. Initial damage is followed by a phase of repair that includes a TGF-β-induced increase in the production of ECM proteins such as fibronectins and collagens. Repeated cycles of injury, inflammation and repair attempts lead to fibrosis. The accumulation of ECM proteins occurs in the space between hepatocytes and endothelial cells that is called space of Disse (Figure 11).

Bile duct ligation is as efficient as CCl_4 administration in the induction of liver fibrosis even though the two models are mechanically different. In both cases, damage to hepatocyte plasma membrane is the starting point of liver fibrosis. Bile secretion normally depends on the function of a number of membrane transport systems in hepatocytes and cholangiocytes (epithelial cells of the bile duct), and on the structural and functional integrity of the bile-secretory apparatus. Ligation of the extra-hepatic bile duct provokes

blocking of the free bile flow excretory pathway between liver and duodenum, generating stagnation of the bile constituents within hepatocytes (Rodriguez-Garay, 2003). Alterations in membrane functionality are rapidly produced. Since the hydrophobic bile acids are strong detergents, they damage the plasma membrane proteins and the cell tight-junctions, provoking impairment of membrane functions (Rodriguez-Garay, 2003).

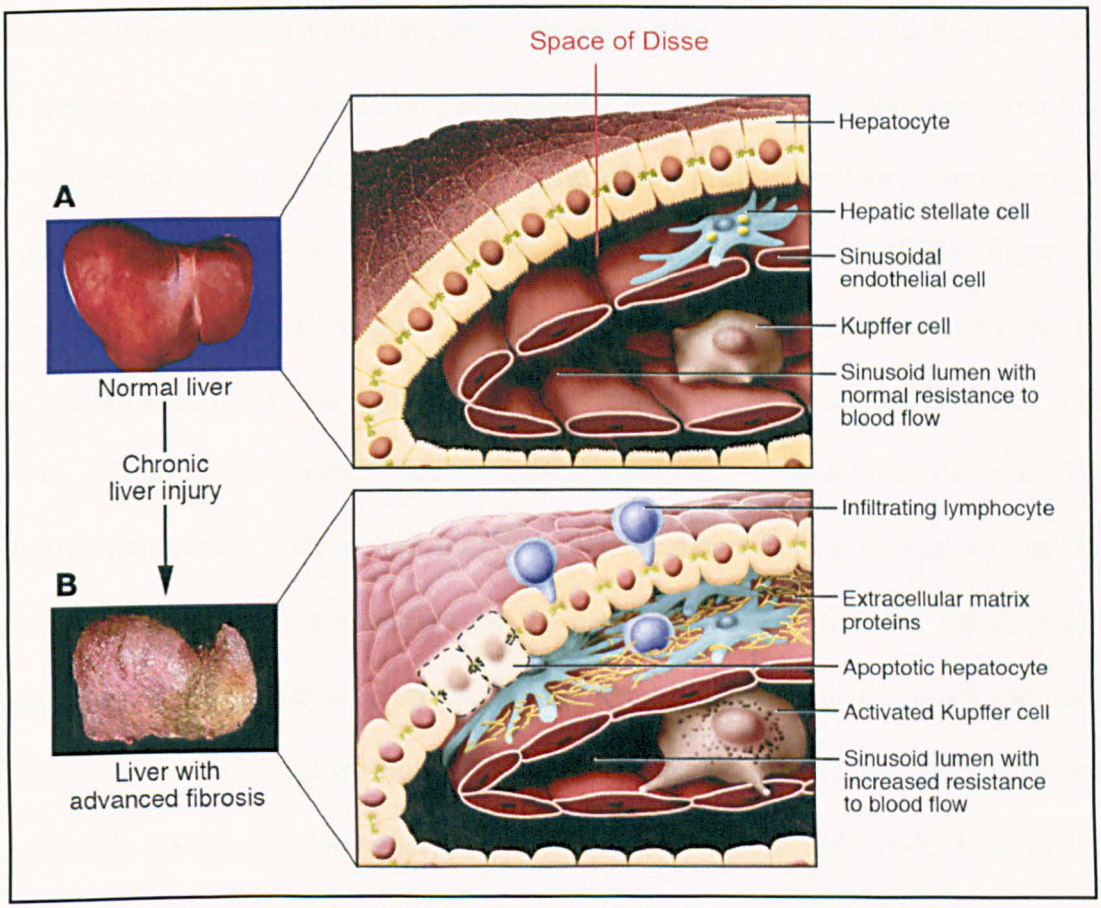

Figure 11. Changes in the hepatic architecture (Panel A) associated with advanced hepatic fibrosis (Panel B).
Following chronic liver injury, inflammatory lymphocytes infiltrate the hepatic parenchyma. Some hepatocytes undergo apoptosis, and Kupffer cells activate, releasing fibrogenic mediators. Hepatic stellate cells (HSCs) proliferate and undergo a dramatic phenotypical activation, secreting large amounts of extracellular matrix proteins such as $EDA^{+}FN$ and collagens. Sinusoidal endothelial cells lose their fenestrations, and the tonic contraction of HSCs causes increased resistance to blood flow in the hepatic sinusoid (Bataller and Brenner, 2005).

The presence of damaged or apoptotic hepatocytes trigger both the inflammatory and repair response leading to fibrosis. In both models, accumulation of ECM proteins in the space of Disse distorts the hepatic architecture due to the formation of a fibrous scar. The subsequent development of nodules of regenerating hepatocytes leads to cirrhosis. If the hepatic injury persists and the liver regeneration fails, the necrotic or apoptotic cells are substituted with abundant ECM, including fibrillar collagen. Cirrhosis produces hepatocellular dysfunction and increased intrahepatic resistance to blood flow that result in hepatic insufficiency and portal hypertension, respectively (Bataller and Brenner, 2005). Following chronic injury, HSCs or perisinusoidal lipocytes activate and transdifferentiate into myofibroblast-like cells, acquiring contractile, proinflammatory, and fibrogenic properties (Friedman et al., 1985; Geerts, 2001; Jarnagin et al., 1994) (Figure 11). Activated HSCs proliferate, migrate and accumulate at the sites of tissue repair, secreting large amounts of ECM and regulating ECM degradation (Bataller and Brenner, 2005). Several different molecules are involved in the modulation of the HCSs transdifferentiation: i) TGF-β and the $EDA^{+}FN$ variant mainly produced by the SECs (George et al., 2000) are responsible for the activation of the quiescent HSCs and their subsequent synthesis of ECM proteins, cytokine and growth factor receptors and αSMA; ii) PDGF and EGF, mainly produced by Kupffer cells, are the predominant mitogens for the activated HSCs; iii) Chemotactic signals as well as specialized cell-ECM interactions modulate the migration of the myofibroblasts to the injured areas, instead iv) Endothelins modulate their contraction (Bissell, 2001). Quiescent HSCs express markers that are characteristic of adipocytes (PPARγ, SREBP-1c, and leptin), while the activated HSCs express myogenic markers (αSMA, c-myb, and myocyte enhancer factor-2) (Bataller and Brenner, 2005). Hepatocytes are the target for most hepatotoxic agents such as carbon tetrachloride, diamethylnitrosamine and thioacetamide (Constandinou et al., 2005), including alcohol metabolites, bile acids and hepatitis viruses (Higuchi and Gores, 2003). Damaged hepatocytes release reactive oxygen species (ROS) and fibrogenic mediators and

induce the recruitment of white blood cells and inflammatory cells such as leucocytes, lymphocytes, macrophages, polymorphonuclear cells and platelets. Apoptosis of damaged hepatocytes and the recruited inflammatory cells stimulates the fibrogenic actions of the myofibroblasts. Activated HSCs secrete inflammatory chemokines, express cell adhesion molecules, and modulate the activation of the inflammatory cells. Therefore, a sort of "vicious circle" or "synergic effect" in which inflammatory and fibrogenic cells stimulate each other is likely to occur (Bataller and Brenner, 2005).

The identification of activated HSCs or myofibroblasts as the major fibrogenic cell types as well as the recognition of the key cytokines and growth factors involved in the liver fibrosis process is facilitating the design of promising new antifibrotic therapies. These therapies are aimed at inhibiting the accumulation of activated HCSs at the sites of liver injury and preventing the deposit of extracellular matrix and scar formation. To date, removal of the causative agent is the only effective therapy to stop or even reverse liver fibrosis. The development of effective antifibrotic therapies represents a challenge for modern hepatology. Experimental antifibrotic strategies tested in rodents involve the use of antagonist of cytokines or cytokine receptors, specific inhibitors of the HSC activation and anti-collagen agents (Bataller and Brenner, 2001; Bissell, 2001). Antibodies like anti-TGF-β or "soluble TGF-β receptors" that consist of the extracellular portion of the TGF-β receptor, may function as competitive binders of TGF-β, preventing interaction of the cytokine with its receptor (George et al., 1999). Antioxidant compounds such as vitamine E, sylimarin, phosphatidylcoline, S-adenosyl-L-methionine, inhibit HSC activation, protect hepatocytes from apoptosis, and attenuate experimental liver fibrosis (Bataller and Brenner, 2005). The use of modifiers of collagen cross-linking as well as inhibitors of collagen synthesis or promotion of its degradation (Bataller and Brenner, 2001) can be a valid alternative approach. Moreover, the finding of a direct participation of EDA domain in the activation of the HSCs opens a novel pathway towards the identification of new antifibrotic therapies having as a potential target the EDA domain itself or its receptors.

1.8 AIM OF THE THESIS.

As previously described, the FN-EDA exon undergoes alternative splicing and its inclusion/exclusion pattern is strictly regulated in a developmental and tissue specific manner (Chauhan et al., 2004). The adult liver tissue is characterized by the total absence of EDA domain from the FN polypeptide. Both embryonic and pathologic livers are instead characterized by an upregulation of $EDA^{+}FN$ mRNA (Jarnagin et al., 1994; Oyama et al., 1989b). The main objective of this thesis is to address the functions of the FN isoforms produced by the liver, containing or not the EDA domain, during physiological and pathological situations such as i) the supply of pFN to tissues and ii) tissue repair/progressive fibrosis, respectively.

To address these issues we have used two mouse strains devoid of EDA-exon alternative splicing (Muro et al., 2003). The strain called $EDA^{+/+}$ modified to constitutively include the EDA exon into the FN mRNA was used to address the contribution of liver to the formation of the tissue FN matrix. The strain called $EDA^{-/-}$ bearing a deletion of the EDA exon from the genome was used to study the involvement of EDA domain in the activation of the hepatic stellate cells, the key cells of the fibrotic process in liver.

To demonstrate the first issue, we generated and characterized a liver-specific EDA-null mouse ($EDA^{+/+CRE}$) bearing an $EDA^{-/-}$ liver inside an $EDA^{+/+}$ body. That mouse was simply obtained by crossbreeding our $EDA^{+/+}$ strain with a transgenic mouse expressing the CRE recombinase only in the hepatocytes (Kellendonk et al., 2000).

To demonstrate the *in vivo* role of the EDA domain in liver fibrosis, we challenged our $EDA^{-/-}$ and control mice with two well-established experimental models of liver fibrosis: carbon tetrachloride (CCl_4) intoxication and the bile duct ligation (BDL) models (Constandinou et al., 2005).

2. MATERIALS AND METHODS

2.1 CHEMICAL REAGENTS.

General chemicals were purchased from Sigma-Aldrich, Merck, Gibco BRL, Life Technologies and Analar, BDH Laboratory Supplies, Fluka, Riedel-de-Hael, BD Bioscience, Amersham Biosciences, Pharmacia, Analyticals and Invitrogen.

2.1.1 Standard solutions.

All solutions are identified in the text where used, except for the following:

a) 5X DNA Loading Buffer: 500 gr/L Sucrose, 240 gr/L Urea, 500 ml/L 10X TBE, 1% 10-20 ml/L 1% w/v Bromophenolo blue in H_2O.

b) 50X Denhardts Solution: 5 gr Ficoll (Type 400, Pharmacia), 5 gr Polyvinylpyrrolidone, 5 gr Bovine Serum Albumin (BSA) and H_2O to 500 ml. Filtered and stored at −20°C.

c) 20X SSPE: 3M NaCl, 0.2M NaH_2PO_4, 0.02M EDTA. pH adjusted to 7.4 with NaOH.

d) 20X SSC: 3M NaCl, 0.3M Na_3Citrate. pH adjusted to 7.0 with HCl.

e) 10X TBE: 108 gr/L Tris, 55 gr/L Boric acid, 9.5 gr/L EDTA.

f) 1X PBS: 137 mM NaCl, 2.7 mM KCl, 10 mM Na_2HPO_4, 1.8 mM KH_2PO_4 (pH7.4).

g) 10X Protein Loading Buffer: 20% w/v SDS, 1M DTT, 0.63 M Tris pH 7, 0.2% w/v Bromophenol blue, 12% w/v sucrose, 10 mM EDTA pH 7.

h) 5X Running Buffer for SDS-PAGE: 30 gr/L Tris base, 144 gr/L Glycine, 5 gr/L SDS.

i) 10X Protein Blotting Buffer: 30 gr/L Tris base, 144 gr/L Glycine.

2.1.2 Radioactive isotopes.

[α-^{32}P]-dCTP isotope was purchased from Amersham Biosciences and used to label the probe for the Southern blot experiments. ^{35}S-Methionine and ^{35}S-Cysteine isotopes (ProMix, Amersham Biosciences) were used for the *in vivo* labeling of cultured hepatocytes.

2.2 GENERATION OF THE GENETICALLY MODIFIED MICE.

The generation and genetic background of the mice devoid of regulated splicing at the EDA exon ($EDA^{+/+}$ and $EDA^{-/-}$) has been previously described by Muro *at al.* (Muro et al., 2003), see also the introduction section of this thesis. $EDA^{-/-}$ and $EDA^{+/+}$ mice have been backcrossed > 6 generations onto a C57Bl/6 background. The liver-specific EDA-null mice ($EDA^{+/+CRE}$) were generated by crossbreeding the floxed $EDA^{+/+}$ mice, which have two loxP sites in the introns flanking the EDA exon, with the transgenic strain Tg Alf pCRE, which has the CRE recombinase gene under the control of the albumin promoter and enhancer (Kellendonk et al., 2000). The heterozygous mice having the CRE recombinase ($EDA^{wt/+CRE}$) were mated with $EDA^{+/+}$ animals in order to obtain the homozygous $EDA^{+/+}$ strain with the CRE transgene ($EDA^{+/+CRE}$). These strains express the CRE recombinase exclusively in hepatocytes. All murine strains (C57BL/6 control mice, $EDA^{+/+}$, $EDA^{-/-}$, $EDA^{wt/+}$, $EDA^{wt/+CRE}$, $EDA^{+/+CRE}$ and Tg Alf pCRE mice) were bred at the International Centre for Genetic Engineering and Biotechnology animal house, and housed in rooms at 25°C with 12 hr light/dark cycles. Mice were fed with standard food and water *ad libitum*. In all experiments, mice were males and age-matched (2/4-month-old), except in the CCl_4 mortality experiment in which both males and females were used, or specifically indicated in the text.

2.3 PREPARATION OF HEPATOCYTE PRIMARY CULTURE.

Hepatocytes from $EDA^{wt/wt}$, $EDA^{+/+}$, $EDA^{-/-}$ and $EDA^{+/+CRE}$ whole livers were

purified by the two-step collagenase perfusion method (Seglen, 1976) using Liver Digest Medium (Gibco) as described by manufacturers. About 1.3 x 10^6 hepatocytes per each genotype were plated in 1% rat-tail collagen-containing 60 mm Petri's dishes and incubated at 37°C with 5 ml of culture medium (Dulbecco's Modified Eagle Medium supplemented with 10% fetal bovine serum, Gibco) until use for RNA and protein extraction or *in vivo* labelling.

2.4 NUCLEIC ACID ANALYSIS.

2.4.1 Genomic DNA extraction from organs.

Organ biopsies were digested overnight (O/N) with 600 µl of Lysis Buffer (50 mM Tris pH 8.0, 100 mM EDTA pH8, 0.5% SDS, 200 µg/ml Proteinase K by Boehringer Mannheim), in a water bath at 58°C (Laird et al., 1991). The mix was then centrifuged for 15 min at 14000 rpm. 500 µl of supernatants were recovered and added to 500 µl of isopropanol to allow DNA precipitation, by tube invertion. The DNA pellets were washed with 80% ethanol, resuspended in 200 µl of TE Buffer (10 mM Tris pH 7.4, 0.1 mM pH 8) prewarmed at 65°C, left O/N at 37°C to facilitate the dissolution, and quantitated by measuring the absorbance at 260 nm and 280 nm with a spectrophotometer (Jenway Genova). The DNA integrity was checked by electrophoresis on 1% w/v agarose gel and stored at 4°C until use either for PCRs or Southern blot analysis.

2.4.2 Polymerase Chain Reaction (PCR) for genotyping.

The genotype of mice was determined by PCR analysis of DNA samples from tail biopsies (0.5-0.8 cm). The reaction was performed in a final volume of 50 µl with 250-500 ng of genomic DNA, 1X Taq Buffer, dNTP mix (200 µM each, final concentration), appropriate sense and anti-sense oligonucleotide primers (15 µM each, final concentration) and 2.5-5 U of Taq DNA polymerase (BioLabs). For the amplification of the CRE-

transgene the following primers were used: Forward primer 5'-CGAGTGATGAGGTTCGCAAG-3'; Reverse primer 5'-TGAGTGAACGAACCTGGTCG-3'. Conditions for PCR were: 1 cycle (initial denaturation step at 95°C for 2 min), 45 cycles (denaturation step at 95°C for 30 sec; annealing step at 58°C for 30 sec; extension step at 72°C for 1 min), 1 cycle (final extension step at 72°C for 10 min). The amplified fragment was 390 bp long. To amplify the EDA exon, primers pairing into the EDA-flanking introns were used: Forward primer 5'-CTTCAGGGTGTCTACATAC-3'; Reverse primer 5'-ACCGAGGTGTCTCACTTAG-3'. Conditions for PCR were: 1 cycle (initial denaturation step at 95°C for 2 min), 30 cycles (denaturation at 95°C for 30 sec; annealing step at 54°C for 30 sec; extension step at 72°C for 1 min), 1 cycle (final extension step at 72°C for 10 min). The amplified fragments were: EDA^{wt} band, 860 bp; EDA^{+} band, 1152 bp; EDA^{-} band, 350 bp (Figure 12). All PCR products (1/5 of the PCR volume) were separated in a 1% w/v agarose gel prestained with ethidium bromide and verification of the correct size was done by visualization of their migration relative to the molecular weight standards.

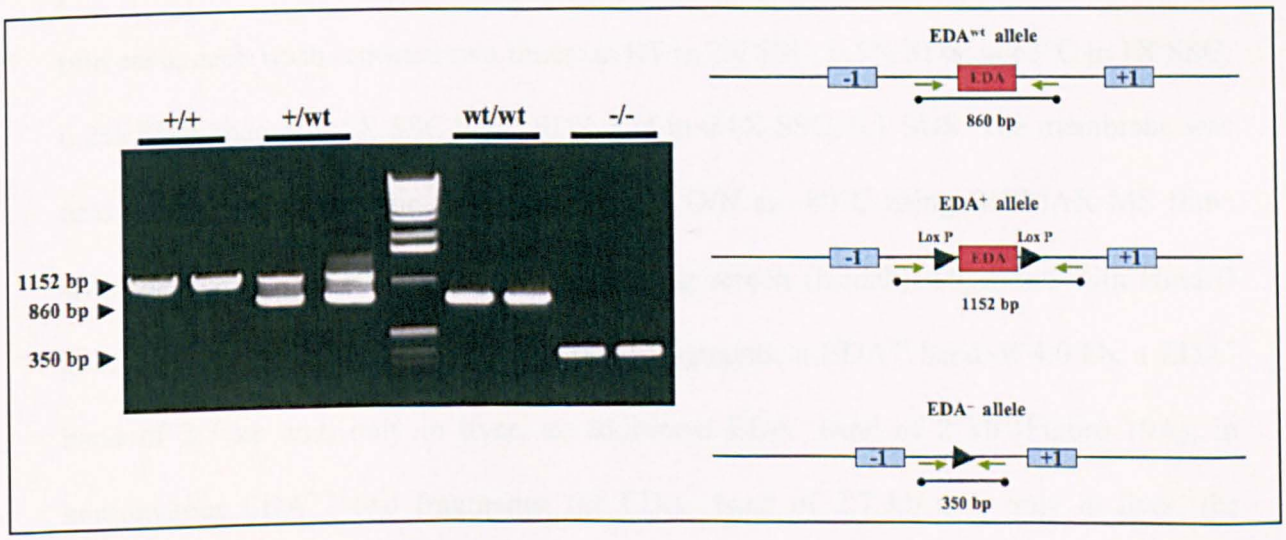

Figure 12. PCR-genotyping for the EDA exon.
PCR analysis was performed using DNA samples from tail biopsis. To amplified the EDA exon, primers (green arrows) pairing into the EDA-flanking introns were used. 1152 bp-band, EDA-floxed allele; 860 bp-band, WT allele; 350 bp-band, EDA-null allele.

2.4.3 Southern blot analysis.

DNA was extracted from tissues as described above. 15-20 μg of DNA were digested O/N at 37°C in a final volume of 400 μl with 1X NEBuffer 2 and 200 U of the restriction enzyme Hind III (BioLabs). The DNA was than precipitated (1/10 volume of 3M Sodium Acetate pH 5.3, 2 volumes of 100% Ethanol) washed in 70% Ethanol, resuspended in 40-50 μl of 1X DNA Loading Buffer, and run O/N at 20 V in a 0.8% (w/v) agarose gel. The gel was then soaked in the Denaturing Solution (0.5M NaOH, 1.5M NaCl) for 15 min with slight agitation (two times) at room temperature (RT). The DNA was blotted for 16 hrs onto a Z-Probe nylon membrane (Bio-Rad) by capillary blotting using the denaturing solution. Next, the membrane was neutralized with 1M Tris pH 8.0 and 1.5M NaCl by incubating at RT for 15 min (two times), dried, UV crosslinked, and prehybridized in a minimum amount of Hybridization Solution (6X SSPE, 10X Denhardt's Solution, 2% SDS, 200 μg/ml of denatured Salmon Sperm) for 2-3 hrs at 65°C. The radioactive labeled DNA probe (see below) was denatured at 95°C for 5 min, quickly chilled on ice, and then added to the hybridization solution. The hybridization reaction was performed O/N at 65°C. The membrane was then subjected to successive washes of 10-15 min each, each wash repeated two times: at RT in 2X SSC, 0.5% SDS; at 65°C in 1X SSC, 0.2% SDS, then in 0.5X SSC 0.1% SDS, and in 0.1X SSC, 0.1 SDS. The membrane was next covered with a plastic wrap and exposed O/N at -80°C using BIOMAX MS films with the help of the BIOMAX MS intensifying screen (Kodak). Digestion with HindIII generated in heterozygous $EDA^{wt/+CRE}$ three fragments: a EDA^{wt} band of 4.0 kb, a EDA^{+} band of 2.7 kb and, only in liver, an additional EDA^{-} band of 2 kb (Figure 19A); in homozygous $EDA^{+/+}$ two fragments: the EDA^{+} band of 2.7 kb and, only in liver, the additional EDA^{-} band of 2 kb (Figure 19B).

2.4.4 Hybridization probe.

A DNA fragment corresponding to the exon downstream to the EDA exon was used as a probe for the Southern blot analysis (Muro et al., 2003). 50 ng of DNA were radioactive labeled with [α-^{32}P] dCTP isotope by the random priming method using the oligolabelling kit (Amersham Biosciences) and then purified from unincorporated nucleotides by passing the probe mixture through a Nick column (Amersham Biosciences). Both the labeling and the probe purification were carried out according to the manufacturers' instructions.

2.4.5 Isolation of total RNA from organs.

Total RNA was prepared from tissues by the Guanidinium Thiocyanate method (Chomczynski and Sacchi, 1987). Organs were removed, quickly frozen in liquid nitrogen and stored at –80°C until use. Then, 8 ml of ice-cold Solution D (4M Guanidine Thiocynate, 25 mM Sodium Citrate, 100 mM β-Mercaptoethanol, 0.5% w/v Lauroylsarcosine) was added to organs and completely homogenized in series of 20 sec by using the UTRA-TURRAX T-25 Basic homogenizer (Ika-Werke). To the homogenate, 0.8 ml of 2M Sodium Acetate pH 4, 8 ml of Phenol (saturated with water) and 1.6 ml of Chloroform were then added. The whole mix was vortexed, kept on ice for 15 min and centrifuged in a 5810-R rotor (Eppendorf) at 3500 rpm for 20 min (4°C). The aqueous phase was then separated and subjected to a second phenol-chloroform extraction to improve the sample purification from proteins and fatty acids. The RNA was precipitated by addition of one volume of Isopropanol, kept for one hour at –20°C and centrifuged in a 5415-D rotor (Eppendorf) at 14000 rpm for 15 min (4°C). RNA pellets were washed once in ice-cold 70% Ethanol, resuspended in 200-400 µl of DEPC-treated ddH_2O, separated in aliquots frozen immediately in dry-ice, and kept at –80°C until use. RNA integrity was confirmed by running the samples on 1% w/v agarose gel with 7% formaldehyde and quantitated by measuring absorbance at 260 nm and 280 nm with a spectrophotometer

(Jenway Genova).

2.4.6 Isolation of total RNA from cultured hepatocytes.

To a 60 mm Petri dish containing ~ 1.3 x 10^6 cells was added 1.6 ml of Solution D (4M Guanidine Thiocynate, 25 mM Sodium Citrate, 100 mM β-Mercaptoethanol, 0.5% w/v Lauroylsarcosine), 1.6 ml of Phenol (saturated in H_2O) and 160 µl of 2M Sodium Acetate pH 4, following removal of the culture medium and two washes in cold 1X PBS. Lysis was carried out by shaking for 15 min at 4°C. To the lysate was added 1/10 volume of Chloroform, and the mix was then vortexed, incubated for 15 min on ice, and centrifuged at 14000 rpm for 15 min (4°C). The aqueous phase was separated, added of one volume of Phenol (saturated in H_2O) and ¼ volume of Chloroform, reincubated on ice and recentrifuged. The supernatant was added of one volume of ice-cold Isopropanol, left for one hour at –20°C and centrifuged. The pellet was then washed with 70% Ethanol and resuspended in 50-100 µl of DEPC-treated ddH_2O. RNA integrity was confirmed by running the samples on 1% agarose gel with 7% formaldehyde and quantitated by measuring absorbance at 260 nm and 280 nm with a spectrophotometer (Jenway Genova).

2.4.7 FN cDNA synthesis and RT-PCR for the EDA exon.

To synthesize FN cDNA, 1-2 µg of total RNA were used in the following 20 µl reaction: 1µl of random primers (hexanucleotides, 200 ng/µl), 1 µl of dNTP mix (100 mM), 4 µl of RT buffer (5X), 2 µl of 0.1 M DTT (10X), 1µl of RNAsin (40 U/µl) and 50 units of M-MLV reverse transcriptase (RT) (Invitrogen). The reaction was incubated for one hour at 37°C. Following RT reaction, the PCR reaction was carried out in a final volume of 50 µl with 1-2 µl of the RT reaction (cDNA), 1X Taq buffer, dNTP mix (200 µM each, final concentration), FN-EDA forward (5'-ACCATCACCCTGTATGCTGTCACT3') and reverse (5'-ATGAGTCCTGACACAATCAC-3') oligonucleotide primers (2 ng/µl each, final

concentration) pairing in the two exons flanking the EDA, and 2.5 U of Taq DNA polymerase (Eppendorf). Conditions for PCR were: 1 cycle (initial denaturation step at 95°C for 2 min), 35 cycles (denaturation step at 95°C for 30 sec; annealing step at 58°C for 30 sec; extension step at 68°C for 1 min), 1 cycle (final extension step at 68°C for 10 min). The amplified fragments were: EDA^+ band, 805 bp; EDA^- band, 535 bp (Figure 20A and 29). The PCR products (1/5 of the PCR volume) were separated in a 1% w/v agarose gel prestained with ethidium bromide and verification of the correct size was done by visualization of their migration relative to the molecular weight standards.

2.4.8 Agarose gel for nucleic acid routine screening electrophoresis.

All agarose gels were prepared dissolving the right weight of agarose (EuroClone) in 1X TBE Buffer and heating in a microwave oven (DeLonghi). All DNA samples were diluted in 1X DNA Loading Buffer, loaded into the gels prestained with ethidium bromide (1:20000) and run in 1X TBE Buffer at 80-100V according to the gel size. The DNA bands were sized by confront to the molecular weight standards (1 kb DNA ladder, Invitrogen).

2.5 PROTEIN ANALYSIS.

2.5.1 Plasma and bile fluid preparation.

Blood was drawn by puncture of the internal maxillary artery from $EDA^{wt/wt}$, $EDA^{+/+}$, $EDA^{-/-}$, $EDA^{wt/+}$, $EDA^{wt/+CRE}$, $EDA^{+/+CRE}$ mice of different ages, from 6 day- to 30 month-old. A quantity of 200-300 µl of blood was mix with 2-3 µl of 0.5M EDTA pH 8, centrifuged at 4000 rpm for 15 min (RT), to separate the cell component from plasma. Plasma was then recovered, recentrifugated and stored at –80°C until use. The 18.5-day post-coitus (PC) and 1-day blood was pooled from 6-7 $EDA^{wt/wt}$ and $EDA^{+/+}$ embryos and newborns, respectively. Bile fluid was drawn directly from the gallbladder of $EDA^{wt/wt}$ and $EDA^{+/+}$ mice, following laparatomy. The whole content of bile was recovered by means of

a 0.5 ml insulin syringe (BD MICRO-FINE +), holding the gallbladder with forceps.

2.5.2 *In vivo* labelling of cultured hepatocytes.

About 1.3 x 10^6 $EDA^{wt/wt}$, $EDA^{+/+}$ and $EDA^{-/-}$ hepatocytes were plated in 60 mm 1% rat-tail collagen-containing Petri dishes and incubated for 1 h at 37°C with 5 ml of culture medium (Dulbecco's Modified Eagle Medium supplemented with 10% fetal bovine serum, Gibco). Next, cells were incubated immediately, after 24 and 48 hrs with 1.5 ml Methionine/Cysteine free culture medium (DMEM –Met/–Cys, Gibco) supplemented with 300 μCi/ml of ^{35}S-Methionine/^{35}S-Cysteine (ProMix, Amersham) for additional 24 hrs, following removal of the former medium. The conditional media were then collected and a fraction of 500 μl was affinity-purified with Gelatin-Sepharose as described (Owens and Baralle, 1986) (Ruoslahti et al., 1982). Next, 40 μl of the conditional media and 25 μl of the affinity-purified eluted of each sample were run in a 6% SDS-PAGE. Gels were then fixed in 10% glacial acetic acid, 25% methanol, 65% H_2O, dried by the use of a gel-dryer (Bio-Rad) and autoradiographed O/N using BIOMAX MR films (Kodak) at RT.

2.5.3 Total protein extract from cultured hepatocytes.

To a 60 mm Petri dish containing ~ 1.3 x 10^6 hepatocytes was added 100 μl of Protein Lysis Buffer (150 mM NaCl, 50 mM Tris pH 8, 1% NP-40, protease inhibitors by Roche). The lysate, after mild shaking, was collected by the use of a cell scraper, sonicated three times for 10 sec by the Soniprep-150 sonicator (Cellai) at the maximum power, and centrifuged for 15 min at 14000 rpm at 4°C. The supernatant was then separated, aliquoted and stored at –80°C until use.

2.5.4 Total protein extracts from tissues.

Mice used for the study of the origin of the tissue FN ($EDA^{wt/wt}$, $EDA^{+/+}$, $EDA^{+/+CRE}$) were firstly perfused with 25 ml of cold 1X PBS through the left ventricle of

the heart, following anesthetizing with 2.5% Avertin (15 µl per gram of body weight). Normally, all organs were immediately dissected from animals and snap-frozen in liquid nitrogen until use. All tissues were homogenized in 2 ml of Protein Lysis Buffer (150 mM NaCl, 50 mM Tris pH 8, 1% NP-40, protease inhibitors by Roche), whereas fibrotic livers and controls were homogenized in 0.5% Sodium Deoxycholate, 0.1% SDS, and protease inhibitors by Roche. Homogenization was carried out in series of 20 sec by using the UTRA-TURRAX T-25 basic homogenizer (Ika-Werke) and the homogenates were next sonicated two times for 15 sec by the Soniprep-150 sonicator (Cellai) at the maximum power, and centrifuged in a 5415-D rotor (Eppendorf) at 14000 rpm for 15 min. The liquid phase was separated and recentrifiged always at 4°C. Samples were then aliquoted and stored at –80°C until use. Protein sample concentration was determined by Bradford assay (Bio-Rad Protein Assay).

2.5.5 Sodium Dodecyl Sulfate-PolyAcrylamide Gel Electrophoresis (SDS-PAGE).

Proteins were separated running 20 to 150 µg of tissue or cellular samples or 0.2 µl of plasma or 2 µl of bile on a polyacrylamide gels. Proteins were mixed with 2X Protein Loading Buffer, denatured for 5 min at 95°C, ice-cooled and then loaded into the gels. The electrophoretic run was performed at 25-30 mA for 4-5 hrs using 1X Running Buffer for SDS-PAGE. 6% SDS-PAGEs were performed to visualize both pFN and cFN (~ 220 kDa). 10 % SDS-PAGEs were done to visualize vitronectin (VN, ~ 75 kDa), and 12 % SDS-PAGEs for β-Tubulin (~ 55 kDa), smooth muscle α-actin (αSMA, 45 kDa) and IgG (heavy chain ~ 58 kDa, light chain ~ 28 kDa). Solutions used for preparing the 5% stacking gels were: 30% acrylamide mix (Ultra pure Protogel, National Diagnostics) diluted 1:6, ½ volume of 0.5M Tris pH 6.8, 0.1% SDS, 0.1% Ammonium persulfate, 1µl/ml TEMED. Solutions used for preparing the running gels were: the right volume of 30% acrylamide mix, ½ volume of 1.5M Tris pH 8.8, 0.1% SDS, 0.1% Ammonium persulfate, 1µl/ml TEMED.

2.5.6 Western blot analysis.

Following electrophoresis, separated proteins were Coomassie-blue stained (see below) or blotted onto nitrocellulose membranes (Hybond-C Extra, Amersham Bioscience) at 200 mA for 2 hrs using 1X Protein Blotting Buffer supplemented with Methanol at 5, 10 or 20%. Next, membranes were blocked in 5-10% milk in 1X PBS for 1 hr at RT or O/N at 4 °C, stained with the primary antibody, washed 3 times for 5 min in 0.2-0.5% Tween-20 or Triton X-100 (Sigma) in 1X PBS, stained with a polyclonal horseradish-peroxidase-conjugated (HRP)-antibody (Dako Cytomation, 1:2000) directed against mouse, rabbit or goat Immunoglobulins (IgG) for 1 hr at RT, and washed again. A chemiluminescent reaction, generated by adding 3-4 ml of a chemiluminescent ECL-substrate (PIERCE) to the membrane, was used to impress films (Hyperfilm-ECL, Amersham Biosciences). Serial ECL expositions of the membranes were performed to determine the optimum linear range to quantify the signals. Films were then scanned with the Versadoc scanner (Bio-Rad) and quantified with the help of the Quantity One software package (Bio-Rad). Normally, two or three animals per genotype ($EDA^{wt/wt}$, $EDA^{+/+}$ $EDA^{-/-}$ $EDA^{wt/+}$, $EDA^{wt/+CRE}$ and $EDA^{+/+CRE}$) were analyzed.

2.5.7 Western blot conditions for the total FN detection in tissues, plasma and bile fluid.

To perform the 6% SDS-PAGE, 50 μg of tissue or cellular protein extract, 0.2 μl of plasma and 2 μl of bile were used. The gel blotting was done in presence of 5% methanol and the membrane blocking was done in 5% milk. The primary antibody was an anti-total FN polyclonal antibody developed in goat (Sigma), used diluted 1:2000 in 1% BSA, 0.2% Tween-20, 1X PBS for one hour at RT. The secondary antibody was an anti-goat IgG HRP-antibody (Dako), used diluted 1:2000 in 1% BSA, 0.2% Tween-20, 1X PBS for one hour at RT. Washes were performed in 0.2% Tween-20. The tissues analyzed were perfused liver, brain, lung, heart and testis.

2.5.8 Western blot conditions for EDA$^+$FN detection in plasma and tissues.

To perform the 6% SDS-PAGE, 150 μg of tissue protein extract and 2.5 μl of plasma were used. The gel blotting was done in presence of 5% methanol. The membrane blocking was done in 5% milk, followed by antigen unmasking by soaking the membrane in 6 M urea for 2 min in a microwave oven at half power. The primary antibody was an anti FN-EDA monoclonal antibody developed in mouse (Clone FN-3E2, Sigma), used diluted 1:300 in 1X PBS O/N at 4°C. The secondary antibody was an anti-mouse IgG HRP-antibody (Dako), used diluted 1:2000 in 1X PBS for one hour at RT. Washes were performed in 1X PBS. The tissues analyzed were perfused liver, brain, lung and testis.

2.5.9 Western blot conditions for VN detection in plasma and liver.

To perform the 10% SDS-PAGE, 50 μg of liver protein extract and 0.2 μl of plasma were used. The gel blotting was done in presence of 10% methanol; the membrane blocking was done in 5% milk. The primary antibody was an anti-total VN polyclonal antibody developed in rabbit (kindly provided by D. Seiffert, Scripps Research Institute, (Zheng et al., 1995)), used diluted 1:2000 in 0.5% Tween-20, 1X PBS for one hour at RT. The secondary antibody was an anti-rabbit IgG HRP-antibody (Dako), used diluted 1:2000 in 0.5% Tween-20, 1X PBS for one hour at RT. Washes were performed in 0.5% Tween-20. Membrane was then stripped and analyzed for the β-Tubulin (see below).

2.5.10 Western blot conditions for αSMA detection in liver.

To perform the 12% SDS-PAGE, 60 μg of tissue protein extract were used. The gel blotting was done in presence of 20% methanol; the membrane blocking was done in 10% milk. The primary antibody was an anti-αSMA monoclonal antibody developed in mouse (clone 1A4, Dako), used diluted 1:500 in 5% BSA, 0.2% Triton X-100, 1X PBS for 6 hrs at RT. The secondary antibody was an anti-mouse IgG HRP-antibody (Dako), used diluted 1:2000 in 5% BSA, 0.2% Triton X-100, 1X PBS for one hour at RT. Washes were

performed in 0.2% Triton X-100.

2.5.11 Western blot condition for IgG detection in liver and brain.

To determine the efficiency of perfusion and elimination of plasma proteins in each of the organs analyzed, a Western blot analysis of protein extract from liver and brain was performed using an anti-mouse IgG polyclonal HRP-antibody (Dako) as unique antibody. 50 μg of protein were run in a 12% SDS-PAGE. The gel blotting was done in presence of 20% methanol; the membrane blocking was done in 5% milk. The antibody was used diluted 1:2000 in 0.2% Tween-20, 1X PBS for one hour at RT. Washes were performed in 0.2% Tween-20. Membrane was then stripped and analyzed for the β-Tubulin (see below).

2.5.12 Western blot conditions for β-Tubulin detection in tissues.

To normalize the protein loads, 20 μg of protein from the same tissue extracts were run in a 12% SDS-PAGE. The gel blotting was done in presence of 20% methanol; the membrane blocking was done in 10% milk. The primary antibody was an anti β-Tubulin monoclonal antibody (Developmental Studies Hybridoma Bank, University of Iowa, E7), used diluted 1:3000 in 5% BSA, 0.2% Triton X-100, 1X PBS for one hour at RT. The secondary antibody was an anti-mouse IgG HRP-antibody (Dako), used diluted 1:2000 in 5% BSA, 0.2% Triton X-100, 1X PBS for one hour at RT. Washes were performed in 0.2% Triton X-100. The tissues analyzed were liver, brain, lung, heart and testis. When the β-Tubulin analysis was done by stripping of the membrane, were used the same antibody dilution buffers and washes of the primary antibody.

2.5.13 Stripping of the membranes.

Stripping was performed by soaking membranes in 200 ml of 2% SDS, 65.5 mM Tris pH 6.8 supplemented with 1.4 ml of β-Mercaptoethanol and incubation at 65°C for 45

min. After two washes in 1X PBS for 15 min and blocking in milk, membranes were stained with a different antibody.

2.5.14 Coomassie blue staining.

Following 10% SDS-PAGE, gels were soaked O/N in Coomassie Staining Solution (0.2% w/v Coomassie brilliant blue R, 10% glacial acetic acid, 40% methanol, 50% H_2O) and destained in 10% glacial acetic acid, 25% methanol, 65% H_2O until appearance of the bands.

2.5.15 Hydroxyproline assay.

Total collagen content was measured in fibrotic livers and controls via a conventional hydroxyproline assay (Bergman and Loxley, 1970). Briefly, the technique consists in the quantification of the hydroxyproline content of the collagen. Hydroxyproline is a very rare amino acid but it is particularly abundant in the collagen protein (14% of the total amino acid amount) and in a few other proteins. Experimental results were quantitated by comparison to a standard curve of known linear hydroxyproline (cis-4-Hydroxy-l-proline, Sigma) concentrations (from 200 μg/ml to 6.25 μg/ml) in 6N HCl solution. The whole liver was weighted, added to distilled H_2O to a final concentration of 400 mg/ml and homogenized. One ml of the homogenate was then added to 1 ml of 12N HCl (37%). Two 1 ml glass-vials (Sigma) were filled up with 500 μl of the acid mix, sealed with the help of a portable Bunsen's burner and baked at 120°C for 24 hrs in order to hydrolyze the proteins and release amino acids. Next, the amino acid mix was centrifuged in order to remove the burnt particles. In a 96 well plate, the following reaction was performed: to 5 μl of each amino acid sample and standard (in triplicate) was added 5 μl of Citrate-Acetate Buffer pH 6 (5% Citric acid, 1.2% Glacial Acetic acid, 7.24% Sodium Acetate, 3.4% Sodium Hydroxide, in H_2O) and 100 μl of Chloramine T solution (0.282 gr Chloramine T by Aldrich dissolved in 2 ml N-Propanol, 2 ml H_2O, 16 ml Citrate-

Acetate Buffer, and heated in water bath at 37°C until completely clear) to oxidate the hydroxypolines to pyrroles. Following incubation at RT for 30 min, 100 µl of Ehrlich's solution (2.5 gr Ehrlich's reagent [4-(Dimethylamino) benzaldehyde] by Sigma dissolved in 9.3 ml N-Propanol, 3.9 ml 70% Perchloric acid) was added to each well. The plate was next incubated at 65°C for 30 min to condensate the pyrroles to a red dyestuff. The concentration of the red dyestuff was evaluated by reading the plate at 540 nm in a plate-reader (SpectraCount, PACKARD).

2.6 EXPERIMENTAL MODELS FOR LIVER FIBROSIS.

Liver injury was induced either by Carbon Tetrachloride (CCl_4) administration as described (Constandinou et al., 2005) or by bile duct ligation (BDL) as described (Xia et al., 2006). At the indicated time (see below) animals were sacrificed, livers were excised and samples of the same portion of the left lobe were taken for RNA, protein and histological analysis (Figure 13).

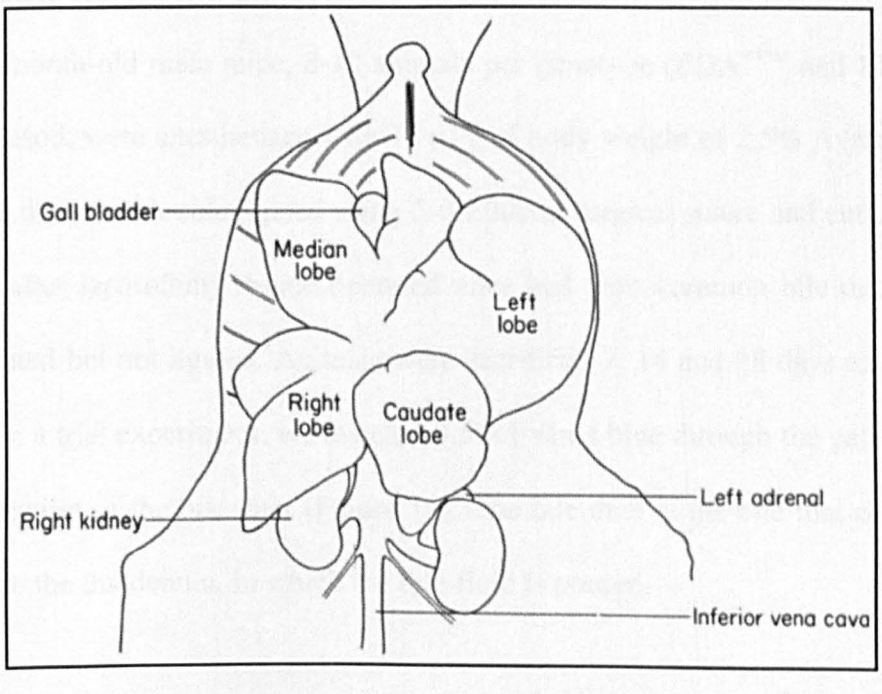

Figure 13. Schematic view of the mouse abdominal surface of the liver.
The left lobe was excised and the upper part was used for RNA extraction, the central part was fixed in 4% formaldehyde, the lower part was used for protein extraction.

2.6.1 Carbon Tetrachloride (CCl_4) intraperitoneal administration.

A chronic liver injury was induced in mice by intraperitoneal (IP) administration of CCl_4. All mice were 2/4-month-old male and age-mated. 8-10 animals were used for each genotype ($EDA^{wt/wt}$, $EDA^{+/+}$ and $EDA^{-/-}$) in each experiment. CCl_4 (Fluka) was diluted 1:4 (v/v) in mineral oil (Sigma) used as toxin vehicle. The mix was IP injected by a 0.5 ml insulin syringe (BD MICRO-FINE +) twice a week. Control mice were treated with mineral oil alone. A low- and middle-CCl_4 dose of 0.5 and 1.0 µl/gr of body weight, respectively, was administrated for a period of 5 weeks, whereas a high- and very high-CCl_4 dose of 1.5 and 2.0 µl/gr of body weight, respectively, was administrated for a period of 6 weeks. Following the intoxication period, mice were sacrificed three days after the last injection. For the CCl_4 surviving curve a total number of 30 animals per genotype ($EDA^{wt/wt}$ and $EDA^{-/-}$), 15 for each sex were IP injected with 2.0 µl/gr of body weight of CCl_4. The number of survivors was daily graph reported.

2.6.2 Bile duct ligation (BDL).

Two-month-old male mice, 8-10 animals per genotype ($EDA^{wt/wt}$ and $EDA^{-/-}$) and each BDL-period, were anesthetized with 15 µl/g of body weight of 2.5% Avertin and the common bile duct was double ligated using 5-0 Ethicon surgical suture and cut in between the stitches, after laparotomy. Sham-operated mice had their common bile duct exposed and manipulated but not ligated. Animals were sacrificed 7, 14 and 18 days after ligation of the duct. In a trial experiment, we injected 0.5% Evan's blue through the gall bladder to detect the position of the bile duct (Figure 14). The bile duct is the one that connects the gall bladder to the duodenum, in which the bile fluid is poured.

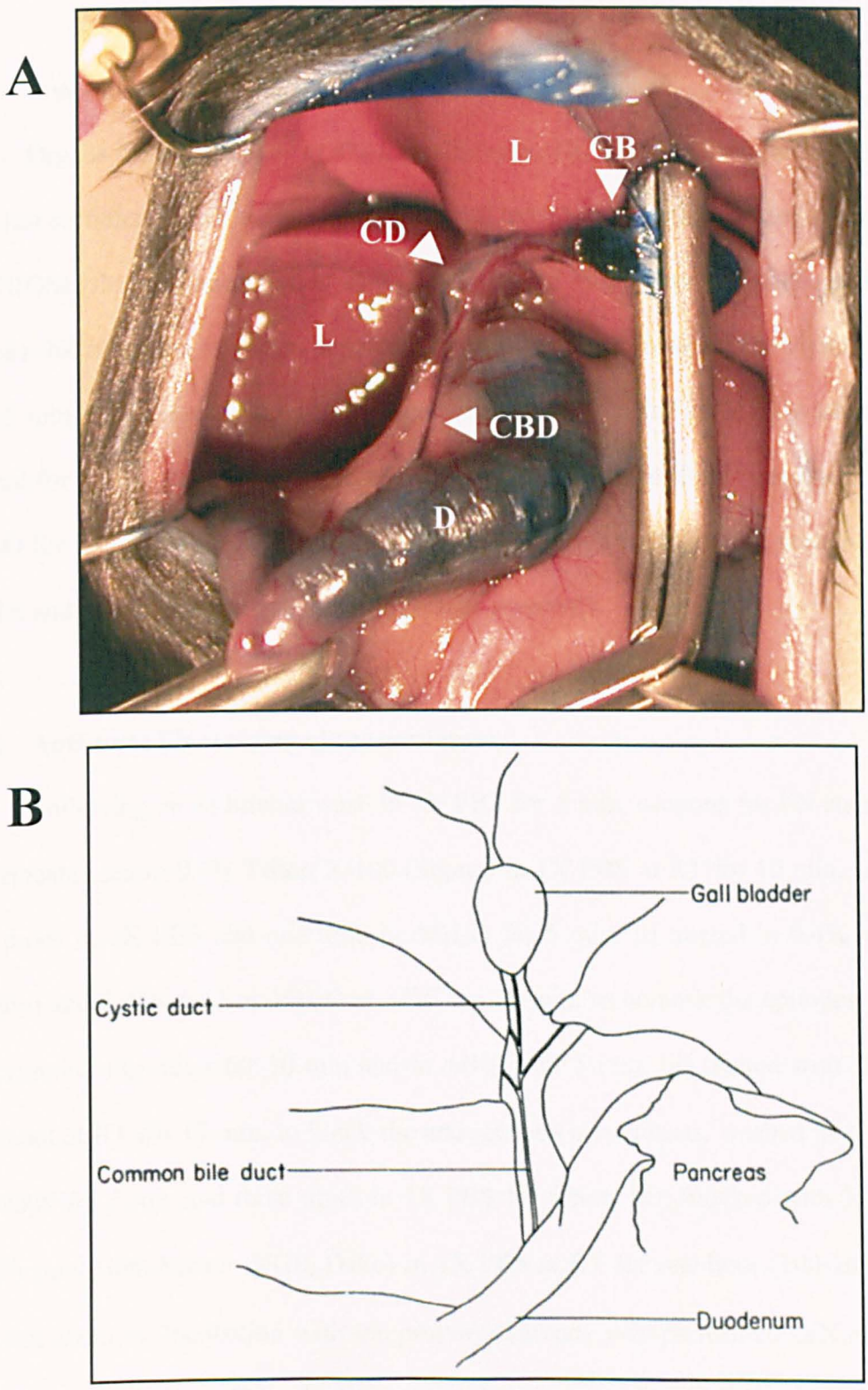

Figure 14. Mouse gall bladder and bile-duct.
A. The whole bile duct was identified by injection of 0.5% Evan's blue through the gall bladder. The common bile duct was double ligated with surgical suture and cut in between the stitches. **B.** Schematic representation of the of the upper real image. The bile duct connects the gall bladder to the duodenum. L, liver lobes; GB, gall bladder; CD, cystic duct; CBD, common bile duct; D, duodenum.

2.7 HISTOLOGICAL ANALYSIS.

2.7.1 Immunohistochemistry of tissue sections.

Organs were fixed O/N in 4% formaldehyde, 1X PBS and then paraffin embedded. Four μm sections of each tissue (liver, brain and testis) were cut by the use of a microtome (MICROM HM 400) and dried at 37°C for 24 hrs on microscope slides (SuperFrost/Plus, Kaltek). Each section was then deparaffined by soaking of the slides in Xylene (Aldrich) for 15 min (two times) and hydrated by the following alcohol scale: 2 washes in 100% ethanol for 5 min, 1 wash in 95%, 80%, 70%, and 50% ethanol for 5 min, and 2 washes in ddH_2O for 5 min. Hydrated sections were then stained for the following proteins: total FN, αSMA and collagen, accordingly the following protocols:

2.7.2 Anti-total FN staining of the sections.

Following an additional wash in 1X PBS for 5 min, sections for FN staining were: i) permeabilized in 0.5% Triton X-100 (Sigma) in 1X PBS at RT for 10 min, and washed two times in 1X PBS and one time in ddH_2O for 5 min; ii) treated in 0.4% w/v Pepsin (Sigma) and 0.01N HCl in ddH_2O at 37°C for 30 min, to unmask the epitopes, washed in cold running tap water for 10 min and in ddH_2O for 5 min; iii) treated with 3% H_2O_2 in methanol at RT for 15 min, to block the endogenous peroxidases, washed in cold running tap water for 5 min and three times in 1X PBS for 5 min; iiii) blocked with 3% BSA and 1% Normal Goat Serum (NGS, Dako) in 1X PBS at RT for one hour (100-200 μl of mix for each section). Incubation with the primary antibody was performed O/N at 4°C using an affinity-purified anti-FN polyclonal antibody developed in rabbit (Sigma) diluted 1:200 in 3% BSA, 1X PBS (100-200 μl of mix for each section), following blocking-buffer removal by slide inversion. Slides were then washed in 0.05% Tween-20 (Sigma), 1X PBS three times for 5 min. Incubation with the secondary antibody was performed for one hour at RT using a biotinylated anti-rabbit IgG developed in goat (Vector) diluted to a final

concentration of 5 μg/ml in 3% BSA, 2% NGS in 1X PBS (100-200 μl of mix for each section). Slides were then washed in 0.05% Tween-20, 1X PBS three times for 5 min. Incubation with the biotinylated secondary antibody was followed by incubation with a preformed Avidin and Biotinylated Horseradish Peroxidase macromolecular complex (1-2 drops of R.T.U. ABC reagent for each section, Vector) for one hour at RT. Slides were then washed in 0.05% Tween-20, 1X PBS three times for 5 min. As a peroxidase substrate the DAB substrate mix (Vector) was used. Incubation was done with 100-200 μl of DAB mix for each section for 4 min, followed by one wash in cold running tap water and one in ddH_2O for 5 min. Sections were then stained for 2 min in Gill's Hematoxylin (Vector), washed with cold running tap water and ddH_2O for 5 min, dehydrated repeating the alcohol scale but up-side-down, up to the xilene. Each slide was mount with a micro cover glass (Prestige) using Eukitt quick-hardening mounting medium (Fluka). A Leica DM LA microscope was used to visualize and photograph the sections.

2.7.3 Anti-αSMA staining of the liver sections.

Hydrated sections were firstly subjected to antigen unmasking with 10 mM Sodium Citrate buffer pH 6 (18 ml/L 0.1M Citric acid, 82 ml/L 0.1M Sodium Citrate in H_2O) for 20 min at a sub-boiling temperature on a hot stirrer. Slides were then cooled on the bench for 20 min. After washing with cold running tap water for 10 min, sections were treated with 3% H_2O_2 in methanol at RT for 30 min, to block the endogenous peroxidases. After washing in cold running tap water for 5 min and three times in 1X PBS for 5 min, sections were blocked with 5% BSA and 5% Normal Goat Serum (NGS, Dako) in 1X PBS at RT for 2 hrs (100-200 μl of mix for each section). Incubation with the primary antibody was performed for one hour at RT using anti-αSMA monoclonal antibody developed in mouse (clone 1A4, Dako) diluted 1:80 in 5% BSA, 1X PBS (100-200 μl of mix for each section), following blocking buffer removal by slide inversion. Slides were then washed in 0.2% Tween-20 (Sigma), 1X PBS three times for 5 min. Incubation with the secondary antibody

was performed for one hour at RT using a biotinylated anti-mouse IgG developed in goat (Vector) diluted to a final concentration of 2.5 μg/ml in 5% BSA, 5% NGS, 2% Normal Mouse Serum in 1X PBS (100-200 μl of mix for each section). Slides were then washed in 0.2% Tween-20, 1X PBS three times for 5 min. Incubation with the biotinylated secondary antibody was followed by incubation with a preformed Avidin and Biotinylated Horseradish Peroxidase macromolecular complex (1-2 drops of R.T.U. ABC reagent for each section, Vector) for 30 min at RT. Slides were then washed in 0.2% Tween-20, 1X PBS three times for 5 min. As a peroxidase substrate, the DAB substrate mix (Vector) was used. Incubation was done with 100-200 μl of DAB mix for each section for 10 min, followed by one wash in cold running tap water and one in ddH_2O for 5 min. Sections were next dehydrated repeating the alcohol scale up to the xilene. Each slide was mount with a micro cover glass (Prestige) using Eukitt quick-hardening mounting medium (Fluka). A Leica DM LA microscope was used to visualize and photograph the sections.

2.7.4 Trichrome staining of the liver sections.

Liver sections were subjected to the Gomori's Trichrome staining for collagen fibers (Accustain Trichrome Stain Gomori, Sigma-Aldrich) accordingly to the manufacturers' protocol. Briefly, slides were soaked in Bouin's Solution (Sigma-Diagnostics) for 15 min in a water bath at 56°C, to intensify the final coloration of the tissue. After cooling on the bench up to RT, slides were washed in cold running tap water until removal of the yellow color from the sections and in ddH_2O for 5 min. Next, the slides were soaked in the working Weigert's Iron Hematoxylin solution for 1.5 min to stain nuclei blue-black. Working solution was prepared by mixing 1:1 the solution A (1% Certified Hematoxylin by Sigma, in ethanol) with the solution B (1.2% w/v Ferric Chloride and 1% v/v Hydrochloric acid). After washing in cold running tap water and in ddH_2O for 5 min, sections were stained by socking the slides in Trichrome Stain AB Solution (Sigma-Aldrich) for 5min, to stain collagen fibers blue. Next slides were briefly rinsed in ddH_2O

and in 0.5% Acetic acid for 1.5 min to remove the color in excess and to render the shades of color more delicate and transparent, respectively. Slides were again rinsed in ddH_2O, dehydrated through alcohol, cleared in xilene, mounted and photographed as described above.

2.7.5 Immunofluorescence of cultured hepatocytes.

Purified hepatocytes from $EDA^{wt/wt}$ $EDA^{+/+}$ livers were plated on 15 mm 1% rat-tail collagen-containing glass disk in a 12 well plate and incubated at 37°C with 1 ml of culture medium (Dulbecco's Modified Eagle Medium supplemented with 10% fetal bovine serum, Gibco) for 24 and 48 hrs before staining for total FN. Each disk-containing well was emptied out of the culture medium, washed with 1 ml of cold 1X PBS for two times and cells were fixed with 1 ml of 3% paraformaldeyde at RT for 20 min. After washing with 1 ml of 1X PBS for two times, cells were permeabilized with 1 ml of 0.5% Triton X-100 (Sigma) for 5 min, washed, saturated with 1 ml of 0.2% BSA, 20 mM Glycine in 1X PBS at RT for 30 min, and washed again. Next, each disk was incubated with 20 µl of affinity-purified anti-FN polyclonal antibody developed in rabbit (Sigma) diluted 1:400 in 0.2% BSA, 1X PBS at RT for one hour. After 2 washes with 1 ml of 0.05% Tween X-100, 1X PBS, disks were incubated with 20 µl of anti-rabbit fluorescein-conjugated immunoglobulins (FITC green, DAKOPATTS) diluted 1:80 in 0.2% BSA, 1X PBS at RT for one hour. After washing, nuclei were stained with 1 ml of 4',6-diamidino-2-phenylindole (DAPI blue, Invitrogen) diluted 1:10000 in 1X PBS at RT for 5 min (Hoetscht staining). After 2 washes in 1X PBS and one in ddH_2O, disks were mounted up-side-down on microscope slides (SuperFrost/Plus, Kaltek) with the Faramount aqueous mounting medium (Dako). A Leica DM LB fluorescent microscope was used to visualize and photograph the cells.

2.8 STATISTICAL ANALYSIS.

All bar graphs, the Standard Deviation (SD) and the Student's T-test were drawn and calculated, respectively, with the help of Microsoft Excel software. A p-value of 0.05 was chosen as the limit of statistical significance in the T-test. Quantification of the collagen-positive areas (trichrome staining) of liver sections was carried out by counting of the pixels of the fibrotic areas with the help of the Adobe Photoshop software. Log-rank test statistical analysis was used to evaluate the survival curves (Kaplan-Meier graph).

3.1 ORIGIN OF TISSUE FIBRONECTIN.

3.1.1 Plasma from EDA$^{+/+}$ mice does not contain normal levels of pFN.

We have previously observed that the mouse strain that constitutively include the EDA exon of the FN gene (EDA$^{+/+}$) have a significant decrease of FN in plasma and in most tissues (Chauhan et al., 2004; Muro et al., 2003). Further characterization of pFN levels of embryos, young and adult EDA$^{+/+}$ mice showed very low amounts of FN compared to EDA$^{wt/wt}$ and EDA$^{-/-}$ mice (Figure 15). Same amounts of plasma proteins were run in a 6% SDS-PAGE and blotted onto nitrocellulose. The nitrocellulose membrane was subsequently stained with an antibody anti total FN (Figure 15A). Quantification of the Western blots revealed that embryos had 60% of the pFN levels of the control samples (Figure 15B). A further decrease in pFN levels occurred in 1-day-old newborns and 7-day-old EDA$^{+/+}$ pups. The pFN levels stabilized at 20% of control levels in mice older than 7 days (Figure 15B). Western blot analysis of the same samples using an EDA-specific monoclonal antibody revealed the complete absence of EDA domain in pFN of the EDA$^{wt/wt}$ mice at all time points analyzed (Figure 15C). As expected, a positive signal was present only in the EDA$^{+/+}$ samples, confirming the progressive decrease of the pFN levels in EDA$^{+/+}$ blood (Figure 15C) associated with age.

3.1.2 Liver from EDA$^{+/+}$ mice contains normal levels of ECM-FN and other extracellular matrix (ECM) proteins.

Next, we examined whether the depletion of pFN from EDA$^{+/+}$ plasma could be correlated to variations of other ECM proteins or FN itself in liver. As previously shown, EDA$^{+/+}$ animals revealed evident decreased levels of FN in almost all EDA$^{+/+}$ tissues when compared to the control mice (Muro et al., 2003).

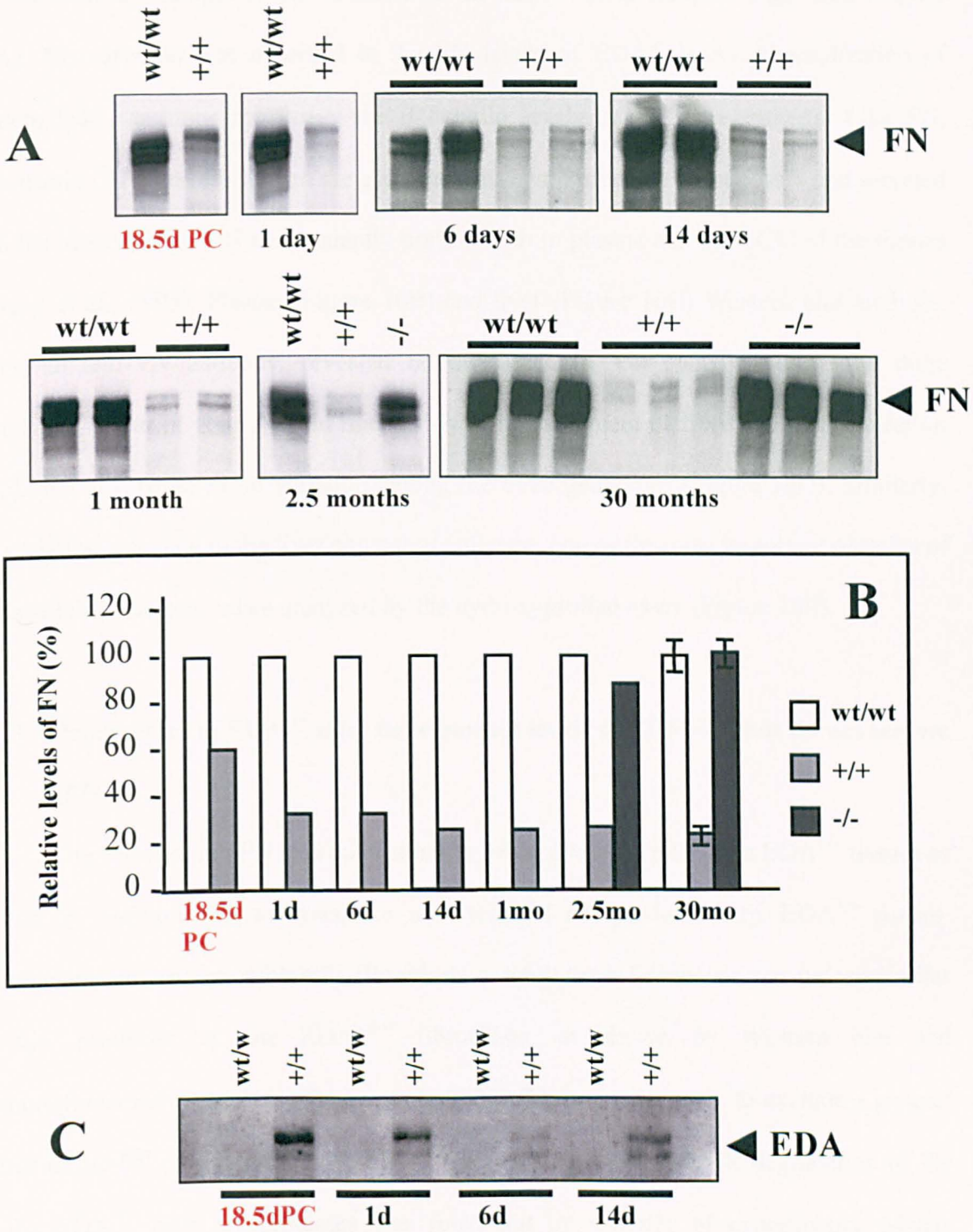

Figure 15. Plasma from EDA$^{+/+}$ mice does not contain normal levels of pFN.
A. Western-blot analysis of pFN from 18.5 pc embryos, 1, 6 and 14 day-old babies, 1, 2.5 and 30 month-old young and adult mice from EDA$^{wt/wt}$, EDA$^{+/+}$ and EDA$^{-/-}$ animals. Equal quantities of plasma were separated in a 6% SDS-PAGE, blotted onto nitrocellulosa and probed for FN with an anti-FN polyclonal antibody, followed by chemiluminescence. **B.** Quantification of the chemiluminescent signals. Serial ECL expositions of the membranes were performed to determine the optimum linear range before quantifying the signals. pFN levels are relative to the wild-type levels considered as 100%. **C.** Western-blot analysis of pFN from 18.5 pc embryos, 1, 6 and 14 day-old babies from EDA$^{wt/wt}$ and EDA$^{+/+}$ animals using an anti-EDA monoclonal antibody.

On the contrary, similar levels of ECM-FN in $EDA^{+/+}$ liver samples were seen (Figure 16A). No variation was observed in the FN levels of $EDA^{-/-}$ livers. Normalization of protein load was done measuring the β-Tubulin levels in the same extracts. Like FN, vitronectin (VN) and fibrinogen are glycoproteins synthesized by hepatocytes and secreted into the bloodstream. VN is abundantly present both in plasma and the ECM of the tissues (Zheng et al., 1995). Plasma (Figure 16B) and liver (Figure 16C) Western blot analysis, using an anti-VN antibody, revealed no difference in VN content among the three genotypes, either in young or old mice. *In vitro* measurement of fibrinogen concentration in plasma also revealed no variation among the three genotypes (Figure 16D). Similarly, no variation was seen in the liver content of collagen, one of the most important proteins of extracellular matrixes, when analyzed by the hydroxyproline assay (Figure 16E).

3.1.3 Hepatocytes of $EDA^{+/+}$ mice have normal levels of ECM-FN but do not secrete pFN.

The decrease in pFN was due neither to lower levels of mRNA in $EDA^{+/+}$ tissues as shown by Northern-blot analysis, nor to a reduced FN production by $EDA^{+/+}$ tissues. Fibronectin secreted by embryonic fibroblasts or adult heart fibroblasts was indeed similar to that produced by the $EDA^{wt/wt}$ fibroblasts, as shown by Western blot and immunofluorescence analyses (Muro et al., 2003). These results seem to exclude a general defect in the FN production by the $EDA^{+/+}$ tissues. Moreover, specific degradation of FN in the $EDA^{+/+}$ mice by proteases was ruled out by a series of experiments. Matrix metalloproteinases (MMPs) are enzymes responsible for remodeling of the extracellular matrixes (Nagase et al., 2006). Consequently, we evaluated the MMPs activity present in plasma and tissues. The same amount of plasma and tissue samples from $EDA^{wt/wt}$, $EDA^{+/+}$ and $EDA^{-/-}$ mice was loaded in a gelatin-SDS polyacrylamide gel and the activity of metalloproteinases was determined by gelatin zymography analysis.

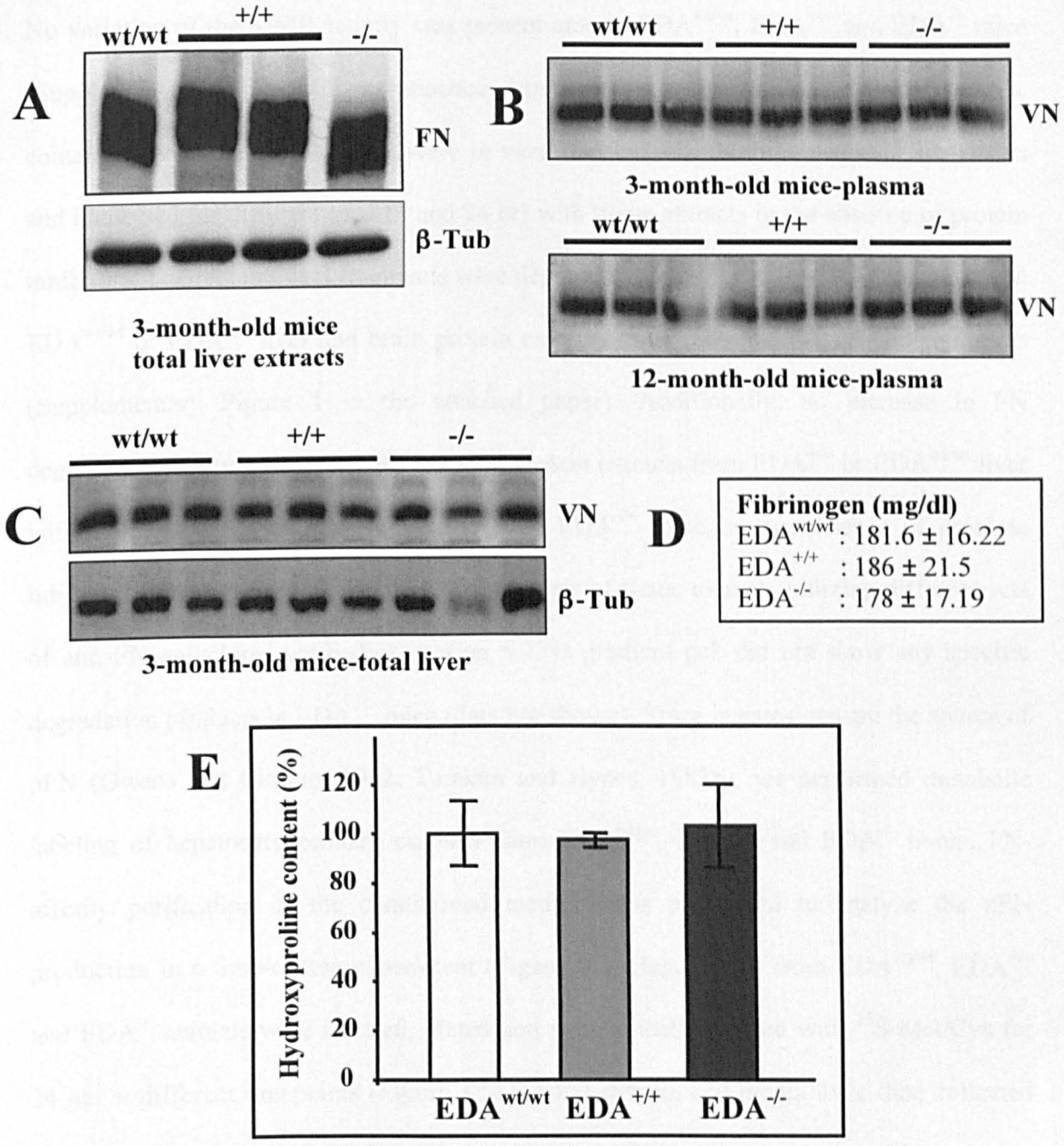

Figure 16. Liver from EDA$^{+/+}$ mice contains normal levels of ECM-FN and other extracellular matrix (ECM) proteins.

A. Western-blot analysis of ECM-FN of total liver extracts from EDA$^{wt/wt}$, EDA$^{+/+}$ and EDA$^{-/-}$ animals. Equal quantities of protein were separated in a 6% SDS-PAGE, blotted onto nitrocellulose and probed for FN with an anti-FN polyclonal antibody, followed by chemiluminescence. **B. and C.** Western-blot analysis of vitronectin (VN) in plasma (Panel B) and total liver extracts (Panel C) from EDA$^{wt/wt}$, EDA$^{+/+}$ and EDA$^{-/-}$ young and old animals. Equal quantities of protein were separated in a 12% SDS-PAGE and probed for VN with an anti-VN polyclonal antibody. Normalization was done by measurement of the β-Tubulin levels after stripping of the anti-FN and anti-VN membranes. **D.** *In vitro* measurement of fibrinogen levels in plasma of the three geneotypes. **E.** Quantification of liver collagen by hydroxyproline (HP) assay. The content of HP is relative to the wild-type levels considered as 100%. N = 4 for each genotype.

No variation of the MMP activity was present among $EDA^{wt/wt}$, $EDA^{+/+}$ and $EDA^{-/-}$ mice (Supplementary Figure 1 in the attached paper). Moreover, recombinant FN fragments, containing or not the EDA exon, were *in vitro* translated in the presence of ^{35}S-Met/Cys and incubated for different time (3 and 24 hr) with tissue extracts in the absence of protein inhibitors. The recombinant fragments were degraded at the same rate when incubated with $EDA^{wt/wt}$ or $EDA^{+/+}$ liver and brain protein extracts in the absence of protease inhibitors (Supplementary Figure 1 in the attached paper). Additionally, no increase in FN degradation rate was observed after mixing protein extracts from $EDA^{+/+}$ or $EDA^{wt/wt}$ liver with different organ extracts or plasma from $EDA^{+/+}$ mice, in the absence of protease inhibitors (data not shown). Western blot analysis of tissue extracts utilizing different sets of anti-FN polyclonal antibodies, run on 5-17% gradient gel, did not show any specific degradation products in $EDA^{+/+}$ mice (data not shown). Since hepatocytes are the source of pFN (Owens and Cimino, 1982; Tamkun and Hynes, 1983b), we performed metabolic labeling of hepatocyte primary cultures from $EDA^{wt/wt}$, $EDA^{+/+}$ and $EDA^{-/-}$ livers. FN-affinity purification of the conditioned medium was performed to analyze the pFN production in a time-course experiment (Figure 17). Hepatocytes from $EDA^{wt/wt}$, $EDA^{+/+}$ and $EDA^{-/-}$ animals were isolated, plated and metabolically labeled with ^{35}S-Met/Cys for 24 hrs at different timepoints (Figure 17A). Total conditioned media were then collected and run on a 6% SDS-PAGE (Figure 17C). Additionally, equal quantities of total conditional media from the three genotypes were affinity purified with a gelatin-agarose resin, eluted and separated through a SDS-PAGE (Figure 17D). Autoradiograph analysis (Figure 17C and D) revealed a clear decrease in soluble FN levels in the $EDA^{+/+}$ mice, due to reduced secretion of pFN by the $EDA^{+/+}$ hepatocytes. Cellular extracts prepared from equal number of cultured hepatocytes from $EDA^{wt/wt}$, $EDA^{+/+}$ and $EDA^{-/-}$ mice were analyzed by Western blot with a polyclonal anti-FN antibody. Similarly to what occurs *in vivo* (Figure 16A), the FN levels were similar in the three genotypes (Figure 17B).

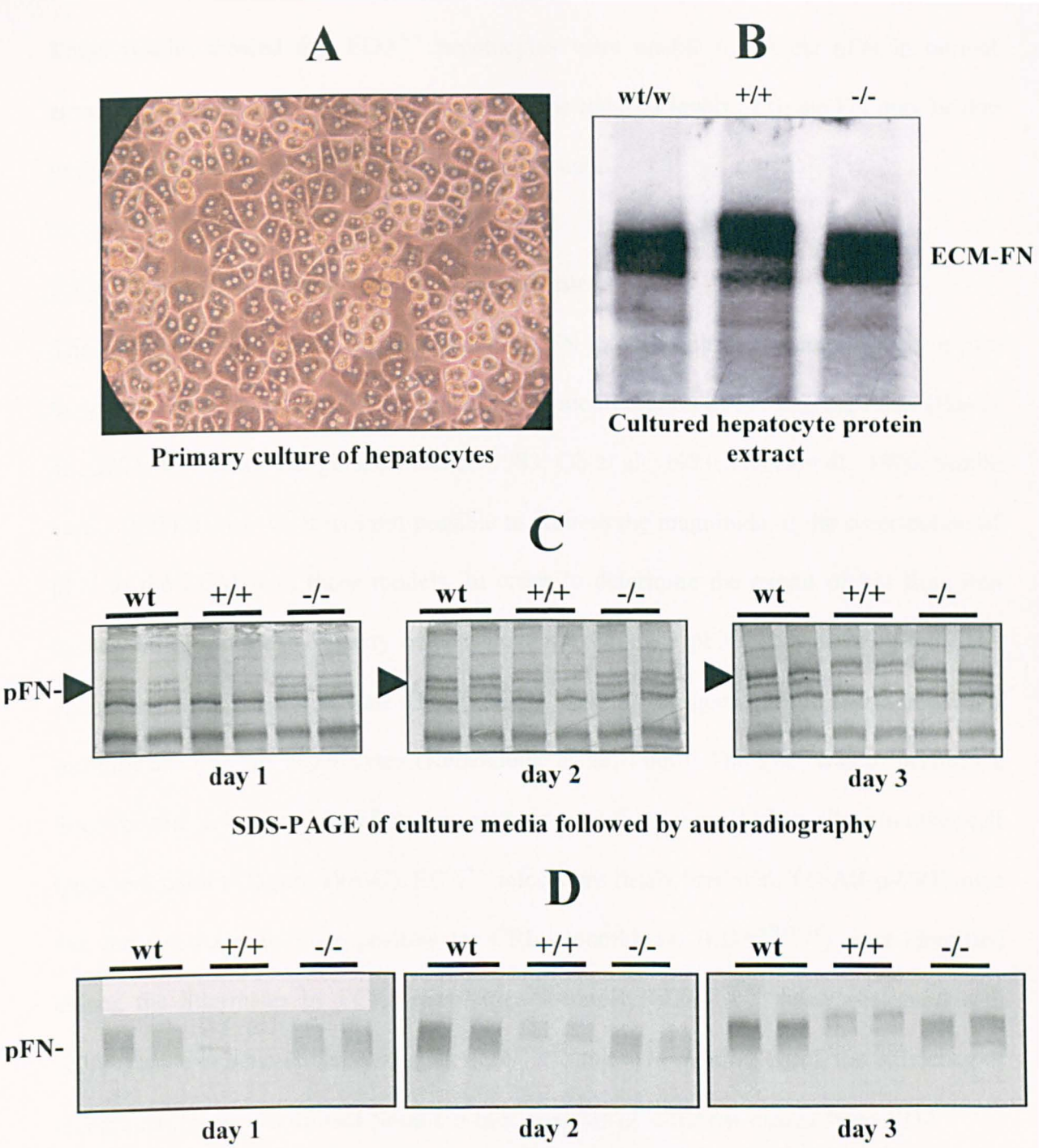

Figure 17. Hepatocytes of EDA$^{+/+}$ mice have normal levels of ECM-FN but do not secrete pFN.

A. Hepatocytes from a primary culture. **B.** Cell extracts prepared with an equal number of hepatocytes from EDA$^{wt/wt}$, EDA$^{+/+}$ and EDA$^{-/-}$ livers were analyzed by Western blot using an anti-FN polyclonal antibody. **C.** Hepatocytes from EDA$^{wt/wt}$, EDA$^{+/+}$ and EDA$^{-/-}$ livers were isolated, plated and metabolically labeled with ^{35}S-Met/Cys for 24 hrs. An autoradiographic analysis of equal amounts of the conditioned medium run on a 6% SDS-PAGE is shown. **D.** Equal quantities of samples prepared in C were affinity purified with a gelatin-agarose resin, eluted, separated in an SDS-PAGE and autoradiographed.

These results showed that $EDA^{+/+}$ hepatocytes were unable to secrete pFN in normal amounts. Consequently, we hypothesized that the reduced levels of tissue FN may be due to the decreased supply of FN from plasma to tissues.

3.1.4 Generation of liver-specific EDA-null mice.

The addition or injection of exogenous soluble FN into the culture medium of cells or into the plasma of mice, respectively, resulted in the incorporation of FN into the ECM (Bae et al., 2004; McKeown-Longo and Mosher, 1983; Oh et al., 1981; Peters et al., 1990; Sottile et al., 1998). However, it was not possible to address the magnitude of the contribution of pFN to the ECM with those models. In order to determine the extent of FN flow into tissues we restored the capacity of hepatocytes to produce pFN not containing the EDA exon: we crossbred our floxed $EDA^{+/+}$ strain with a transgenic strain expressing CRE recombinase only in hepatocytes (Kellendonk et al., 2000). The goal was to perform a liver-specific deletion of the EDA exon without modifying the $EDA^{+}FN$ allele in other cell types and tissues (Figure 18A-C). $EDA^{+/+}$ mice were firstly bred with TG-Alf-p-CRE mice and the heterozygous mice positive for CRE recombinase ($EDA^{wt/+CRE}$) were identified among the littermates by PCR genotyping. Secondly, $EDA^{wt/+CRE}$ mice were bred with $EDA^{+/+}$ mice to generate homozygous $EDA^{+/+CRE}$ mice. In order to check the efficiency of recombination we performed Southern blot analysis of different tissues from $EDA^{wt/+CRE}$ and $EDA^{+/+CRE}$, both strains carrying the liver-specific CRE recombinase (Figure 19). Hybridization of the membranes with a probe corresponding to the exon downstream of the EDA exon (Figure 19C) showed CRE-mediated recombination only in the liver and not in other tissues (Figure 19A and B). The recombination efficiency in the liver was ~ 60-70% and, consequently, in hepatocytes was close to 100% considering that they constitute ~ 60% of the total number of cells present in the liver, although they occupy 80% of volume of parenchyma (Malarkey et al., 2005). To further check the efficiency of recombination, we performed analyses of the transcription and translation products (Figure 20). RT-PCR

analysis of total RNA clearly showed the absence of the EDA exon both in liver and purified hepatocytes from $EDA^{+/+CRE}$ mice (Figure 20A). In agreement with the RT-PCR result, Western blot analysis using an anti-EDA monoclonal antibody confirmed the absence of the domain both in $EDA^{+/+CRE}$ plasma and liver FN, similarly to the wild-type condition (Figure 20B). As expected, a positive signal was present only in the $EDA^{+/+}$ protein samples.

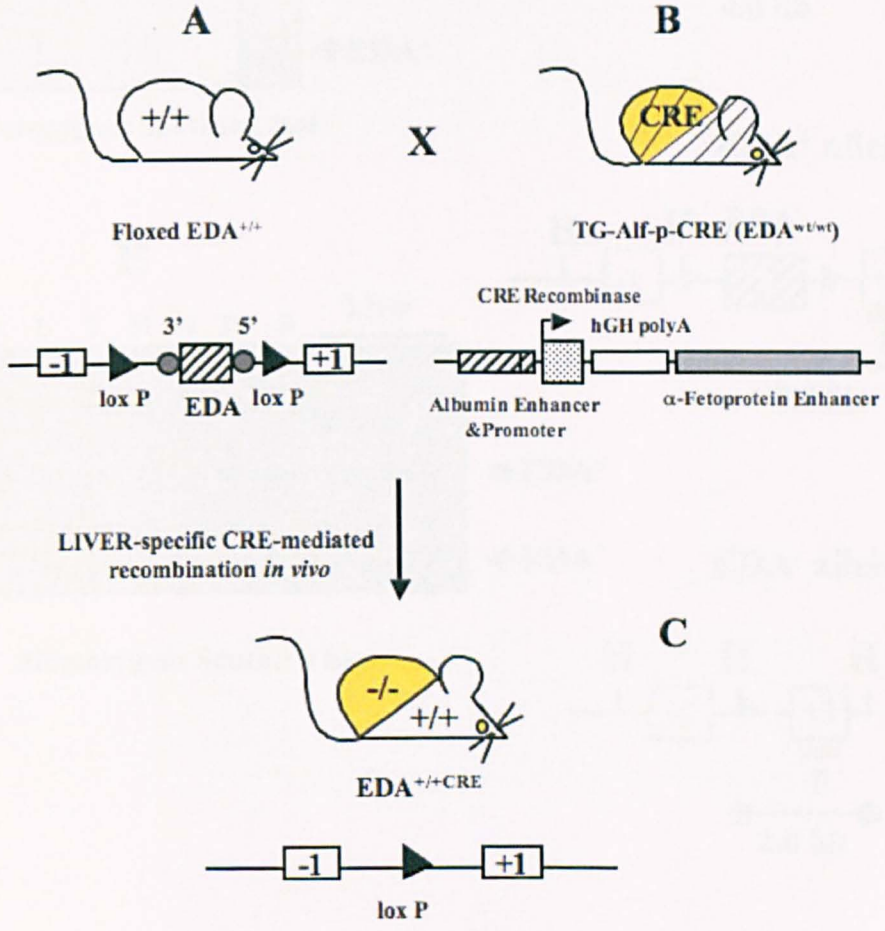

Figure 18. Generation of liver-specific EDA-null mice.
The floxed $EDA^{+/+}$ mice (Panel A) were crossed with a transgenic strain expressing the CRE-recombinase in hepatocytes (Panel B) in order to obtain a liver-specific deletion of the EDA exon and maintain the EDA^{+} condition in the rest of the body (Panel C). Schemes of the floxed and optimized EDA^{+} and that of the EDA^{-} FN alleles are shown (Panels A and C). The EDA exon is indicated as a dashed box, the loxP sites as black triangles, -1 and +1 are the exons upstream and downstream of EDA, respectively. A scheme of the Alf-P-CRE transgene is shown (Panel B). The CRE recombinase (dotted box) is expressed under the control of the mouse albumin enhancer and promoter (dashed box) and the mouse alpha-fetoprotein enhancer (gray box). Correct polyadenylation was directed by the hGH fragment (empty box).

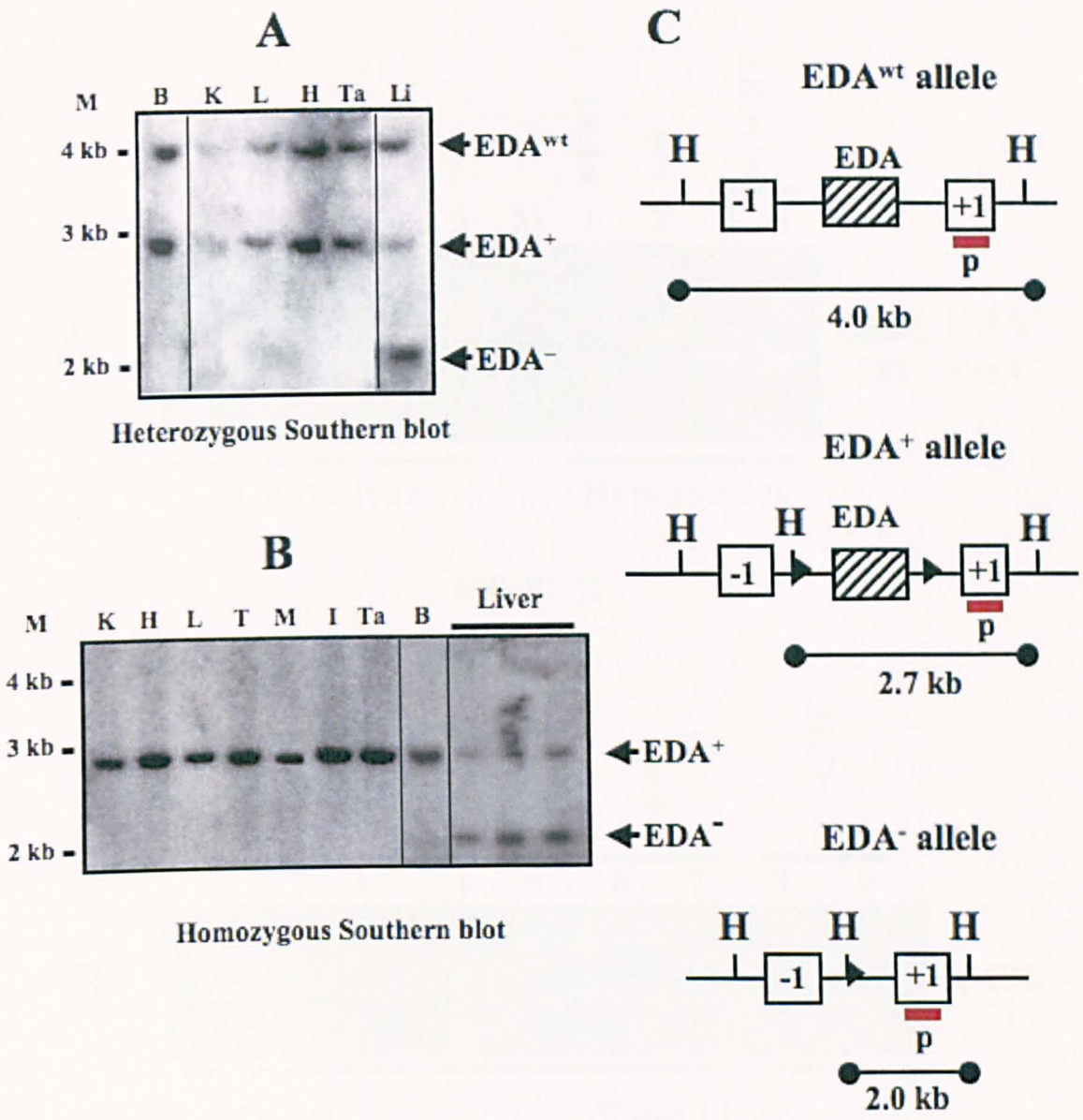

Figure 19. Liver-specific deletion of the EDA exon.

A. and B. Southern blot analysis of different tissues from heterozygous $EDA^{wt/+CRE}$ (Panel A) and homozygous $EDA^{+/+CRE}$ (Panel B) mice. Specific recombination was observed only in the liver. EDA^{wt}, EDA^{+} and EDA^{-} bands are indicated. Liver DNA samples from three mice are shown in Panel B. Tissues are as indicated: K, kidney; H, heart; L, lung; T, testis; M, skeletal muscle; I, intestine; Ta, tail; B, brain; Li, liver. **C.** Schematic representation of the EDA^{wt}, EDA^{+} and EDA^{-} FN alleles. The EDA exon is indicated as a dashed box, the loxP sites as black triangles. Hind III sites (H), the probe used in Panel A and B (red line below +1 exon), the flanking exons (-1 and +1) and the expected size of Hind III-digested fragments are indicated.

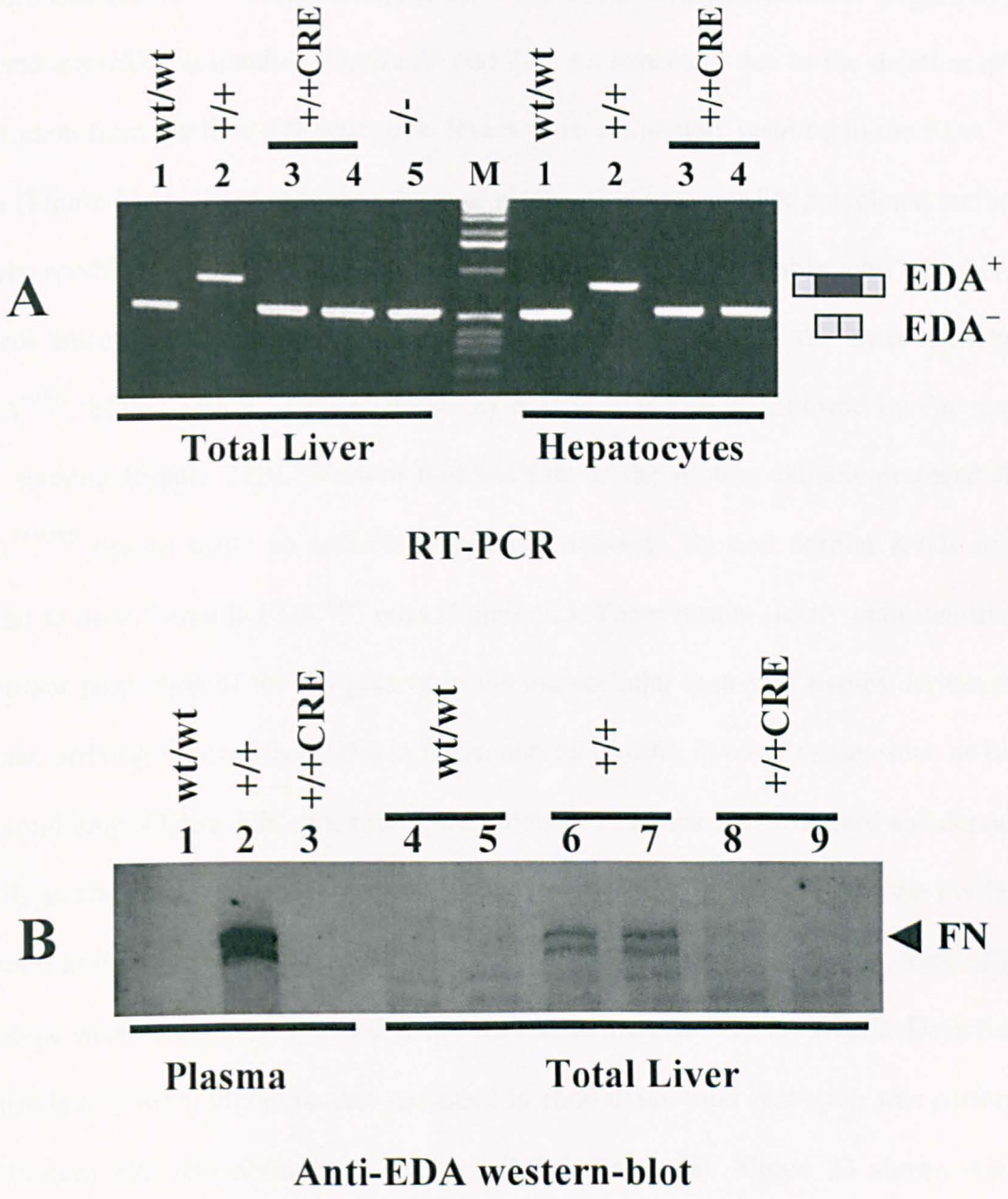

Figure 20. EDA exon and domain are missing from the liver FN mRNA and protein, respectively, of EDA$^{+/+CRE}$ animals.

A. RT-PCR analysis showing the inclusion/exclusion of the EDA exon in total RNA prepared from liver and purified hepatocytes from different genotypes. The position of the EDA^{+} and EDA^{-} bands are indicated. **B.** Plasma and liver protein extracts prepared from EDA$^{wt/wt}$, EDA$^{+/+}$ and EDA$^{+/+CRE}$ mice were analyzed for the presence of the EDA domain using the anti-EDA monoclonal antibody 3E2.

3.1.5 FN levels are restored in $EDA^{+/+CRE}$ mice.

Plasma and tissues from $EDA^{+/+}$ mice expressing the hepatocyte-specific CRE recombinase ($EDA^{+/+CRE}$) were analyzed by Western blot with anti-total FN (Figure 21 and 22) and anti-EDA antibodies (Figure 20 and 24). As expected, due to the deletion of the EDA exon from the liver FN gene, pFN levels were completely restored in the $EDA^{+/+CRE}$ mice (Figure 21A). Western blot analysis of plasma using an anti-FN polyclonal antibody, clearly revealed in $EDA^{+/+CRE}$ mice normal levels of pFN comparable with those of the control mice ($EDA^{wt/wt}$). Plasma protein loads were similar in the three genotypes ($EDA^{wt/wt}$, $EDA^{+/+}$, $EDA^{+/+CRE}$) as shown by a 10% SDS-PAGE followed by Coomassie blue staining (Figure 21B). Western blot analysis of the protein extracts prepared from $EDA^{+/+CRE}$ organs using an anti-FN polyclonal antibody showed normal levels of FN similar to those found in $EDA^{wt/wt}$ ones (Figure 22). These results clearly indicated that an important proportion of the FN present in the extracellular matrix of tissues derives from plasma, arriving to more than 60% in testis, and up to 40% in other tissues such as brain, heart and lung (Figure 22B). Therefore, the amount of FN that is synthesized and deposited locally in the tissues is much lower than believed. In order to rule out that the FN levels detected in the tissues could be contaminated by circulating plasma proteins, mice of each genotype were abundantly perfused with PBS before dissection of the organs. Detection of the levels of plasma globulins that remained in each tissue after perfusion was performed by Western blot and normalized with the β-Tubulin signal. Figure 23 shows that the remaining globulin levels after tissue perfusion were less than 10% of the levels seen in the non-perfused organs. This finding indicated that the differences of FN levels among the different strains were not due to residual contamination of pFN, since most of plasma proteins were washed-out from the perfused organs. To confirm that the variation of FN levels detected in tissues were only due to variation of pFN and not cFN, we performed Western blot analysis using a monoclonal antibody to specifically detect the EDA-containing FN isoform. As expected, we could observe no differences in EDA^{+}cFN levels

of the $EDA^{wt/wt}$, $EDA^{+/+}$and $EDA^{+/+CRE}$ brain, lung and testis (Figure 24A-C) tissues. Quantification of the testis FN and its normalization with β-Tubulin is shown in the bar graph (Figure 24D).

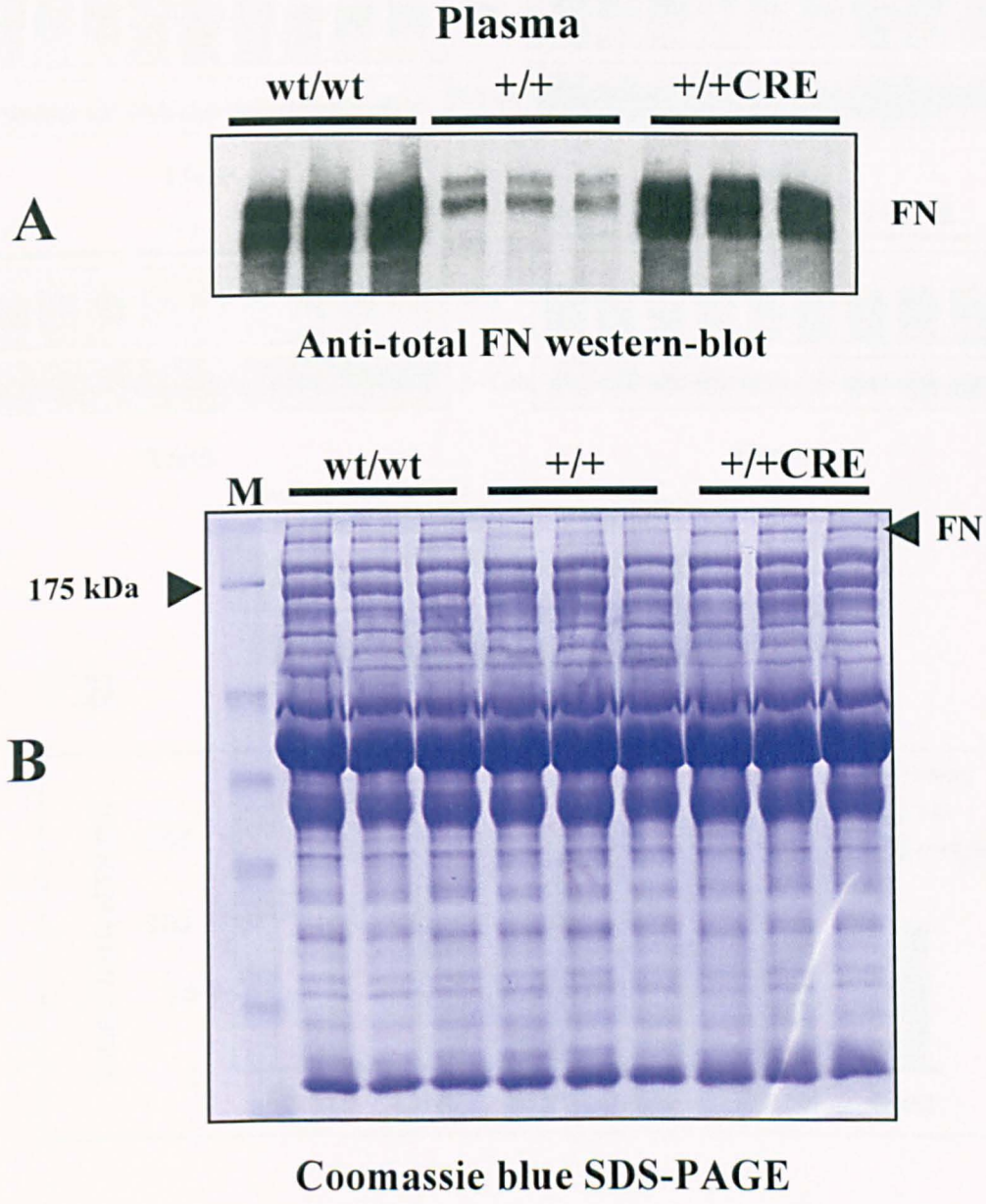

Figure 21. Plasma from $EDA^{+/+CRE}$ mice has normal FN levels.
A. Plasma was prepared from $EDA^{wt/wt}$, $EDA^{+/+}$ and $EDA^{+/+CRE}$ mice (3 month-old) and total FN levels were detected by Western blot analysis. **B.** The protein load was controlled performing a coomassie blue staining of a 10% SDS-PAGE containing equal amounts of plasma from the three genotypes. The intensity of the signals in Panel A was quantified with the help of the Quantity One Software and the results are shown in Figure 22B. The signal obtained in the $EDA^{wt/wt}$ samples was considered 100%. The Mean ± SD of three independent experiments is shown.

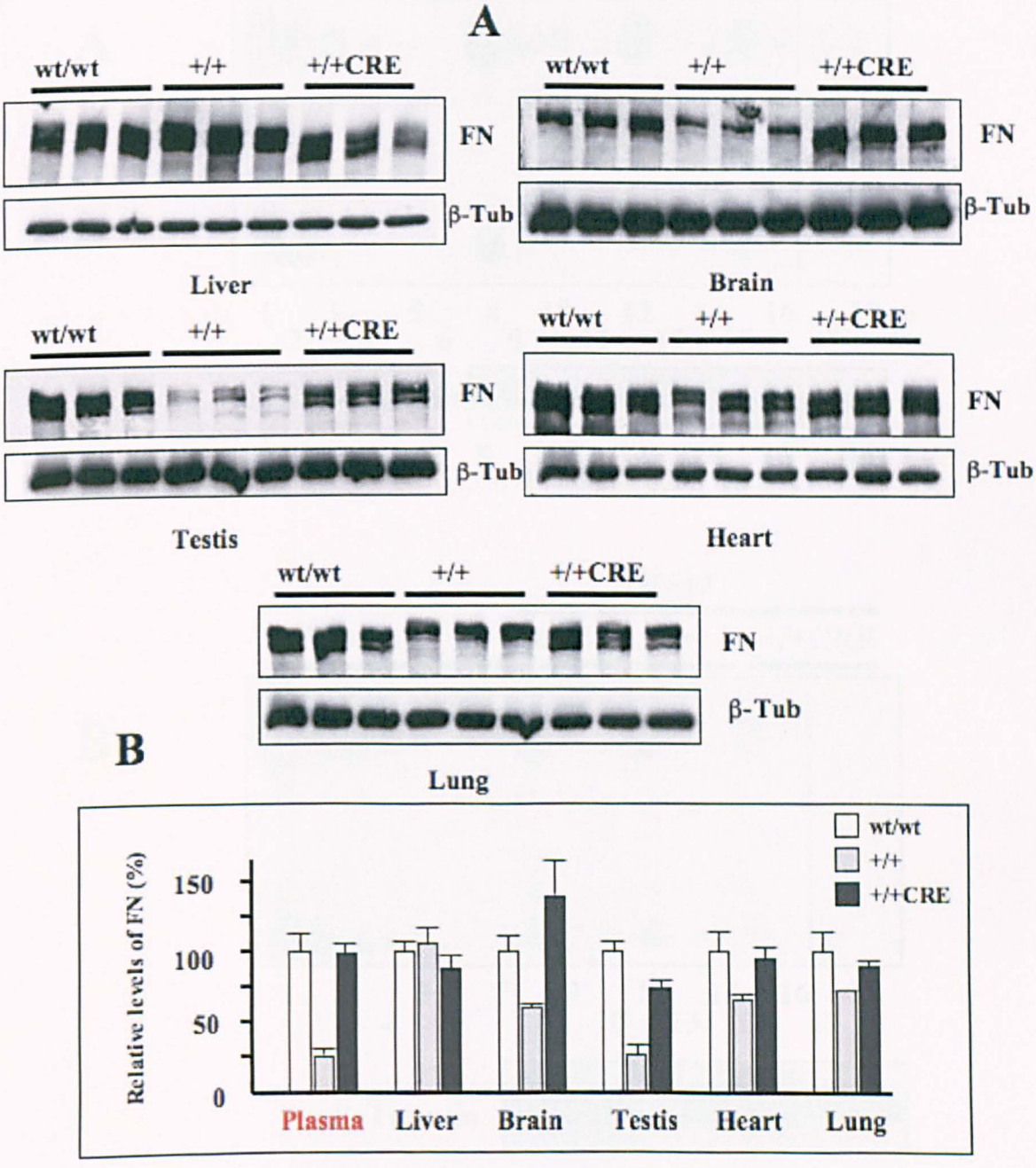

Figure 22. Tissues from EDA$^{+/+CRE}$ mice have normal FN levels.
A. Protein extracts were prepared from EDA$^{wt/wt}$, EDA$^{+/+}$ and EDA$^{+/+CRE}$ mice (3 month-old) and total FN levels were detected by Western blot analysis. The protein load was controlled by detection of β-Tubulin in the same extracts. **B.** The intensity of the signals in Panel A was quantified with the help of the Quantity One Software. The signal obtained in the EDA$^{wt/wt}$ samples was considered 100%. The Mean ± SD of three independent experiments is shown.

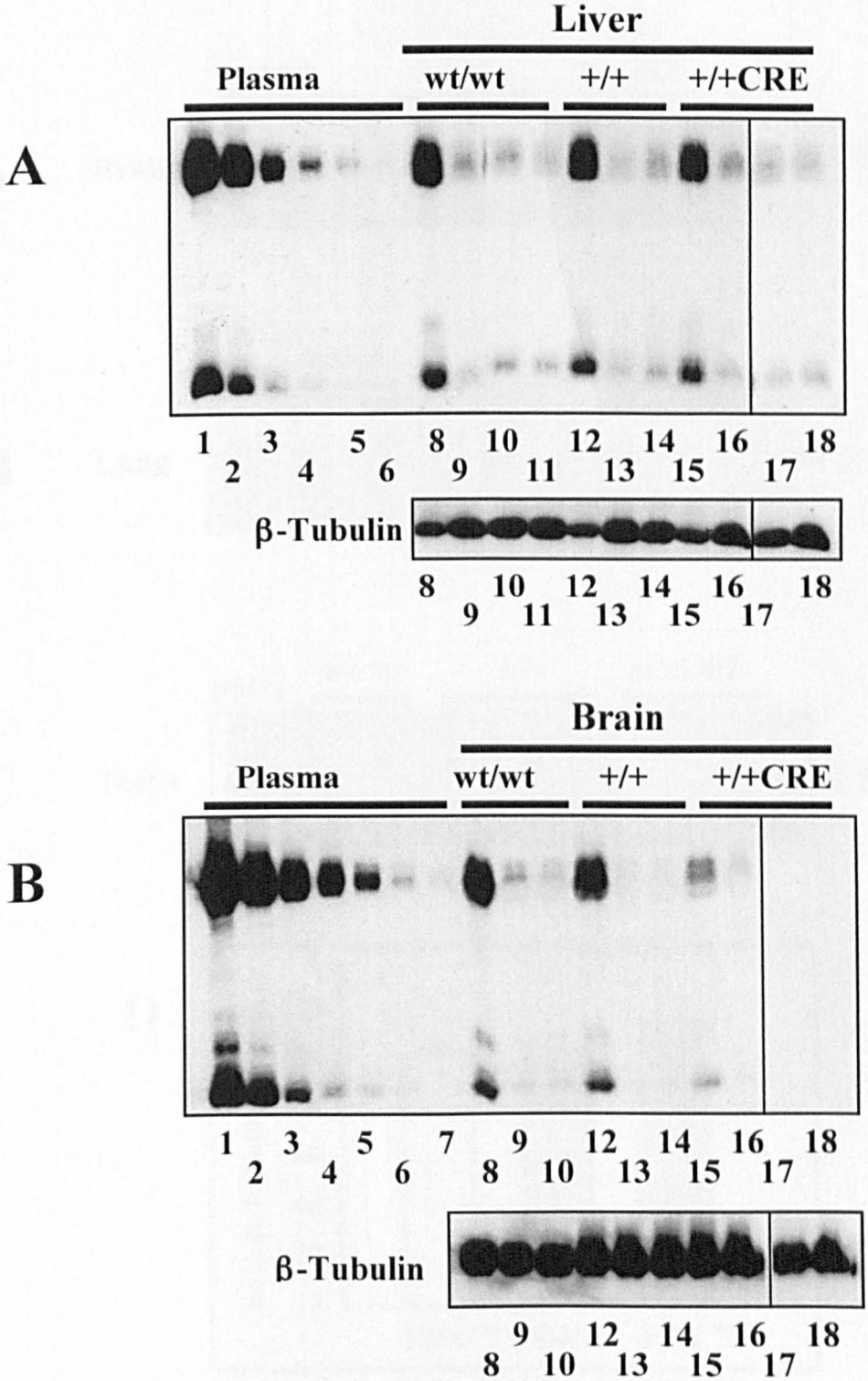

Figure 23. Perfusion of tissues showed almost no residual plasma proteins.
Equal amounts of proteins extracts (50 μg) from liver (Panel A) and brain (Panel B) were loaded, run on a 12% SDS-PAGE and analyzed by Western blot for the presence of plasma gamma globulins. The protein load was controlled by detection of β-Tubulin in the same extracts. Lanes 1-7 correspond to serial dilutions of $EDA^{wt/wt}$ plasma (each lane is 1:2 of the previous one, starting from 0.05 μl to 0.00078 μl). Lanes 8, 12 and 15 correspond to non-perfused samples. Lanes 9-11, 13-14 and 16-18 correspond to perfused samples. The protein load was quantified by detection of β-Tubulin in the stripped membrane (lower panels).

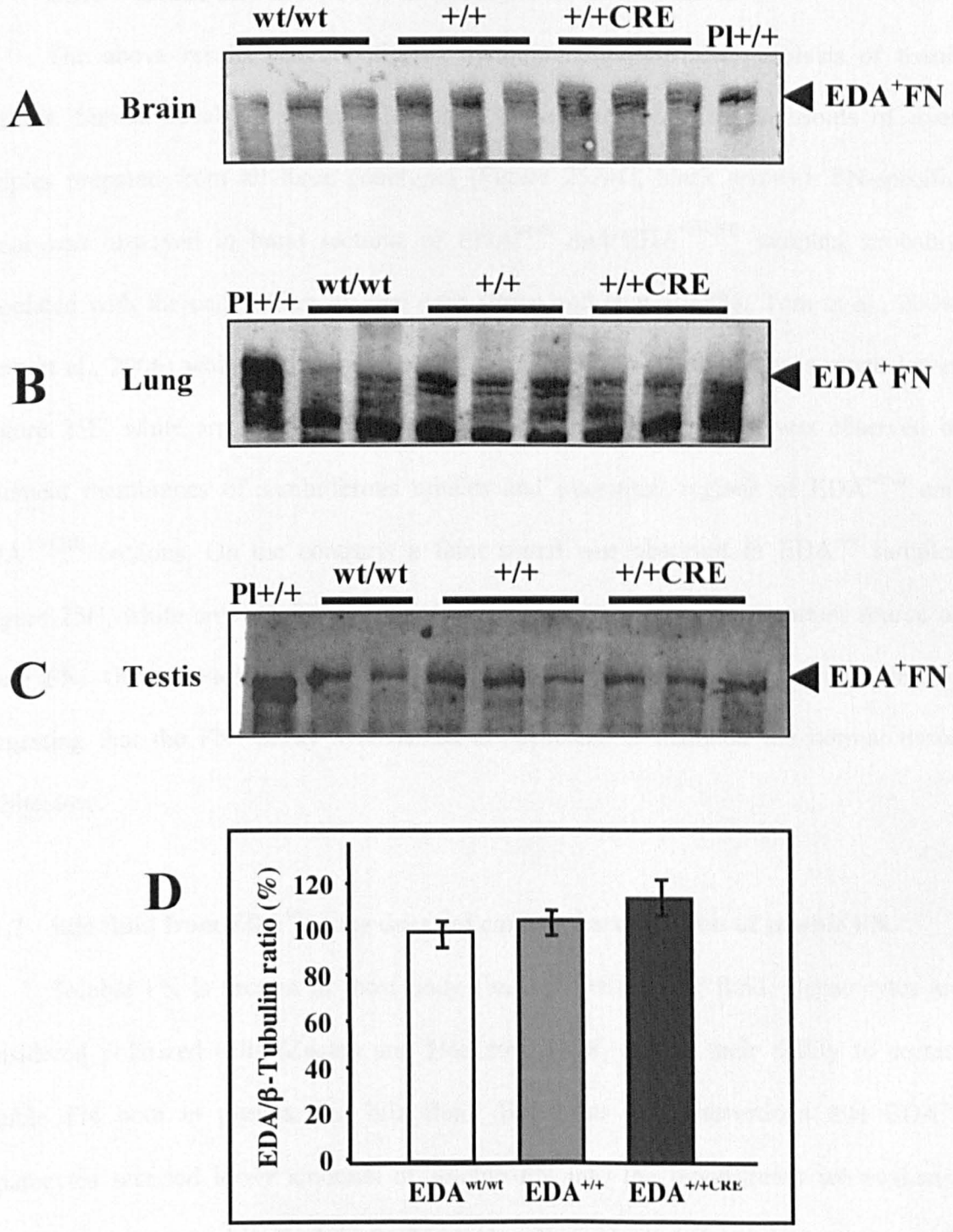

Figure 24. Similar levels of EDA^{+}FN were observed in tissues from all three genotypes.

A., B. and C. The same protein extracts from brain (Panel A), lung (Panel B) and testis (Panel C) used in Figure 22 were analyzed by Western Blot using the anti-EDA monoclonal antibody 3E2. **D.** The ratio between EDA^{+}FN and β-Tubulin signals was used for normalization and results are shown in the bar graph. The ratio obtained in the EDA$^{wt/wt}$ samples was considered 100%.

3.1.6 Immunostaining of tissue sections confirmed the decrease of FN levels in $EDA^{+/+}$ tissues and the recover in tissues of $EDA^{+/+CRE}$ mice.

The above results were confirmed by immunohistochemical analysis of tissue sections. Similar levels of FN-specific signal were detected in the sinusoids of liver samples prepared from all three genotypes (Figure 25A-C, black arrows). FN-specific signal was observed in brain sections of $EDA^{wt/wt}$ and $EDA^{+/+CRE}$ samples, probably associated with the cell surface of glial cells (Price and Hynes, 1985; Tom et al., 2004; Yang et al., 2006) while the intensity of the signal in $EDA^{+/+}$ samples was much lower (Figure 25E, white arrows). In the case of testis, a strong FN signal was observed in basement membranes of seminiferous tubules and interstitial regions of $EDA^{wt/wt}$ and $EDA^{+/+CRE}$ sections. On the contrary, a faint signal was observed in $EDA^{+/+}$ samples (Figure 25H, white arrows). These results suggest that plasma is an important source of tissue FN. Gross histology of tissue samples from all three genotypes was similar, suggesting that the FN locally synthesized is sufficient to maintain the normal tissue architecture.

3.1.7 Bile fluid from $EDA^{+/+}$ mice does not contain normal levels of soluble FN.

Soluble FN is present in most body fluids including bile fluid. Hepatocytes are considered polarized cells (Zegers and Hoekstra, 1998) due to their ability to secrete soluble FN both in plasma and bile fluid. Based on the observations that $EDA^{+/+}$ hepatocytes secreted lower amounts of soluble FN into the bloodstream we evaluated whether FN sectretion into the bile fluid was also diminished. A decrease in FN levels in the bile fluid of $EDA^{+/+}$ mice was observed by Western blot analysis using and anti-FN polyclonal antibody (Figure 26A). This result suggests both the absence of an EDA-dependent polarization of FN secretion in hepatocytes, as postulated for airway epithelial cells (Wang et al., 1991) and endothelial cells (Kowalczyk et al., 1990), and the presence of a general defect in the secretory pathway of the soluble FN by $EDA^{+/+}$ hepatocytes.

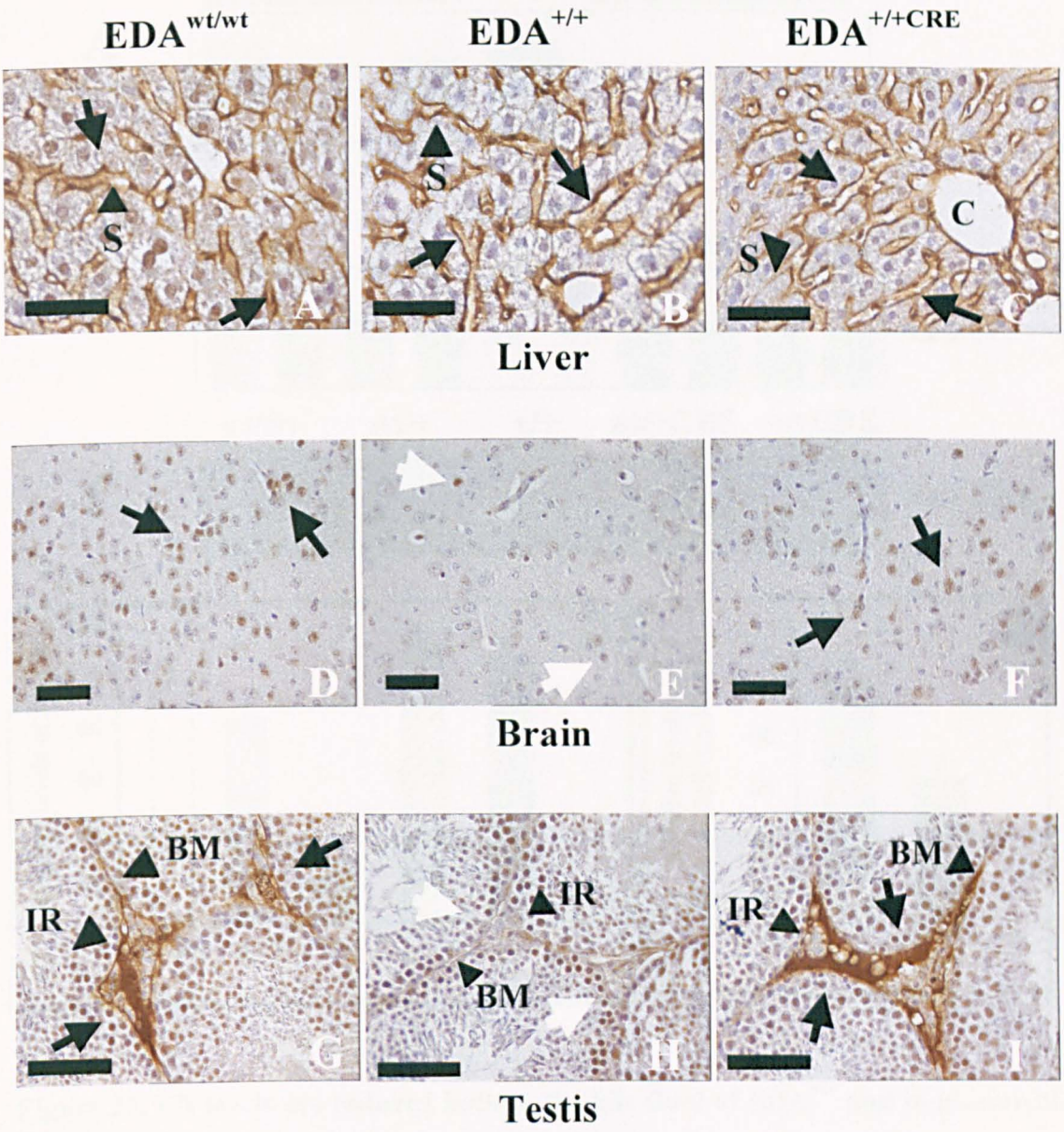

Figure 25. Immunohistochemical analysis of liver, brain and testis tissues.
Tissue sections of liver (Panel A-C), brain (Panel D-F) and testis (Panel G-I) from $EDA^{wt/wt}$ (panel A, D and G), $EDA^{+/+}$ (Panel B, E and H) and $EDA^{+/+CRE}$ (Panel C, F and I) mice were stained with an affinity purified anti-FN polyclonal antibody. The black arrows indicate FN in the extracellular matrix of $EDA^{wt/wt}$ and $EDA^{+/+CRE}$ from different tissues and $EDA^{+/+}$ liver. White arrows indicate the decrease in levels of FN from the same areas of brain and testis only in $EDA^{+/+}$ mice. S, sinusoids; BM, basement membrane; and IR, interstitial region are indicated by black arrowheads. The black bars correspond to 50 μm.

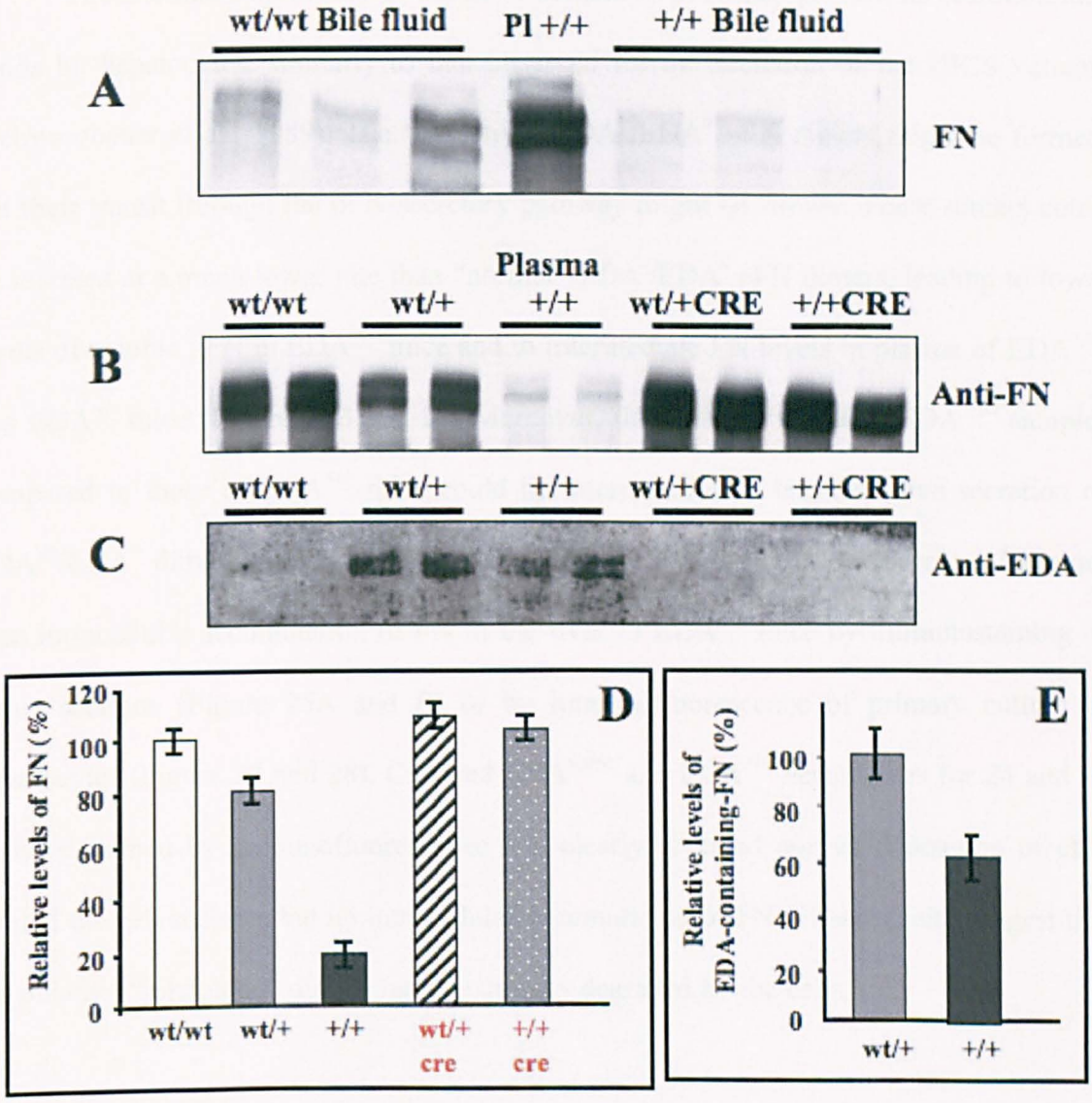

Figure 26. FN levels are reduced both in the bile fluid of $EDA^{+/+}$ and in plasma of $EDA^{wt/+}$ mice.

A. The same amount of bile fluid (2µ undiluted) was loaded and analyzed by Western-blot using an anti-FN polyclonal antibody. The bile of $EDA^{+/+}$ mice contained less FN than control mice. A control from $EDA^{+/+}$ plasma is shown (lane 4). **B.** Plasma samples were prepared from $EDA^{wt/wt}$, $EDA^{wt/+}$, $EDA^{+/+}$, $EDA^{wt/+CRE}$, and $EDA^{+/+CRE}$ mice and total FN levels were detected by Western-blot analysis using an anti-FN polyclonal antibody. Plasma of $EDA^{wt/+}$ heterozygous mice contained intermediate amounts of FN levels. **C.** Same samples of Panel B were stained with an anti-EDA monoclonal antibody. **D. and E.** The intensity of the signals in Panel B and C was quantified with the help of the Quantity One Software and the values were bar graphed in the Panel D and E, respectively. The signal obtained in the $EDA^{wt/wt}$ samples was considered 100%. Plasma of $EDA^{wt/+}$ heterozygous mice contained more $EDA^{+}FN$ than the $EDA^{+/+}$ homozygous mice (Panel C and E).

3.1.8 $EDA^{+/+}$ hepatocytes do not show intracellular accumulation of FN.

The anomalous presence of the EDA domain in pFN may prevent its secretion into fluids by hepatocytes, similarly to that observed for the secretion of the IIICS variants (Schwarzbauer et al., 1989). The "defective" EDA^{+}/EDA^{+} pFN dimers might be formed, but their transit through the pFN-secretory pathway might be slower. These dimers could be secreted at a much lower rate than "normal" EDA^{-}/EDA^{-} pFN dimers, leading to lower levels of soluble pFN in $EDA^{+/+}$ mice and to intermediate FN levels in plasma of $EDA^{+/wt}$ and $EDA^{+/-}$ mice (Figure 26B and D). Moreover, the stronger signal in $EDA^{+/wt}$ samples compared to those of $EDA^{+/+}$ mice could be interpreted as a less-defective secretion of EDA^{wt}/EDA^{+} dimers than EDA^{+}/EDA^{+} ones (Figure 26C and E). However, we have not seen intracellular accumulation of FN in the liver of $EDA^{+/+}$ mice by immunostaining of tissue sections (Figure 25A and B) or by immunofluorescence of primary culture of hepatocytes (Figure 27 and 28). Cultured $EDA^{wt/wt}$ and $EDA^{+/+}$ hepatocytes for 24 and 48 hr were stained by immunofluorescence and clearly revealed normal deposition of cFN around the cell surfaces but no intracellular accumulation of FN. These results suggest that the putative "misfolded" dimers may be quickly degraded by the cells.

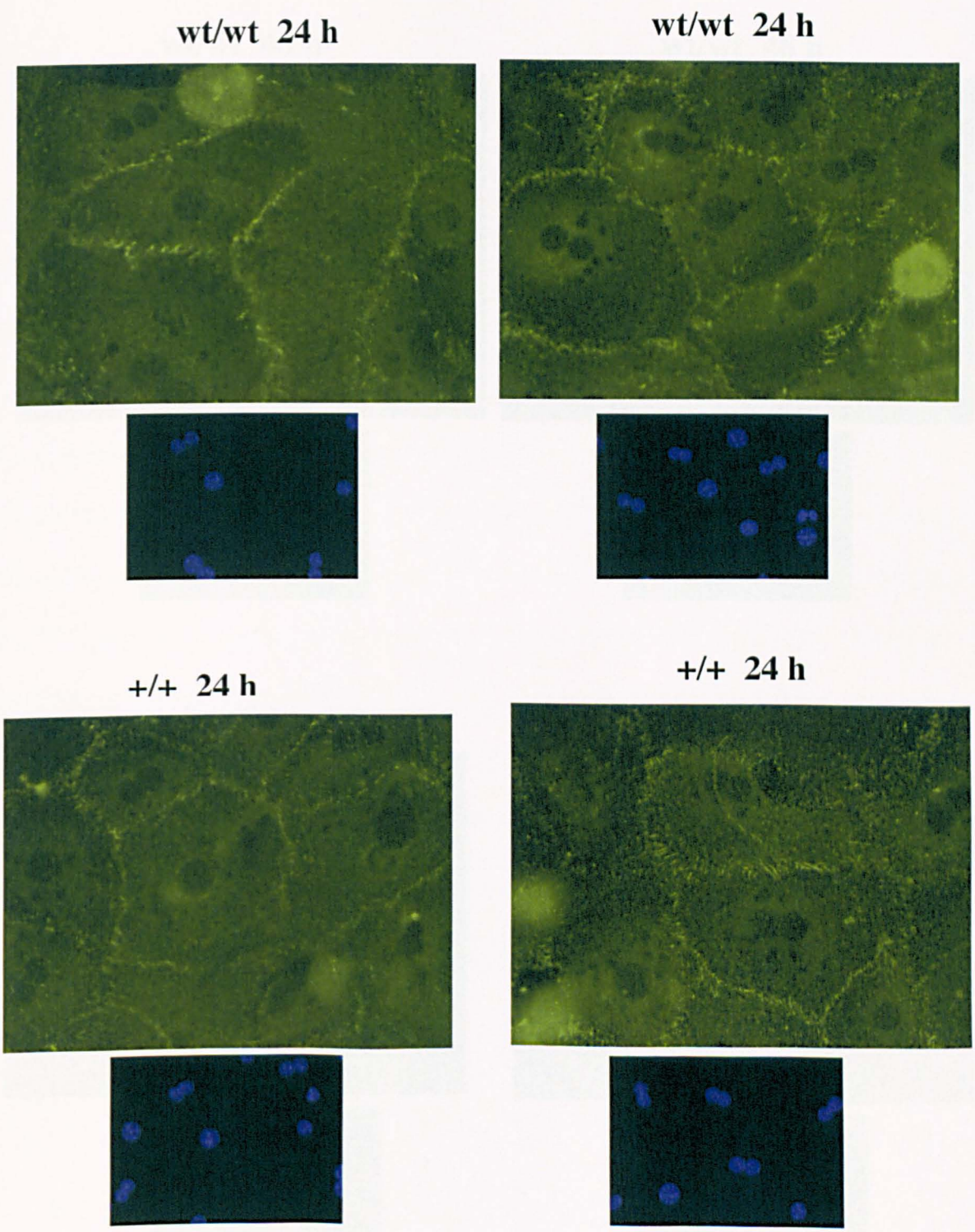

Figure 27. Immunofluorescence analysis of primary culture of hepatocytes (I). Hepatocytes were purified from $EDA^{wt/wt}$ and $EDA^{+/+}$ mice and plated onto rat tail collagen coated glass-slips for 24 hrs. Cells were fixed and stained with an affinity purified anti-FN polyclonal antibody. Nuclei of the same fields are shown (Hoetscht staining).

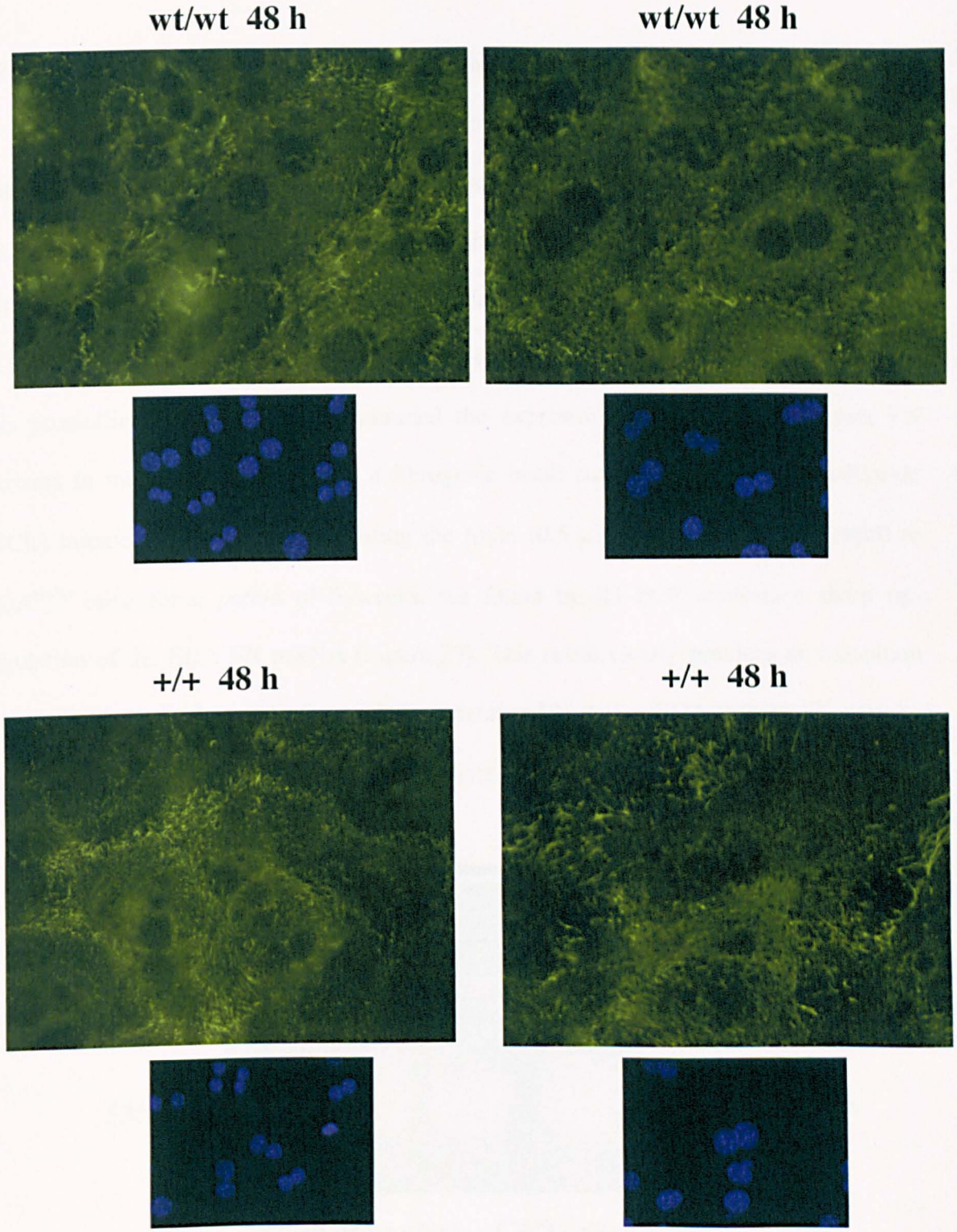

Figure 28. Immunofluorescence analysis of primary culture of hepatocytes (II). Hepatocytes were purified from $EDA^{wt/wt}$ and $EDA^{+/+}$ mice and plated onto rat tail collagen coated glass-slips for 48 hrs. Cells were fixed and stained with an affinity purified anti-FN polyclonal antibody. Nuclei of the same fields are shown (Hoetscht staining).

3.2 EDA$^+$FN AND LIVER FIBROSIS.

3.2.1 EDA$^+$FN mRNA is up-regulated as consequence of a liver injury.

Since EDA$^+$ cFN expression has been observed both *in vivo* (in fibroblastic foci of human fibrotic liver and hepatocellular carcinoma (Matsui et al., 1997), and rat regenerating liver (Caputi et al., 1995b)) and *in* vitro (in cultured rat hepatic cells after experimental induction of liver fibrogenesis (Jarnagin et al., 1994)), we postulated that EDA$^+$ cFN may be an important contributor to liver fibrosis also in mice. In order to assess this possibility, we qualitatively examined the expression of the EDA-containing FN variants in murine livers following a fibrogenic insult such as the carbon tetrachloride (CCl_4) intoxication. After administrating the toxin (0.5 µl per gram of body weight) to EDA$^{wt/wt}$ mice for a period of 5 weeks, we found by RT-PCR analysis a sharp up-regulation of the EDA$^+$FN mRNA (Figure 29). This result clearly provides an indication that an increase in the ratio of the EDA-containing FN vs the EDA-lacking FN may be associated to the onset of the fibrotic process in mouse liver.

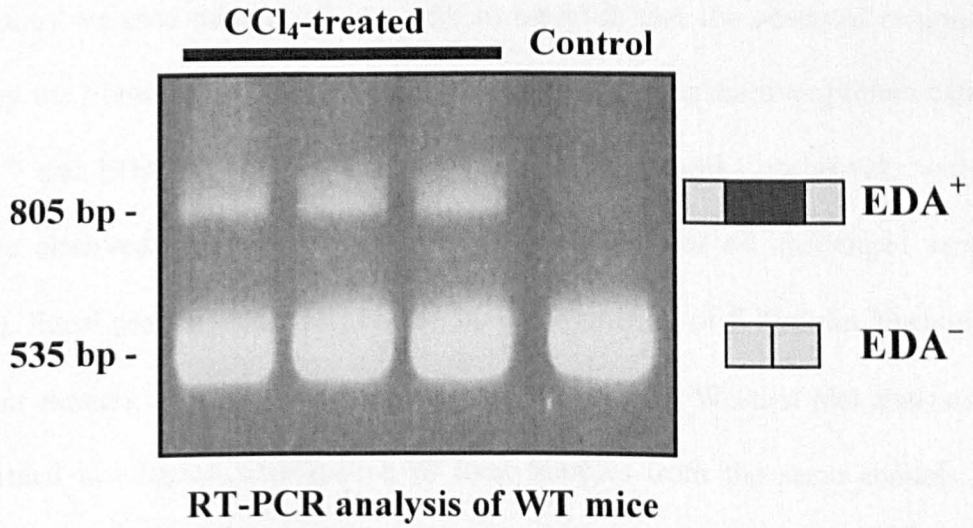

Figure 29. EDA$^+$FN mRNA is upregulated as a consequence of liver injury.
RT-PCR analysis of the EDA-inclusion pattern in the FN mRNA using total RNA extracts from CCl_4-treated WT livers. Lane 1-3, RNA samples extracted from 3 animals treated for 5 weeks with 0.5 µl/gr of CCl_4. Lane 4, Control sample. The EDA$^+$ and EDA$^-$ band are indicated.

3.2.2 Reduced αSMA levels in $EDA^{-/-}$ mice following liver fibrosis induced by low-dose CCl_4 administration.

We have previously shown that $EDA^{-/-}$ mice are incapable of adequately healing cutaneous wounds (Muro et al., 2003). This is due to ulceration of the newly formed epidermis, abnormal re-epithelialization, and ongoing proliferation of infiltrating inflammatory cells. In order to explore the role of EDA^{+} cFN in liver fibrosis, $EDA^{-/-}$ and $EDA^{wt/wt}$ control mice received intraperitoneal (IP) injections of the fibrogenic toxin CCl_4. A dose of 0.5 μl per gram of body weight was administrated twice a week for a period of 5 weeks (Maher and McGuire, 1990). We observed that both the $EDA^{-/-}$ and $EDA^{wt/wt}$ animals developed a significant degree of fibrosis in the liver. Western blot analysis of liver protein extracts evidenced elevated levels of one of the markers used to determine activated fibrotic cells (or myofibroblasts), the smooth muscle α-actin (αSMA). However, $EDA^{-/-}$ mice failed to develop significant increases in αSMA levels as it was observed in $EDA^{wt/wt}$ mice (Figure 31A). αSMA signals were quantified and normalized for β-Tubulin levels and the αSMA/β-Tubulin ratios were bar graphed (Figure 31B). As a vehicle for CCl_4 injections we used mineral oil. In order to establish that the observed response is provoked by the fibrotic toxin, we evaluated the αSMA level in the liver protein extracts from $EDA^{-/-}$ and $EDA^{wt/wt}$ animals that were treated for 5 weeks exclusively with the vehicle. We observed no αSMA signal in any of the mineral oil challenged samples (Figure 30). Equal protein load was checked by determination of β-Tubulin levels in the same protein extracts. In order to confirm the data obtained by Western blot analysis, we next performed histological examination of liver samples from the same animals. The immunostaining of serial sections using the same anti-αSMA antiboby, revealed less intense αSMA-positive areas in the $EDA^{-/-}$ sections than in the $EDA^{wt/wt}$ ones. This finding indicated that a lower number of myofibroblasts were present in the $EDA^{-/-}$ liver (Figure 32).

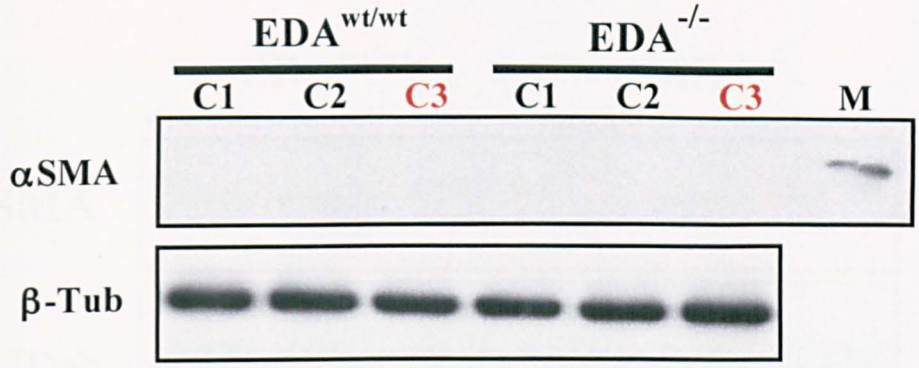

Figure 30. The CCl_4-vehicle mineral oil does not activate hepatic stellate cells. $EDA^{wt/wt}$ and $EDA^{-/-}$ mice were IP injected twice a week for 5 weeks with the vehicle. The whole liver protein was extracted and immunoblotted for αSMA expression. β-Tubulin was assessed as a protein loading control. Western-blot analysis showed that no αSMA signal was present either in the $EDA^{wt/wt}$ or in the $EDA^{-/-}$ protein samples. **C1-2**, mineral oil challenged samples; **C3**, unchallenged samples. **M**, protein extract from rat aorta was used as a αSMA molecular weight marker.

3.2.3 Quantification of the collagen content in the $EDA^{wt/wt}$ and $EDA^{-/-}$ mice following liver fibrosis induced by low-dose CCl_4 administration.

Previous studies have shown that fibroproliferative disorders are characterized by increased production and deposit of ECM proteins in tissues by mesenchymal cell phenotypes (Bissell, 1990; Bissell, 2001). Indeed, activated tissue fibroblasts and hepatic stellate cells are retained responsible not only for the abnormal deposition of FNs in areas of active fibrogenesis (Jarnagin et al., 1994; Serini et al., 1998) but also for other important proteins such as collagens (Maher and McGuire, 1990). Actually, collagens are the predominant ECM proteins identified in fibrotic lesions and are the hallmark of fibroproliferative diseases. For this reason we evaluated the collagen content in the $EDA^{wt/wt}$ and $EDA^{-/-}$ mice following liver fibrosis induced by the CCl_4 insult. The collagen amount was measured by an indirect method based on the determination in tissues of a peculiar and rare amino acid called hydroxyproline that is higly abundant in collagen.

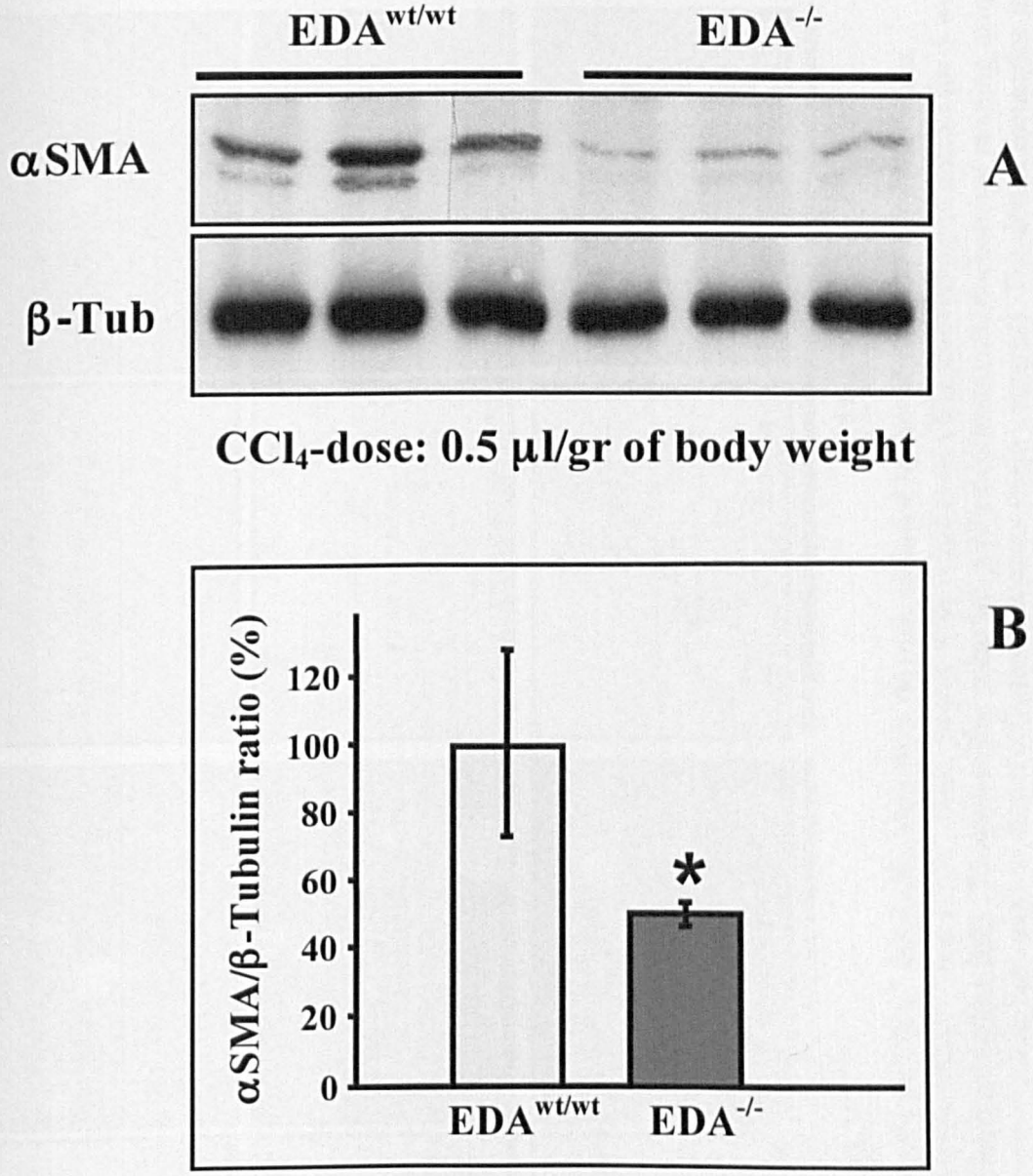

Figure 31. Reduced αSMA levels in $EDA^{-/-}$ mice following liver fibrosis induced by low-dose CCl_4 administration.

A. $EDA^{wt/wt}$ and $EDA^{-/-}$ mice were IP injected twice a week for 5 weeks with CCl_4 (0.5 µl/gr of body weight) or vehicle (Figure 30). The whole liver protein was extracted and immunoblotted for αSMA expression. β-Tubulin was assessed as a protein loading control. **B.** Densitometry of αSMA bands (normalized for β-tubulin) is shown in the bar graph (mean ± SD of three independent animals per genotype). The ratio obtained in the $EDA^{wt/wt}$ samples was considered 100%. Quantification of the bands was done with the help of Quantity-one software. The difference between $EDA^{wt/wt}$ and $EDA^{-/-}$ ratios was statistically significant, according to the T-test (*$p < 0.04$).

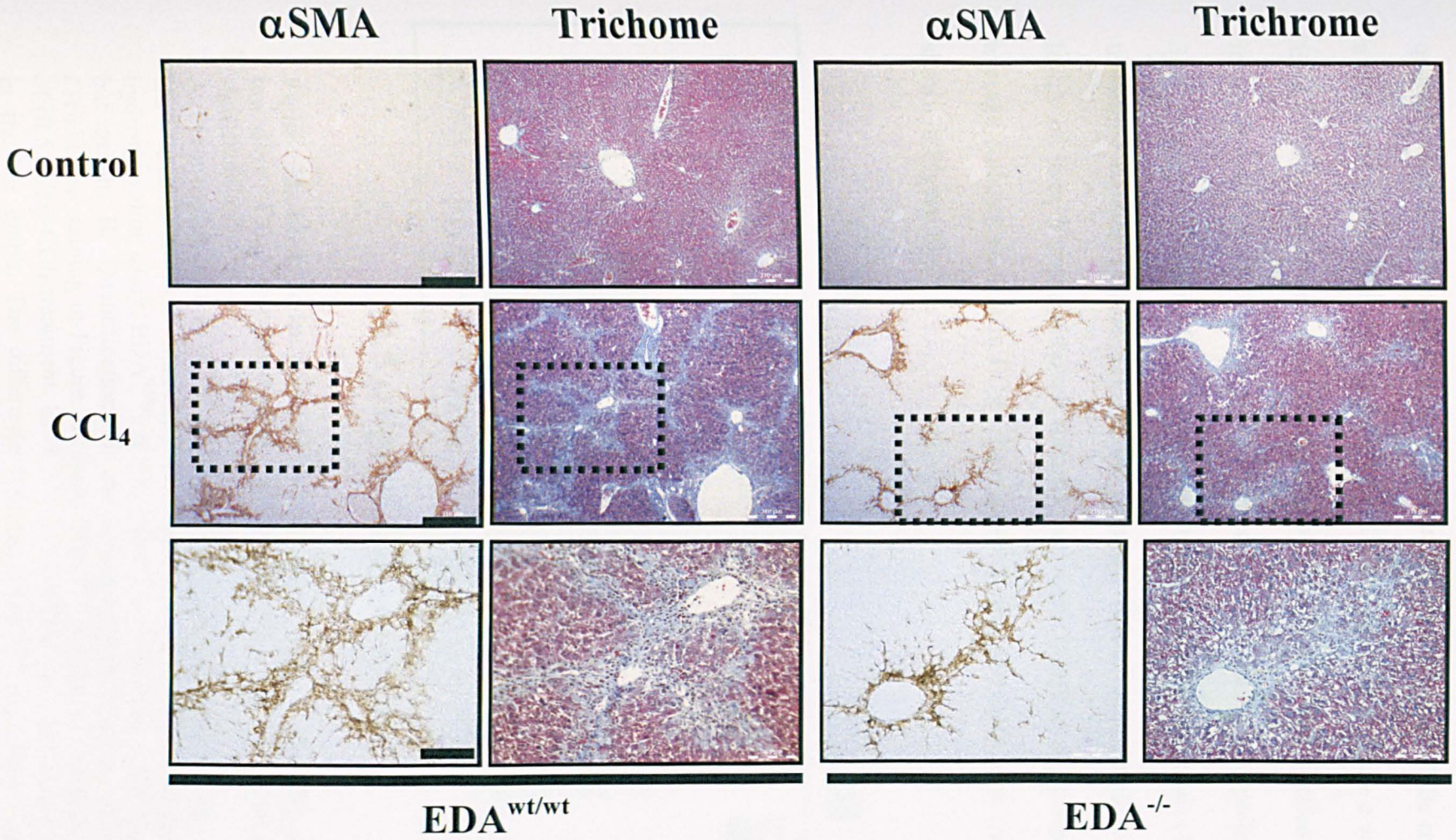

Figure 32. Reduced αSMA and collagen levels in EDA$^{-/-}$ mice following liver fibrosis induced by low-dose CCl_4 administration.
Serial histological sections of liver samples from EDA$^{wt/wt}$ and EDA$^{-/-}$ mice, treated with 0.5μl/gr of CCl_4 and vehicle (Control) for 5 weeks, were analyzed for the presence of activated hepatic stellate cells. To address this issue we performed immunohistochemical staining using an anti-αSMA antibody (left columns). Trichrome staining was used to detect collagen-rich areas (right columns). The dotted rectangles in the middle panels indicate the magnified area shown in the bottom panels. Shown are photomicrographs of a representative field. The black bar in the right-bottom corner of the photographs corresponds to 310 μm and 100 μm for the top and middle rows, and the bottom row, respectively.

It has been evaluated that ~ 14% of collagen amino acids is represented by hydroxyproline (Nelson, 2005). Since it is found in a reduced number of proteins other than collagens, the quantification of hydroxyproline content gives a good estimation of the collagen present in a tissue. As expected, following 0.5 μl/gr CCl_4 administration, twice a week for 5 weeks, $EDA^{wt/wt}$ mice developed significant degree of liver fibrosis. The elevated level of collagen in the fibrotic $EDA^{wt/wt}$ livers was measured by both the hydroxyproline assay (Figure 33A) and quantification of the collagen-positive areas of liver sections (Figure 33B) after trichrome staining (Figure 32). On the contrary, $EDA^{-/-}$ mice failed to develop similar levels of liver fibrosis, although this did not reach statistical significance. Indeed, the average collagen content in $EDA^{-/-}$ liver samples was decreased after the CCL_4 insult as shown in Figure 33.

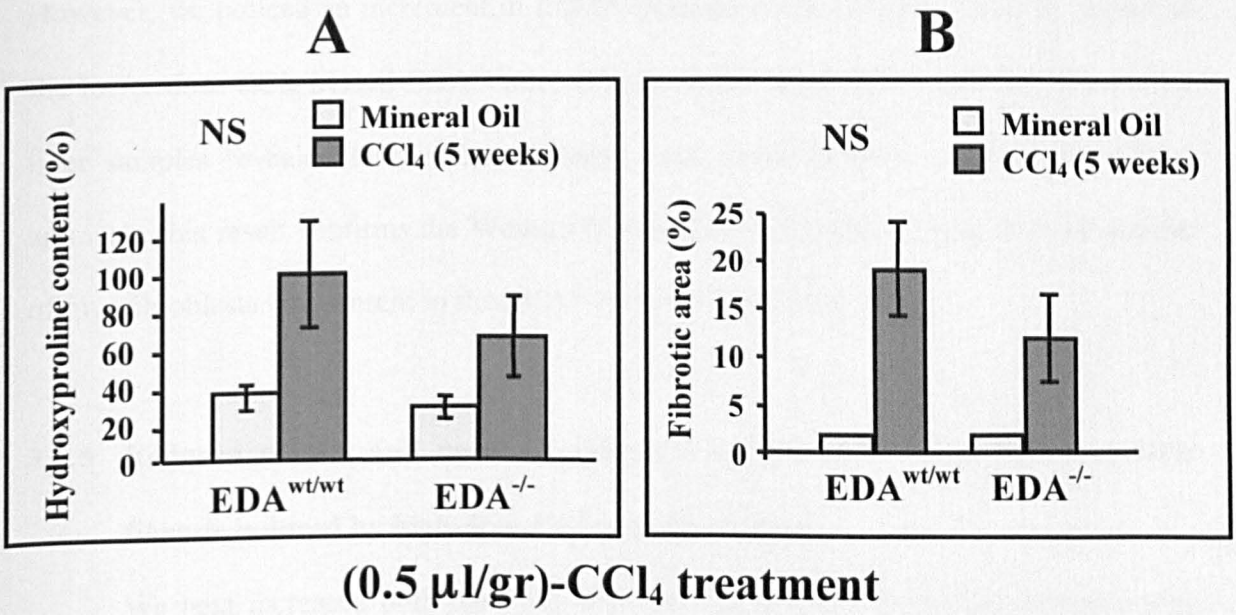

Figure 33. $EDA^{-/-}$ mice failed to develop high levels of liver fibrosis following low-dose CCl_4 administration, although this did not reach statistical significance.

A. Liver tissues from $EDA^{wt/wt}$ and $EDA^{-/-}$ animals following 5 weeks of (0.5 μl/gr)-CCl_4 treatment were harvested and assessed for total collagen content by hydroxyproline assay. $EDA^{wt/wt}$, n = 6; $EDA^{-/-}$, n = 7; mean ± SD are shown in the bar graph. **B.** Quantification of the collagen-positive areas of liver sections (Trichrome staining in Figure 32) from $EDA^{wt/wt}$ and $EDA^{-/-}$ animals after 5 weeks of (0.5 μl/gr)-CCl_4 treatment. $EDA^{wt/wt}$, n = 4; $EDA^{-/-}$, n = 4; mean ± SD are shown in the bar graph. The difference between $EDA^{wt/wt}$ and $EDA^{-/-}$ ratios was not statistically significant, according to the T-test ($p > 0.05$). NS, not significant.

3.2.4 Reduced αSMA levels in $EDA^{-/-}$ mice following liver fibrosis induced by middle-dose CCl_4 administration.

In order to better understand the mechanisms participating in the fibrotic process, we evaluated the relationship between the activation rate of the hepatic stellate cells (HSCs) to a myofibroblast-like phenotype and the dose of the injected toxin. To address this issue we repeated the same intoxication experiment injecting increasing doses of CCl_4 (1.0 to 2.0 μl/gr). In this section 1μl of CCl_4 per gram of body weight was administrated to $EDA^{-/-}$ and $EDA^{wt/wt}$ mice. Both αSMA and β-Tubulin levels were evaluated by Western blot (Figure 34A) and the normalized αSMA levels were bar graphed (Figure 34B). The reduction in αSMA levels in the $EDA^{-/-}$ mice in respect to the $EDA^{wt/wt}$ animals was evident and statistically significant, confirming the previous result (0.5μl/gr CCl_4). However, we noticed an increment in αSMA average levels in $EDA^{-/-}$ mice in respect to the lower dose CCl_4-treated $EDA^{-/-}$ mice (Figure 31B). Histological analysis of the same liver samples revealed less intense collagen- and αSMA-positive areas in the $EDA^{-/-}$ animals. This result confirms the Western blot analysis and indicates that a lower number of myofibroblasts was present in the $EDA^{-/-}$ liver sections (Figure 35).

3.2.5 Reduced αSMA and normal collagen levels in $EDA^{-/-}$ mice following liver fibrosis induced by high-dose CCl_4 administration

We next increased both the CCl_4 dose and the intoxication period administrating 1.5 μl of CCl_4 per gram of body weight, always twice a week but for a period of 6 weeks. Even though the mean value of αSMA level in $EDA^{-/-}$ mice was lower than that of the control mice, the differences between $EDA^{wt/wt}$ and $EDA^{-/-}$ samples were not statistically significant according to the T-test (Figure 36). However, we cannot rule out that the high variability in the response of the $EDA^{wt/wt}$ mice to the toxin may have affected the significance of the test. Indeed, when we performed the histological analysis we still noticed a reduction of the αSMA signal in all the $EDA^{-/-}$ sections (Figure 37) as previously

observed with lower CCl_4 doses. On the contrary, a similar degree of liver fibrosis was observed in $EDA^{wt/wt}$ and $EDA^{-/-}$ mice as shown by the elevated levels of collagen evaluated by both trichrome coloration of the liver sections (Figure 37) and hydroxyproline assay (Figure 38).

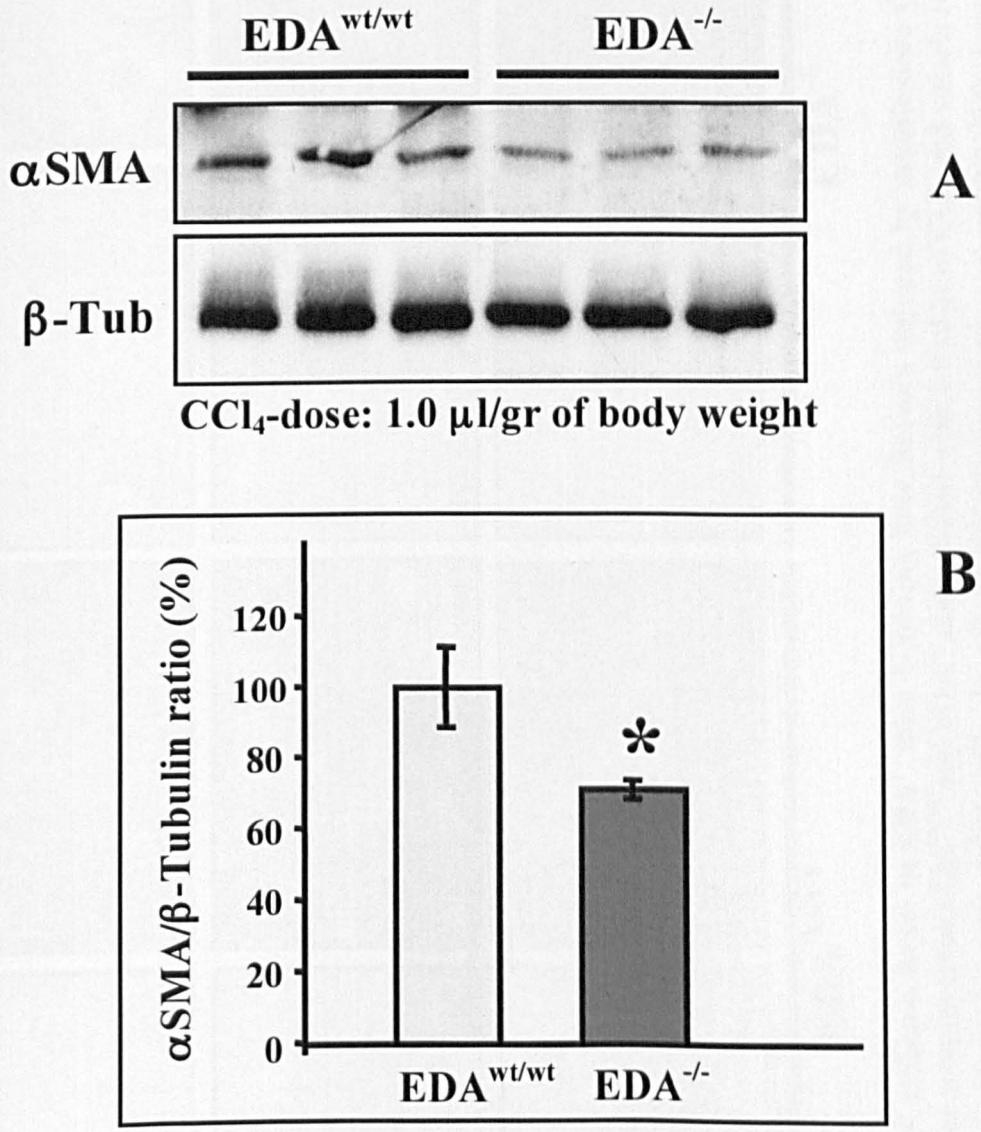

Figure 34. Reduced αSMA levels in $EDA^{-/-}$ mice following liver fibrosis induced by middle-dose CCl_4 administration.
A. $EDA^{wt/wt}$ and $EDA^{-/-}$ mice were IP injected twice a week for 5 weeks with CCl_4 (1.0 µl/gr of body weight) or vehicle. The whole liver protein was extracted and immunoblotted for αSMA expression. β-Tubulin was assessed as a protein loading control. **B.** Densitometry of αSMA bands (normalized for β-Tubulin) is shown in the bar graph (mean ± SD of three independent animals per genotype). The ratio obtained in the $EDA^{wt/wt}$ samples was considered 100%. Quantification of the bands was done with the help of Quantity-one software. The difference between $EDA^{wt/wt}$ and $EDA^{-/-}$ ratios was statistically significant, according to the T-test (*p = 0.01).

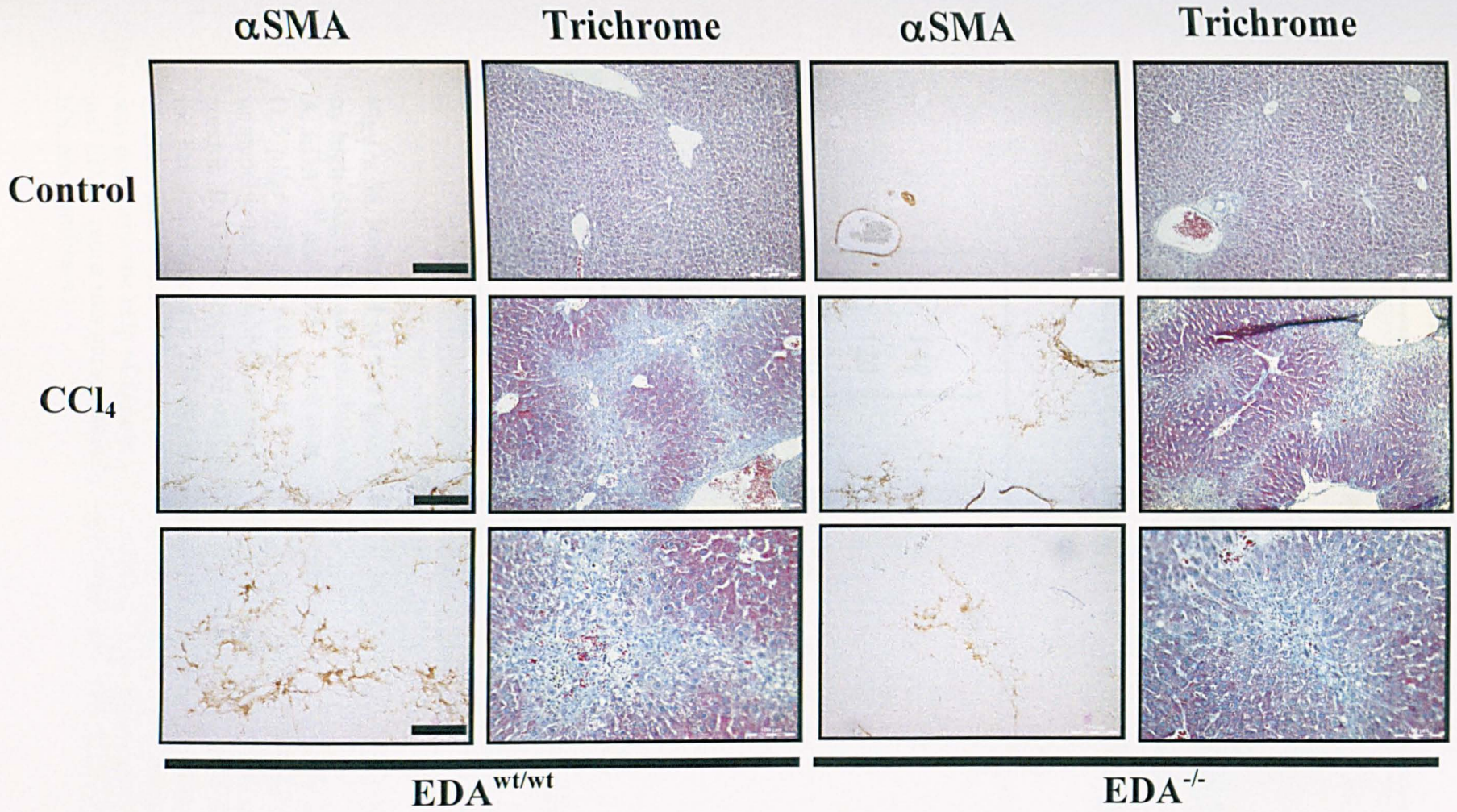

Figure 35. Reduced αSMA and collagen levels in $EDA^{-/-}$ mice following liver fibrosis induced by middle-dose CCl_4 administration. Serial histological sections of liver samples from $EDA^{wt/wt}$ and $EDA^{-/-}$ mice, treated with 1.0 μl/gr of CCl_4 and vehicle (Control) for 5 weeks, were analyzed for the presence of activated hepatic stellate cells. To address this issue we performed immunohistochemical staining using an anti-αSMA antibody (left columns). Trichrome staining was used to detect collagen-rich areas (right columns). Shown are photomicrographs of a representative field. The black bar in the right-bottom corner of the photographs corresponds to 200 μm and 100 μm for the top and middle rows, and the bottom row, respectively.

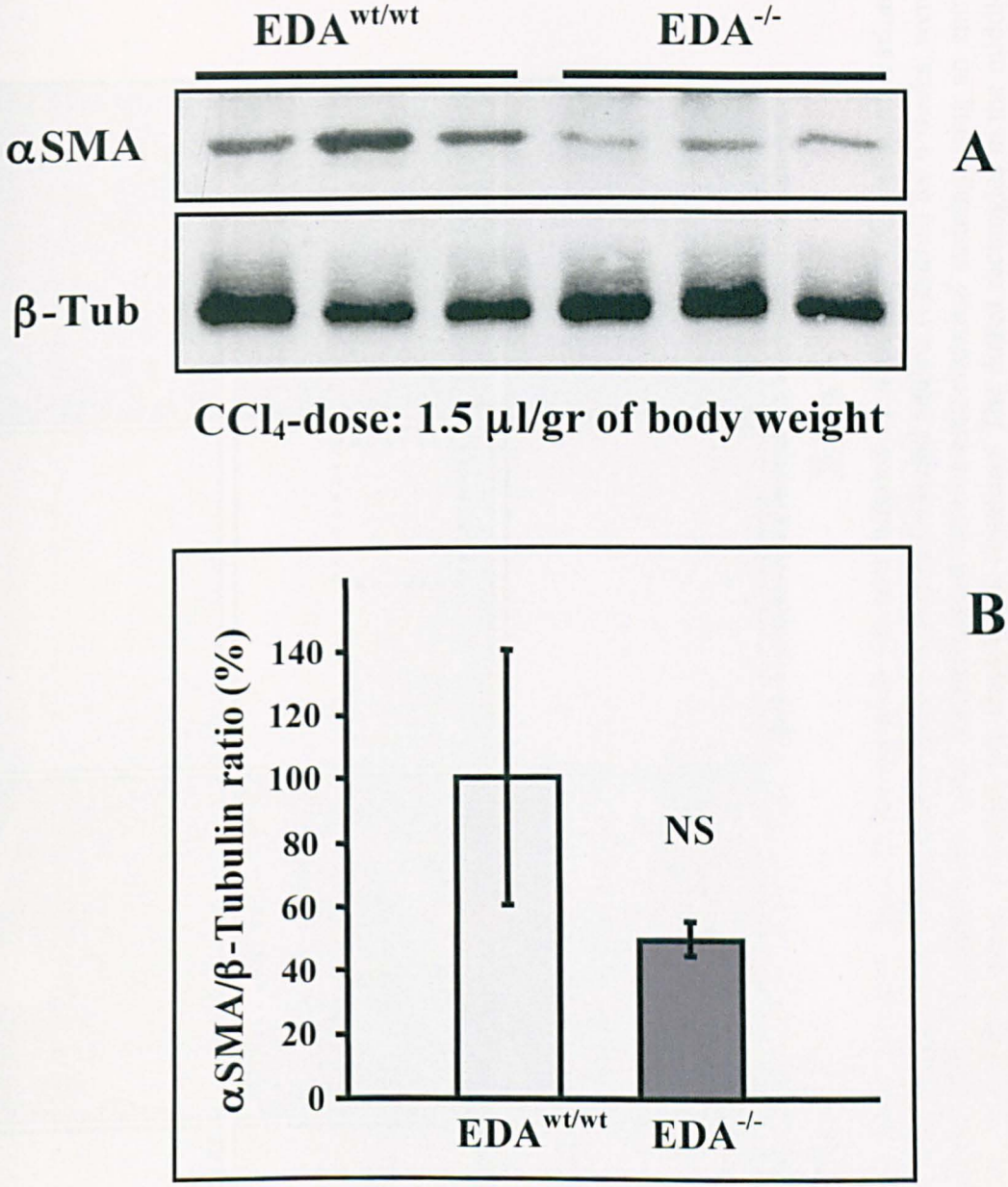

Figure 36. Reduced αSMA levels in EDA$^{-/-}$ mice following liver fibrosis induced by high-dose CCl_4 administration.

A. EDA$^{wt/wt}$ and EDA$^{-/-}$ mice were IP injected twice a week for 6 weeks with CCl_4 (1.5 µl/gr of body weight) or vehicle. The whole liver protein was extracted and immunoblotted for αSMA expression. β-Tubulin was assessed as a protein loading control. **B.** Densitometry of αSMA bands (normalized for β-Tubulin) is shown in the bar graph (mean ± SD of three independent animals per genotype). The ratio obtained in the EDA$^{wt/wt}$ samples was considered 100%. Quantification of the bands was done with the help of Quantity-one software. The difference between EDA$^{wt/wt}$ and EDA$^{-/-}$ ratios was not statistically significant, according to the T-test ($p > 0.05$). NS, not significant.

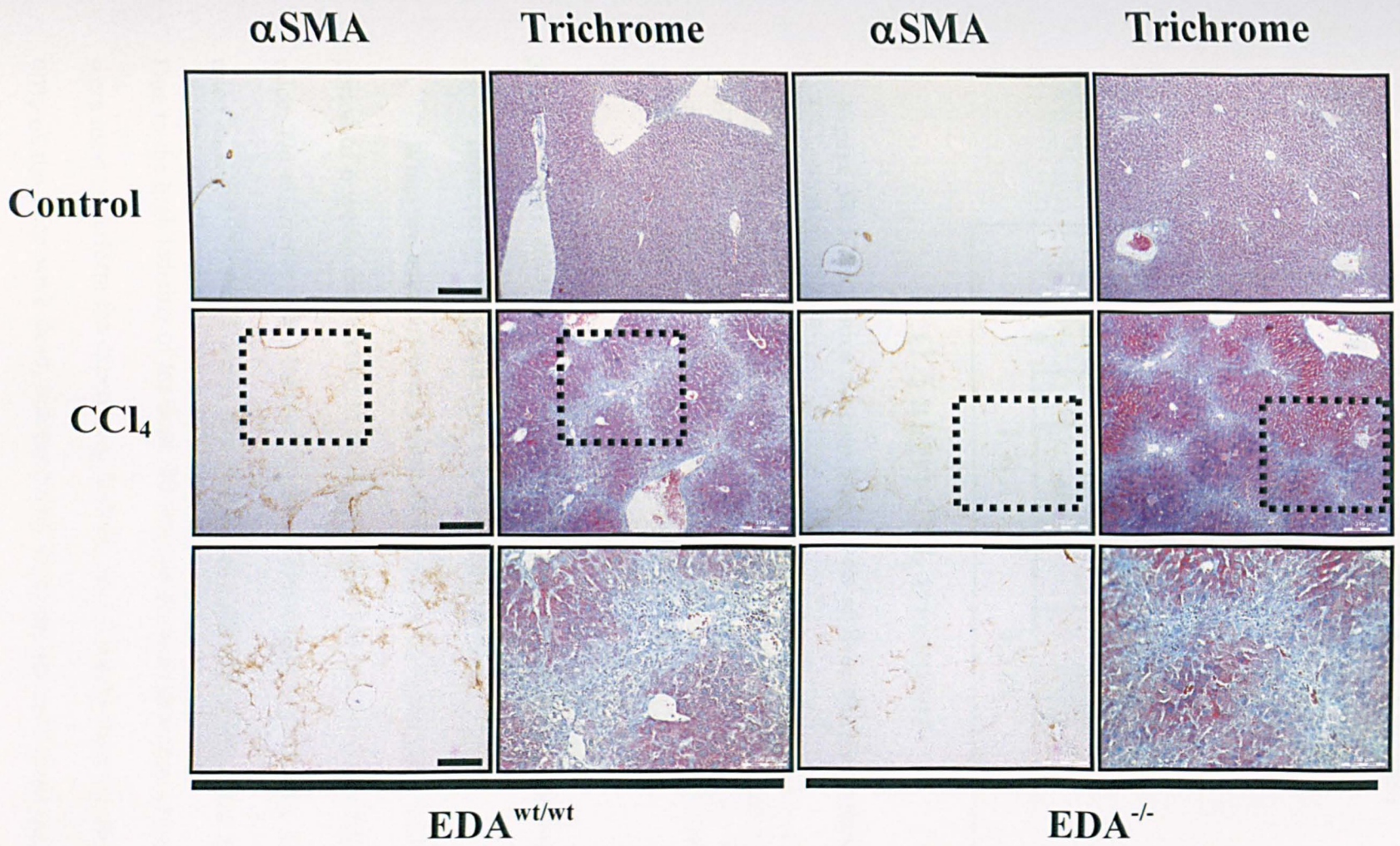

Figure 37. Reduced αSMA and normal collagen levels in $EDA^{-/-}$ mice following liver fibrosis induced by high-dose CCl_4 administration. Serial histological sections of liver samples from $EDA^{wt/wt}$ and $EDA^{-/-}$ mice, treated with 1.5 μl/gr of CCl_4 and vehicle (Control) for 6 weeks, were analyzed for the presence of activated hepatic stellate cells. To address this issue we performed immunohistochemical staining using an anti-αSMA antibody (left columns). Trichrome staining was used to detect collagen-rich areas (right columns). The dotted rectangles in the middle panels indicate the magnified area shown in the bottom panels. Shown are photomicrographs of a representative field. The black bar in the right-bottom corner of the photographs corresponds to 310 μm and 100 μm for the top and middle rows, and the bottom row, respectively.

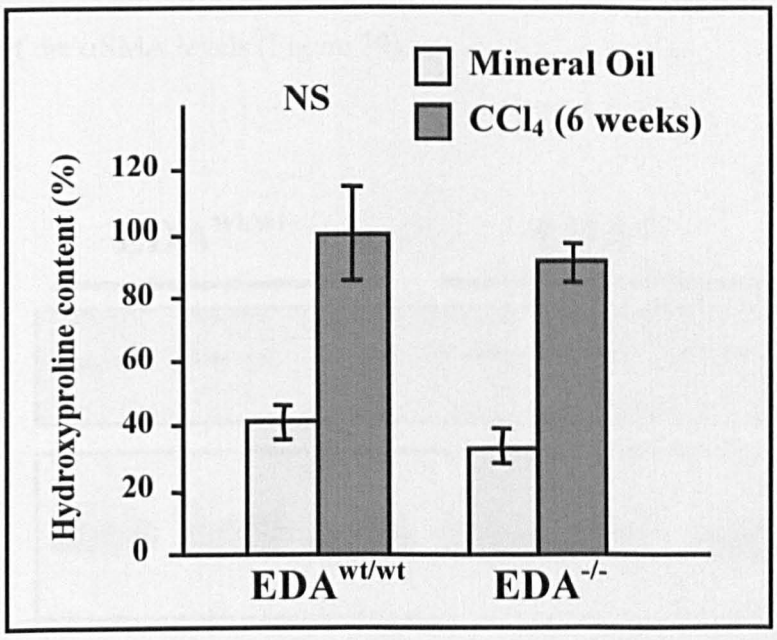

Figure 38. EDA$^{-/-}$ mice develop high levels of liver fibrosis followind high-dose CCl_4 administration.
Liver tissues from EDA$^{wt/wt}$ and EDA$^{-/-}$ animals following 6 weeks of CCl_4 treatment were harvested and assessed for total collagen content by hydroxyproline assay. EDA$^{wt/wt}$, n = 4; EDA$^{-/-}$, n = 4; mean ± SD are shown in the bar graph. The difference between EDA$^{wt/wt}$ and EDA$^{-/-}$ ratios was not statistically significant, according to the T-test ($p > 0.50$). NS, not significant.

3.2.6 Similar αSMA levels in EDA$^{wt/wt}$ and EDA$^{-/-}$ mice following liver fibrosis induced by very-high-dose CCl_4 administration.

When we administrated a dose of 2.0 µl of CCl_4 per gram of body weight for a period of 6 weeks the reaction to the intoxication was similar in the EDA$^{-/-}$ and EDA$^{wt/wt}$ mice. No difference was observed in the αSMA levels between the EDA$^{-/-}$ and control mice as shown by the Western blot analysis and quantification of the bands (Figure 39). Due to the high lethality of the dose, 30 animals for each genotype (15 mice for each sex) were used to perform the experiment. Indeed, after 3 weeks from the first injection, about 90% of the mice were dead, independently from the sex and genotype, as shown in the Kaplan-Meier graphical representation (Figure 40). Since no difference was seen in the CCl_4 mortality curve between the two genotypes, we retained dispensable performing any

histological analysis of the dead mice. The survivors were instead used for the quantification of the αSMA levels (Figure 39).

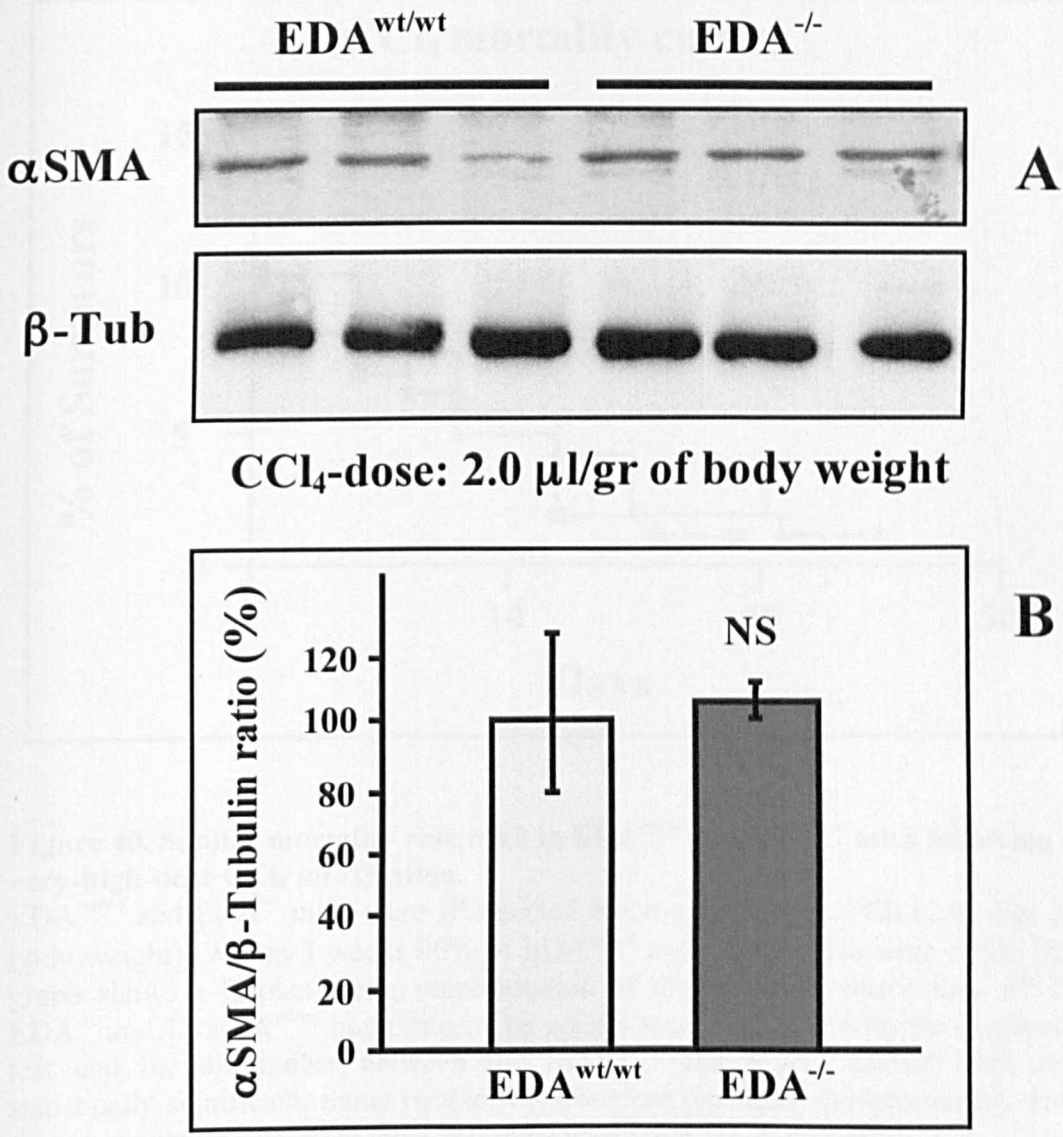

Figure 39. Similar αSMA levels in EDA$^{wt/wt}$ and EDA$^{-/-}$ mice following liver fibrosis induced by very-high-dose CCl_4 administration.
A. EDA$^{wt/wt}$ and EDA$^{-/-}$ mice were IP injected twice a week for 6 weeks with CCl_4 (2.0 µl/gr of body weight) or vehicle. The whole liver protein was extracted and immunoblotted for αSMA expression. β-Tubulin was assessed as a protein loading control. **B.** Densitometry of αSMA bands (normalized for β-Tubulin) is shown in the bar graph (mean ± SD of three independent animals per genotype). The ratio obtained in the EDA$^{wt/wt}$ samples was considered 100%. Quantification of the bands was done with the help of Quantity-one software. The difference between EDA$^{wt/wt}$ and EDA$^{-/-}$ ratios was not statistically significant, according to the T-test ($p > 0.50$). NS, not significant.

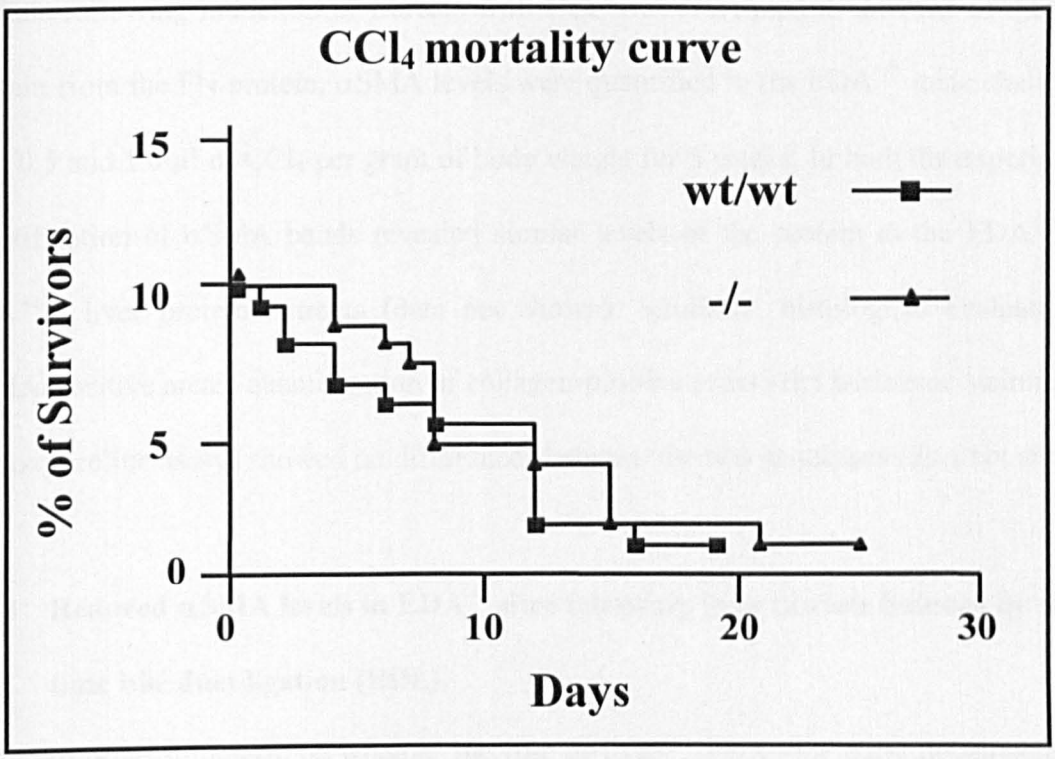

Figure 40. Similar mortality rate both in $EDA^{wt/wt}$ and $EDA^{-/-}$ mice following a very-high-dose CCl_4 intoxication.
$EDA^{wt/wt}$ and $EDA^{-/-}$ mice were IP injected twice a week with CCl_4 (2.0 µl/gr of body weight). Within 3 weeks 90% of $EDA^{wt/wt}$ and $EDA^{-/-}$ mice were dead. The graph shows a Kaplan-Meier representation of the survivals versus time of 15 $EDA^{-/-}$ and 15 $EDA^{wt/wt}$ male mice. The results were analyzed with the Log-rank test and the differences between the $EDA^{wt/wt}$ and $EDA^{-/-}$ curves were not statistically significant. Same course was observed repeating the experiment with the same number of female mice. All mice used were 3/4-month-old.

3.2.7 Similar αSMA levels in $EDA^{wt/wt}$ and $EDA^{+/+}$ mice following liver fibrosis induced by CCl_4 administration.

In order to confirm that the reduction in αSMA levels observed in the $EDA^{-/-}$ animals following induction of fibrosis with CCl_4 was correlated to the lack of the EDA domain from the FN protein, αSMA levels were quantified in the $EDA^{+/+}$ mice challenged with 0.5 and 1.0 μl of CCl_4 per gram of body weight for 5 weeks. In both the experiments, quantification of αSMA bands revealed similar levels of the protein in the $EDA^{+/+}$ and $EDA^{wt/wt}$ liver protein extracts (data not shown). Similarly, histological evaluation of αSMA-positive areas, quantification of collagen-positive areas after trichrome staining and hydroxyproline assays showed no differences between the two genotypes (data not shown).

3.2.8 Reduced αSMA levels in $EDA^{-/-}$ mice following liver fibrosis induced by short-time bile duct ligation (BDL).

In order to determine whether the role of EDA^{+} cFN in the early development of liver fibrosis could be extended to other fibrosis models, we used the bile duct ligation (BDL) model (Maher and McGuire, 1990). Mice were subjected to laparatomy and ligation of the common bile duct as described in Material & Methods (Figure 14). We observed a significant increase in the levels of αSMA after 7-day-BDL in $EDA^{wt/wt}$ mice but not in $EDA^{-/-}$ mice (Figure 42A) confirming the Western blot results obtained with the low-dose CCl_4 insult. Seven days after the operation, livers were excised and protein extracts were prepared. As for the CCl_4 experiments, equal amounts of protein were loaded and run in a 12% SDS-PAGE. The membrane was stained with an anti-αSMA monoclonal antibody following gel blotting. The αSMA signals were quantified and normalized according to β-Tubulin levels. The αSMA/β-Tubulin ratios were bar graphed (Figure 42B). As a control, sham-operated mice were used. The sham operation consisted in the manipulation of the bile duct following laparatomy, without ligation and cut of the common bile duct. As expected, no αSMA signal was evident in any of the liver samples from the sham-operated

animals (Figure 41). In order to confirm the result obtained by Western blot analysis, we next assessed serial BDL-liver sections for the presence of αSMA within HSCs, indicating the presence of activated myofibroblasts. The fibrotic regions in the liver of the $EDA^{wt/wt}$ mice contained clusters of αSMA-expressing myofibroblasts in higher amounts than the $EDA^{-/-}$ samples (Figura 43). As expected and similarly to the low-dose CCl_4-administration experiment, $EDA^{wt/wt}$ mice developed higher degree of fibrosis as shown by the increased levels of collagen, measured by quantification of the collagen-positive areas of liver sections (Figure 44) after trichrome staining (Figure 43). On the contrary, $EDA^{-/-}$ mice failed to develop similar levels of liver fibrosis as shown by the reduction of the collagen-positive areas, although this did not reach statistical significance.

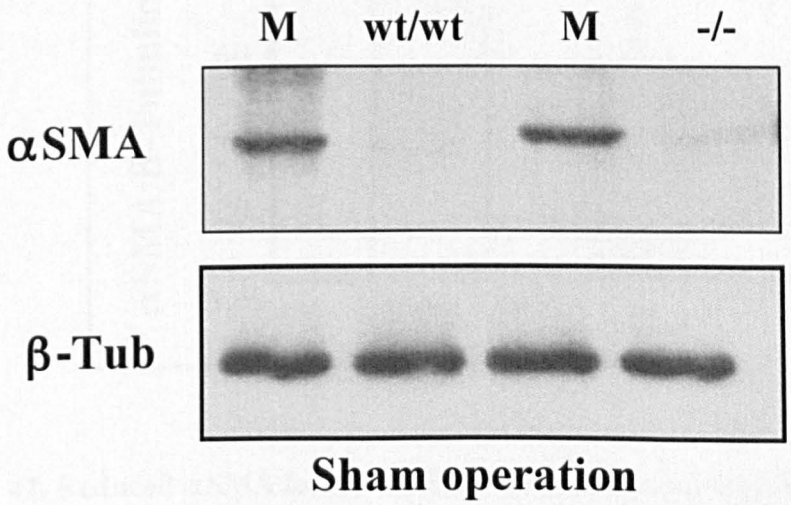

Figure 41. The sham operation as a control for the bile duct ligation (BDL). Sham operation is consistent with laparotomy and manipulation but not ligation and cut of the common bile duct. Protein samples from sham operated $EDA^{wt/wt}$ and $EDA^{-/-}$ mice were separated in 12% SDS-PAGE and immuno-blotted for αSMA expression. β-Tubulin was assessed as a protein loading control. M, liver samples from BDL WT animals were used as marker.

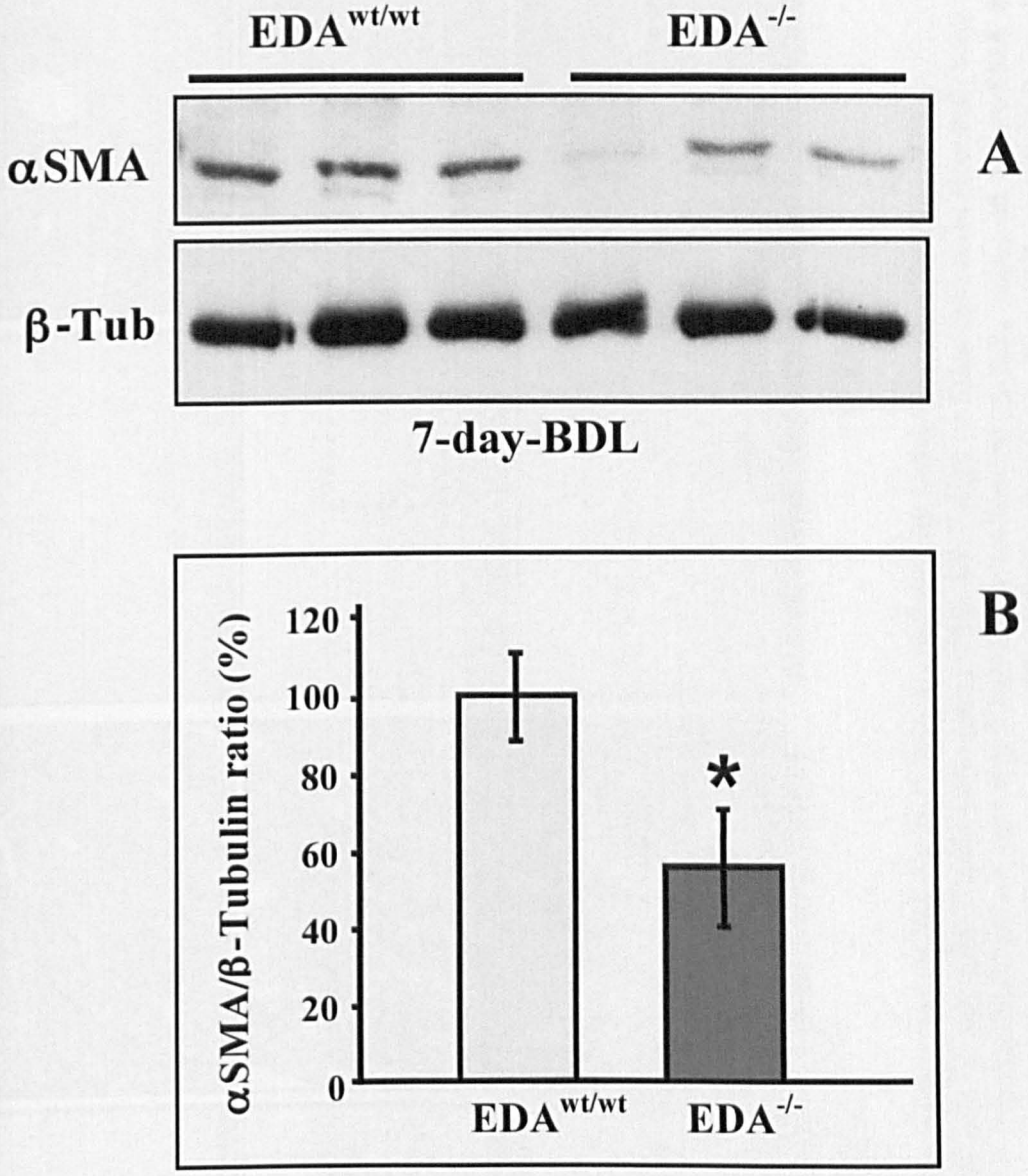

Figure 42. Reduced αSMA levels in EDA$^{-/-}$ mice following liver fibrosis induced by short-time BDL.

A. EDA$^{wt/wt}$ and EDA$^{-/-}$ mice were subjected to laparotomy and BDL or sham operation (Figure 36). The whole liver protein was extracted and immunoblotted for αSMA expression. β-Tubulin was assessed as a protein loading control. **B.** Densitometry of αSMA bands (normalized for β-tubulin) is shown in the bar graph (mean ± SD of three independent animals per genotype). The ratio obtained in the EDA$^{wt/wt}$ samples was considered 100%. Quantification of the bands was done with the help of Quantity-one software. The difference between EDA$^{wt/wt}$ and EDA$^{-/-}$ ratios was statistically significant, according to the T-test (*$p < 0.02$).

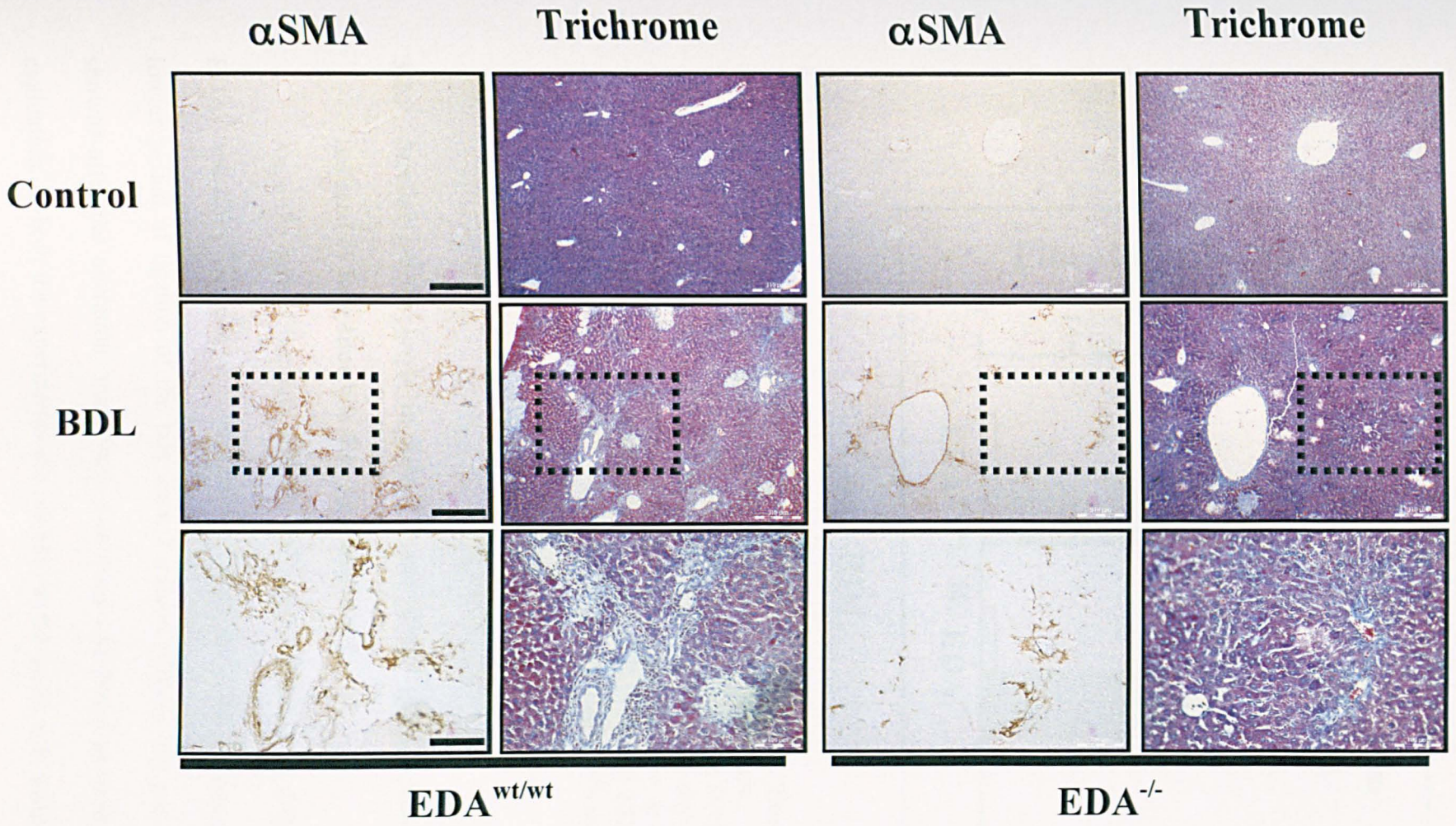

Figure 43. Reduced αSMA and collagen levels in EDA$^{-/-}$ mice following liver fibrosis induced by 7-day-bile duct ligation (BDL).
Serial histological sections of liver samples from EDA$^{wt/wt}$ and EDA$^{-/-}$ mice undergoing BDL for 7 days or sham operation (Control) were analyzed for the presence of activated hepatic stellate cells. To address this issue we performed immunohistochemical staining using an anti-α-SMA antibody (left columns). Trichrome staining was used to detect collagen-rich areas (right columns). The dotted rectangles in the middle panels indicate the magnified area shown in the bottom panels. Shown are photomicrographs of a representative field. The black bar in the right-bottom corner of the photographs corresponds to 310 μm and 100 μm for the top and middle rows, and the bottom row, respectively.

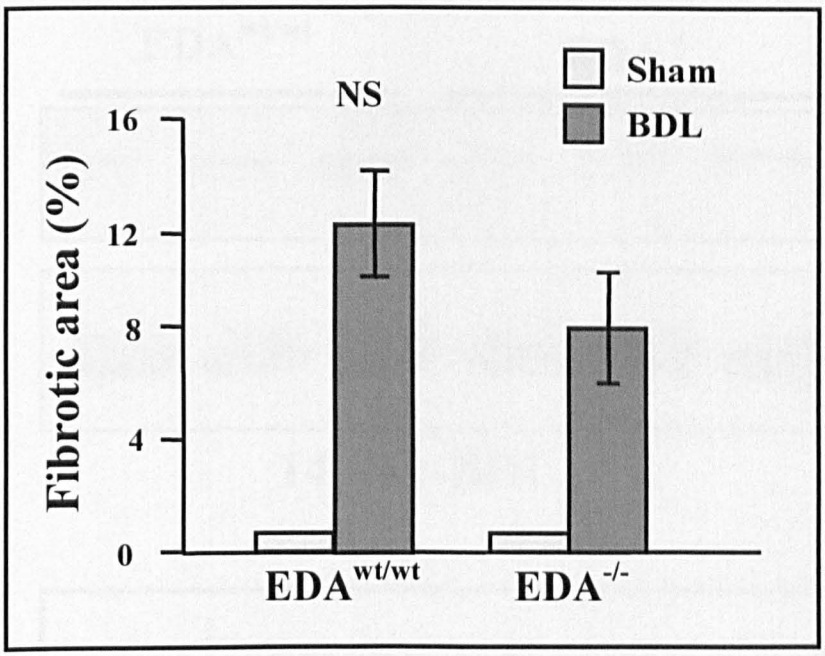

Figure 44. EDA$^{-/-}$ mice failed to develop high levels of liver fibrosis following 7-day-BDL, although this did not reach statistical significance.
Quantification of collagen-positive areas in the liver sections (Trichrome staining in Figure 43) from EDA$^{wt/wt}$ and EDA$^{-/-}$ animals, following 7-day-ligation of the bile duct is represented in the chart. EDA$^{wt/wt}$, n = 4; EDA$^{-/-}$, n = 4; mean ± SD are shown in the bar graph. The difference between EDA$^{wt/wt}$ and EDA$^{-/-}$ ratios was not statistically significant, according to the T-test ($p > 0.05$). NS, not significant.

3.2.9 Similar αSMA levels in EDA$^{wt/wt}$ and EDA$^{-/-}$ mice following liver fibrosis induced by long-time bile duct ligation (BDL).

As in the case of the high doses of CCl_4, the differences in αSMA levels between EDA$^{-/-}$ and EDA$^{wt/wt}$ mice vanished after an increment in the fibrogenic insult such as a longer period of ligation of the bile duct. Fourteen (Figure 45) and eighteen day (not shown) after the operation, mice were sacrificed and livers excised for αSMA signal evaluation. In both the experiments the reaction to the insult was similar in EDA$^{wt/wt}$ and EDA$^{-/-}$ mice.

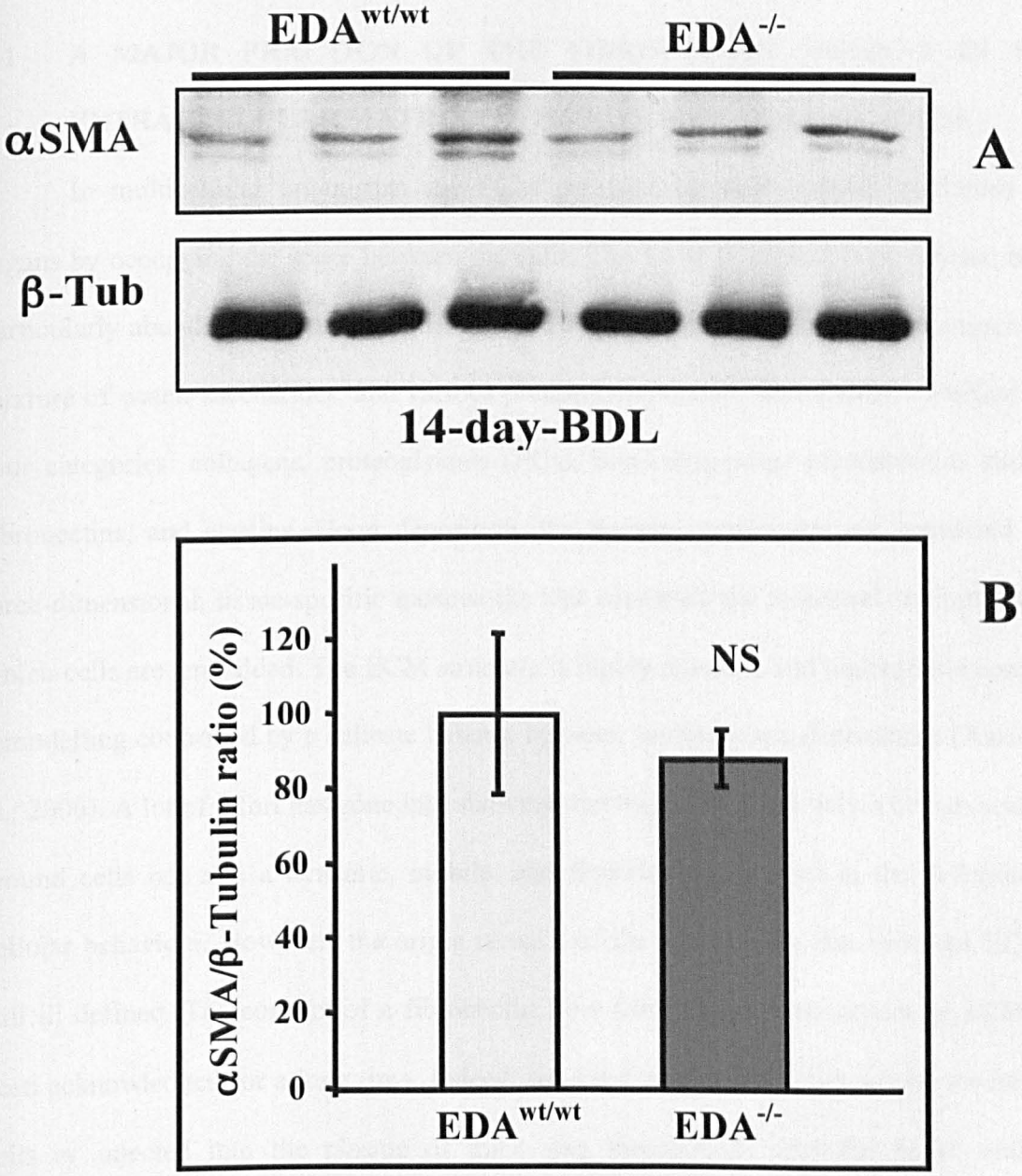

Figure 45. Similar αSMA levels in EDA$^{wt/wt}$ and EDA$^{-/-}$ mice following liver fibrosis induced by long-time BDL.

A. EDA$^{wt/wt}$ and EDA$^{-/-}$ mice were subjected to laparotomy and BDL or sham operation. The whole liver protein was extracted and immunoblotted for αSMA expression. β-Tubulin was assessed as a protein loading control. **B.** Densitometry of αSMA bands (normalized for β-Tubulin) is shown in the bar graph (mean ± SD of three independent animals per genotype). The ratio obtained in the EDA$^{wt/wt}$ samples was considered 100%. Quantification of the bands was done with the help of Quantity-one software. The difference between EDA$^{wt/wt}$ and EDA$^{-/-}$ ratios was not statistically significant, according to the T-test ($p > 0.40$). NS, not significant.

4. DISCUSSION

4.1 A MAJOR FRACTION OF THE FIBRONECTIN PRESENT IN THE EXTRACELLULAR MATRIX OF TISSUES IS PLASMA-DERIVED.

In multicellular organisms, the ECM provides physical support to tissues and organs by occupying the space between the cells. The ECM is present in all tissues, being particularly abundant in connective tissue and basement membranes. It is a heterogeneous mixture of water, saccharides, and various protein components traditionally classified into four categories: collagens, proteoglycans (PGs), non-collagenous glycoproteins such as fibronectins, and elastins. Upon deposition, the protein constituents are organized into three-dimensional, tissue-specific meshworks that constitute the structural environment in which cells are embedded. The ECM structure is highly dynamic and undergoes a constant remodelling controlled by a delicate balance between synthesis and degradation (Aszodi et al., 2006). A lot of effort has gone into showing that the ECM is not only a benign scaffold around cells but also a dynamic, mobile, and flexible key element in the definition of cellular behaviour. However, the origin of each of the components that form the ECM is still ill defined. The concept of a fibronectin flow from plasma into tissues or ECM has been acknowledged for a long time. Indeed, soluble FN added into the culture medium of cells or injected into the plasma of mice was incorporated into the ECM, with its distribution being undistinguishable from that of endogenous FN (Bae et al., 2004; McKeown-Longo and Mosher, 1983; Oh et al., 1981; Peters et al., 1990; Sottile et al., 1998). These initial findings suggested that both local tissue production and transfer from plasma of FN contribute to form the ECM of tissues. However, the extent of this phenomenon has never been addressed. The reported reduction of pFN levels in mice heterozygous for the targeted FN allele ($FN^{wt/-}$) (George et al., 1993) and in conditional pFN-null mice (Sakai et al., 2001) has given a hint to evaluate the levels of FN also in the mouse tissues, but neither of these authors addressed this issue. We had previously

reported that mice with a constitutive inclusion of the EDA domain in FN ($EDA^{+/+}$) showed a significant decrease of FN both in plasma and in most of the tissues of adult animals (Chauhan et al., 2004; Muro et al., 2003). During the present work, pFN levels in young, adult and old $EDA^{+/+}$ mice have been shown to be of about 20% of the pFN levels in control mice ($EDA^{wt/wt}$) (Figure 15A). Additionally, analysis of $EDA^{+/+}$ embryos revealed an apparent decrease of FN levels in plasma of up to 60% of control levels (Figure 15A). We hypothesized that the main reason for this important decrease in FN levels in the ECM of $EDA^{+/+}$ tissues could be related to the reduction of pFN in those animals, which implicates that a major proportion of the FN present in the ECM is probably plasma derived. Moreover, we suspected that the reason for the pFN reduction in the $EDA^{+/+}$ bloodstream was an incapability of hepatocytes to release soluble FN bearing the EDA domain. Not only hepatocytes are known to be the main source of the pFN (Tamkun and Hynes, 1983a), but we also observed that $EDA^{+/+}$ hepatocytes in culture are unable to release as much soluble FN to the medium as those $EDA^{wt/wt}$ (Figure 17C and D). Our previous experiments had also shown that the decrease in pFN was due neither to lower levels of mRNA in $EDA^{+/+}$ tissues, as shown by Northern blot analysis, nor to a reduced FN production by non-hepatic $EDA^{+/+}$ tissues, since the amount of FN secreted by embryonic and adult heart fibroblasts was similar to that produced by $EDA^{wt/wt}$ fibroblasts (Muro et al., 2003). Furthermore, the proteolytic degradation of FN in $EDA^{+/+}$ plasma and tissues was also excluded. Overall, these data seem to exclude a general defect in FN production by $EDA^{+/+}$ tissues, and show that the deficiency in FN secretion was limited to $EDA^{+/+}$ hepatocytes. This was confirmed when we crossed our "floxed" $EDA^{+/+}$ mice with a transgenic mouse expressing CRE recombinase in hepatocytes (Figure 8), in order to generate a liver-specific EDA-null mouse ($EDA^{+/+CRE}$) having an $EDA^{-/-}$ liver inside an $EDA^{+/+}$ body (Figure 18). We observed that the levels of FN present both in plasma and tissue ECM in these mice were restored to normal (Figure 21 and 22). Furthermore, the finding that EDA^{+} cFN levels were similar in the same tissues of $EDA^{+/+}$ and $EDA^{+/+CRE}$

mice confirmed that the variation in total FN content was only due to a difference in pFN (Figure 24). Our results clearly indicated that an important proportion of the FN present in the extracellular matrix of tissues derives from plasma, reaching more than 60% in testis and up to 40% in other tissues such as brain, heart and lung. Our *in vivo* results confirmed previous evidence that plasma could behave as a sort a reservoir of FN for tissue maintenance, and showed for the first time that the contribution of pFN to the ECM of tissues is roughly equal to the FN locally produced in all major tissues. The present results contribute significantly to the understanding of the role of pFN, and perhaps of other plasma proteins, in the modulation of cellular activities and in the formation of the extracellular matrix of tissues.

Sakai *et al.* have recently shown that pFN supports neuronal survival and reduces brain injury following transient focal cerebral ischemia, suggesting the incorporation of pFN into the injured brain (Sakai et al., 2001). Our results confirmed and extended their observations, since we have shown that pFN is incorporated in non-injured brain. Additionally, we also demonstrate that this is a general mechanism occurring in most normal tissues, which import up to 60% of their FN from plasma.

The observation that $EDA^{+/+}$ embryos and young mice (of up to 1-2 months of age) had a reduced pFN (Figure 15A) but contained normal levels of tissue FN (Muro et al., 2003) suggests that the ratio between tissue FN requirements and tissue FN production might be higher in adults than in embryos. Adults, therefore demand an important supply of FN from plasma, which is instead prevented in the $EDA^{+/+}$ mouse.

Here we have presented evidence that the inclusion of the EDA domain in hepatocyte FN affects its secretion into both the bloodstream and bile fluid. The reason why $EDA^{+/+}$ hepatocytes are not able to secrete as much FN as $EDA^{wt/wt}$ hepatocytes is still unclear. Soluble pFN is normally a dimer, with its dimerization occurring in the lumen of the endoplasmic reticulum (ER) of hepatocytes, shortly after its synthesis (Choi and Hynes, 1979). The assembly of dimers seems to occur by random assortment of monomers, but

only certain types of dimers are selected for secretion (Schwarzbauer et al., 1987a). In fact, experiments co-expressing recombinant FN fragments (deminectins) containing or not the IIICS domain (V120 and V0, respectively) in cultured fibroblasts showed that among the three possible types of dimers (V0/V0, V120/V120 and V0/V120), only those containing V120 are found in the medium. This selective retention of V0 homodimers within the ER indicates that the V region may be required for the formation and secretion of native FN dimers (Schwarzbauer et al., 1989). In an analogous *in vivo* situation, it has been shown that rat plasma FN also lacks V0 homodimers and consists only of V0/V+ and V+/V+ combinations (Schwarzbauer et al., 1989). Similarly to V0/V0 dimers, the EDA^{+}/EDA^{+} dimers produced by $EDA^{+/+}$ hepatocytes might not be efficiently secreted into either plasma (Figure 15) or culture medium (Figure 17) and could therefore be selectively retained and degraded due to a possibly unfolded or misfolded conformation. Intracellular protein degradation is an important mechanism of cellular regulation not only to eliminate waste products due to aberrant protein folding or failed protein secretion but also to regulate the protein output to the needs of the cell. It could be possible that hepatocytes are programmed to eliminate and/or to maintain at very low levels the $EDA^{+}FN$. One of the reasons to avoid high $EDA^{+}FN$ levels in plasma could be linked to its pro-thrombotic activity (see Introduction §1.4.4). It could also be possible that the degradation process of FN resembled the degradation pathway that governs the output of another huge hepatic glycoprotein such as apolipoprotein B (apoB). The intracellular degradation process of newly synthesized apoB has been shown to occur at every stage of the secretory pathway, from protein translation and polypeptide translocation across the membrane of the ER to vesicular transport (Yao et al., 1997). The proteolysis of nascent apoB can be performed by the ubiquitin-proteasome system in the cytosol as well as by resident ER proteases (Davidson and Shelness, 2000). Thus, $EDA^{+}FN$ proceeding along the normal secretory pathway may be stopped by a rapid and efficient proteolytic degradation at one or more of the steps of the process. In keeping with this hypothesis, we did not observe any

intracellular accumulation of FN in $EDA^{+/+}$ hepatocytes by immunostaining of tissue sections (Figure 25A-C) or immunofluorescence staining of primary culture hepatocytes (Figure 27 and 28).

Western blot analysis of plasma from heterozygous mice ($EDA^{wt/+}$) showed intermediate levels of total FN in comparison with $EDA^{wt/wt}$ and $EDA^{+/+}$ animals (Figure 26B), supporting the idea that $EDA^{+}FN$ is produced less efficiently because dimers containing only one $EDA^{+}FN$ monomer (EDA^{wt}/EDA^{+} heterodimers) would be secreted more efficiency than EDA^{+}/EDA^{+} homodimers. It is noteworthy that the "presence" of the EDA domain seems to negatively affect FN production by the hepatocyte. Indeed, following the *in vivo* removal of the EDA exon from the FN gene, a normal production of pFN is restored in $EDA^{+/+}$ mice. On the contrary, in the case of IIICS, the "absence" of the domain in both subunits of the dimer (V0/V0 variant) affects dimer formation and/or secretion, as shown by Schwarzbauer et al. This finding, though, has been demonstrated only *in vitro* by expressing cDNA encoding truncated FN fragments (or deminectins) in fibroblasts (Schwarzbauer et al., 1989).

Surprisingly, analysis of the FN content of both $EDA^{+/+}$ perfused liver (Figure 16A) and total cellular (Figure 17B) extracts revealed that, unlike in other tissues, the ECM does not contain a reduced level of FN. Indeed, FN content was similar in $EDA^{wt/wt}$ and $EDA^{+/+}$ mice. The normal level of FN in the ECM of liver and purified hepatocytes from $EDA^{+/+}$ mice raises several questions regarding FN export mechanisms in hepatocytes. The current model of FN assembly into the ECM or "fibrillogenesis" (Figure 46) postulates that soluble, inactive and compactly folded FN dimers bind $\alpha5\beta1$ integrins through the RGD cell binding sequence present in the type III_{10} module along with the synergy sequence located in the adjacent type III_9 module (Mao and Schwarzbauer, 2005; Schwarzbauer, 1991). Other integrins can also support FN-matrix assembly but with lower efficiency (Geiger et al., 2001) (Figure 46A). Although initially distributed diffusely over the cell surface, the Integrin/FN complexes soon cluster. Integrin clustering recruits signaling and

cytoskeletal proteins into "focal complexes", stimulating a number of distinct intracellular responses, including reorganization of the actin cytoskeleton and changes in gene expression (Figure 46B). The tension exerted on FN dimers as a consequence of integrin translocation along the actin stress fibers and out of the focal contacts, stretches and unfolds the FN subunits (Wierzbicka-Patynowski and Schwarzbauer, 2003) (Figure 46C). Consequently, the FN-binding domains that were hidden in the compact form are now exposed and become involved in FN-FN interactions. Soluble FN dimers are thus incorporated into a network of insoluble fibrils (Choi and Hynes, 1979). However, the precise mechanism of the initial binding between FN and integrins is not yet clear. The observation that $EDA^{+/+}$ hepatocytes secrete low amounts of soluble FN while the $EDA^{+/+}$ liver has normal FN levels suggests that inclusion of the EDA domain, which is placed near the RGD and the synergy sequences, could facilitate the unfolding or stretching of dimers. Consequently, FN cell-binding sites would be more accessible to integrins (Manabe et al., 1999; Manabe et al., 1997). The conformation of the FN molecule may be globally altered upon insertion of the EDA segment and the possible increased exposure of the RGD motif in the type III_{10} module, and/or other cryptic sites could render the EDA^{+}/EDA^{+} dimers stickier or less soluble. Thus, an augmented "stickiness" of the EDA^{+}/EDA^{+} dimers could not only explain the normal level of FN in the $EDA^{+/+}$ liver ECM (Figure 16A and 17B) but also the enhanced thrombus formation in injured arterioles in the presence of $EDA^{+}FN$ (see Introduction §1.4.4). The initial step of fibrillogenesis may be the intracellular binding of FN to integrin receptors. Once all the cell-surface receptors are fully occupied by the FN dimers, the excess of dimers could be released into the bloodstream, explaining the presence of 20% of $EDA^{+}FN$ in $EDA^{+/+}$ plasma. However, all these hypotheses need demonstrating.

Recently, $\alpha4\beta1$ and $\alpha9\beta1$ integrins have been shown to specifically bind to the EDA segment of FN. This interaction therefore provides a novel mechanism by which both cell adhesion and signal transduction are regulated by alternative splicing (Liao et al., 2002).

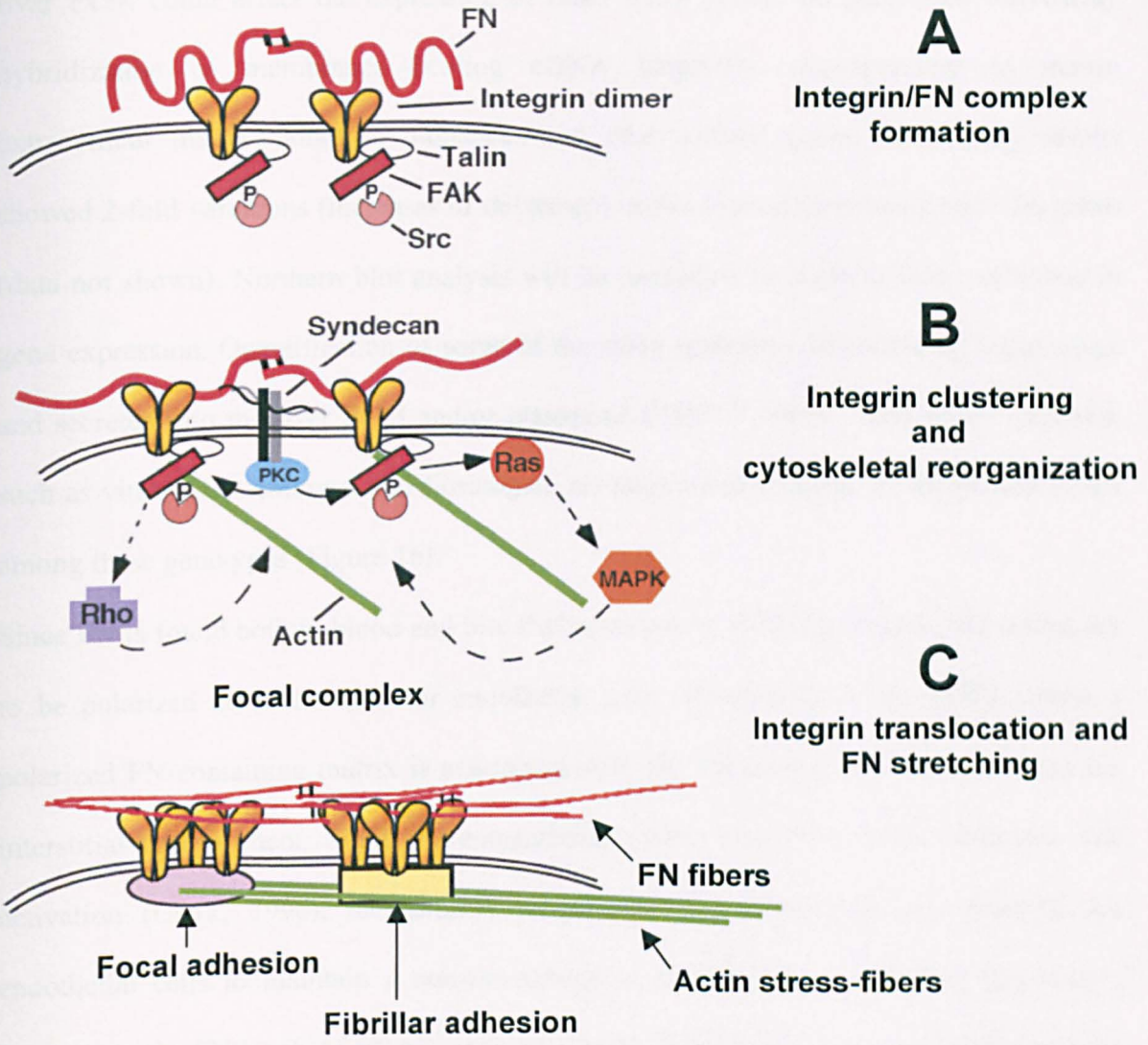

Figure 46. Fibronectin matrix assembly model.
A. Binding of soluble, compactly folded and inactive FN dimers to diffusely distributed integrins induces receptor clustering and co-localization of talin (white ovals) and focal adhesion kinase (FAK, red rectangle). FAK autophosphorylation (P) recruits Src (pink circle), and these two kinases regulate the very early step of assembly. **B.** Clustered integrins and co-localized syndecan (gray and black bars), a transmembrane proteoglycan that can bind to FN, organize the actin cytoskeleton (green lines) and activate signaling molecules including Ras/MAP kinase (orange), Rho GTPase (violet) and protein kinase C (PKC) (blue) at the "focal complexes". **C.** FN fibrillogenesis is driven by cooperation of two distinct types of cell-surface adhesion: "focal adhesion" and "fibrillar adhesion". These cooperate in a process by which integrins and dynamic tension forces seem to unmask cryptic FN assembly sites that mediate FN polarization and generate networks of fibrillar ECM. Ligand-bound $\alpha5\beta1$ integrins actively translocate from the focal adhesions to the fibrillar adhesions parallel to the actin microfilament bundles. This concerted movement could provide a mechanism by which tensile forces stretch FN and induce fibrillogenesis (Wierzbicka-Patynowski and Schwarzbauer, 2003).

Thus, to assess whether the constitutive presence or absence of the EDA domain in mouse liver ECM could affect the expression of other ECM genes, we performed microarray hybridization of membranes bearing cDNA fragments corresponding to mouse extracellular matrix, adhesion molecules and other related genes. Preliminary results showed 2-fold variations (increases or decreases) in the expression of some specific genes (data not shown). Northern blot analysis will be necessary to confirm these variations in gene expression. Quantification of some of the main proteins synthesized by hepatocytes and secreted into the liver ECM and/or plasma of $EDA^{wt/wt}$, $EDA^{+/+}$ and $EDA^{-/-}$ animals, such as vitronectin, collagen and fibrinogen, revealed no differences in the protein levels among these genotypes (Figure 16).

Since FN is found both in blood and bile fluids, secretion of FN by hepatocytes seems not to be polarized as is the case for endothelial cells (Kowalczyk et al., 1990), where a polarized FN-containing matrix is assembled onto the basolateral cell surface facing the interstitial compartment. Since the extracellular matrix promotes platelet adhesion and activation (Clark, 1996), mechanisms to polarize ECM formation are essential for endothelial cells to maintain a non-thrombogenic apical surface. We have observed a decrease in the FN levels of $EDA^{+/+}$ mice bile fluids (Figure 26A) that suggests an absence of an EDA-dependent polarization of the process of FN secretion in hepatocytes, similarly to airway epithelial cells (Wang et al., 1991). These cells secrete FN from both apical and basal surfaces, although the $EDA^{+}FN$ isoform is preferentially secreted apically to the airway lumen.

Overall, the present findings highlight the extraordinary structural and behavioral diversity between pFN and the FN present in the ECM, and attempt to explain the incapacity of hepatocytes to synthesize and secrete a potentially pro-thrombogenic $EDA^{+}FN$ isoform into the bloodstream.

4.2 THE FN-EDA DOMAIN PARTICIPATES IN THE ACTIVATION OF HEPATIC STELLATE CELLS.

The pathogenesis of progressive tissue fibrosis is not completely understood, and has been likened to an exuberant and dysregulated wound healing response. Therefore, understanding why normal wound healing is triggered and tissue injury is limited is of critical importance. Here we present evidence in support of the important role of $EDA^{+}FN$ in tissue repair/progressive fibrosis following liver injury. Carbon tetrachloride (CCl_4) administration and bile duct ligation (BDL) represent two well-established models to induce experimental liver fibrosis in rodents (Constandinou et al., 2005; Xia et al., 2006). Both models, even though differently, represent a liver insult that leads to the stimulation of hepatic fibrogenic cells, key elements of the fibroproliferative process typical of liver fibrotic diseases (Jarnagin et al., 1994; Maher and McGuire, 1990). Such cells are indeed responsible for an abnormal, intensive production and deposition of extracellular matrix proteins such as collagens and fibronectins in tissue fibrotic foci. The importance of the EDA-containing FN variant in the fibrotic process is shown by the upregulation of $EDA^{+}FN$ mRNA in $EDA^{wt/wt}$ hepatic tissue following CCl_4 treatment or BDL (George et al., 2000; Jarnagin et al., 1994) (Figure 29). We found that mice unable to produce $EDA^{+}FN$ show a reduced fibrotic response to fibrogenic insults. Therefore, expression of $EDA^{+}FN$ by non-parenchymal cells is a critical early event for the liver response to injury. In fact, histopathologic evidences (Figure 32, 35, 37 and 43) supported by Western blot analysis (Figure 31, 34 and 42) have shown a significant reduction of αSMA-expressing myofibroblasts in $EDA^{-/-}$ mice compared with $EDA^{wt/wt}$ controls. Additionally, primary lung fibroblasts from $EDA^{wt/wt}$, $EDA^{+/+}$ and $EDA^{-/-}$ mice were able to express comparable αSMA levels when plated on FN matrices bearing the EDA domain, in the presence of TGF-β (Eric White's personal communication, University of Michigan Medical Center, Chicago, USA). Interestingly, $EDA^{wt/wt}$ and $EDA^{+/+}$ fibroblasts were also able to express αSMA when plated on $EDA^{-}FN$ matrices, implying that either exogenous (matrix-derived)

or endogenous (cell-derived) $EDA^{+}FN$ supports myofibroblast differentiation. Instead, $EDA^{-/-}$ fibroblasts were not able to express high levels of αSMA when plated on the same $EDA^{-}FN$ matrices, again confirming that the presence of $EDA^{+}FN$, regardless of its origin, is important for the differentiation to myofibroblasts. However, when the same experiment was repeated in the absence of TGF-β, no induction of αSMA was observed, indicating that $EDA^{+}FN$ is necessary, but not sufficient for myofibroblast differentiation. We also observed that following a stronger liver insult such as the administration of a higher dose of CCl_4 for a longer period (Figure 36 and 39), or a longer BDL duration (Figure 45), the level of αSMA in $EDA^{-/-}$ livers paralleled that of $EDA^{wt/wt}$ livers. These data support the idea that other factors participate in myofibroblast transformation in addition to $EDA^{+}FN$. Since the $EDA^{+}FN$ variant is one of the ECM components to be earlier expressed after injury, we speculate that the EDA domain could be one of the first elements that trigger the activation of HSCs after mild liver insult, at the onset of the fibrotic process. When the insult is greater, however, other factors such as some cytokines, growth factors and ECM proteins may play a role in the activation process along with the EDA domain.

TGF-β has been shown to be directly involved in the differentiation of both skin (Balza et al., 1988; Borsi et al., 1990; Serini et al., 1998) and lung (Giri et al., 1997) fibroblasts, and indirectly involved in HSC differentiation (George et al., 2000). It stimulates the inclusion of the EDA exon into FN mRNA. Taken together, the data available and our results seem to indicate a biologically active role for the EDA domain in the *in vivo* conversion of HSCs and fibroblasts into myofibroblasts, supporting the contention that $EDA^{+}FN$ is necessary for TGF-β-mediated α-SMA expression *in vivo*. However, the precise mechanism by which TGF-β stimulates the production of $EDA^{+}FN$ mRNA is not yet well understood. In general, the FN-EDA splicing depends on the recognition of a splicing enhancer element located within the EDA exon itself by splicing factors termed SR proteins because they abound in serine-arginine motifs (Buratti et al., 2004; Caputi et al., 1994; Muro et al., 1999) (Figure 4). It is thought that TGF-β-induced alterations in the intracellular levels

and/or the phosphorylation state of these factors might result in an increase of splicing activity (Blaustein et al., 2005; Li and Sun, 1997; Maehama and Dixon, 1998).

The fibrotic process is mainly characterized by a strong production and deposition of collagen into the ECM. Previous studies have shown that both HSCs (Maher and McGuire, 1990) and skin fibroblasts (Serini et al., 1998) produce increased amounts of collagens following a fibrogenic insult. Histochemical staining of $EDA^{wt/wt}$ mouse lung sections obtained after inducing fibrosis by administering bleomycin showed an abundant deposition of collagen in fibrotic foci. These areas were also characterized by increased amounts of αSMA in comparison with untreated mice (Eric White's unpublished data, University of Michigan Medical Center, Chicago, USA). Interestingly, the levels of collagen and αSMA in bleomycin-treated $EDA^{-/-}$ samples were reduced in comparison with those from $EDA^{wt/wt}$ mice, and similar to the basal levels of untreated mice (Eric White's unpublished data, University of Michigan Medical Center, Chicago, USA). These results suggest that: a) the EDA domain of FN plays a critical role in the development of fibrosis in both lung and liver; b) the mechanisms triggering lung and liver fibrosis may be similar, and c) the role of the EDA domain in the differentiation and activation of hepatic stellate cells and skin fibroblasts (Jarnagin et al., 1994; Serini et al., 1998; Serini and Gabbiani, 1999) can be extended to lung fibroblasts. However, the differences we observed between lung and liver fibrosis suggest the involvement of other factors and a more complex fibrotic process in the liver. In fact, while the levels of αSMA and collagen in the lung of $EDA^{-/-}$ animals following bleomycin injury were similar to those of untreated mice (Eric White's unpublished data, University of Michigan Medical Center, Chicago, USA), the liver from both control and $EDA^{-/-}$ mice showed an increase in the levels of αSMA (Figure 30-31 and 41-42) and collagen (Figure 33 and 44) after fibrogenic challenge. Although liver levels of αSMA and collagen increased significantly in mutant mice following both CCl_4 treatment and BDL, these increases were markedly lower than in $EDA^{wt/wt}$ mice. This suggests that the lack of the EDA domain attenuated the development

of a full fibrotic response to liver injury. However, even though $EDA^{-/-}$ mice failed to develop collagen levels as high as those $EDA^{wt/wt}$, the difference between $EDA^{wt/wt}$ and $EDA^{-/-}$ livers in the levels of collagen, measured both by hydroxyproline assay or by quantification of the extent of collagen-positive areas in liver sections, were not statistically significant (Figure 33 and 44). The reason for the disparity in collagen production when comparing fibrotic lung and liver models is not clear, and might reflect the fact that other pathways could be bypassing the requirement for $EDA^{+}FN$ in the liver. At least three different cell lineages, expressing only αSMA, only collagen or both αSMA and collagen, contribute to the fibrogenic response in the liver while having different stellate cell marker gene profiles (Magness et al., 2004). This fact raises the question of discrete hepatic stellate cell populations that may have different $EDA^{+}FN$ requirements and respond to separate sets of stimuli regarding differentiation and activation.

Besides HSCs, the main fibrogenic cell type in pericentral areas of the liver, other hepatic cell types have been recently shown to exhibit fibrogenic potential (Figure 47). Perivascular fibroblasts of portal and central veins and periductural fibroblasts in close contact with bile ducts can be additional sources of fibrogenic myofibroblasts in the injured liver. Thus, a complex interplay involving different hepatic cell types may take place during hepatic fibrogenesis (Lotersztajn et al., 2005). Further work is needed to clarify the precise contribution of each of these cell types to the liver fibrotic process and the role of $EDA^{+}FN$ in their transformation to myofibroblasts.

Although we have presented evidence here that $EDA^{+}FN$ is necessary for α-SMA expression in myofibroblasts, a previous report demonstrated that $EDA^{-/-}$ mice show no defect in α-SMA induction in vascular smooth muscle cells or pericytes during tumor angiogenesis (Astrof et al., 2004). This observation, while seemingly contradicting our findings, is intriguing and may be explained in alternative ways.

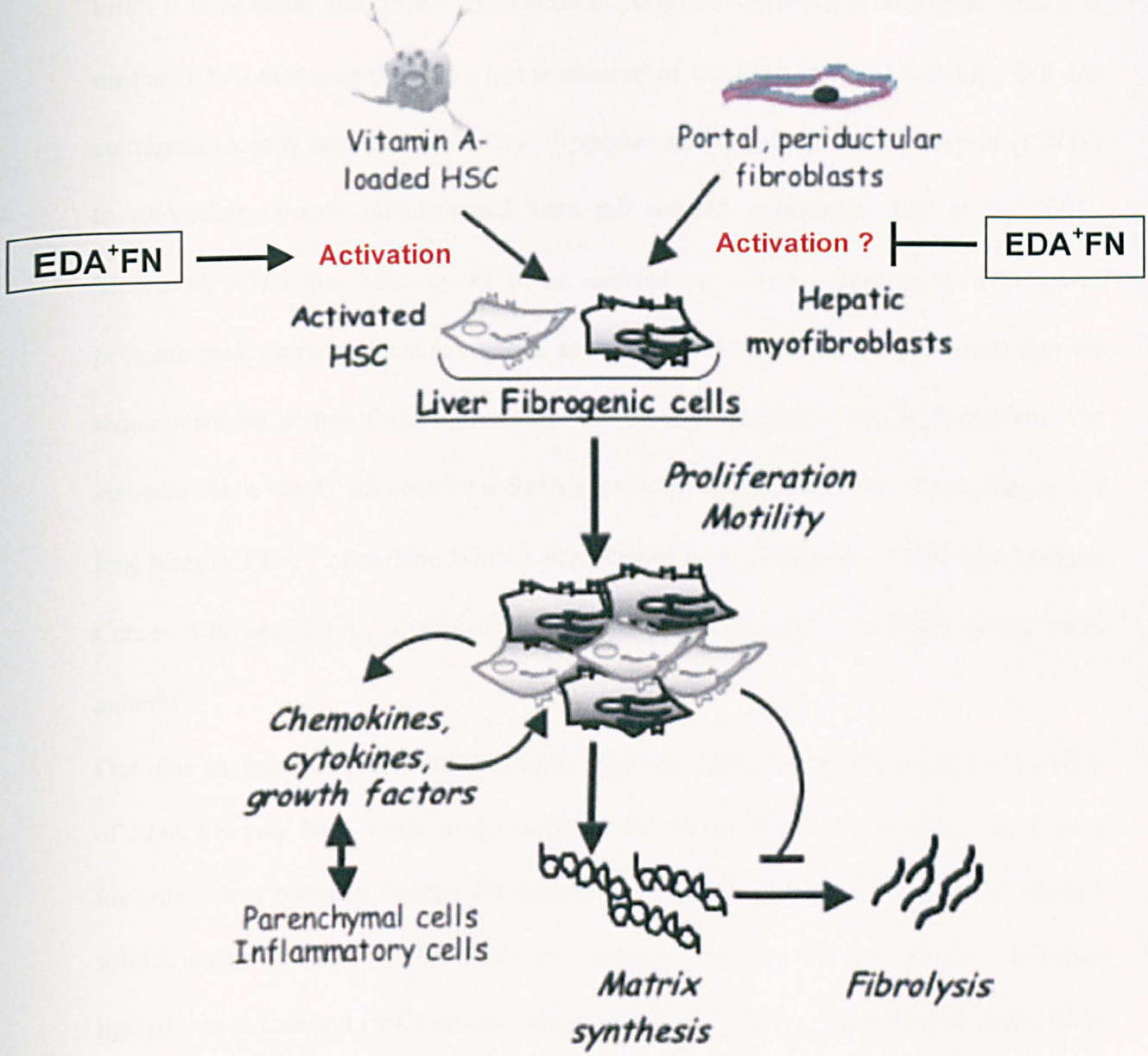

Figure 47. Heterogeneity in hepatic fibrogenic cell populations.
Matrix accumulation during chronic liver diseases originates from different fibrogenic myofibroblasts deriving from the "activation" of distinct cell populations such as the hepatic stellate cells (HSCs), and the perivascular and peribiliary fibroblasts (hepatic myofibroblasts). Following acute or chronic liver injury, they undergo phenotypic changes switching from a quiescent, vitamin A-rich phenotype to a myofibroblastic phenotype. Myofibroblasts show *de novo* fibrogenic properties, including proliferation and accumulation in areas of parenchymal cell necrosis, secretion of proinflammatory cytokines and chemokines, and synthesis of a large panel of matrix proteins and of inhibitors of matrix degradation, leading to progressive scar formation. Phenotypic and functional properties of hepatic myofibroblasts are grossly similar overall to those of activated hepatic stellate cells. However, culture studies have clearly established that several phenotypic markers distinguish both cell types (Lotersztajn et al., 2005). EDA^+FN could be involved in the activation of the HSCs but not in the activation of the hepatic myofibroblast.

First, it is possible that αSMA expression in pericytes surrounding angiogenic vessels is mediated by other growth factors in the absence of the EDA domain. Notably, Ball and colleagues recently reported the ability of platelet-derived growth factor receptor (PDGF) to upregulate directly mesenchymal stem cell α-SMA expression (Ball et al., 2007). Moreover, PDGF has been shown to be secreted by certain neoplasms as a means to promote pericyte recruitment (Furuhashi et al., 2004). Alternatively, it is possible that the requirement for certain factors governing α-SMA expression is cell-type dependent. For instance, while we do not observe α-SMA expressing myofibroblasts in bleomycin-injured lung areas of $EDA^{-/-}$ mice (Eric White's unpublished data, University of Michigan Medical Center, Chicago, USA), airway smooth muscle cells do express α-SMA in the same animals.

Our data suggest that therapeutic strategies targeting either the production or the function of $EDA^{+}FN$ may have a role in the treatment of fibroproliferative disorders. An attempt towards a new potential therapy for hepatic fibrosis was made by George *et al.* using a soluble antagonist of the TGF-β receptor extracellular domain. Treatment of bile-duct ligated rats *in vivo* and HSCs *ex vivo* with a soluble TGF-β receptor inhibited both αSMA and collagen production and hepatic fibrosis (George et al., 1999). These same investigators subsequently showed that the effect of soluble TGF-β receptor in hepatic fibrosis was mediated through the inhibition of $EDA^{+}FN$ production both *in vitro* and *in vivo* (George et al., 2000). Preventing the accumulation of activated HSCs by modulating their activation and/or proliferation or by promoting their apoptosis may be a viable approach for the treatment of fibrotic disorders, and $EDA^{+}FN$ is a plausible target.

5. BIBLIOGRAPHY

Ali, I. U., and Hunter, T. (1981). Structural comparison of fibronectins from normal and transformed cells. J Biol Chem *256*, 7671-7677.

Arai, M., Yokosuka, O., Chiba, T., Imazeki, F., Kato, M., Hashida, J., Ueda, Y., Sugano, S., Hashimoto, K., Saisho, H., *et al.* (2003). Gene expression profiling reveals the mechanism and pathophysiology of mouse liver regeneration. J Biol Chem *278*, 29813-29818.

Assoian, R. K., and Schwartz, M. A. (2001). Coordinate signaling by integrins and receptor tyrosine kinases in the regulation of G1 phase cell-cycle progression. Curr Opin Genet Dev *11*, 48-53.

Astrof, S., Crowley, D., George, E. L., Fukuda, T., Sekiguchi, K., Hanahan, D., and Hynes, R. O. (2004). Direct test of potential roles of EIIIA and EIIIB alternatively spliced segments of fibronectin in physiological and tumor angiogenesis. Mol Cell Biol *24*, 8662-8670.

Aszodi, A., Legate, K. R., Nakchbandi, I., and Fassler, R. (2006). What mouse mutants teach us about extracellular matrix function. Annu Rev Cell Dev Biol *22*, 591-621.

Bae, E., Sakai, T., and Mosher, D. F. (2004). Assembly of exogenous fibronectin by fibronectin-null cells is dependent on the adhesive substrate. J Biol Chem *279*, 35749-35759.

Ball, S. G., Shuttleworth, C. A., and Kielty, C. M. (2007). Platelet-derived growth factor receptor-[alpha] is a key determinant of smooth muscle [alpha]-actin filaments in bone marrow-derived mesenchymal stem cells. Int J Biochem Cell Biol *39*, 379-391.

Balza, E., Borsi, L., Allemanni, G., and Zardi, L. (1988). Transforming growth factor beta regulates the levels of different fibronectin isoforms in normal human cultured fibroblasts. FEBS Lett *228*, 42-44.

Baron, M., Main, A. L., Driscoll, P. C., Mardon, H. J., Boyd, J., and Campbell, I. D. (1992). 1H NMR assignment and secondary structure of the cell adhesion type III module of fibronectin. Biochemistry *31*, 2068-2073.

Baron, M., Norman, D., Willis, A., and Campbell, I. D. (1990). Structure of the fibronectin type 1 module. Nature *345*, 642-646.

Bataller, R., and Brenner, D. A. (2001). Hepatic stellate cells as a target for the treatment of liver fibrosis. Semin Liver Dis *21*, 437-451.

Bataller, R., and Brenner, D. A. (2005). Liver fibrosis. J Clin Invest *115*, 209-218.

Berget, S. M. (1995). Exon recognition in vertebrate splicing. J Biol Chem *270*, 2411-2414.

Bergman, I., and Loxley, R. (1970). New spectrophotometric method for the determination of proline in tissue hydrolyzates. Anal Chem *42*, 702-706.

Bissell, D. M. (1990). Hepatic fibrosis: cellular aspects. Ital J Gastroenterol *22*, 83-87.

Bissell, D. M. (2001). Chronic liver injury, TGF-beta, and cancer. Exp Mol Med *33*, 179-190.

Black, D. L. (2003). Mechanisms of alternative pre-messenger RNA splicing. Annu Rev Biochem *72*, 291-336.

Blaustein, M., Pelisch, F., Tanos, T., Munoz, M. J., Wengier, D., Quadrana, L., Sanford, J. R., Muschietti, J. P., Kornblihtt, A. R., Caceres, J. F., *et al.* (2005). Concerted regulation of nuclear and cytoplasmic activities of SR proteins by AKT. Nat Struct Mol Biol *12*, 1037-1044.

Borsi, L., Castellani, P., Risso, A. M., Leprini, A., and Zardi, L. (1990). Transforming growth factor-beta regulates the splicing pattern of fibronectin messenger RNA precursor. FEBS Lett *261*, 175-178.

Brow, D. A. (2002). Allosteric cascade of spliceosome activation. Annu Rev Genet *36*, 333-360.

Brown, L. F., Dubin, D., Lavigne, L., Logan, B., Dvorak, H. F., and Van de Water, L. (1993). Macrophages and fibroblasts express embryonic fibronectins during cutaneous wound healing. Am J Pathol *142*, 793-801.

Buratti, E., Muro, A. F., Giombi, M., Gherbassi, D., Iaconcig, A., and Baralle, F. E. (2004). RNA folding affects the recruitment of SR proteins by mouse and human polypurinic enhancer elements in the fibronectin EDA exon. Mol Cell Biol *24*, 1387-1400.

Caputi, M., Baralle, F. E., and Melo, C. A. (1995a). Analysis of the linkage between fibronectin alternative spliced sites during ageing in rat tissues. Biochim Biophys Acta *1263*, 53-59.

Caputi, M., Casari, G., Guenzi, S., Tagliabue, R., Sidoli, A., Melo, C. A., and Baralle, F. E. (1994). A novel bipartite splicing enhancer modulates the differential processing of the human fibronectin EDA exon. Nucleic Acids Res *22*, 1018-1022.

Caputi, M., Melo, C. A., and Baralle, F. E. (1995b). Regulation of fibronectin expression in rat regenerating liver. Nucleic Acids Res *23*, 238-243.

Chauhan, A. K., Iaconcig, A., Baralle, F. E., and Muro, A. F. (2004). Alternative splicing of fibronectin: a mouse model demonstrates the identity of in vitro and in vivo systems and the processing autonomy of regulated exons in adult mice. Gene *324*, 55-63.

Choi, M. G., and Hynes, R. O. (1979). Biosynthesis and processing of fibronectin in NIL.8 hamster cells. J Biol Chem *254*, 12050-12055.

Chomczynski, P., and Sacchi, N. (1987). Single-step method of RNA isolation by acid guanidinium thiocyanate-phenol-chloroform extraction. Anal Biochem *162*, 156-159.

Clark, R. A. (1990). Fibronectin matrix deposition and fibronectin receptor expression in healing and normal skin. J Invest Dermatol *94*, 128S-134S.

Clark, R. A., Winn, H. J., Dvorak, H. F., and Colvin, R. B. (1983). Fibronectin beneath reepithelializing epidermis in vivo: sources and significance. J Invest Dermatol *80 Suppl*, 26s-30s.

Clark, R. A. F. (1996). The Molecular and Cellular Biology of Wound Repair (New York: Plenum Press).

Constandinou, C., Henderson, N., and Iredale, J. P. (2005). Modeling liver fibrosis in rodents. Methods Mol Med *117*, 237-250.

Constantine, K. L., Ramesh, V., Banyai, L., Trexler, M., Patthy, L., and Llinas, M. (1991). Sequence-specific 1H NMR assignments and structural characterization of bovine seminal fluid protein PDC-109 domain b. Biochemistry *30*, 1663-1672.

Davidson, N. O., and Shelness, G. S. (2000). APOLIPOPROTEIN B: mRNA editing, lipoprotein assembly, and presecretory degradation. Annu Rev Nutr *20*, 169-193.

Du, K., Peng, Y., Greenbaum, L. E., Haber, B. A., and Taub, R. (1997). HRS/SRp40-mediated inclusion of the fibronectin EIIIB exon, a possible cause of increased EIIIB expression in proliferating liver. Mol Cell Biol *17*, 4096-4104.

Dunham, J. S., and Hynes, R. O. (1978). Differences in the sulfated macromolecules synthesized by normal and transformed hamster fibroblasts. Biochim Biophys Acta *506*, 242-255.

Ellingsworth, L. R., Brennan, J. E., Fok, K., Rosen, D. M., Bentz, H., Piez, K. A., and Seyedin, S. M. (1986). Antibodies to the N-terminal portion of cartilage-inducing factor A

and transforming growth factor beta. Immunohistochemical localization and association with differentiating cells. J Biol Chem *261*, 12362-12367.

ffrench-Constant, C. (1995). Alternative splicing of fibronectin--many different proteins but few different functions. Exp Cell Res *221*, 261-271.

Ffrench-Constant, C., and Hynes, R. O. (1988). Patterns of fibronectin gene expression and splicing during cell migration in chicken embryos. Development *104*, 369-382.

Ffrench-Constant, C., and Hynes, R. O. (1989). Alternative splicing of fibronectin is temporally and spatially regulated in the chicken embryo. Development *106*, 375-388.

Ffrench-Constant, C., Van de Water, L., Dvorak, H. F., and Hynes, R. O. (1989). Reappearance of an embryonic pattern of fibronectin splicing during wound healing in the adult rat. J Cell Biol *109*, 903-914.

Friedman, S. L. (2000). Molecular regulation of hepatic fibrosis, an integrated cellular response to tissue injury. J Biol Chem *275*, 2247-2250.

Friedman, S. L. (2003). Liver fibrosis -- from bench to bedside. J Hepatol *38 Suppl 1*, S38-53.

Friedman, S. L., Roll, F. J., Boyles, J., Arenson, D. M., and Bissell, D. M. (1989). Maintenance of differentiated phenotype of cultured rat hepatic lipocytes by basement membrane matrix. J Biol Chem *264*, 10756-10762.

Friedman, S. L., Roll, F. J., Boyles, J., and Bissell, D. M. (1985). Hepatic lipocytes: the principal collagen-producing cells of normal rat liver. Proc Natl Acad Sci U S A *82*, 8681-8685.

Fukuda, T., Yoshida, N., Kataoka, Y., Manabe, R., Mizuno-Horikawa, Y., Sato, M., Kuriyama, K., Yasui, N., and Sekiguchi, K. (2002). Mice lacking the EDB segment of fibronectin develop normally but exhibit reduced cell growth and fibronectin matrix assembly in vitro. Cancer Res *62*, 5603-5610.

Furuhashi, M., Sjoblom, T., Abramsson, A., Ellingsen, J., Micke, P., Li, H., Bergsten-Folestad, E., Eriksson, U., Heuchel, R., Betsholtz, C., *et al.* (2004). Platelet-Derived Growth Factor Production by B16 Melanoma Cells Leads to Increased Pericyte Abundance in Tumors and an Associated Increase in Tumor Growth Rate. Cancer Res %R 101158/0008-5472CAN-03-1489 *64*, 2725-2733.

Garcia, J. H., Liu, K. F., Yoshida, Y., Lian, J., Chen, S., and del Zoppo, G. J. (1994). Influx of leukocytes and platelets in an evolving brain infarct (Wistar rat). Am J Pathol *144*, 188-199.

Geerts, A. (2001). History, heterogeneity, developmental biology, and functions of quiescent hepatic stellate cells. Semin Liver Dis *21*, 311-335.

Geiger, B., Bershadsky, A., Pankov, R., and Yamada, K. M. (2001). Transmembrane crosstalk between the extracellular matrix--cytoskeleton crosstalk. Nat Rev Mol Cell Biol *2*, 793-805.

George, E. L., Georges-Labouesse, E. N., Patel-King, R. S., Rayburn, H., and Hynes, R. O. (1993). Defects in mesoderm, neural tube and vascular development in mouse embryos lacking fibronectin. Development *119*, 1079-1091.

George, J., Roulot, D., Koteliansky, V. E., and Bissell, D. M. (1999). In vivo inhibition of rat stellate cell activation by soluble transforming growth factor beta type II receptor: a potential new therapy for hepatic fibrosis. Proc Natl Acad Sci U S A *96*, 12719-12724.

George, J., Wang, S. S., Sevcsik, A. M., Sanicola, M., Cate, R. L., Koteliansky, V. E., and Bissell, D. M. (2000). Transforming growth factor-beta initiates wound repair in rat liver through induction of the EIIIA-fibronectin splice isoform. Am J Pathol *156*, 115-124.

Georges-Labouesse, E. N., George, E. L., Rayburn, H., and Hynes, R. O. (1996). Mesodermal development in mouse embryos mutant for fibronectin. Dev Dyn *207*, 145-156.

Gesteland, R. F., Cech, T. R., and Atkins, J. F. (1999). The RNA World, Second edn (Cold Spring Harbor, NY: Cold Spring Harb. Lab.).

Giancotti, F. G., and Ruoslahti, E. (1999). Integrin signaling. Science *285*, 1028-1032.

Giri, S. N., Hyde, D. M., Braun, R. K., Gaarde, W., Harper, J. R., and Pierschbacher, M. D. (1997). Antifibrotic effect of decorin in a bleomycin hamster model of lung fibrosis. Biochem Pharmacol *54*, 1205-1216.

Glukhova, M. A., Frid, M. G., Shekhonin, B. V., Balabanov, Y. V., and Koteliansky, V. E. (1990). Expression of fibronectin variants in vascular and visceral smooth muscle cells in development. Dev Biol *141*, 193-202.

Glukhova, M. A., Frid, M. G., Shekhonin, B. V., Vasilevskaya, T. D., Grunwald, J., Saginati, M., and Koteliansky, V. E. (1989). Expression of extra domain A fibronectin sequence in vascular smooth muscle cells is phenotype dependent. J Cell Biol *109*, 357-366.

Grabowski, P. J., and Black, D. L. (2001). Alternative RNA splicing in the nervous system. Prog Neurobiol *65*, 289-308.

Graveley, B. R. (2000). Sorting out the complexity of SR protein functions. Rna *6*, 1197-1211.

Gutman, A., and Kornblihtt, A. R. (1987). Identification of a third region of cell-specific alternative splicing in human fibronectin mRNA. Proc Natl Acad Sci U S A *84*, 7179-7182.

Hayashi, M., and Yamada, K. M. (1981). Differences in domain structures between plasma and cellular fibronectins. J Biol Chem *256*, 11292-11300.

Hershberger, R. P., and Culp, L. A. (1990). Cell-type-specific expression of alternatively spliced human fibronectin IIICS mRNAs. Mol Cell Biol *10*, 662-671.

Higuchi, H., and Gores, G. J. (2003). Mechanisms of liver injury: an overview. Curr Mol Med *3*, 483-490.

Hinz, B., and Gabbiani, G. (2003). Mechanisms of force generation and transmission by myofibroblasts. Curr Opin Biotechnol *14*, 538-546.

Hynes, R. O. (1990). Fibronectins (New York: Springer-Verlag).

Hynes, R. O. (1992). Integrins: versatility, modulation, and signaling in cell adhesion. Cell *69*, 11-25.

Hynes, R. O., and Yamada, K. M. (1982). Fibronectins: multifunctional modular glycoproteins. J Cell Biol *95*, 369-377.

Jarnagin, W. R., Rockey, D. C., Koteliansky, V. E., Wang, S. S., and Bissell, D. M. (1994). Expression of variant fibronectins in wound healing: cellular source and biological activity of the EIIIA segment in rat hepatic fibrogenesis. J Cell Biol *127*, 2037-2048.

Kellendonk, C., Opherk, C., Anlag, K., Schutz, G., and Tronche, F. (2000). Hepatocyte-specific expression of CRE recombinase. Genesis *26*, 151-153.

Knowlton, A. A., Connelly, C. M., Romo, G. M., Mamuya, W., Apstein, C. S., and Brecher, P. (1992). Rapid expression of fibronectin in the rabbit heart after myocardial infarction with and without reperfusion. J Clin Invest *89*, 1060-1068.

Komoriya, A., Green, L. J., Mervic, M., Yamada, S. S., Yamada, K. M., and Humphries, M. J. (1991). The minimal essential sequence for a major cell type-specific adhesion site (CS1) within the alternatively spliced type III connecting segment domain of fibronectin is leucine-aspartic acid-valine. J Biol Chem *266*, 15075-15079.

Kornblihtt, A. R., Pesce, C. G., Alonso, C. R., Cramer, P., Srebrow, A., Werbajh, S., and Muro, A. F. (1996). The fibronectin gene as a model for splicing and transcription studies. Faseb J *10*, 248-257.

Kornblihtt, A. R., Vibe-Pedersen, K., and Baralle, F. E. (1983). Isolation and characterization of cDNA clones for human and bovine fibronectins. Proc Natl Acad Sci U S A *80*, 3218-3222.

Kornblihtt, A. R., Vibe-Pedersen, K., and Baralle, F. E. (1984a). Human fibronectin: cell specific alternative mRNA splicing generates polypeptide chains differing in the number of internal repeats. Nucleic Acids Res *12*, 5853-5868.

Kornblihtt, A. R., Vibe-Pedersen, K., and Baralle, F. E. (1984b). Human fibronectin: molecular cloning evidence for two mRNA species differing by an internal segment coding for a structural domain. Embo J *3*, 221-226.

Kowalczyk, A. P., Tulloh, R. H., and McKeown-Longo, P. J. (1990). Polarized fibronectin secretion and localized matrix assembly sites correlate with subendothelial matrix formation. Blood *75*, 2335-2342.

Krecic, A. M., and Swanson, M. S. (1999). hnRNP complexes: composition, structure, and function. Curr Opin Cell Biol *11*, 363-371.

Laird, P. W., Zijderveld, A., Linders, K., Rudnicki, M. A., Jaenisch, R., and Berns, A. (1991). Simplified mammalian DNA isolation procedure. Nucleic Acids Res *19*, 4293.

Lavigueur, A., La Branche, H., Kornblihtt, A. R., and Chabot, B. (1993). A splicing enhancer in the human fibronectin alternate ED1 exon interacts with SR proteins and stimulates U2 snRNP binding. Genes Dev *7*, 2405-2417.

Leikina, E., Mertts, M. V., Kuznetsova, N., and Leikin, S. (2002). Type I collagen is thermally unstable at body temperature. Proc Natl Acad Sci U S A *99*, 1314-1318.

Li, D. M., and Sun, H. (1997). TEP1, encoded by a candidate tumor suppressor locus, is a novel protein tyrosine phosphatase regulated by transforming growth factor beta. Cancer Res *57*, 2124-2129.

Liao, Y. F., Gotwals, P. J., Koteliansky, V. E., Sheppard, D., and Van De Water, L. (2002). The EIIIA segment of fibronectin is a ligand for integrins alpha 9beta 1 and alpha 4beta 1 providing a novel mechanism for regulating cell adhesion by alternative splicing. J Biol Chem *277*, 14467-14474.

Libri, D., Piseri, A., and Fiszman, M. Y. (1991). Tissue-specific splicing in vivo of the beta-tropomyosin gene: dependence on an RNA secondary structure. Science *252*, 1842-1845.

Lotersztajn, S., Julien, B., Teixeira-Clerc, F., Grenard, P., and Mallat, A. (2005). Hepatic fibrosis: molecular mechanisms and drug targets. Annu Rev Pharmacol Toxicol *45*, 605-628.

Maehama, T., and Dixon, J. E. (1998). The tumor suppressor, PTEN/MMAC1, dephosphorylates the lipid second messenger, phosphatidylinositol 3,4,5-trisphosphate. J Biol Chem *273*, 13375-13378.

Magness, S. T., Bataller, R., Yang, L., and Brenner, D. A. (2004). A dual reporter gene transgenic mouse demonstrates heterogeneity in hepatic fibrogenic cell populations. Hepatology *40*, 1151-1159.

Magnuson, V. L., Young, M., Schattenberg, D. G., Mancini, M. A., Chen, D. L., Steffensen, B., and Klebe, R. J. (1991). The alternative splicing of fibronectin pre-mRNA is altered during aging and in response to growth factors. J Biol Chem *266*, 14654-14662.

Maher, J. J., and McGuire, R. F. (1990). Extracellular matrix gene expression increases preferentially in rat lipocytes and sinusoidal endothelial cells during hepatic fibrosis in vivo. J Clin Invest *86*, 1641-1648.

Malarkey, D. E., Johnson, K., Ryan, L., Boorman, G., and Maronpot, R. R. (2005). New insights into functional aspects of liver morphology. Toxicol Pathol *33*, 27-34.

Manabe, R., Oh-e, N., and Sekiguchi, K. (1999). Alternatively spliced EDA segment regulates fibronectin-dependent cell cycle progression and mitogenic signal transduction. J Biol Chem *274*, 5919-5924.

Manabe, R., Ohe, N., Maeda, T., Fukuda, T., and Sekiguchi, K. (1997). Modulation of cell-adhesive activity of fibronectin by the alternatively spliced EDA segment. J Cell Biol *139*, 295-307.

Mao, Y., and Schwarzbauer, J. E. (2005). Fibronectin fibrillogenesis, a cell-mediated matrix assembly process. Matrix Biol *24*, 389-399.

Marceau, N., Goyette, R., Valet, J. P., and Deschenes, J. (1980). The effect of dexamethasone on formation of a fibronectin extracellular matrix by rat hepatocytes in vitro. Exp Cell Res *125*, 497-502.

Mardon, H. J., Sebastio, G., and Baralle, F. E. (1987). A role for exon sequences in alternative splicing of the human fibronectin gene. Nucleic Acids Res *15*, 7725-7733.

Matsui, S., Takahashi, T., Oyanagi, Y., Takahashi, S., Boku, S., Takahashi, K., Furukawa, K., Arai, F., and Asakura, H. (1997). Expression, localization and alternative splicing pattern of fibronectin messenger RNA in fibrotic human liver and hepatocellular carcinoma. J Hepatol *27*, 843-853.

Matuskova, J., Chauhan, A. K., Cambien, B., Astrof, S., Dole, V. S., Piffath, C. L., Hynes, R. O., and Wagner, D. D. (2006). Decreased plasma fibronectin leads to delayed thrombus growth in injured arterioles. Arterioscler Thromb Vasc Biol *26*, 1391-1396.

McKeown-Longo, P. J., and Mosher, D. F. (1983). Binding of plasma fibronectin to cell layers of human skin fibroblasts. J Cell Biol *97*, 466-472.

Montesano, R., and Orci, L. (1988). Transforming growth factor beta stimulates collagen-matrix contraction by fibroblasts: implications for wound healing. Proc Natl Acad Sci U S A *85*, 4894-4897.

Mostafavi-Pour, Z., Askari, J. A., Whittard, J. D., and Humphries, M. J. (2001). Identification of a novel heparin-binding site in the alternatively spliced IIICS region of fibronectin: roles of integrins and proteoglycans in cell adhesion to fibronectin splice variants. Matrix Biol *20*, 63-73.

Muro, A. F., Caputi, M., Pariyarath, R., Pagani, F., Buratti, E., and Baralle, F. E. (1999). Regulation of fibronectin EDA exon alternative splicing: possible role of RNA secondary structure for enhancer display. Mol Cell Biol *19*, 2657-2671.

Muro, A. F., Chauhan, A. K., Gajovic, S., Iaconcig, A., Porro, F., Stanta, G., and Baralle, F. E. (2003). Regulated splicing of the fibronectin EDA exon is essential for proper skin wound healing and normal lifespan. J Cell Biol *162*, 149-160.

Muro, A. F., Iaconcig, A., and Baralle, F. E. (1998). Regulation of the fibronectin EDA exon alternative splicing. Cooperative role of the exonic enhancer element and the 5' splicing site. FEBS Lett *437*, 137-141.

Nagase, H., Visse, R., and Murphy, G. (2006). Structure and function of matrix metalloproteinases and TIMPs. Cardiovasc Res *69*, 562-573.

Nelson, D. L. a. C., M. M. (2005). Lehninger's Principles of Biochemistry, 4th Edition edn (W. H. Freeman and Company, New York: W. H. Freeman and Company).

Ni, H., Yuen, P. S., Papalia, J. M., Trevithick, J. E., Sakai, T., Fassler, R., Hynes, R. O., and Wagner, D. D. (2003). Plasma fibronectin promotes thrombus growth and stability in injured arterioles. Proc Natl Acad Sci U S A *100*, 2415-2419.

Norton, P. A., and Hynes, R. O. (1987). Alternative splicing of chicken fibronectin in embryos and in normal and transformed cells. Mol Cell Biol *7*, 4297-4307.

Novobrantseva, T. I., Majeau, G. R., Amatucci, A., Kogan, S., Brenner, I., Casola, S., Shlomchik, M. J., Koteliansky, V., Hochman, P. S., and Ibraghimov, A. (2005). Attenuated liver fibrosis in the absence of B cells. J Clin Invest *115*, 3072-3082.

Odenthal, M., Neubauer, K., Baralle, F. E., Peters, H., Meyer zum Buschenfelde, K. H., and Ramadori, G. (1992). Rat hepatocytes in primary culture synthesize and secrete cellular fibronectin. Exp Cell Res *203*, 289-296.

Oh, E., Pierschbacher, M., and Ruoslahti, E. (1981). Deposition of plasma fibronectin in tissues. Proc Natl Acad Sci U S A *78*, 3218-3221.

Olden, K., Pratt, R. M., and Yamada, K. M. (1979). Role of carbohydrate in biological function of the adhesive glycoprotein fibronectin. Proc Natl Acad Sci U S A *76*, 3343-3347.

Owens, M. R., and Cimino, C. D. (1982). Synthesis of fibronectin by the isolated perfused rat liver. Blood *59*, 1305-1309.

Owens, R. J., and Baralle, F. E. (1986). Mapping the collagen-binding site of human fibronectin by expression in Escherichia coli. Embo J *5*, 2825-2830.

Oyama, F., Hirohashi, S., Sakamoto, M., Titani, K., and Sekiguchi, K. (1993). Coordinate oncodevelopmental modulation of alternative splicing of fibronectin pre-messenger RNA at ED-A, ED-B, and CS1 regions in human liver tumors. Cancer Res *53*, 2005-2011.

Oyama, F., Hirohashi, S., Shimosato, Y., Titani, K., and Sekiguchi, K. (1989a). Deregulation of alternative splicing of fibronectin pre-mRNA in malignant human liver tumors. J Biol Chem *264*, 10331-10334.

Oyama, F., Murata, Y., Suganuma, N., Kimura, T., Titani, K., and Sekiguchi, K. (1989b). Patterns of alternative splicing of fibronectin pre-mRNA in human adult and fetal tissues. Biochemistry *28*, 1428-1434.

Pagani, F., Zagato, L., Vergani, C., Casari, G., Sidoli, A., and Baralle, F. E. (1991). Tissue-specific splicing pattern of fibronectin messenger RNA precursor during development and aging in rat. J Cell Biol *113*, 1223-1229.

Pankov, R., and Yamada, K. M. (2002). Fibronectin at a glance. J Cell Sci *115*, 3861-3863.

Peters, D. M., Portz, L. M., Fullenwider, J., and Mosher, D. F. (1990). Co-assembly of plasma and cellular fibronectins into fibrils in human fibroblast cultures. J Cell Biol *111*, 249-256.

Peters, J. H., and Hynes, R. O. (1996). Fibronectin isoform distribution in the mouse. I. The alternatively spliced EIIIB, EIIIA, and V segments show widespread codistribution in the developing mouse embryo. Cell Adhes Commun *4*, 103-125.

Petersen, T. E., Thogersen, H. C., Skorstengaard, K., Vibe-Pedersen, K., Sahl, P., Sottrup-Jensen, L., and Magnusson, S. (1983). Partial primary structure of bovine plasma fibronectin: three types of internal homology. Proc Natl Acad Sci U S A *80*, 137-141.

Pierschbacher, M. D., and Ruoslahti, E. (1984). Cell attachment activity of fibronectin can be duplicated by small synthetic fragments of the molecule. Nature *309*, 30-33.

Plow, E. F., Haas, T. A., Zhang, L., Loftus, J., and Smith, J. W. (2000). Ligand binding to integrins. J Biol Chem *275*, 21785-21788.

Plump, A. S., Smith, J. D., Hayek, T., Aalto-Setala, K., Walsh, A., Verstuyft, J. G., Rubin, E. M., and Breslow, J. L. (1992). Severe hypercholesterolemia and atherosclerosis in apolipoprotein E-deficient mice created by homologous recombination in ES cells. Cell *71*, 343-353.

Price, J., and Hynes, R. O. (1985). Astrocytes in culture synthesize and secrete a variant form of fibronectin. J Neurosci *5*, 2205-2211.

Prowse, K. R., Tricoli, J. V., Klebe, R. J., and Shows, T. B. (1986). Assignment of the human fibronectin structural gene to chromosome 2. Cytogenet Cell Genet *41*, 42-46.

Rodriguez-Garay, E. A. (2003). Cholestasis: human disease and experimental animal models. Ann Hepatol *2*, 150-158.

Ruoslahti, E., Hayman, E. G., Pierschbacher, M., and Engvall, E. (1982). Fibronectin: purification, immunochemical properties, and biological activities. Methods Enzymol *82 Pt A*, 803-831.

Sakai, T., Johnson, K. J., Murozono, M., Sakai, K., Magnuson, M. A., Wieloch, T., Cronberg, T., Isshiki, A., Erickson, H. P., and Fassler, R. (2001). Plasma fibronectin supports neuronal survival and reduces brain injury following transient focal cerebral ischemia but is not essential for skin-wound healing and hemostasis. Nat Med *7*, 324-330.

Sauer, B., and Henderson, N. (1988). Site-specific DNA recombination in mammalian cells by the CRE recombinase of bacteriophage P1. Proc Natl Acad Sci U S A *85*, 5166-5170.

Schwarzbauer, J. E. (1991). Identification of the fibronectin sequences required for assembly of a fibrillar matrix. J Cell Biol *113*, 1463-1473.

Schwarzbauer, J. E., Mulligan, R. C., and Hynes, R. O. (1987a). Efficient and stable expression of recombinant fibronectin polypeptides. Proc Natl Acad Sci U S A *84*, 754-758.

Schwarzbauer, J. E., Patel, R. S., Fonda, D., and Hynes, R. O. (1987b). Multiple sites of alternative splicing of the rat fibronectin gene transcript. Embo J *6*, 2573-2580.

Schwarzbauer, J. E., Spencer, C. S., and Wilson, C. L. (1989). Selective secretion of alternatively spliced fibronectin variants. J Cell Biol *109*, 3445-3453.

Schwarzbauer, J. E., Tamkun, J. W., Lemischka, I. R., and Hynes, R. O. (1983). Three different fibronectin mRNAs arise by alternative splicing within the coding region. Cell *35*, 421-431.

Seglen, P. O. (1976). Preparation of isolated rat liver cells. Methods Cell Biol *13*, 29-83.

Serini, G., Bochaton-Piallat, M. L., Ropraz, P., Geinoz, A., Borsi, L., Zardi, L., and Gabbiani, G. (1998). The fibronectin domain ED-A is crucial for myofibroblastic phenotype induction by transforming growth factor-beta1. J Cell Biol *142*, 873-881.

Serini, G., and Gabbiani, G. (1999). Mechanisms of myofibroblast activity and phenotypic modulation. Exp Cell Res *250*, 273-283.

Skow, L. C., Adkison, L., Womack, J. E., Beamer, W. G., and Taylor, B. A. (1987). Mapping of the mouse fibronectin gene (Fn-1) to chromosome 1: conservation of the Idh-1-Cryg-Fn-1 synteny group in mammals. Genomics *1*, 283-286.

Sottile, J., Hocking, D. C., and Swiatek, P. J. (1998). Fibronectin matrix assembly enhances adhesion-dependent cell growth. J Cell Sci *111 (Pt 19)*, 2933-2943.

Su, A. I., Guidotti, L. G., Pezacki, J. P., Chisari, F. V., and Schultz, P. G. (2002). Gene expression during the priming phase of liver regeneration after partial hepatectomy in mice. Proc Natl Acad Sci U S A *99*, 11181-11186.

Tajiri, M., Yoshida, S., and Wada, Y. (2005). Differential analysis of site-specific glycans on plasma and cellular fibronectins: application of a hydrophilic affinity method for glycopeptide enrichment. Glycobiology *15*, 1332-1340.

Tamkun, J. W., and Hynes, R. O. (1983a). Plasma fibronectin is synthesized and secreted by hepatocytes. J Biol Chem *258*, 4641-4647.

Tamkun, J. W., and Hynes, R. O. (1983b). Plasma fibronectin is synthesized and secreted by hepatocytes. J Biol Chem *258*, 4641-4647.

Tan, M. H., Sun, Z., Opitz, S. L., Schmidt, T. E., Peters, J. H., and George, E. L. (2004). Deletion of the alternatively spliced fibronectin EIIIA domain in mice reduces atherosclerosis. Blood *104*, 11-18.

Tavian, D., De Petro, G., Colombi, M., Portolani, N., Giulini, S. M., Gardella, R., and Barlati, S. (1994). RT-PCR detection of fibronectin EDA+ and EDB+ mRNA isoforms: molecular markers for hepatocellular carcinoma. Int J Cancer *56*, 820-825.

Teng, M. H., and Rifkin, D. B. (1979). Fibronectin from chicken embryo fibroblasts contains covalently bound phosphate. J Cell Biol *80*, 784-791.

Tom, V. J., Doller, C. M., Malouf, A. T., and Silver, J. (2004). Astrocyte-associated fibronectin is critical for axonal regeneration in adult white matter. J Neurosci *24*, 9282-9290.

Torres, R. M., Kuhn, R. (1997). Laboratory protocols for conditional gene targeting (Oxford, UK: Oxford University Press).

Veit, B. E., and Fangman, W. L. (1988). Copy number and partition of the Saccharomyces cerevisiae 2 micron plasmid controlled by transcription regulators. Mol Cell Biol *8*, 4949-4957.

Voss, B., Allam, S., Rauterberg, J., Ullrich, K., Gieselmann, V., and von Figura, K. (1979). Primary cultures of rat hepatocytes synthesize fibronectin. Biochem Biophys Res Commun *90*, 1348-1354.

Wang, A., Cohen, D. S., Palmer, E., and Sheppard, D. (1991). Polarized regulation of fibronectin secretion and alternative splicing by transforming growth factor. J Biol Chem *266*, 15598-15601.

Wierzbicka-Patynowski, I., and Schwarzbauer, J. E. (2003). The ins and outs of fibronectin matrix assembly. J Cell Sci *116*, 3269-3276.

Xia, J. L., Dai, C., Michalopoulos, G. K., and Liu, Y. (2006). Hepatocyte growth factor attenuates liver fibrosis induced by bile duct ligation. Am J Pathol *168*, 1500-1512.

Yamada, K. M. (1983). Cell surface interactions with extracellular materials. Annu Rev Biochem *52*, 761-799.

Yamada, K. M. (2000). Fibronectin peptides in cell migration and wound repair. J Clin Invest *105*, 1507-1509.

Yamada, K. M., and Kennedy, D. W. (1979). Fibroblast cellular and plasma fibronectins are similar but not identical. J Cell Biol *80*, 492-498.

Yang, Z., Suzuki, R., Daniels, S. B., Brunquell, C. B., Sala, C. J., and Nishiyama, A. (2006). NG2 glial cells provide a favorable substrate for growing axons. J Neurosci *26*, 3829-3839.

Yao, Z., Tran, K., and McLeod, R. S. (1997). Intracellular degradation of newly synthesized apolipoprotein B. J Lipid Res *38*, 1937-1953.

Zegers, M. M., and Hoekstra, D. (1998). Mechanisms and functional features of polarized membrane traffic in epithelial and hepatic cells. Biochem J *336 (Pt 2)*, 257-269.

Zheng, X., Saunders, T. L., Camper, S. A., Samuelson, L. C., and Ginsburg, D. (1995). Vitronectin is not essential for normal mammalian development and fertility. Proc Natl Acad Sci U S A *92*, 12426-12430.

Zhu, B. C., and Laine, R. A. (1985). Polylactosamine glycosylation on human fetal placental fibronectin weakens the binding affinity of fibronectin to gelatin. J Biol Chem *260*, 4041-4045.

APPENDIX

The first part of this thesis, related to the study of the origin of fibronectin present in the tissue extracellular matrix, has been accepted for publication in the Journal of Biological Chemistry (JBC):

Federico A. Moretti, Anil K. Chauhan, Alessandra Iaconcig, Fabiola Porro, Francisco E. Baralle and Andrés F. Muro (2007). **A major fraction of fibronectin present in the extracellular matrix of tissues is plasma-derived.** J Biol Chem Sep 21;282(38):28057-62. Epub 2007 Jul 19

An electronic reprint of this article can be viewed in the subsequent pages.

APPENDIX

The first part of this thesis, related to the study of the origin of fibronectin present in the tissue extracellular matrix, has been accepted for publication in the Journal of Biological Chemistry (JBC):

Federico A. Moretti, Anil K. Chauhan, Alessandra Iaconcig, Fabiola Porro, Francisco E. Baralle and Andrés F. Muro (2007). **A major fraction of fibronectin present in the extracellular matrix of tissues is plasma-derived.** J Biol Chem Sep 21;282(38):28057-62. Epub 2007 Jul 19

An electronic reprint of this article can be viewed in the subsequent pages.

THE JOURNAL OF BIOLOGICAL CHEMISTRY VOL. 282, NO. 38, pp. 28057–28062, September 21, 2007

A Major Fraction of Fibronectin Present in the Extracellular Matrix of Tissues Is Plasma-derived*[S]

Received for publication, December 11, 2006, and in revised form, May 9, 2007 Published, JBC Papers in Press, July 19, 2007, DOI 10.1074/jbc.M611315200

Federico A. Moretti, Anil K. Chauhan[1], Alessandra Iaconcig, Fabiola Porro, Francisco E. Baralle, and Andrés F. Muro[2]

From the International Centre for Genetic Engineering and Biotechnology, 34012 Trieste, Italy

The origin of the fibronectin (FN) found in the extracellular matrix of tissues has not been defined experimentally. Previous studies suggest that there is contribution from both local tissue production and transfer from plasma, but the extent of this phenomenon has not been addressed. We have shown before that engineered mice constitutively expressing extra domain A-containing FN (EDA$^+$FN) have a significant decrease of FN levels in plasma and most tissues. We showed that hepatocytes modified to produce EDA$^+$FN have normal extracellular matrix-FN levels but secrete less soluble FN. When we performed a liver-specific EDA-exon deletion in these animals, FN levels were restored both in plasma and tissues. Therefore, an important fraction of tissue FN, approximately an equal amount of that produced by the tissue itself, is actually plasma-derived, suggesting that plasma is an important source of tissue FN. The present results have potential significance for understanding the contributions of plasma FN, and perhaps other plasma proteins, in the modulation of cellular activities and in the formation of the extracellular matrix of tissues.

Fibronectins (FN)[3] are a family of multifunctional glycoproteins known to play key roles in fundamental processes related to adhesive and migratory behavior of cells, such as embryogenesis, malignancy, homeostasis, wound healing, and maintenance of tissue integrity (1). FN generates protein diversity as a consequence of alternative processing of a single primary transcript at three different sites, the extra domain A (EDA), the extra domain B (EDB), and the type III homologies connecting segment (IIICS) (2–4). Two major forms of FN exist, plasma FN (pFN) and cellular FN. pFN is a soluble dimeric form that is secreted into the bloodstream by hepatocytes (5, 6) and found at 300 and 580 μg/ml in plasma of humans and mice, respectively (1, 7). pFN lacks both the EDA and EDB domains, whereas cellular FN is locally produced and deposited as insoluble fibrils in the extracellular matrix of tissues and contains these domains at variable proportions (1, 8, 9). Previous studies suggested that circulating pFN contributes to the extracellular matrix of tissues (10, 11) but the extent of the phenomenon has not been addressed.

The levels of FN in plasma are critical for hemostasis, tissue repair, and susceptibility to infections. Depletion of pFN (liver-specific knockout of FN) results in increased brain injury after transient focal cerebral ischemia (12), a delay in thrombus formation and decreased thrombus stability (13), decreased angiogenesis (14), and increased susceptibility to bacterial infections (15). Heterozygous null FN mice appear healthy and fertile (7) but show delayed thrombus growth in injured arterioles (16). Regrettably, the levels of FN present in the tissues of heterozygous null FN and in the pFN null mice have not been reported.

We have previously shown that knock-in mice having constitutive inclusion of the EDA exon of the FN gene (EDA$^{+/+}$ strain) had up to 70–80% reduction in the levels of plasma and tissue FN (17). Taking advantage of the "floxed" EDA exon present in those mice, we generated liver-specific EDA-null mice (EDA$^{+/+CRE}$) after crossing EDA$^{+/+}$ animals with a transgenic strain expressing the CRE recombinase only in hepatocytes (18). Consequently, hepatocytes of EDA$^{+/+CRE}$ mice, without the EDA exon, were able to produce and secrete pFN at normal levels.

We show here that the levels of pFN were restored in those mice and also that the levels of tissue FN were similar to those observed in EDA$^{WT/WT}$ animals. These results showed a major flow of pFN into the extracellular matrix of tissues and suggest the importance of the pFN as an essential source of FN for the tissues. The presented results might have potential significance for understanding the contributions of pFN, and perhaps other plasma proteins, to cellular activities and in the formation of the extracellular matrix of tissues.

EXPERIMENTAL PROCEDURES

Mice—The generation and genetic background of the mice devoid of regulated splicing at the EDA exon have been previously described (17). EDA$^{+/+}$ mice were mated with the transgenic strain Tg Alf pCRE mice, which have CRE recombinase under the control of the albumin promoter and enhancer (18). EDA$^{+/WT}$ mice having the CRE recombinase were mated in order to obtain EDA$^{+/+}$ mice with the CRE transgene (EDA$^{+/+CRE}$). This strain expresses the CRE recombinase exclusively in hepatocytes (18). The genotype of mice was determined by PCR from tail biopsies.

* The costs of publication of this article were defrayed in part by the payment of page charges. This article must therefore be hereby marked "*advertisement*" in accordance with 18 U.S.C. Section 1734 solely to indicate this fact.
[S] The on-line version of this article (available at http://www.jbc.org) contains supplemental Figs. S1–S3 and supplemental Materials and Methods.
[1] Present Address: CBR Institute for Biomedical Research and Dept. of Pathology, Harvard Medical School, Boston, MA 02115.
[2] To whom correspondence should be addressed: International Centre for Genetic Engineering and Biotechnology, Padriciano 99, I 34012, Trieste, Italy. Tel.: 39-040-3757312; Fax: 39-040-226555; E-mail: muro@icgeb.org.
[3] The abbreviations used are: FN, fibronectin; pFN, plasma FN; EDA, extra domain A; IIICS, type III homologies connecting segment; WT, wild type; RT-PCR, reverse transcription PCR.

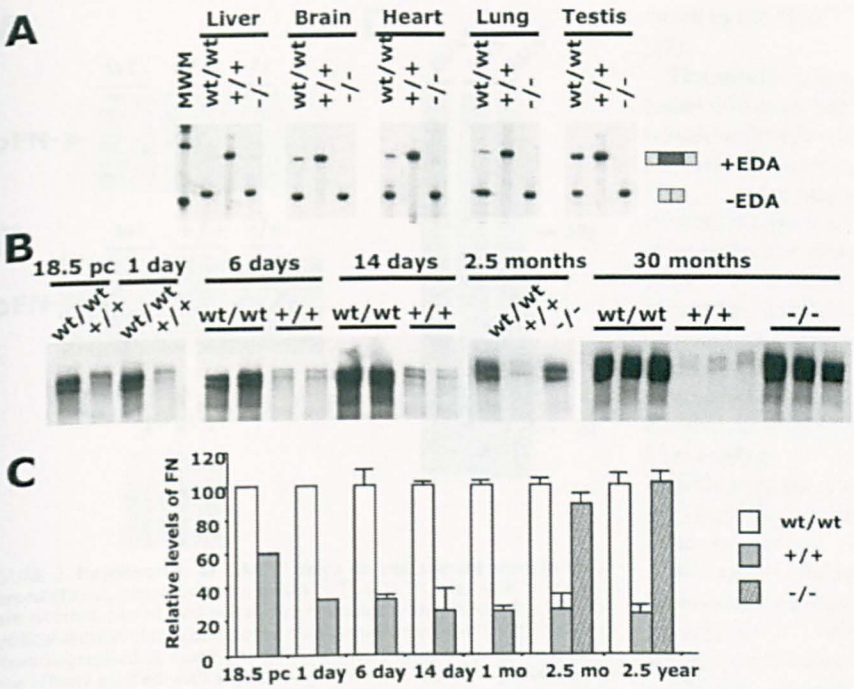

FIGURE 1. **EDA$^{+/+}$ embryos have a decrease in the levels of pFN.** *A*, radioactive RT-PCR analysis of the EDA exon of total RNA extracted from liver, brain, heart, lung, and testis from EDA$^{WT/WT}$, EDA$^{+/+}$, and EDA$^{-/-}$ mice. The position of the EDA-containing (+*EDA*) and the EDA-lacking (−*EDA*) bands are indicated. *B*, Western blot analysis of pFN from 18.5-pc embryos, 1-, 6-, and 14-day-old babies, 2.5- and 30-month-old adult mice from EDA$^{WT/WT}$, EDA$^{+/+}$, and EDA$^{-/-}$ animals. The samples corresponding to 18.5-pc and 1-day-old time points are pools of 4–6 animals/genotype. Note that the EDA^{+}FN migrates at a different size from the EDA^{-} FN by SDS-PAGE. *C*, the intensity of the signals in *panel B* was quantified with the help of the Quantity One software. The signal obtained in the EDA$^{WT/WT}$ samples was considered 100%. Data are presented as the mean ± S.D. of three independent animals/genotype.

RNA Preparation and Reverse Transcription (RT)-PCR Analysis—Total RNA was prepared from freshly extracted tissues and cells as described (19). The radioactive RT-PCR reactions were performed and quantified as previously described (20).

Protein Extracts and Western Blot Analysis—Mice were anesthetized with 2.5% Avertin (300 μl/20 g mouse), and organs were perfused with 25 ml of cold phosphate-buffered saline through the left ventricle of the heart. Organs were immediately dissected and snap-frozen in liquid nitrogen. Organs were homogenized, and protein content was determined by Bradford protein assay (Bio-Rad). Identical amounts of protein sample were run on a 6% SDS-PAGE and analyzed by Western blot with polyclonal rabbit anti-FN antibody (50 μg of protein extract, 1:1500; Sigma), anti-EDA 3E2 monoclonal antibody (100 μg of protein extract, 1:300; Sigma), or anti β-tubulin monoclonal antibody (20 μg of protein extract, E7, 1:3000; Developmental Studies Hybridoma Bank, University of Iowa) as described (17). Three animals per genotype were analyzed. To determine the efficiency of perfusion and elimination of plasma proteins in each of the organs analyzed, a Western blot analysis of 50 μg of protein extract was performed using an anti-mouse IgG antibody (1:2000; DAKO). Serial ECL expositions of the membranes were performed to determine the optimum linear range to quantify the signals. Films were scanned with the Versadoc (Bio-Rad) and quantified with the help of the Quantity One software package (Bio-Rad).

Bile was collected by holding the gallbladder with forceps. Two μl of each sample were mixed with protein loading buffer (0.125 Tris-HCl, pH 6.8, 4% SDS, 20% glycerol, and 0.002% bromphenol blue) and boiled for 5 min. Bile FN was analyzed by Western blot as described above.

In Vivo Labeling of Hepatocytes—Hepatocytes were purified by the two-step collagenase perfusion method (21), using Liver Digest Medium (Invitrogen) as described by the manufacturers. Hepatocytes were plated in rat tail collagen for 1 h, washed, and then incubated for 24 h with Met-Cys-free medium supplemented with 300 μCi/ml of [^{35}S]Met/Cys (ProMix; Amersham Biosciences). The supernatant was collected, and a fraction was affinity-purified with gelatin-Sepharose as described (22, 23).

Southern Blot Analysis of Tissues—DNA was extracted from tissues, and 15 μg were digested with HindIII. The DNA was then run in an agarose gel and blotted onto Z-Probe membrane. A probe corresponding to the exon downstream to the EDA exon was used as described (17).

Immunohistochemistry of Tissue Sections—Organs were fixed in 4% formaldehyde and paraffin-embedded. 4-μm sections of each tissue were cut and incubated with affinity-purified polyclonal rabbit anti-FN antibody (1:200; Sigma). Then sections were incubated with biotinylated goat anti-rabbit IgG (5 μg/ml; VectaStain) followed by avidin-biotin-peroxidase mix (ABC Reagent; Vector Laboratories), 3,3′-diaminobenzidine peroxidase substrate (Vector Laboratories), and Gill's hematoxylin (Vector Laboratories). An AS LMD Leica microscope was used to visualize and photograph the sections.

RESULTS

Hepatocytes of EDA$^{+/+}$ Mice Have Normal Levels of Extracellular Matrix-FN but Do Not Secrete pFN—We have previously observed that mice having constitutive inclusion of the EDA exon of the FN gene (Fig. 1*A*) had a significant decrease of FN in plasma and in most tissues (17, 20). Further characterization of pFN levels (embryo, young, and adult mice) from EDA$^{+/+}$ mice showed very low amounts compared with EDA$^{WT/WT}$ and EDA$^{-/-}$ mice (Fig. 1, *B* and *C*). Embryos had 60% of the pFN levels in the control sample, whereas young and adult EDA$^{+/+}$ mice showed a higher decrease in pFN levels. The decrease in pFN was due neither to lower levels in mRNA in tissues of EDA$^{+/+}$ mice (17) nor to a reduced FN production by EDA$^{+/+}$ tissues, as FN secreted by EDA$^{+/+}$ embryonic fibroblasts or adult heart fibroblasts was similar to that pro-

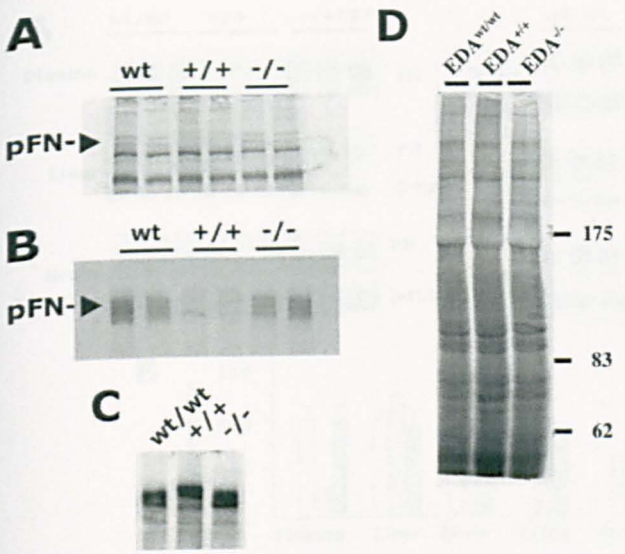

FIGURE 2. **Hepatocytes of EDA$^{+/+}$ mice do not secrete soluble EDA^{+} fibronectin.** *A*, hepatocytes from EDA$^{WT/WT}$, EDA$^{+/+}$, and EDA$^{-/-}$ animals were isolated, plated, and metabolically labeled with [^{35}S]Met/Cys for 24 h. Identical aliquots of the conditioned medium were run in a 6% SDS-PAGE and autoradiographed. *B*, equal quantities of the samples prepared in *panel A* were affinity-purified with a gelatin-agarose resin, eluted, separated in an SDS-PAGE, and autoradiographed. *C*, total cell extracts prepared from equal number of hepatocytes from EDA$^{WT/WT}$, EDA$^{+/+}$, and EDA$^{-/-}$ mice cultured in non-radioactive medium were collected after 24 h and analyzed by Western blot with a polyclonal anti-FN antibody. *D*, total cell extracts from the hepatocytes used in *panel A* were collected, and identical aliquots were run in a 6% SDS-PAGE and autoradiographed. Molecular weight markers are indicated.

duced by the EDA$^{WT/WT}$ fibroblasts, excluding a general defect (17).

The specific degradation of FN in the EDA$^{+/+}$ mice by proteases was ruled out by a series of experiments: 1) Metalloproteinase activity levels in plasma and tissues by gelatin zymography analysis were similar among EDA$^{WT/WT}$, EDA$^{+/+}$, and EDA$^{-/-}$ mice (supplemental Fig. S1, *A* and *B*); 2) [^{35}S]Met-labeled fragments of FN containing or not containing the EDA exon were not differentially degraded when incubated with EDA$^{WT/WT}$ or EDA$^{+/+}$ tissue extracts or plasma in the absence of protease inhibitors (supplemental Fig. S1, *C* and *D*); 3) no increase in FN degradation rate was observed after mixing protein extracts from EDA$^{+/+}$ or EDA$^{WT/WT}$ liver with those originating from different organs or plasma from EDA$^{+/+}$ mice in the absence of protease inhibitors (data not shown); 4) Western blot analysis of tissue extracts done with different sets of anti-FN polyclonal antibodies, run on 5–17% gradient gel, did not show any specific degradation products in EDA$^{+/+}$ mice (data not shown).

Because the hepatocytes are the source of pFN (5, 6), we performed metabolic labeling of hepatocyte primary cultures from EDA$^{WT/WT}$, EDA$^{+/+}$, and EDA$^{-/-}$ livers followed by FN affinity purification of the conditioned medium to analyze pFN production. We observed a decreased secretion of pFN by the EDA$^{+/+}$ hepatocytes, suggesting that the reduced levels in pFN in the EDA$^{+/+}$ mice were the consequence of a defect in hepatocytes (Fig. 2, *A* and *B*). However, the FN amounts detected by Western blot in hepatocyte cell extracts were similar (Fig. 2*C*). Additionally, the decrease of pFN in EDA$^{+/+}$ embryos (Fig. 1*B*) but not in embryonic tissues (17) confirmed that the deficiency in FN secretion was limited only to EDA$^{+/+}$ hepatocytes. These results showed that EDA$^{+/+}$ hepatocytes were unable to secrete pFN in normal amounts. We hypothesized that the reduced levels of tissue FN could be due to the decreased supply of FN from plasma to tissues.

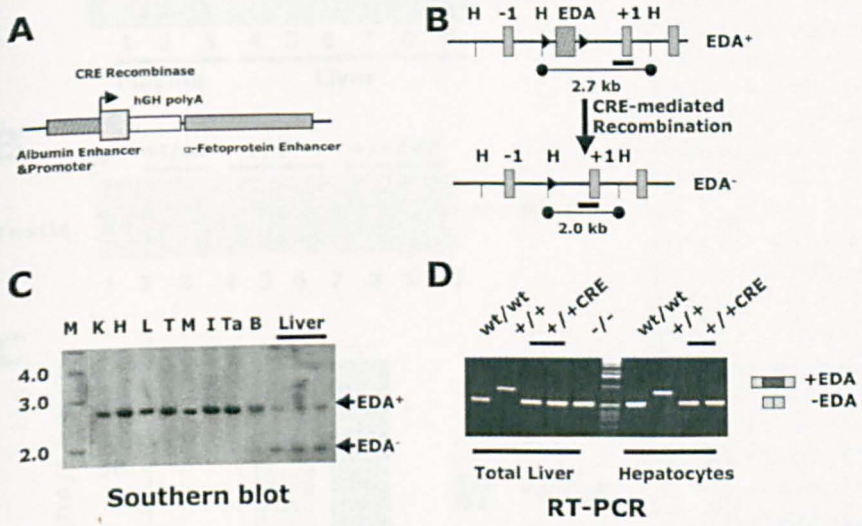

FIGURE 3. **Liver-specific deletion of the EDA exon.** *A*, scheme of the Alf P-Cre transgene. The CRE recombinase (*dotted box*) is expressed under the control of the mouse albumin enhancer and promoter (*dashed box*) and the mouse α-fetoprotein enhancer (*gray box*). Correct polyadenylation was directed by the hGH fragment (*empty box*). *B*, partial map of the EDA^{+} and EDA^{-} FN alleles. The EDA exon is indicated as a *dashed box* and the lox-P sites as *black triangles*. HindIII sites (*H*), the probe used in *panel C* (*black line below +1 exon*), the flanking exons (*−1* and *+1*), and the expected size of HindIII-digested fragments are as indicated. *C*, EDA$^{+/+}$ mice were crossed with a transgenic strain expressing the CRE recombinase in hepatocytes. Southern blot analysis of the different tissues from EDA$^{+/+CRE}$ mice was performed, and specific recombination was observed only in the liver. EDA^{+} and EDA^{-} bands are indicated. Liver DNA samples from three mice are shown. Tissues are as indicated: *K*, kidney; *H*, heart; *L*, lung; *T*, testis; *M*, skeletal muscle; *I*, intestine; *Ta*, tail; *B*, brain; *M*, molecular weight markers. *D*, RT-PCR analysis showing the inclusion/exclusion of the EDA exon in total RNA prepared from liver and purified hepatocytes from the different genotypes. The position of the EDA^{+} and EDA^{-} bands is indicated.

Generation of Liver-specific EDA Null Mice—To determine the extent of FN flow into tissues we restored the capacity of hepatocytes to produce pFN not containing the EDA exon by cross-breeding EDA$^{+/+}$ mice with a transgenic strain expressing the CRE recombinase only in hepatocytes (18). The aim was to perform a tissue-specific deletion of the EDA exon without modifying the EDA^{+} allele in other cell types and tissues (Fig. 3, *A* and *B*). Southern blot analysis of different tissues from the EDA$^{+/+}$ mice carrying the liver-specific CRE recombinase (EDA$^{+/+CRE}$ mice) showed CRE-mediated recombination only in the liver (Fig. 3*C*). The percentage

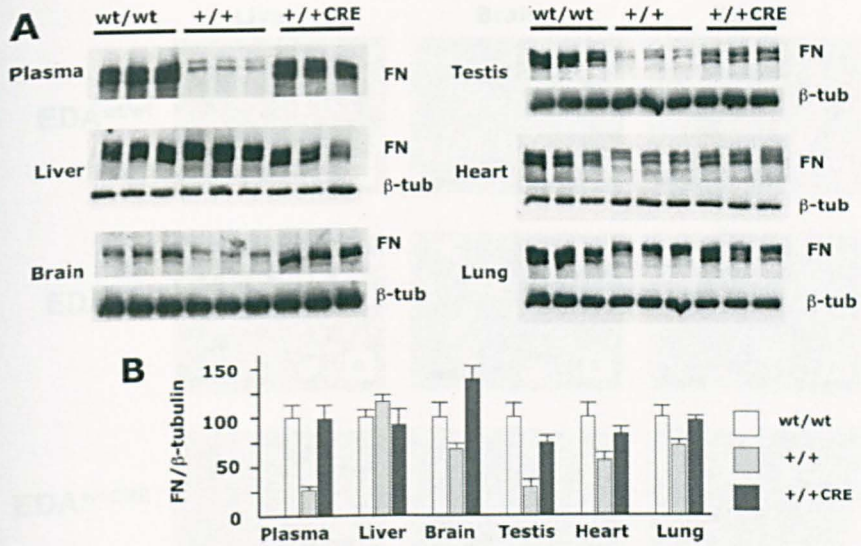

FIGURE 4. **Plasma and tissues from EDA$^{+/+CRE}$ mice have normal FN levels.** *A*, plasma and protein extracts were prepared from EDA$^{WT/WT}$, EDA$^{+/+}$, and EDA$^{+/+CRE}$ mice (3 month-old), and total FN levels were detected by Western blot analysis. The protein load was controlled by detecting β-tubulin in the same extracts. *B*, the intensity of the signals in *panel A* was quantified with the help of the Quantity One software. The ratio between FN and β-tubulin signals was used for normalization, and results are shown in the bar graph. The ratio obtained in the EDA$^{WT/WT}$ samples was considered 100%. The mean ± S.D. of three independent experiments is shown.

of recombination in liver was ~60–70%. Because hepatocytes constitute 60% of the total number of cells present in the liver (24), one can consider that the percentage of recombination in hepatocytes was close to 100%. RT-PCR analysis confirmed the absence of the EDA exon in the FN mRNA both in liver and purified hepatocytes from EDA$^{+/+CRE}$ mice (Fig. 3*D*).

FN Levels Are Restored in EDA$^{+/+CRE}$ Mice—Tissues and plasma from EDA$^{+/+}$ mice expressing the hepatocyte-specific CRE recombinase were analyzed by Western blot with polyclonal anti-FN and anti-EDA-specific antibodies. As expected, pFN levels were completely restored in the EDA$^{+/+CRE}$ mice (Fig. 4*A*). Tissue extracts prepared from EDA$^{+/+CRE}$ mice contained amounts of FN similar to that found in EDA$^{WT/WT}$ mice (Fig. 4*A*). The amount of FN present in the extracellular matrix of tissues from EDA$^{+/+CRE}$ mice that was derived from plasma was ~60% in testis and ~40% in other tissues such as brain, heart, and lung (Fig. 4*B*). These results clearly indicate that an important proportion of the FN present in the extracellular matrix of adult tissues derives from plasma. Consequently, the amount of FN that is synthesized and deposited locally in tissues is much lower than believed.

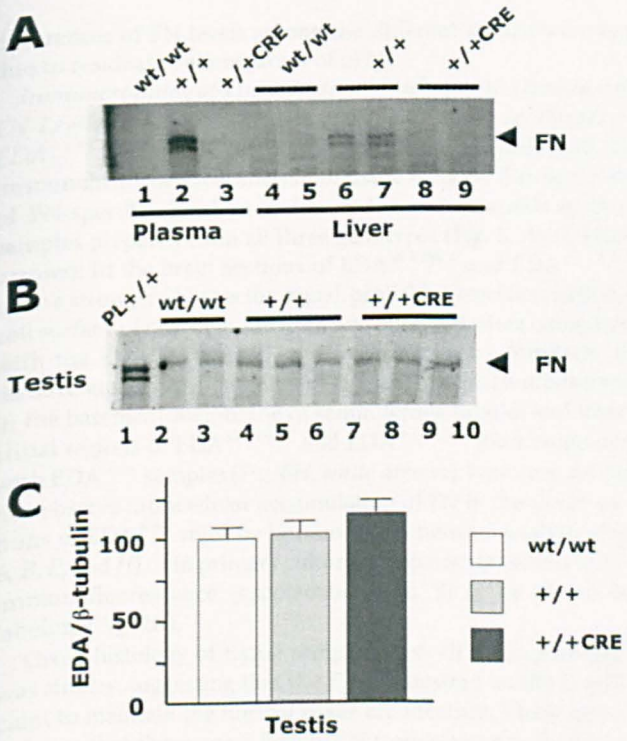

FIGURE 5. *A*, plasma from EDA$^{+/+CRE}$ mice has no EDA-containing FN. Plasma and liver protein extracts prepared from EDA$^{WT/WT}$, EDA$^{+/+}$, and EDA$^{+/+CRE}$ mice were analyzed for the presence of the EDA domain with the 3E2 anti-EDA monoclonal antibody. *B*, similar levels of EDA^{+}FN were seen in tissues from all three genotypes. The same protein extracts from testis used in Fig. 4 were analyzed by Western blot with the 3E2 anti-EDA monoclonal antibody. *C*, the ratio between EDA^{+}FN and β-tubulin signals was used for normalization, and results are shown in the bar graph. The ratio obtained in the EDA$^{WT/WT}$ samples was considered 100%. Data are presented as the mean ± S.D. of three independent animals/genotype.

We then used the monoclonal antibody 3E2 to specifically detect the EDA-containing FN isoform. As expected, no EDA^{+}FN was present in the plasma of EDA$^{WT/WT}$ mice. Additionally, we did not detect EDA^{+}FN in the plasma of EDA$^{+/+CRE}$ mice, indicating a high efficiency of CRE-mediated recombination in hepatocytes. The EDA^{+}FN isoform in liver was clearly visible only in the EDA$^{+/+}$ samples (Fig. 5*A*, *lanes 4–9*), confirming again the Southern blot and RT-PCR data (Fig. 3, *C* and *D*). The absence of EDA^{+}FN in the plasma of EDA$^{+/+CRE}$ mice also suggests that the FN flow is mainly from plasma to tissues and not vice versa (Fig. 5*A*, *lanes 1–3*). No differences were observed in the levels of EDA^{+}FN in testis (Fig. 5, *B* and *C*) and in other tissues (data not shown) between the EDA$^{WT/WT}$ and EDA$^{+/+CRE}$ samples, suggesting that the observed differences in tissue FN among the different genotypes corresponded to EDA^{-}FN incorporated from plasma into the extracellular matrix of tissues.

To ensure that the detected levels of FN in tissues were not due to non-complete perfusion of the organs, we performed Western blot analysis of the plasma globulins that remained in each tissue after perfusion and normalized the protein load with the β-tubulin signal. Supplemental Fig. S2 shows that the remaining globulin levels after tissue perfusion were ~10% of the levels seen in the non-perfused organs. Because most plasma proteins were washed out from the perfused organs, the

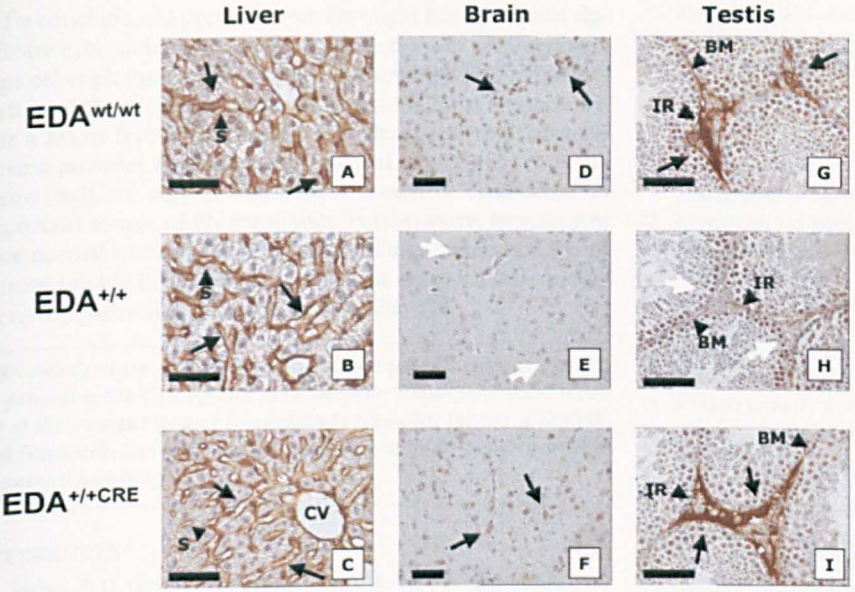

FIGURE 6. **Immunohistochemical analysis of liver, brain, and testis.** Tissue sections of liver (*A–C*), brain (*D–F*), and testis (*G–I*) from $EDA^{WT/WT}$ (*A, D,* and *G*), $EDA^{+/+}$ (*B, E,* and *H*), and $EDA^{+/+CRE}$ mice (*C, F,* and *I*) were stained with an affinity-purified polyclonal anti-FN antibody. The *black arrows* indicate FN in the extracellular matrix of $EDA^{WT/WT}$ and $EDA^{+/+CRE}$ from different tissues and $EDA^{+/+}$ liver. *White arrows* indicate the decrease in levels of FN from the same areas of brain and testis only in $EDA^{+/+}$ mice. *S*, sinusoids, *BM*, basement membrane, and *IR*, interstitial region, are indicated by *black triangles*. The *black bars* correspond to 50 μm.

differences of FN levels among the different strains were not due to residual contamination of pFN.

Immunostaining of Tissue Sections Confirmed the Decrease of FN Levels in $EDA^{+/+}$ Tissues and the Recovery in Tissues of $EDA^{+/+CRE}$ Mice—The above results were confirmed by immunohistochemical analysis of tissue sections. Similar levels of FN-specific signal were detected in the sinusoids of liver samples prepared from all three genotypes (Fig. 6, *A–C, black arrows*). In the brain sections of $EDA^{WT/WT}$ and $EDA^{+/+CRE}$ mice a stronger FN-specific signal, probably associated with the cell surface of glial cells (25–27), was observed when compared with the $EDA^{+/+}$ mice (Fig. 6*E*, *white arrows*). Similarly, in testis tissue sections, a stronger FN-specific signal was observed in the basement membrane of seminiferous tubules and interstitial regions of $EDA^{WT/WT}$ and $EDA^{+/+CRE}$ mice compared with $EDA^{+/+}$ samples (Fig. 6*H*, *white arrows*). However, we did not observe intracellular accumulation of FN in the tissue sections of $EDA^{+/+}$ mice by immunohistochemical analysis (Fig. 6, *B, E,* and *H*) or in primary culture of hepatocytes either by FN immunofluorescence (supplemental Fig. 3) or by metabolic labeling (Fig. 2*D*).

Gross histology of tissue samples from all three genotypes was similar, suggesting that the FN synthesized locally is sufficient to maintain the normal tissue architecture. These results indicate that there was a flow of FN from plasma to the extracellular matrix of tissues and plasma is an important source of tissue FN.

DISCUSSION

Our data demonstrate an important and novel role for plasma proteins, in particular that of fibronectin, in the formation of the extracellular matrix of tissues and, probably, in the modulation of cellular activities in tissues. The concept that there is FN flow from plasma into tissues or extracellular matrix of cells has been known for a long time. Addition or injection of soluble FN into the culture medium of cells or into the plasma of mice, respectively, resulted in the incorporation of FN into the extracellular matrix (10, 11, 28–30). However, the magnitude of the contribution of pFN to the extracellular matrix was not possible to address with either model. In the present report we have shown that in some tissues up to 60% of the fibronectin present in the extracellular matrix could be plasma-derived.

Sakai *et al.* (12) have recently shown that pFN supports neuronal survival and reduces brain injury following transient focal cerebral ischemia, suggesting the incorporation of pFN into the injured brain. Our results confirmed and extended their observations to non-injured tissues as we showed pFN incorporation into most normal organs, including brain. In fact, we are also demonstrating that this is a general mechanism that occurs in most normal tissues, and we suggest that other plasma proteins could also become incorporated into the extracellular matrix of tissues, modulating cellular activities.

Because FN is found both in blood and bile fluids, secretion of FN by hepatocytes seems not to be polarized as proposed for endothelial cells (31). Furthermore, we also observed a decrease in FN levels in the bile fluid of $EDA^{+/+}$ mice (data not shown), suggesting the absence of an EDA-dependent polarization of FN secretion in hepatocytes, as postulated for airway epithelial cells (32). The low levels of soluble FN in the plasma of $EDA^{+/+}$ mice and intermediate levels in $EDA^{+/WT}$ and $EDA^{+/-}$ mice (data not shown) point toward the existence of a mechanism, analogous to that observed for the secretion of the IIICS variants (33), that detects the EDA domain during the secretory pathway of pFN from hepatocytes and prevents the release of EDA^{+}FN into the bloodstream. The "defective" EDA^{+}/EDA^{+} pFN dimers might be formed but their transit through the pFN secretory pathway might be slower compared with EDA^{-}/EDA^{-} dimers. However, immunostaining of tissue sections, immunofluorescence of primary culture of hepatocytes, or metabolic labeling of hepatocytes did not reveal any intracellular accumulation of FN in the liver of $EDA^{+/+}$ mice, suggesting that the putative "misfolded" dimers are quickly degraded. We observed that the amount of pFN supplied to the extracellular matrix of tissues varied among the different organs analyzed, suggesting that there might be equilibrium between the amount of FN locally produced by the tissues and the availability of cellular receptors to incorporate FN from the plasma pool.

A Major Fraction of Tissue Fibronectin Is Plasma-derived

To conclude, the presented results might have potential significance for understanding the contributions of pFN, and perhaps other plasma proteins, to cellular activities and in the formation of the extracellular matrix of tissues, as we have shown that a major fraction of tissue FN is plasma-derived. Because plasma provides approximately an equal amount of FN as the tissue itself, we suggest that plasma should be considered an important source of FN for tissues. Furthermore, hepatocytes have normal levels of FN in the extracellular matrix but do not secrete soluble EDA^+FN, suggesting the existence of separate secretory pathways for soluble and fibrillar FN.

Acknowledgments—We thank Marcello Raspa and Günther Schütz for providing the Tg Alf pCRE mice, Meghan Walsh for critical reading of the manuscript and for comments regarding the use of English, and Giancarlo Lunazzi, Mauro Sturnega, and Stefano Artico for help in animal handling.

REFERENCES

1. Hynes, R. O. (1990) in *Fibronectins* (Rich, A., ed) Springer-Verlag, New York
2. Kornblihtt, A. R., Vibe-Pedersen, K., and Baralle, F. E. (1984) *EMBO J.* **3,** 221–226
3. Gutman, A., and Kornblihtt, A. R. (1987) *Proc. Natl. Acad. Sci. U. S. A.* **84,** 7179–7182
4. Schwarzbauer, J. E., Tamkun, J. W., Lemischka, I. R., and Hynes, R. O. (1983) *Cell* **35,** 2 Pt. 1, 421–431
5. Owens, M. R., and Cimino, C. D. (1982) *Blood* **59,** 1305–1309
6. Tamkun, J. W., and Hynes, R. O. (1983) *J. Biol. Chem.* **258,** 4641–4647
7. George, E. L., Georges-Labouesse, E. N., Patel-King, R. S., Rayburn, H., and Hynes, R. O. (1993) *Development* **119,** 1079–1091
8. ffrench-Constant, C. (1995) *Exp. Cell Res.* **221,** 261–271
9. Kornblihtt, A. R., Pesce, C. G., Alonso, C. R., Cramer, P., Srebrow, A., Werbajh, S., and Muro, A. F. (1996) *FASEB J.* **10,** 248–257
10. McKeown-Longo, P. J., and Mosher, D. F. (1983) *J. Cell Biol.* **97,** 466–472
11. Oh, E., Pierschbacher, M., and Ruoslahti, E. (1981) *Proc. Natl. Acad. Sci. U. S. A.* **78,** 3218–3221
12. Sakai, T., Johnson, K. J., Murozono, M., Sakai, K., Magnuson, M. A., Wieloch, T., Cronberg, T., Isshiki, A., Erickson, H. P., and Fassler, R. (2001) *Nat. Med.* **7,** 324–330
13. Ni, H., Yuen, P. S., Papalia, J. M., Trevithick, J. E., Sakai, T., Fassler, R., Hynes, R. O., and Wagner, D. D. (2003) *Proc. Natl. Acad. Sci. U. S. A.* **100,** 2415–2419
14. Yi, M., Sakai, T., Fassler, R., and Ruoslahti, E. (2003) *Proc. Natl. Acad. Sci. U. S. A.* **100,** 11435–11438
15. Nyberg, P., Sakai, T., Cho, K. H., Caparon, M. G., Fassler, R., and Bjorck, L. (2004) *EMBO J.* **23,** 2166–2174
16. Matuskova, J., Chauhan, A. K., Cambien, B., Astrof, S., Dole, V. S., Piffath, C. L., Hynes, R. O., and Wagner, D. D. (2006) *Arterioscler. Thromb. Vasc. Biol.* **26,** 1391–1396
17. Muro, A. F., Chauhan, A. K., Gajovic, S., Iaconcig, A., Porro, F., Stanta, G., and Baralle, F. E. (2003) *J. Cell Biol.* **162,** 149–160
18. Kellendonk, C., Opherk, C., Anlag, K., Schutz, G., and Tronche, F. (2000) *Genesis* **26,** 151–153
19. Chomczynski, P., and Sacchi, N. (1987) *Anal. Biochem.* **162,** 156–159
20. Chauhan, A. K., Iaconcig, A., Baralle, F. E., and Muro, A. F. (2004) *Gene* **324,** 55–63
21. Seglen, P. O. (1976) *Methods Cell Biol.* **13,** 29–83
22. Owens, R. J., and Baralle, F. E. (1986) *EMBO J.* **5,** 2825–2830
23. Ruoslahti, E., Hayman, E. G., Pierschbacher, M., and Engvall, E. (1982) *Methods Enzymol.* **82,** Pt. A, 803–831
24. Malarkey, D. E., Johnson, K., Ryan, L., Boorman, G., and Maronpot, R. R. (2005) *Toxicol. Pathol.* **33,** 27–34
25. Price, J., and Hynes, R. O. (1985) *J. Neurosci.* **5,** 2205–2211
26. Tom, V. J., Doller, C. M., Malouf, A. T., and Silver, J. (2004) *J. Neurosci.* **24,** 9282–9290
27. Yang, Z., Suzuki, R., Daniels, S. B., Brunquell, C. B., Sala, C. J., and Nishiyama, A. (2006) *J. Neurosci.* **26,** 3829–3839
28. Peters, D. M., Portz, L. M., Fullenwider, J., and Mosher, D. F. (1990) *J. Cell Biol.* **111,** 249–256
29. Sottile, J., Hocking, D. C., and Swiatek, P. J. (1998) *J. Cell Sci.* **111,** Pt. 19, 2933–2943
30. Bae, E., Sakai, T., and Mosher, D. F. (2004) *J. Biol. Chem.* **279,** 35749–35759
31. Kowalczyk, A. P., Tulloh, R. H., and McKeown-Longo, P. J. (1990) *Blood* **75,** 2335–2342
32. Wang, A., Cohen, D. S., Palmer, E., and Sheppard, D. (1991) *J. Biol. Chem.* **266,** 15598–15601
33. Schwarzbauer, J. E., Spencer, C. S., and Wilson, C. L. (1989) *J. Cell Biol.* **109,** 6 Pt. 2, 3445–3453

SUPPLEMENTAL DATA

Supplementary Material and Methods

In vitro translation: cDNAs with or without the EDA exon were prepared from $EDA^{+/+}$ and $EDA^{-/-}$ mice by RT-PCR using the following primers: Forward 5' CGGGGTACCACCATGGGCACCATCACCCTGTATGCTGTCACT 3' and Reverse 5' CGCGGATCCTTATCAGAGTCCTGACACAATCACCGA 3' which produce a fragment of 803 bp and 533 bp, respectively. The PCR amplified products (EDA^+ and EDA^-) were cloned in pBS-SKII vector. The *in vitro* translation was done by a single tube protein system (Novagen), based on a linked reaction in which transcription by a bacteriophage RNA polymerase is directly followed by translation with rabbit reticulocytes lysate. The translation products were analyzed by 10% SDS-PAGE followed by ON autoradiography. Fixed amount of the in vitro translated products were incubated in the absence of protease inhibitors with protein extracts (prepared in the absence of protease inhibitors) from tissues for 3h and 24h.

Gelatin Zymography: A total of 20 μg of tissue protein extract or 0.2 μl of plasma were diluted in 2X sample buffer (1:1) without adding any reducing agent. The samples were run on a 10% polyacrylamide gel polymerized in the presence of 0.2% gelatin. After electrophoresis, the gel was washed once for 15 minutes and then overnight in 100 ml wash buffer (2.5% Triton-X100, 50 mM Tris-HCl, pH 7.5 and 5 mM $CaCl_2$) to remove the sodium dodecyl sulfate (SDS). The gel was rinsed three times in water, followed by a 24 h incubation at 37°C in incubation buffer (50 mM Tris-HCl, pH 7.5 and 5 mM $CaCl_2$) and was stained for 4 hours in Coomassie Brilliant Blue. The absence of coloration indicates the digestion of gelatin by metalloproteinases. In a parallel gel, the same extracts were run and stained with Coomasie Blue.

Immunofluorescence of primary cultures of hepatocytes: Hepatocytes were prepared as described in the Materials and Methods Section, plated onto rat-tail collagen coated cover slips and cultured for the indicated times. Cells were fixed and incubated with an affinity purified anti-FN rabbit antibody, then with a FITC labeled secondary antibody. Nuclei were stained with Hoetscht. Original magnification was 200x.

Legends to the Supplementary Figures.

Supplementary Figure 1. A and B. MMPs activity was similar in tissues from all genotypes. Gelatin zymography analysis of plasma samples of $EDA^{wt/wt}$, $EDA^{+/+}$ and $EDA^{-/-}$ mice. The same amount of plasma was loaded in a gelatin-SDS gel, and the activity of metalloproteinases was determined. The same samples were loaded in a normal SDS-PAGE and stained with Coomassie Blue (Panel B) to normalize protein load. **C and D. EDA^+ FN was not preferentially degraded.** FN fragments containing or not containing the EDA exon were in vitro translated in the presence of ^{35}S-Met/Cys and incubated for different time with tissue extracts in the absence of protein inhibitors.

Supplementary Figure 2. Perfusion of tissues showed almost no residual plasma proteins. Equal amounts of proteins samples (50 μg) were loaded, run on a 12% SDS-PAGE and analyzed by Western blot for the presence of plasma gamma globulins. The protein load was controlled by detecting β-tubulin in the same extracts. Lanes 1-7 correspond to serial dilutions of $EDA^{wt/wt}$ plasma (each lane is 1:2 of the previous one, starting from 0.05 μl to 0.00078 μl). Lanes 8, 12 and 15 correspond to non-perfused samples. Lanes 9-11, 13-14 and 16-18 correspond to perfused samples. The protein load was quantified by the detection of β-tubulin in the stripped membrane (lower panels).

Supplementary Figure 3. No intracellular FN accumulation is seen in EDA+/+ hepatocytes. Hepatocytes were purified from $EDA^{wt/wt}$ and $EDA^{+/+}$ mice and plated onto rat tail collagen coated glass-slips for 24 or 48 h. Cells were fixed and stained with an affinity purified anti-FN polyclonal antibody. Nuclei of the same fields are shown (Hoetscht staining).

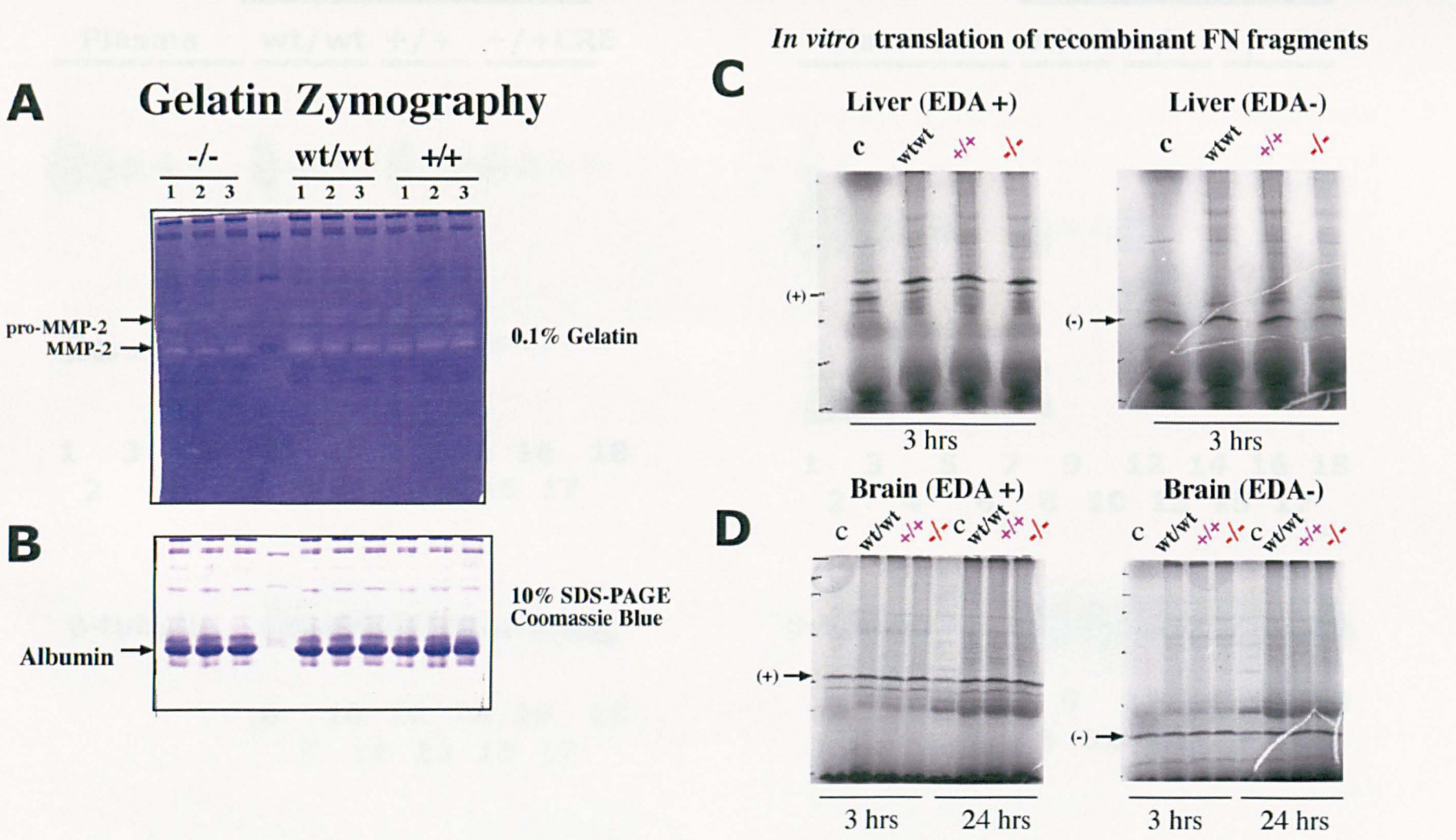

SUPPLEMENTARY FIGURE 1

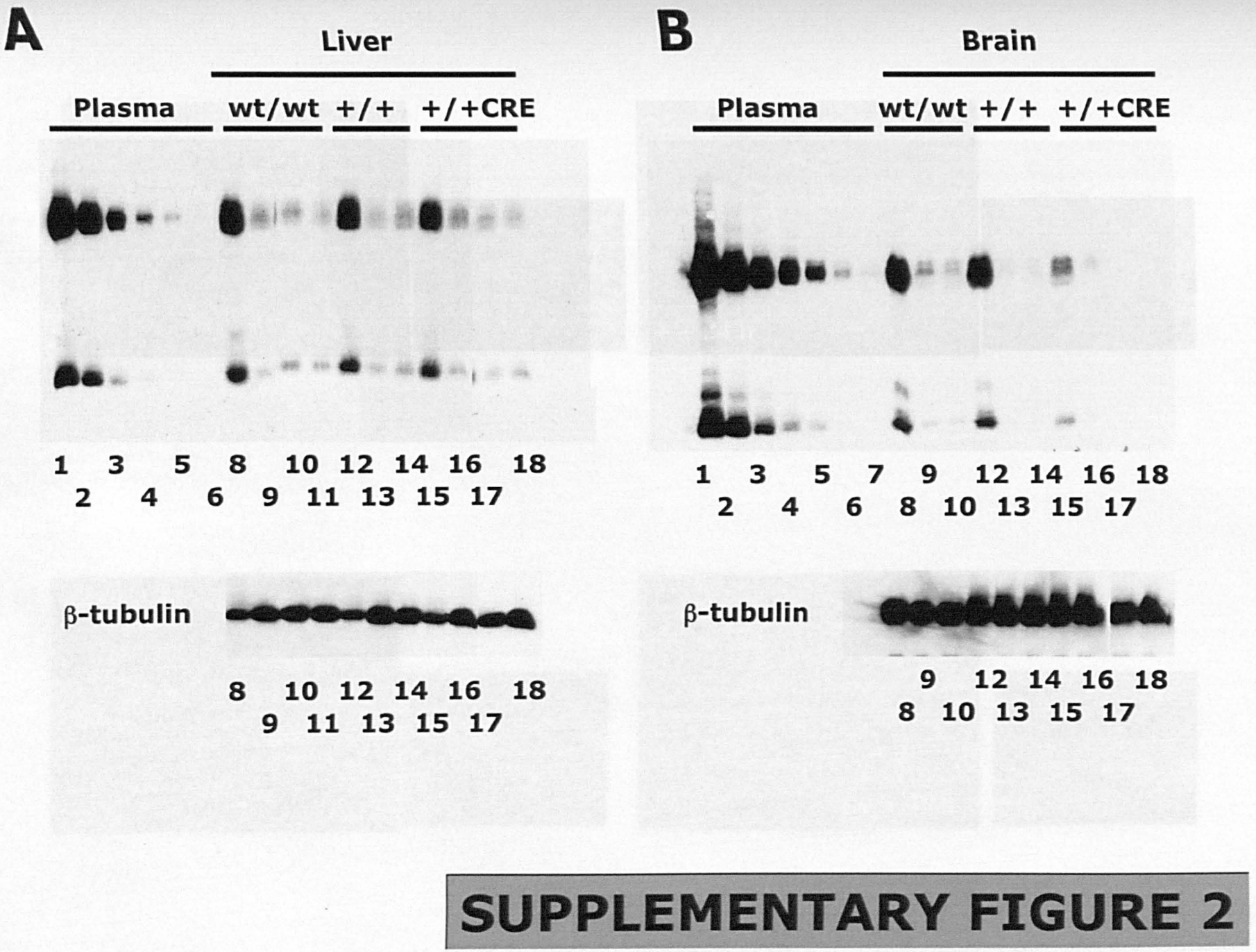

SUPPLEMENTARY FIGURE 2

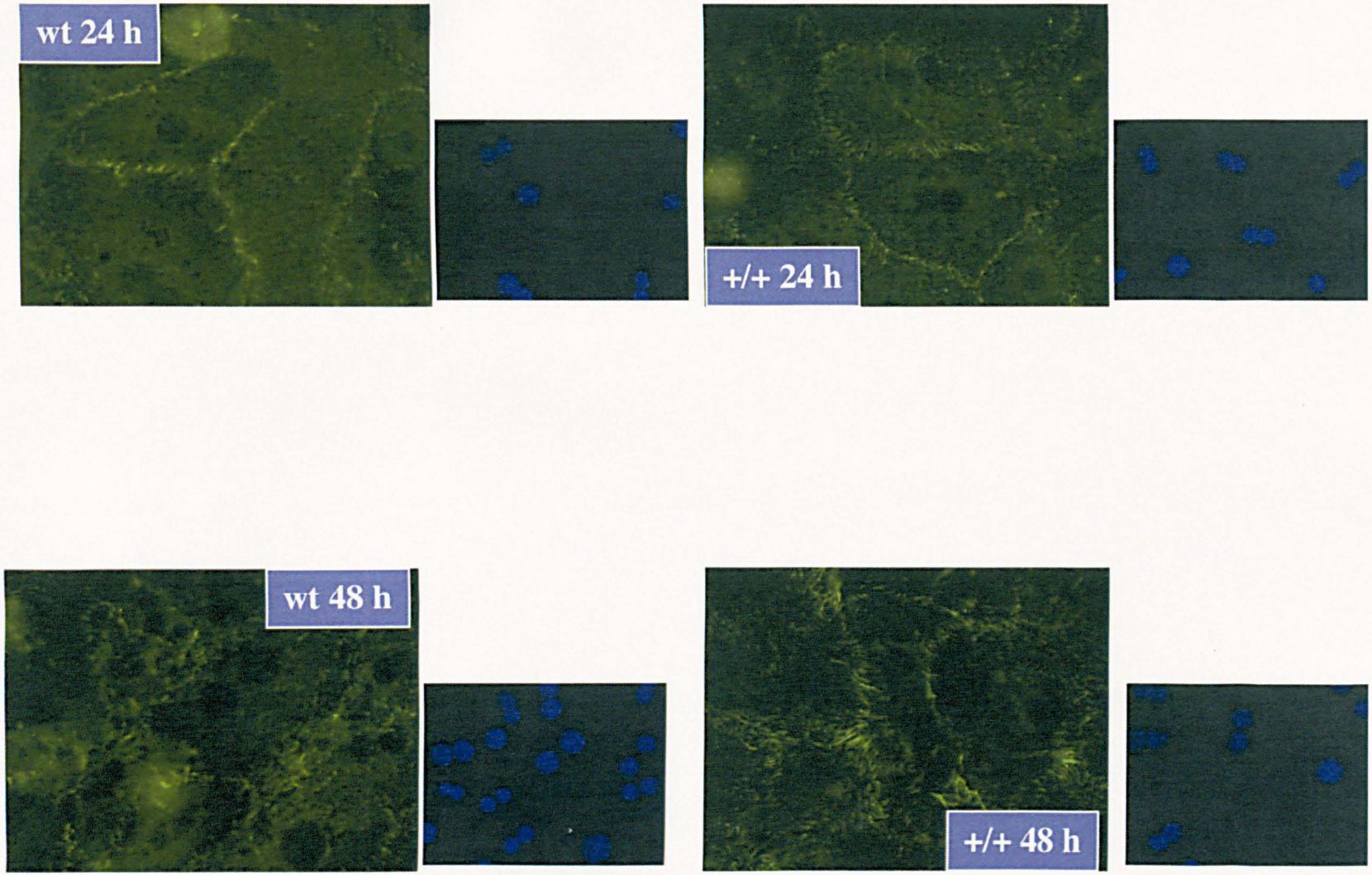

SUPPLEMENTARY FIGURE 3